



HAL
open science

Lead-free ferroelectric ceramics for multilayer ceramic capacitors

Vitoria Mussi Toschi

► **To cite this version:**

Vitoria Mussi Toschi. Lead-free ferroelectric ceramics for multilayer ceramic capacitors. Micro and nanotechnologies/Microelectronics. Université Paris Saclay (COMUE), 2019. English. NNT : 2019SACLC089 . tel-02495353v2

HAL Id: tel-02495353

<https://theses.hal.science/tel-02495353v2>

Submitted on 15 May 2020

HAL is a multi-disciplinary open access archive for the deposit and dissemination of scientific research documents, whether they are published or not. The documents may come from teaching and research institutions in France or abroad, or from public or private research centers.

L'archive ouverte pluridisciplinaire **HAL**, est destinée au dépôt et à la diffusion de documents scientifiques de niveau recherche, publiés ou non, émanant des établissements d'enseignement et de recherche français ou étrangers, des laboratoires publics ou privés.

Lead-free ferroelectric ceramics for multilayer ceramic capacitors

Thèse de doctorat de l'Université Paris-Saclay
préparée à CentraleSupélec

École doctorale n°573 : interfaces : approches interdisciplinaires,
fondements, applications et innovation (Interfaces)
Spécialité de doctorat: Chimie

Thèse présentée et soutenue à Gif-sur-Yvette, le 21/11/2019, par

Vitória Mussi Toschi

Composition du Jury :

Cécile Autret-Lambert Maîtresse de Conférences, Université de Tours	Rapporteuse
Mojca Otonicar Chercheuse, Institut Josef Stefan (Slovénie)	Rapporteuse
Pierre-Eymeric Janolin Professeur, CentraleSupélec	Directeur de thèse
Raphaël Haumont Professeur, Université Paris-Sud	Examineur (Président)
Henri Laville Docteur Ingénieur, responsable R&D, Exxelia	Co-encadrant

Titre : Céramiques ferroélectriques sans plomb pour condensateurs céramiques multicouches

Mots clés : Ferroélectriques, Céramique sans plomb, Condensateur multicouche, Electronique chaude

Résumé : De nos jours, la consommation des condensateurs céramiques multicouches (MLCCs) augmente en raison de leur efficacité et leur fiabilité. La miniaturisation résultant dans une plus grande dissipation volumique de chaleur et les nouvelles applications demandent des MLCCs qui peuvent travailler de 300 à 350°C, au-delà des limites actuelles de 200 – 250°C. De plus, les exigences environnementales augmentent également avec les réglementations REACH et RoHS qui interdisent l'utilisation du plomb en Europe. Il est donc impératif de créer des nouveaux matériaux sans plomb capables de répondre aux nouvelles attentes des MLCC.

Cependant, la compatibilité avec les méthodes de production industrielle, ainsi que les prix du marché sont des limites importantes. Trois familles de matériaux sans plomb ont été examinées : celle du BaTiO₃ (BT), du K_{0.5}Na_{0.5}NbO₃ et du Na_{0.5}Bi_{0.5}TiO₃ (NBT). Le NBT-BT à la MPB (6 % BT) a été choisi comme matériau diélectrique de base.

Plusieurs méthodes et paramètres de synthèse ont ensuite été étudiés pour déterminer les meilleures conditions de synthèse. La synthèse à l'état solide et le frittage traditionnel ont été choisis pour les échantillons en massif et le coulage en bande a été choisi pour les couches. Pour éviter l'évaporation des espèces volatiles, le frittage a été effectué en couvrant le NBT-BT par une poudre de ZrO₂.

Tous les échantillons présentaient des phases secondaires contenant du Ba (Ba₂TiO₄ et Ba₂Ti₉O₂₀) en raison de l'évaporation du Na pendant le frittage. Un effet de peau créé par la coexistence des phases tétragonale, rhomboédrique et cubique a également été observé, lié à la concentration locale de Ba dans le réseau cristallin du NBT.

Les effets des paramètres de synthèse et la stœchiométrie des réactifs sur les propriétés diélectriques, la résistance d'isolement et la séparation des phases ont été analysés.

La stœchiométrie nominale Na_{0.44}Bi_{0.48}Ba_{0.06}TiO₃ était la plus appropriée pour les MLCC en raison de sa résistance d'isolement élevée, de ses faibles pertes diélectriques et de sa stabilité de la permittivité en température. La présence de phases secondaires est initialement bénéfique en raison de l'élimination des lacunes d'oxygène. Au-delà d'une fraction volumique critique (2.5 à 3.0 %) et d'une taille de grain moyenne critique (0.9 à 3.0 m²), la tendance s'inverse en raison de la nature conductrice des phases secondaires.

Pour atteindre la fraction volumique et la taille de grain critiques, un agent dispersant a été utilisé lors du broyage dans la jarre de YSZ, avec du MEK et de l'éthanol comme solvants, et sans sécher les réactifs avant la pesée. Enfin, la relaxation des contraintes a été réalisée à 400°C pendant 3 heures.

Trois modèles ont été utilisés pour expliquer la dispersion des propriétés diélectriques en fréquence : le modèle de Maxwell-Wagner, le modèle de Nyquist et la loi de Curie-Weiss modifiée.

Les incompatibilités entre les propriétés diélectriques du NBT-BT rapportées dans la littérature ont ensuite été analysées soulignant l'importance d'avoir des méthodes de synthèse et de mesure strictes. Les trois principaux facteurs affectant les propriétés diélectriques induisant ces incompatibilités étaient la stœchiométrie, la méthode de métallisation et la fixation des fils électriques à l'aide de la laque d'argent.

Des pertes diélectriques croissantes à haute température a aussi été observée après chaque cycle thermique dépassant les 300°C, indiquant une dégradation thermique des échantillons.

Enfin, les monocouches céramiques ont montré une faible densité (62%) après frittage, limitant la plage de température correspondant aux spécifications d'Exxelia. Cependant, en utilisant un pressage des couches avant frittage, l'échantillon multicouche fritté présentait une densité élevée (89%). Une mesure des propriétés diélectriques doit être effectuée sur cet échantillon multicouche synthétisé, afin de déterminer sa compatibilité avec les spécifications d'Exxelia.



Title: Lead-free ferroelectric ceramics for multilayer ceramic capacitors

Keywords: Ferroelectrics, Lead-free ceramics, Multilayer capacitor, Hot electronics,

Abstract: MLCC consumption is today increasing due to their high efficiency, reliability and frequency characteristics. MLCCs that can work from 300 to 350°C are required both for miniaturization, resulting in greater volume heat dissipation and for new applications.

Moreover, environmental requirements are also increasing, the REACH and RoHS regulations prohibiting the use of lead in Europe. It is imperative to create new lead-free materials that are able to meet those requirements.

However, the compatibility with the production methods, price, and market are important industrial limitations that need to be considered.

Three families of lead-free materials were examined: BaTiO₃-based, K_{0.5}Na_{0.5}NbO₃-based and Na_{0.5}Bi_{0.5}TiO₃-based materials. NBT-BT at the morphotropic phase boundary (6% BT) was chosen as the base dielectric material.

Several synthesis methods and parameters were studied to determine the best synthesis conditions. Solid-state synthesis and traditional sintering were chosen for the bulk samples and tape casting was chosen for the layer samples preparation. Sintering was done under ZrO₂ powder to prevent the evaporation of volatile species.

All samples had secondary Ba-containing phases (Ba₂TiO₄ and Ba₂Ti₉O₂₀) formed because of the evaporation of Na during sintering. A skin-effect was observed due to a phase coexistence (tetragonal, rhombohedral, and cubic) due to the local concentration of Ba in the NBT lattice.

The effects of the synthesis parameters and the stoichiometry of the reactants on dielectric properties, insulation resistance, and phase separation were analysed.

The Na_{0.44}Bi_{0.48}Ba_{0.06}TiO₃ nominal stoichiometry was the most suitable for the MLCCs due to its high insulation resistance, low dielectric losses, and stability of permittivity in temperature.

The phase separation was initially beneficial, due to the resulting elimination of oxygen vacancies. Above a critical volume fraction (2.5 to 3.0%) and a critical mean surface area (0.9 to 3.0 μm²), the trend was reversed due to the conductive nature of the secondary phases.

To achieve the critical volume fraction and surface area of the secondary phases, a dispersing agent was used during ball-milling in YSZ jar, with MEK and ethanol as solvents, and without drying the reactants prior to weighing. Finally, a strain relaxation was done at 400°C for 3 hours.

Three models explained the frequency dispersion of the dielectric properties: the Maxwell-Wagner model, the Nyquist plot and the modified Curie-Weiss law.

Incompatibilities between the dielectric properties of NBT-BT reported in the literature were then analysed, showing the importance of maintaining strict synthesis and measurement methods. The three main factors affected the dielectric properties, creating these incompatibilities in the bulk samples. There were the stoichiometry, the metallization method, and the fixing of the electrical leads using silver paste.

An increase of the high-temperature dielectric losses after each thermal cycle reaching more than 300°C was observed, indicating a thermal degradation of the material.

Finally, the sintered ceramic monolayers showed a low density (62%), limiting the temperature range corresponding to Exxelia's specifications. However, after pressing the layers together before sintering, the sintered multilayer sample showed a high density (89%). Dielectric property measurement should be carried out for these synthesized multilayers.



Acknowledgments

Before entering into the thesis itself, I would like to acknowledge some important people that were essential to the present work.

Firstly, I would like to thank Dr. Cécile Autret-Lambert, Dr. Mojca Otonicar and Dr. Raphael Haumont for accepting being a part of my thesis jury and for their valuable suggestions and comments about my work.

I would also like to thank Prof. Pierre-Eymeric Janolin, professor in CentraleSupélec and supervisor of this work, for his great scientific support during my PhD, for his patience, motivation, knowledge and for accepting supervising my thesis after the loss of my previous supervisor.

I would also like to show my gratitude to Dr. Ing. Henri Laville, responsible for the research and development in the Exxelia company during most of my PhD, for his great technical support and also for his motivation, understanding and help during difficult situations.

I would like to thank everyone in the SPMS laboratory that helped my work directly or indirectly and that made it possible. More specifically, I thank Christine Bogicevic, for her precious help in the chemical synthesis part, in the SEM analysis and also for her emotional support, Fabienne Karolak, for her help in the SEM analysis and metalization, Rossen Tchakalov, for his help with the tape casting synthesis and also for his emotional support, Dr. Pavan Nukala, for the interesting and valuable scientific discussions and for his support and Rohit Pachat, for his help and support and finally all the PhD students in the laboratory, for their support and help during my thesis.

The help of Exxelia company was also essential during my thesis. More specifically, I would like to thank Dr. Ing. Christian Ravagnani, for his support as the head of R&D during the last year of this project, Ing. Anais Anouari, for her suggestions and interesting scientific and technical discussions, Serge Le Deroff, for his help with the insulation resistance measurement, Aurélie Van De Mert, for her support and help with the MEB measurements, and Pascale Escure, for her valuable suggestions and help with the synthesis of the ceramic tapes.

I also thank Prof. Houssny Bouyanfif, professor at the University of Picardie Jules Verne and member of the laboratory of Condensed Matter Physics (LPMC) and Yaovi Gagou, also member of the laboratory of Condensed Matter Physics (LPMC) for their indispensable help with the dielectric measurements, without which this work would not be possible, and for the trust they have given me during these measurements.

I thank again Prof. Rafael Haumont, professor in the university Paris Sud and member of the Institut of Molecular and Materials Chemistry of Orsay (ICMMO), for his precious help with the XRD measurements and also Dr. Lúcio de Abreu Corrêa, doctor by the Soil, Structures and Materials Mechanics Laboratory (MSSMAT) in CentraleSupélec, for his help with the data treatment and for the emotional support.

I would also like to thank my mother Ing. Sonia Maria Mussi Toschi and my brother Ing. Guilherme Mussi Toschi, for their support and motivation during these three years.

Finally, I would like to acknowledge two people that were essential for this work and that, sadly, are not among us anymore: Prof. Jean Michel Kiat, an excellent professor and researcher on the SPMS laboratory in CentraleSupélec and my supervisor during the first year my thesis, without whom this work would not have been possible and my motivation

for the scientific research would not be the same, and my father Ing. Gelson Donizeti Toschi, this great and intelligent man and engineer who was always my first advisor, role model as a person and a professional and who motivated and supported me during my entire thesis, even after he was gone.

This PhD thesis was done within a collaboration between the laboratory Structures, Properties and Modeling of Solids (SPMS) in CentraleSupélec and the Exxelia company, formalized through the CIFRE project number 2016/0982.

Contents

Acknowledgments	v
1 Introduction	1
1.1 Presentation of Exxelia	1
1.2 Industrial Context of multilayers ceramic capacitors (MLCC)	2
1.2.1 Presentation and importance of the MLCC for the industry	2
1.2.2 MLCC types	3
1.2.2.1 Type I	3
1.2.2.2 Type II	4
1.2.3 MLCCs uses and advantages	5
1.2.4 Tuning	5
1.2.4.1 Decoupling	5
1.2.4.2 Connecting	5
1.2.4.3 Filtering	6
1.2.4.4 Temperature compensation	6
1.2.4.5 Energy storage	6
1.2.4.6 Memory (RC)	6
1.2.5 New applications and requirements	6
1.2.5.1 Industrial temperature classification	6
1.2.5.2 REACH and RoHS	6
1.2.5.3 New high temperature applications and their requirements	9
1.2.6 Industrial production method and limitations	9
1.2.6.1 Slurry production	9
1.2.6.2 Tape casting and drying of the ceramic sheets	10
1.2.6.3 Screen printing of the electrodes	11
1.2.6.4 Stacking, pressing, and cutting	11
1.2.6.5 Sintering	11
1.2.6.6 Polishing (Corner rounding)	12
1.2.6.7 Metallization of the external electric contacts	12
1.3 Industrial Specifications and Limitations	13
1.3.1 Properties specifications	13
1.3.1.1 Temperature and frequency ranges	13
1.3.1.2 Permittivity value and its variation in temperature	13
1.3.1.3 Dielectric losses value	14
1.3.1.4 Insulation resistance	15
1.3.1.5 Variation of permittivity with frequency	15
1.3.1.6 Lifetime and aging	15
1.3.1.7 Layer thickness and grain size	16
1.3.1.8 Dielectric strength	16
1.3.2 Production limitations (industrial compatibility)	16
1.3.2.1 Composition	18
1.3.3 Conclusion and most important properties to chose the base material	18

1.4	Choice of the base dielectric material	19
1.4.1	Lead-free material families	19
1.4.1.1	BaTiO ₃ -based materials	19
1.4.1.2	K _{0.5} Na _{0.5} NbO ₃ -based materials	22
1.4.1.3	Na _{0.5} Bi _{0.5} TiO ₃ -based materials	22
1.4.2	NBT and NBT-BT solid solution	25
1.4.2.1	Pure NBT	25
1.4.2.2	NBT-BT solid solution	26
1.4.2.3	Possible NBT-BT solid solutions with K _{0.5} Na _{0.5} NbO ₃ (KNN) and Bi _{0.2} Sr _{0.7} TiO ₃	31
1.4.2.4	NBT-6%BT choice	32
1.4.2.5	Other possible dopants in NBT-BT	33
1.5	Conclusion	34
2	Synthesis method	37
2.1	Choice of the synthesis method	37
2.1.1	Sol-gel [9, 45, 64]	37
2.1.2	Solid-state reaction	38
2.1.3	Sintering	39
2.1.3.1	"Traditional" sintering in an atmosphere	39
2.1.3.2	Spark Plasma Sintering sintering	40
2.1.3.3	Microwave sintering method	40
2.1.4	Films, tape casting, and MLCC	41
2.2	Industrial limitations for each synthesis method	42
2.2.1	Industrial compatibility of the sintering process	42
2.2.1.1	Sintering atmosphere	42
2.3	Solid-state reaction and improvements in this thesis	43
2.3.1	Reactants weighing and drying	44
2.3.2	Mixture of the reactants	45
2.3.2.1	Ball milling of the reactants	45
2.3.2.2	Influence of the jar and balls material	45
2.3.2.3	Influence of the solvent	51
2.3.2.4	Influence of the grain size of the reactants	52
2.3.2.5	Influence of the speed and duration of ball milling	53
2.3.2.6	Influence of the NBT-BT stoichiometry	55
2.3.3	Slurry preparation and tape casting	59
2.3.3.1	Introduction	59
2.3.4	Calcination and sintering	61
2.3.4.1	Density problem for ceramic samples	61
2.3.4.2	Influence of the pressure before sintering	67
2.3.4.3	Influence of the sintering temperature	67
2.3.4.4	Sintering atmosphere influence	68
2.4	Phase separation and secondary Ba-containing phases formation	72
2.4.1	Phase formation and identification	72
2.4.1.1	ZrO ₂ influence in secondary Ba-containing phases formation	73
2.5	Conclusion and sample synthesis conditions	75

3	Dielectric characterization and compatibility with industrial requirements	81
3.1	Models for dielectric properties calculations and uncertainties	81
3.1.1	Description of electrical measurements: impedance spectroscopy and insulation resistance	81
3.1.2	RC model for permittivity and dielectric losses	83
3.1.2.1	RC model validation	84
3.1.3	Bruggeman model [2, 28]	84
3.1.4	Estimation of measurement uncertainties	86
3.1.5	Temperature drift and corrections	88
3.1.5.1	Wire fixing method	88
3.1.5.2	Silver paste on sample surface and temperature correction	88
3.1.5.3	Simplified electric contact and temperature corrections	91
3.2	Dielectric properties with temperature	91
3.2.1	Influence of stoichiometry, secondary Ba-containing phases, synthesis parameters and polishing and strain relaxation on the dielectric properties vs temperature	92
3.2.1.1	Stoichiometry	92
3.2.1.2	Secondary Ba-containing phases	98
3.2.1.3	Synthesis parameters	107
3.2.1.4	Polishing and strain relaxation	107
3.2.2	Comparison of the measured properties with Exxelia's specifications	110
3.2.2.1	Industrial layout graphics for permittivity, dielectric losses and RI versus temperature	113
3.3	Dielectric spectroscopy	115
3.3.1	Maxwell-Wagner model	116
3.3.1.1	Nyquist analysis	117
3.3.1.2	Relaxor character	121
3.4	Co and Mn additions and properties improvement	124
3.4.1	Co ₃ O ₄	124
3.4.1.1	Phase separation	124
3.4.1.2	Dielectric properties in temperature	127
3.4.2	MnCO ₃	128
3.4.2.1	Phase separation	128
3.4.2.2	Dielectric properties in temperature	130
3.5	Other compatibilities with industrial requirements	131
3.5.1	Dielectric strength	131
3.5.2	Compatibility with the electrodes	131
3.6	Conclusion	132
4	Literature incompatibilities	137
4.1	Dielectric properties differences reported in the literature	137
4.2	Differences in the measured sample dielectric properties	138
4.2.1	Influence of the stoichiometry on the dielectric properties	138
4.2.2	Differences in the dielectric properties of over first heating measurement	140
4.2.2.1	Influence of the structure and secondary Ba-containing phases, the synthesis parameters and the polishing and strain relaxation on the temperature hysteresis	141
4.2.2.2	Influence of the metallization and electric contact on the temperature hysteresis	143

4.2.2.3	Other dielectric properties changes during temperature cycle measurement	147
4.3	Conclusion	150
4.4	Future works for bulk NBT-BT	151
5	NBT-BT Layers	153
5.1	Layer preparation	153
5.1.1	Best NBT-BT bulk sample	153
5.1.2	Monolayer synthesis and sintering improvements	153
5.2	Structure and thickness of the monolayers	155
5.3	Dielectric properties of the monolayers in temperature	158
5.3.1	Compatibility of the dielectric properties with Exxelia's specifications	161
5.4	Structure and density of the pressed multilayers	162
5.5	Conclusion	164
5.6	Future works for NBT-BT layers	165
6	Conclusion	167
	Appendices	175
A	Extract of patent number 17 58575 publication number 3071244	175
B	Résumé de thèse	189
	Bibliography	195

List of Abbreviations

AFE	Anti-FerroElectric
BT	BaTiO₃
BMT	BiMg_{0.5}Ti_{0.5}O₃
BCT	Ba_{0.8}Ca_{0.2}TiO₃
BSZT	Ba_{0.6}Sr_{0.4}Zr_{0.2}TiO₃
BZT	BiZr_{0.5}Ti_{0.5}O₃
BZZ	BiZn_{0.5}Zr_{0.5}O₃
BMZ	BiMg_{0.5}Zr_{0.5}O₃
BMTa	BiMg_{0.67}Ta_{0.33}O₃
BST	Bi_{0.2}Sr_{0.7}TiO₃
KBT	K_{0.5}Bi_{0.5}TiO₃
BZW	BiZn_{0.75}W_{0.25}O₃
BSBT	(Ba_{0.6}Sr_{0.4})_{0.7}Bi_{0.2}TiO₃
EDS	Energy Dispersive X-ray Spectroscopy
ESR	Equivalent Series Resistance
ESL	Equivalent Series Inductance (L)
FE	FerroElectric
IR	Isolation Resistance
KNN	K_{0.5}Na_{0.5}NbO₃
MLCC	Multi Layer Ceramic Capacitor
MPB	Morphotropic Phase Boundary
PNR	Polar Nano Regions
NBT	Na_{0.5}Bi_{0.5}TiO₃
NBT-BT	Na_{0.5}Bi_{0.5}TiO₃ - 6% BaTiO₃
NN	NaNbO₃
SEM	Scanning Electronic Microscope
XRD	X-Ray Diffraction
YSZ	Yttrium Stabilized Zirconium oxide
WC	W(tungsten) Carbide
MEK	Methyl-Ethyl-Ketone

Chapter 1

Introduction

The objective of this chapter is to present the context and the problematic of the thesis, to explain the industrial specifications and limitations that apply to the choice of the base material for the multilayer ceramic capacitors (MLCC).

1.1 Presentation of Exxelia

Founded in 2009, the Exxelia group is the result of the merger of five historical companies with complementary know-how (Eurofarad, Firadec, Sic Safco, Microspire and Astema). The main former company, Eurofarad, was founded in 1965 and it was previously a world leader in the multilayer ceramic capacitors (MLCCs) production.

Since its foundation, Exxelia has continued to grow and strengthen its international presence through strategic acquisitions in the United States, Vietnam, Morocco and France. Today, Exxelia has ten entities all operating in niche industrial markets.

Exxelia specializes in the design and manufacture of high reliability passive electronic components and innovative electromechanical solutions. The products are designed and manufactured to meet the problems and constraints of demanding industrial applications: Space, Aeronautics, Defense, Security, Energy, Medical, Transport, Advanced Industries and Telecommunications. Exxelia is based on two main sites, Chanteloup-en-Brie and Marmoutier.

The *Chanteloup-en-Brie* main site is located close to Paris (77) and it has an area of 11000m². It includes the production of Film, Ceramic, Filters, Sensors and Associated Systems capacitors, as well as the Quality, Logistics, Human Resources, IT and Purchasing departments. The site is EN9100 and ISO 9001 certified.

The *Marmoutier* site is located in Alsace (67) and it has a surface area of 9000 m² to develop its activities around Film, Filters, Sensors and Associated Systems and Precision Mechanics capacitors.

This thesis was done in cooperation with the Chanteloup-en-Brie site, where the expertise is the production of MLCCs. These capacitors have an excellent temperature resistance, volume capacity, electrical properties and reliability. Therefore, they can be used in many fields of application such as medical implants, flight controls in aeronautics, switch mode power supplies in harsh environments, oil drilling probes or space. More details on the ceramic capacitors will be presented in section 1.2.

The MLCCs are manufactured according to rigorous manufacturing procedures. These strict procedures at each production stage have enabled many Exxelia's product lines to obtain certifications, so that they comply with the most rigorous standards applied in the space, aeronautics, rail and other advanced industries.

The research and development sector of Exxelia and, more specifically, of the Chanteloup-en-Brie site have also a great importance for the company. So the R&D and Innovation team are formed of expert and dedicated engineers and researchers. In this context, strategic partnerships with laboratories at universities, grandes écoles and companies in the industrial

sector, like this thesis are a key point for developing new products and methods. Finally, collaborations with European and international programs also contribute to the innovative profile of Exxelia.

Innovation in Exxelia's entities is characterized by the more than 40 patents that were already registered internationally. To maintain this high performance and innovation activities, more than 7% of sales are devoted to Research and Development.

In this industrial context, this thesis was proposed by Exxelia and it was developed in partnership with the SPMS (Structures, Properties and Modeling of Solids) laboratory. The SPMS is an excellence laboratory of CentraleSupélec dedicated to the study and innovation in the fields of functional materials for energy, advanced ferroic materials and electronic structures, modelling and simulation.

1.2 Industrial Context of multilayers ceramic capacitors (MLCC)

The industrial production of MLCC is very important for the electronics industry, since MLCCs are the most consumed capacitor type in the world. Moreover, new industrial requirements are constantly created, due to the miniaturization and need for better and more reliable electronic components.

The MLCCs and their context are introduced, applications and industrial production are presented hereafter.

1.2.1 Presentation and importance of the MLCC for the industry

The model of the simplest capacitor is made of two conducting plates or electrodes separated by a dielectric material. This dielectric material can be characterized by its ability to store charges and by its response to an external applied electric field. The main properties we should focus on are the capacitance value and dielectric losses (linked to the real and imaginary parts of the permittivity), the insulation resistance (linked with the resistivity to a direct voltage) and the dielectric strength (breakdown field).

In the case of ceramic capacitors, the material may be paraelectric, ferroelectric, relaxor, or anti-ferroelectric.

The idea behind the production of multilayer ceramic capacitors is to increase the final capacitance of the device, by connecting in parallel many ceramic capacitors. The capacitance calculation for the MLCC will be described in the section 1.3.1.2.

The structure of a MLCC shown in Fig. 1.1 consists in alternating layers of conducting material (electrodes) and dielectric material (ceramics). Each dielectric layer represents a single mono-layer capacitor. The external electric contacts are also composed of several layers, to ensure the parallelisation of the single-layer capacitors and weldability of the MLCC. The composition and function of each layer will be explained in section 1.2.6.7.

MLCCs are known to have high volume efficiency, high reliability, and good frequency features. For this reason, MLCCs are the most consumed capacitor type in the world today, with an annual production of more than 100 billion units. [8] The market has grown around 20% each year since the beginning of the decade. One of the key factors contributing to this is the electronics production increase, driven by cell phones and personal computers. More than that, MLCCs are also intensively used in new high technology fields, such as controlling systems for transportation, aerospace, and military applications. [77]

For this reason, intensive efforts are being made to create capacitors that can withstand more demanding operating conditions with more controlled and reliable properties.

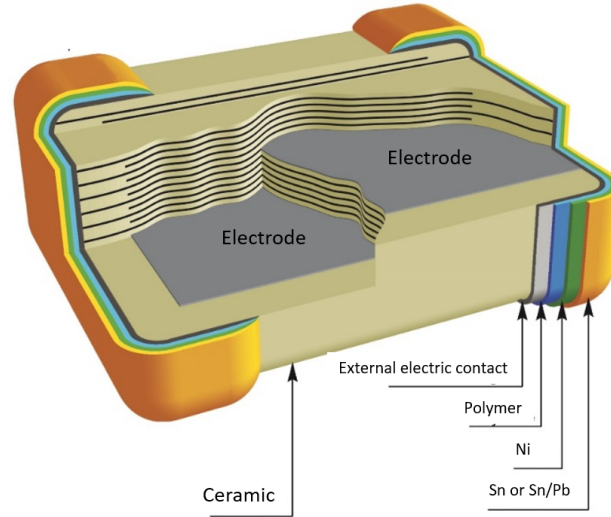


FIGURE 1.1: Schematic representation of a multilayer ceramic capacitor - Exxelia [8]

1.2.2 MLCC types

1.2.2.1 Type I

Type I MLCCs are produced using paraelectric ceramics. For this reason, as it will be explained in details in section 1.2.5.1, their capacitance and permittivity variations with the temperature, voltage, and frequency are reduced. They do not exhibit aging or polarization. However, their dielectric constants and their capacitances are low. This type of MLCCs can be divided in 3 sub-classes depending on their temperature coefficient α (variation of the permittivity by 1°C variation).[67]

NPO (industrial name) or C0G (Electronic Industries Alliance classification)

These MLCCs, as can be seen in Table 1.1, have the most stable permittivity in temperature, with $\alpha = 0 \pm 30 \text{ ppm}/^\circ\text{C}$, which means that the tolerance for permittivity and capacitance variations are 0.3% each 100°C in relation to the permittivity or capacitance value at 25°C , from -55 to 125°C .

Note that, for current application, the value of 25°C is defined as the reference temperature T_0 , since the usage temperature range has the room temperature as its middle point. This permittivity variation limit can be defined as:

$$\Delta\varepsilon(T) = \frac{\varepsilon(T) - \varepsilon(T_0)}{\varepsilon(T_0)} \quad (1.1)$$

NPO dielectrics are normally based on MgTiO_3 or $\text{Nd}_2\text{Ti}_2\text{O}_7$.[67]

P90 and P100

The P90 and P100 MLCCs, as they are normally named in the industry, are equivalent to M7G in the EIA classification. They have $\alpha = 90$ (or 100) $\text{ppm}/^\circ\text{C}$, which means that the permittivity varies linearly with temperature at a rate of 0,9 or 1% each 100°C . These MLCC are usually based on Mg_2TiO_4 .[67]

Others

These MLCCs have a temperature coefficient, which is negative and not quite linear, with

a mean value, at room temperature, ranging from $-33\text{ppm}/^\circ\text{C}$ to $-4700\text{ppm}/^\circ\text{C}$.

1.2.2.2 Type II

Type II capacitors are based on BaTiO_3 (BT), which is a ferroelectric material that undergoes a phase transition from paraelectric to ferroelectric, thereby the permittivity sharply increases around the Curie temperature T_c . For this reason, they can have large capacitance. However, their permittivity varies a lot under temperature, and their voltage constraints and dielectric losses present higher values.[67]

BT and standard additives

In type II MLCCs, BT is the base production material. BT [2] is a well known ferroelectric defined by the existence of a remanent polarization that can be switched by an electric field between two or more directions.

In this material, spontaneous creation of ferroelectric domains are facilitated by long-range interactions between the dipoles in each unit cell. The polarization alignment in each domain under an external electric field results in the growth of the corresponding domains that eventually occupy the entire material. After the external electric field is removed, the domain structure remains. This phenomenon is responsible for the P-E loop (polarization versus electric field cycle). The domains are also responsible for the better energy storage properties and permittivity when compared to most dielectric materials.

BT undergoes three phase transitions in temperature that are accompanied by permittivity peaks: the first one at around -90°C , from rhombohedral to orthorhombic crystalline symmetries, the second one at around 0°C , from orthorhombic to tetragonal and, finally, the third one, at the Curie temperature around 130°C , from tetragonal to cubic. These phase transitions are responsible for a large variation of permittivity in temperature, especially at the Curie temperature, as can be seen in the Fig. 1.2.

For the MLCC production, pure BT is not ideal, due to the large variations of permittiv-

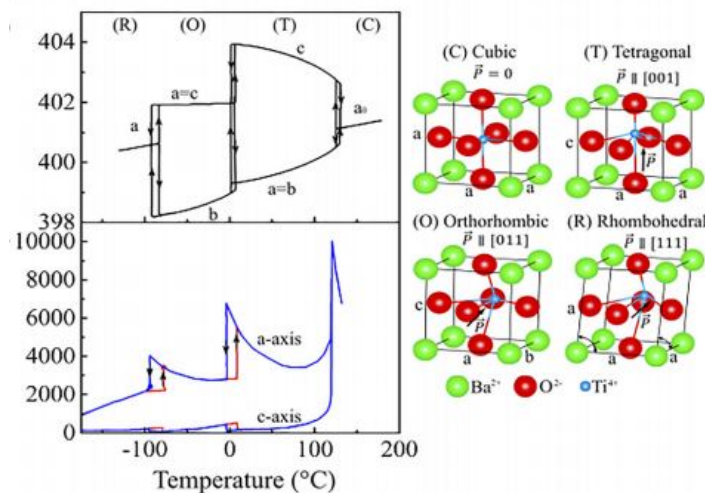


FIGURE 1.2: Phase transitions in temperature for pure BT [1]

ity in temperature. To solve this problem, modifications of the composition through additives are done, in order to increase or decrease the permittivity and to flatten its variation.[67]

Some other problems that would appear if pure BT was used in the MLCC production are:

- The aging phenomenon (steady capacitance decrease over time, as will be presented in the section 1.3.1.6), which is reversible after heating the MLCC above the Curie temperature, something that cannot be done in electronic systems;
- The decrease of the insulation resistance and the permittivity when an external continuous voltage is applied;
- The increase of the dielectric losses during phase transition, which comes from the peaks in permittivity.

Some examples of additives used in the type II MLCC are SrTiO_3 and CaZrO_3 that can form a solid solution with BT to decrease the Curie temperature of the pure BT. The MgZrO_3 and $\text{Bi}_2\text{Sn}_3\text{O}_9$ also form a solid solution with BaTiO_3 to decrease the maximum permittivity value and the permittivity variation with temperature. Other inter-granular doping (that do not form solid solutions) that can be used in MLCC are Co_3O_4 and MnO . These oxides have lower melting points than the BT and can form a liquid phase during sintering, which increases the final density of the ceramics. They also decrease the conductivity of the material as it will be explained in more details in section 3.4.[67]

For the variation of the permittivity with frequency, there is a relative stability for the classical operating frequencies, between 1kHz and a 100MHz.

Fluxing agents

BT is sintered only in the solid-state and the sintering temperature is higher than 1250°C.

Some fluxing agents (glass former) [67] may be added to the composition to create a liquid phase during sintering, increasing the final density and decreasing the sintering temperature to less than 1130°C. However, these agents can evaporate and lead to changes in composition or performance of the dielectrics, for example when using lithium salts. They can also initiate reactions with the electrodes leading to failures, for example, when bismuth-based agents or materials are used (as it will be mentioned in section 1.3.2).

1.2.3 MLCCs uses and advantages

1.2.4 Tuning

Tuning MLCCs are used in oscillating circuits, filters, or time constant circuits. It requires very low losses and high stability as a function of temperature, time, and DC voltage applied. Type I ceramics as well as polystyrene, polypropylene, polycarbonate, and PPS (polyphenylene sulfide) films meet these requirements. These capacitors are applied, for example, in transducer circuits.

1.2.4.1 Decoupling

Decoupling MLCCs are used to reduce or eliminate a parasitic alternating component in a high frequency domain. The capacitor must have a low impedance at the operating frequencies and therefore a high capacitance (e. g. 100 nanoFarads). Type II capacitors are the most suitable. An example of decoupling capacitor application is in output of logic signals.

1.2.4.2 Connecting

Connecting capacitors are used to ensure the connection between 2 points at different continuous potentials. It blocks the DC component and transmits the alternative component.

The capacitor must be able to withstand a high DC voltage and have a high insulation resistance. A typical application is in the output of amplifiers. Either type I or type II MLCC can be used for these applications. [8]

1.2.4.3 Filtering

Filtering capacitors are used to reduce or eliminate a parasitic alternating component of the direct voltage. The capacitor must have a high capacity value as well as low resistance and inductance values. These capacitors are applied, for example, in radios. [8]

1.2.4.4 Temperature compensation

Temperature compensation capacitors have a negative temperature coefficient, to compensate for the positive drift of a component, but also pre-defined and stable over time. Class I ceramics and film (polystyrene) meet these requirements. [8]

1.2.4.5 Energy storage

Energy storage capacitors deliver a very high power in a very short time or a direct voltage for a very long time. An example of their applications is the development of high speed chargers.

1.2.4.6 Memory (RC)

The RC memories store information in the form of an electrical charge. As such, they must have a high insulation resistance and return the stored charge in a very short time. These memories can be used in electronic devices, such as computers and cell phones.

1.2.5 New applications and requirements

1.2.5.1 Industrial temperature classification

Type I and type II MLCC can be classified by their capacitance variation in temperature (temperature class). The temperature classes, expressed in code, describe the minimum operating temperature, the maximum temperature and the temperature drift. This capacitance variation in temperature represents one of the most important characteristics of the MLCC, as will be detailed in section 1.3. The EIA (Electronic Industries Alliance) is the international standard used to classify MLCCs by their temperature coefficients. It is presented in Table 1.1 for type I MLCC and Table 1.2 for type II MLCC.

1.2.5.2 REACH and RoHS

The REACH (Registration, Evaluation, Authorization, and Restriction of Chemicals) and RoHS (Restriction of Hazardous Substances) regulations are the two most important regulations in the electronics industry and, more specifically, for the MLCC production.

Some specifics of those regulations will be explained here.

Products labeling (CLP)

The CLP (Classification, Labelling and Packaging) [58] labeling is used to identify and to make the labeling of dangerous products. It applies to the industrial production (before the marketing of the products).

It is a complementary REACH regulation in the sense that it divides chemical products

Temperature coefficient (ppm/°C)	Code letter	Temperature coefficient multiplier	Code number	Temperature coefficient tolerance (ppm/°C)	Code letter
0.0	C	-1	0	±30	G
1.0	M	-10	1	±60	H
1.5	P	-100	2	±120	J
2.2	R	-1 000	3	±250	K
3.3	S	-10 000	4	±500	L
4.7	T	1	5	±1000	M
7.5	U	10	6	±2500	N
		100	7		
		1 000	8		
		10 000	9		

TABLE 1.1: EIA designation for type I MLCC [8]

Minimum operating temperature (°C)	Code letter	Maximum operating temperature (°C)	Code number	Maximum capacitance variation (%)	Code letter
10	Z	45	2	±1.0	A
-30	Y	65	4	±1.5	B
-55	X	85	5	±2.2	C
		105	6	±3.3	D
		125	7	±4.7	E
				±7.5	F
				±10	P
				±15	R
				±22	S
				± 22 - 33	T
				± 22 - 56	U
				± 22 - 82	V

TABLE 1.2: EIA designation for type II MLCC [8]

into categories, based in their danger. There are 28 hazard classes: 16 classes of physical danger, 10 classes of danger to health, 1 large environmental hazard class.

For certain hazards, and particularly for CMR (carcinogens, mutagens, reprotoxicants), the CLP Regulation uses the principle of classification of mixtures to limit concentrations of dangerous substances (it is the case of Pb, for example, the limit concentration is 0.15%).

REACH Regulation

The REACH (Registration, Evaluation, Authorization and Restriction of Chemicals) [57] is a European Union regulation adopted with the objective of protecting human health and the environment from the risks associated with chemical substances and promoting the competitiveness and innovation.

The regulation is applied for substances present in the final product (so it does not control the products used in production lines, if they are not present in the final product). It also places the responsibility of proof on companies that have to identify and manage the risks of their products. In the long term, the most dangerous substances must be replaced by substances that are less dangerous.

The dangerous substances are defined in the CLP Regulation by the CMR and environmental dangerous products groups.

Companies must register their REACH controlled products with the ECHA (European Chemicals Agency) when they are used in quantities (1 ton) and concentrations (for each product) larger than a limit threshold, in order to be authorized to use them over a limited period (18 months). If no technically and economically viable solution is found during these 18 months, the authorization can be renewed.

The process for registering a product is long and laborious, since the ECHA agency asks for a risk management for each application of the registered substance. Since there is only one register per substance, smaller companies can pay larger ones to take part in their register.

If a new solution is found during the 18 months authorization of a registered product, the company can claim this new product solution. This will be evaluated by a technical committee and the authorization will be withdrawn. The other companies will have 18 months to stop using this previously authorized product. So, the need to find new solutions for REACH controlled products is crucial for companies that sale in Europe.

RoHS Regulation

The RoHS (Restriction of Hazardous Substances) [60] regulation deals with the electric or electronic final products (and not the substances used only during their production). It has the objective of restricting the use of 10 substances in these products: lead (Pb), mercury (Hg), cadmium (Cd), hexavalent chromium (Cr⁶⁺), polybrominated biphenyls (PBB), polybrominated diphenyl ether (PBDE), bis(2-ethylhexyl) phthalate (DEHP) Butyl benzyl phthalate (BBP), dibutyl phthalate (DBP), diisobutyl phthalate (DIBP).

The maximum allowed concentrations in non-exempted products are 0.1wt% (except for Cd, which is limited to 0.01wt%). The restrictions are on each homogeneous material in the product.

In the last review of the RoHS a new category of applications was created, including all the products that have an electrical source in one of their functions, even if this function is not its main one. So, the only excluded fields are the aerospace, the military, and the industrial plant and tools.

The RoHS exemptions have between 12 and 18 months of validity. If no technically and economically viable solution is found during this period, each company should ask from a renewal of the exemption from its country authority. In order to decide if the exemption should be renewed, the authorities evaluate the substitution material and its socio-economic

impact. However, if a new solution is found, the exemption can be withdrawn. So, the need of finding new solutions for RoHS controlled products is also crucial.

In conclusion, these regulations are especially important for the MLCC production since the use of lead will be soon forbidden for non military or aerospace applications. This creates the need to develop new lead-free material that can meet the industrial expectations for new applications.

1.2.5.3 New high temperature applications and their requirements

The MLCC industry is currently going through many technological advances to meet the requirements from modern electronics. Nowadays, investments are done into developing new processes and materials to improve the volume capacity and the capacity of working in harsh environments. [83]

In this context, the rarefaction of fossil resources, which forces to drill ever deeper and the race for miniaturization that leads to dissipate more heat in smaller volumes and, often, closer to hot sources, make the high-temperature MLCC a strategic development for the companies growth.

Some examples include the electronic control of cars or airplanes, where the key modules are placed close to the engines, the development of electric airplane that need small MLCC working constantly close to heat sources. Other examples are the braking control system used in airplanes, where it is estimated that the electronic system should be capable to work around 350°C during every landing and the deep downhole oil and gas industry that requires today an operational temperature of 250°C and higher temperatures in the future. [83]

It is therefore imperative to bring out new materials capable to meet the expectations of electronics in the 300-350°C range.

Today, the high-temperature MLCC production is limited to capacitors that can operate in temperatures up to 200-250°C. Some examples of these products are the AT Series 200°C & 250°C Rated high-temperature type II MLCCs from AVX company that operate at a maximum temperature of 250°C in military and commercial applications, the Knowles HiT250 type II MLCC that works up to 250°C, the X8R and X9M (type II) products from Murata (GCB Series) that can operate up to 200°C, and the KEMET's High Temperature COG (type I) that also operates at a maximum temperature of 200°C.

All in all, the high-temperature MLCC available on the market can work in a maximum temperature of 250°C, which will not be enough for the new market requirements in the near future.

1.2.6 Industrial production method and limitations

The industrial production can be described in a simplified diagram as shown in Fig. 1.3. The various steps are:

1.2.6.1 Slurry production

The first step is the preparation of the slurry[59], where the ceramic powder is mixed with the solvent, a dispersing agent, a deflocculant, a binder, and a plasticizer.

- The ceramic powder is the most important component of the slurry, since it determines the final composition of the ceramic layer and its concentration and also average grain size and shape have a great influence on the final material density.

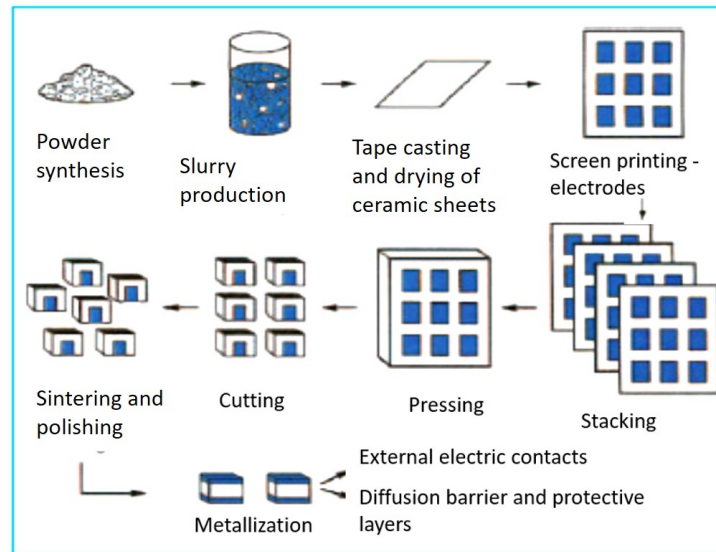


FIGURE 1.3: Simplified diagram of the industrial synthesis method of multilayer ceramic capacitors (adapted from Exxelia's internal document)

- The solvents are the base of the slurry and their properties and concentrations influence the rheological properties of the slurry and the layer drying rate. These properties are extremely important for the synthesis of homogeneous and mechanically strong tapes.
- The function of the dispersing agent, which is often also used as a deflocculant, is to separate particles from each other and hold them in suspension, in order to have a stable slurry in the end. The function of the deflocculant is to avoid the formation of loosely bound groups (*flocs*), in order to increase solid loading, decrease the amount of solvent in the slurry, and increase the surface energy (driving force to the sintering process).
- The binder is there to keep the mechanical integrity of the ceramic sheet. So the green ceramic tape is simply a polymer matrix impregnated with a large amount of ceramics. That is why it is the most important additive of the system.
- The function of the plasticizer is to enable the tape to be bent without cracking. They work on or around the binder polymer chains to allow motions inside the tape matrix without breaking the matrix itself, giving it more flexibility.

1.2.6.2 Tape casting and drying of the ceramic sheets

There are two possible slurry production lines, the first with an aqueous solvent and the second with an organic solvent.

For the production of the ceramic sheets, the slurry is ball-milled and then casted, by tape casting technique, over a film either in silicon-coated Mylar (for thin sheets) or in stainless steel (for thick sheets), to evaporate the solvents in a furnace at a temperature of 50 to 100°C. The dry ceramic thick sheets are then cut and the thin ones are stored as a roll. Defects are identified visually and the thickness of the sheet is measured. Finally, the ceramic sheets are stored in a dry, air-conditioned atmosphere.

1.2.6.3 Screen printing of the electrodes

This part of the production process is where the internal electrodes are created.

Conducting materials

There are two types of conducting materials for MLCC electrodes: [8]

- Base metal electrode (BME): most BMEs are composed of nickel, except in some rare cases, where the electrode is made of copper. This implies sintering in a reducing atmosphere, to avoid deterioration of the electrode.
- Precious metal electrode (PME): the PMEs normally consists of 70% of Ag and 30% of Pd and they are normally co-sintered with the ceramic layers between 1000 and 1150°C. Different Ag and Pd percentages can be used, depending on the sintering temperature, so materials sintered at 1300°C can have more than 30% of Pd while materials sintered at less than 1100°C can use 90% of Ag and 10% of Pd. Sintering is done in an oxidizing atmosphere, to prevent the creation of oxygen vacancies in the ceramic.

In general, the volume variation of the electrodes are more important than the one of the dielectrics during sintering. This may result in defects in the MLCC. One of the solutions is to add to the electrode ink a ceramic filler, which will reduce the volume variation of the electrode.

Method: Silkscreen and mesh

The ceramic sheets are screen printed with the internal pattern electrode. In this process, the 70% Ag - 30% Pd ink, composed of the metal powder, a solvent, a binder, a plasticizer, and a surfactant is applied on the raw ceramic sheet. A mesh is used to create some lines with no ink that allows the communication between two consecutive ceramic layers through small gaps in the electrode. This guarantees the mechanical integrity of the multilayer device.

1.2.6.4 Stacking, pressing, and cutting

The electrode ink is dried in a furnace before the metallized ceramic layers are stacked.

After stacking, the blocks are pressed into an isostatic press, to create a block of alternating layers of ceramic and metal with good cohesion, but not yet sintered. Finally, the blocks are cut into single MLCCs.

1.2.6.5 Sintering

The co-sintering of ceramic and electrode (blocks of alternated layers of ceramic and metal) is carried out between 1000 and 1300°C. In this process, the ceramic and the metallic ink densify and decrease in volume and a monolithic "dielectric-metal electrodes" block is obtained. Sintering is done with a gradual increase of temperature, to avoid thermal shock. To avoid contamination (for example by bismuth, which is used to reduce the melting temperature of some materials), some ceramics are sintered in dedicated furnaces.

Sintering methods

As will be detailed in section 1.3.2, the sintering is done in an industrial furnace where the heating and cooling rates can be controlled. However, the sintering atmosphere in the furnace cannot be controlled, since it is not air tight. No pressure or electric current can be applied during sintering, so the classical sintering method is used.

1.2.6.6 Polishing (Corner rounding)

After sintering, the ceramic and metal blocks are corner rounded, using a vibrating recipient where the blocks are added together with an abrasive. The corner rounding removes sharp corners, edges and the external oxidized layer, to expose the edges of the electrodes and guarantees a homogeneous dielectric layer. This step is not presented in Fig. 1.3 p. 10, even if it is a usual step for the MLCC production.

1.2.6.7 Metallization of the external electric contacts

The metallization is often a succession of several layers, so can we distinguish.

Metal contact

After polishing, the metallization of the external electric contacts [8] is done using a metal ink composed of Ag and Pd (for precious metal electrode) or Cu (for base metal electrode) and glass (silicium oxide), which will ensure the mechanical strength of the contacts by diffusion in the ceramic layers. The ink is placed on the two opposite sides of the capacitors, where the edges of the electrodes are exposed. This creates the final MLCC structure, where the single capacitors (formed by each dielectric layer) are in parallel.

The PME (Ag-Pd) capacitors are then heated at about 700°C to sinter the metallization. In this process, the metallic particles do not melt but the metallization is densified by solid-state mass transfer (sintering) and by the formation of a liquid phase, composed mostly of bismuth and silicium oxides that accumulates at the grain boundaries and in the interface between the metallization and the MLCC, increasing the mechanical strength. This step creates a single MLCC piece.

In the case of capacitors intended for surface mount, a conductive polymer layer (silver filled epoxy) can be used to give some flexibility that allows capacitors to better withstand thermal variations.

Diffusion barrier and weldability

The next step is the surface treatment [8] where electrolytic deposition is used, to create a diffusion barrier of Ni. The role of this barrier is to prevent the dissolution of the silver-based electrical contacts into the solders. Over the Ni barrier, a Sn (or Sn-Pb) layer is added to improve the weldability of the material and to protect it against corrosion and Ni passivation.

Protective layers

The final step in the production process consists in the creation of an exterior resin coating, [8] which is made to increase the resistance of the capacitors to environmental hazards. It is necessary that these layers are waterproof and weldable. Most often Sn / Pb alloys are used (up to 40% Pb) for space and / or military applications or Sn, which is compliant with the REACH and RoHS regulations but that can generate whiskers.

In conclusion, the MLCC is the most consumed capacitor type in the world, due to the variety of applications and to the range of dielectric properties it can have.

Nowadays, the environmental requirements are growing. The most important environmental regulations concerning the MLCCs are the REACH and RoHS that control the level of lead in the final products. This created the need for developing new lead-free materials.

There is also a growing need for the development of new high-temperature MLCCs. These new capacitors would have crucial applications, such as deep oil drilling, use in train and airplane breaks, and also the creation of a new electric airplane. Moreover, the MLCC miniaturization trend intensifies the need to develop new high temperature capacitors.

So the development of a new lead-free material for high-temperature MLCCs is crucial for the electronic components industry.

1.3 Industrial Specifications and Limitations

This section presents the specific requirements for the dielectric material studied in this thesis taking into account its future lead-free high-temperature MLCC application. The requirements related to the dielectric properties and the compatibility with the industry are specified here.

1.3.1 Properties specifications

1.3.1.1 Temperature and frequency ranges

The storage and operating temperatures established by the industry, in which these new high-temperature capacitors should have the appropriate electric properties, are:

Temperature of storage (when the capacitor is not in use): the capacitor should not be damaged when stored at cold temperatures (-55°C and above).

Minimum operating temperature: the expected minimum operating temperature should be the room temperature (from 0 to 25°C). It could also be higher, up to a maximum of 100°C , if a heating system is used. However, the lower the minimum operating temperature (up to a minimum of -55°C) the better.

Maximum operating temperature: The maximum operating temperature should be around 300 to 350°C in continuous operation.

The operating frequencies established by the industry, in which these new high temperature capacitors should have the appropriate electric properties, are:

For *standard applications*, such as oil drilling, is from 1kHz to 100MHz .

For *other applications*, such as classic embedded electronics, the frequency can be around 400Hz .

The *industry standard* is 1kHz for defining the values of the alternative current properties (permittivity and dielectric losses).

So, in general, the frequency can vary from 400Hz up to 1MHz , the standard being 1kHz to define the reference values of the dielectric properties.

1.3.1.2 Permittivity value and its variation in temperature

The capacitance C is one of the most important properties of a capacitor, because it relates to the stored charges Q and to the applied voltage V as it can be seen in equation 1.2:[67]

$$Q = C * V \quad (1.2)$$

The capacitance of a simple capacitor (one dielectric layer) can be calculated, based on the dielectric permittivity of the material as:[67]

$$C = \frac{\epsilon_r \epsilon_0 A}{l} \quad (1.3)$$

where ϵ_r is the relative permittivity of the material (adimensional), ϵ_0 is the permittivity of the vacuum ($8.85 \cdot 10^{-12}\text{F/m}$), A is the surface in m^2 and l the thickness of the dielectric layer in meters.

For a multilayer capacitor, each dielectric layer behaves as a single capacitor and the set behaves as parallel capacitors, increasing the capacitance of the final capacitor. The capacitance of an MLCC containing N electrode layers in can be calculated as: [67]

$$C = \frac{\epsilon_r \epsilon_0 A (N - 1)}{l} \quad (1.4)$$

In order to obtain a relatively high capacitance value and to respect the capacitance variation in temperature for the type II MLCC, the relative permittivity should *ideally be of approximately 2000 and of a minimum of 1000* and flat over the operating temperature range.

Since the new MLCC developed here does not exist in the industrial standards, there is no predefined variation of the permittivity with temperature (or temperature coefficient). However, the standards for X7R ceramics, the most industrially used and produced type II ceramic capacitor have a variation of $\pm 15\%$ compared to the 25°C permittivity (reference) in the temperature range of -55 to 125°C .

From this standard, we chose a permittivity variation of $\pm 15\%$ in the operating temperature range when compared to a reference temperature within this range.

1.3.1.3 Dielectric losses value

Real capacitors can be characterized by their capacitance C , equivalent series resistance (ESR) composed of the resistance of the conductive part (electrodes, electric contacts and connections) and of the dielectric material, and its equivalent series inductance (ESL). [8]

The ESR and the ESL consume a part of the energy sent to the capacitors. Moreover, the relaxation time (used to polarize the dielectric material) also creates an energy loss during the application of an alternative voltage. These energy losses are transformed into heat and the real capacitor diagram can be represented as Fig. 1.4. [67] The $\tan \delta$ represents the dielectric losses of the material.

As can be seen in the Fig.1.4, the consequence of the energy loss is to decrease the phase

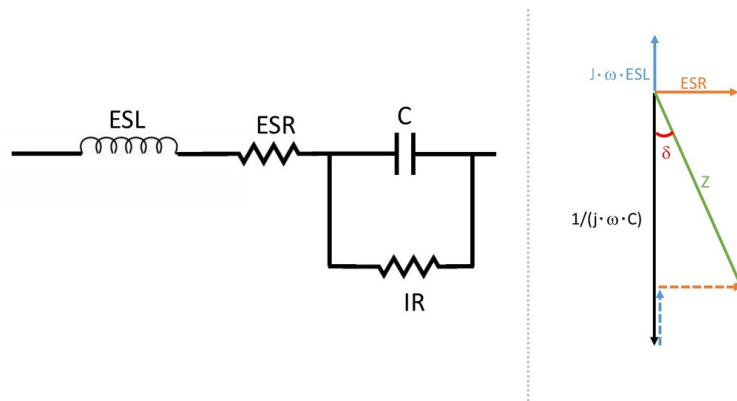


FIGURE 1.4: Complex impedance plane representation of the complex impedance, the equivalent series resistance (ESR), the equivalent series inductance (ESL), the real capacitors C and dielectric losses diagram for real capacitors.

shift between the applied alternative voltage and the current through the capacitor from 90° (ideal capacitor) to $90 - \delta^\circ$

Ideally, to have a low energy loss in the MLCC, the dielectric losses should be *lower than* $\tan \delta < 0.5\%$, however the class II capacitors industrial standard for dielectric losses establishes a *maximum value for* $\tan \delta$ of 2.5% (at 1 kHz). These are therefore the ideal and the maximum values for the dielectric losses in the operating temperatures.

1.3.1.4 Insulation resistance

The insulation resistance (IR) is the property of opposing leakage currents when a direct voltage is applied to a material. Ideally, the insulation resistance should be infinite, to avoid the capacitor discharge. However, real dielectric materials have a limited insulation resistance, due to the presence of crystalline defects and impurities in their structures.[67] The description and origin of the conduction in dielectric materials will be discussed in the section 3.2.1.1.

The insulation resistance corresponds to the product of the material's resistivity by its corresponding permittivity in the same temperature, as detailed in section 3.1.1. So it represents the time constant of the capacitor (the time a capacitor in an opened circuit takes to drop to the value of 36.8% of its initial charge through the internal resistance). [6]

The low value of the insulation resistance is one of the greatest problems of ceramic capacitors that limits its use at high temperatures, since it decreases rapidly when temperature increase (mainly above 150°C for BT-based capacitors). So the IR is an important parameter for the MLCC.

It is desirable that the minimum value of the IR for the high temperature MLCC production is of $IR \cdot C > 10\Omega F$ from 250 to 300°C and $IR * C > 1\Omega F$ from 300 to 350°C.

1.3.1.5 Variation of permittivity with frequency

BT-based capacitors are normally used in the frequency range where there is no variation in capacitance and permittivity with frequency, since the dielectric material is a "normal" ferroelectric (and not a relaxor).

For that reason, there is no standard for this type of permittivity variation. However, for an ideal capacitor, a minimal variation of permittivity within the operation frequency range (10^3 to 10^8 Hz) and the operation temperature range (from room temperature to 350°C) is desirable.

1.3.1.6 Lifetime and aging

The aging phenomenon is characterized by the gradual decrease of the dielectric properties of the capacitors, due to changes in the crystalline structure of the dielectric. It can be canceled by heating the dielectric material above its Curie temperature. However, it has to be minimal to avoid changes in the capacitor properties.

The permittivity aging, for example, can be described for a ferroelectric material by its degradation rate m : [67]

$$\varepsilon_r(t) = \varepsilon_r(t_0) - m \log_{10}(t) \quad (1.5)$$

where $\varepsilon_r(t)$ is the permittivity in time, ε_{r0} is the initial value of permittivity (at $t = t_0$) and t is the time.

For the new high-temperature capacitors, the expected lifetime should be at least 2000 hours of continuous work (in oil drilling, for example).

For applications in train and airplane systems, where the work is done in peaks, the cumulative lifetime under use should be of at least two months (that is, more than 1500h). For an airplane system, for example, it represents around 500 operations with short duration but high demand (this number was estimated for 500 hours of flight between two revisions, an average of one hour per flight and approximately eight flights per day, to maximize service life).

Minimal aging should be observed during the lifetime defined above. This means that the

dielectric material must have a suitable reliability and, therefore, little change in permittivity and losses over time for the defined voltage, frequency and temperature operation ranges. It must, therefore, have a limited variation in capacitance and losses.

1.3.1.7 Layer thickness and grain size

The selected ceramic and grain size should allow the production of ceramic layers with a minimum thicknesses between 5 to 20 μm or less.

Normally the grain size of the ceramics used is of the order of 0.3 to 0.5 μm before sintering and between 0.5 to 2 μm after sintering.

1.3.1.8 Dielectric strength

The dielectric strength is related to the capacity of a dielectric material to withstand high electric fields.

The dielectric failure generates free electrons and, by colliding with the crystal lattice, it creates an avalanche effect resulting in a sudden current increase. This failure is irreparable and the MLCC should be changed after it happens.

The dielectric strength is a secondary parameter in the industrial requirements, because there is no minimum value in the industrial standards. The measured values for BT-based MLCC are between 25 and 30 $\text{V}/\mu\text{m}$ or MV/m for Class II capacitors and between 50 and 60 $\text{V}/\mu\text{m}$ or MV/m for Class I, which can be used as a reference for the new high temperature MLCC studied here.

1.3.2 Production limitations (industrial compatibility)

The compatibility with the current production method in the MLCC industry and, more specifically, in Exxelia is an important limitation, since ideally no major changes should be done to the process, for the new dielectric to be useful for industrial production with reduced costs.

Slurry preparation

As detailed in section 1.2.6.1, the slurry is composed of a mixture of ceramic powder, solvent, deflocculant, binder and plasticizer. The compatibility with the industrial production imposes requirements for the binder: the most common binder in the MLCC industry is the PVB polymer (polyvinyl butyral), so it was chosen to prepare the slurry preparation. It is necessary to verify the compatibility of the ceramic powder with this binder and its influences on the slurry properties.

Tape casting

The Tape Casting process should be used to produce the ceramic sheets, to guarantee the compatibility with the current production method.

Sintering

The heating and cooling rates of the industrial furnace can be controlled, to reduce the possibility of thermal shocks up to 1300°C and the sintering is normally done at a maximum temperature between 1000 and 1300°C.

The sintering atmosphere in the furnace cannot be controlled, which means that the variation of the percentage of O_2 and N_2 in the sintering atmosphere cannot be changed. The

furnace is not airtight, so having a saturated atmosphere to avoid volatilization is difficult. It is conceivable to change the furnace for a airtight one, if the new high-temperature material studied here has good properties and if a controlled atmosphere is needed for sintering.

Compatibility with the electrode materials

The compatibility of the ceramic material with the electrodes are important to allow the MLCC production.

For the BT-based MLCCs, the most common electrode type is composed of 70% of Ag and 30% of Pd, even if the percentages of each metal can vary, depending on the sintering temperature.

To guarantee a good co-sintering of the ceramic and the electrode material, the melting

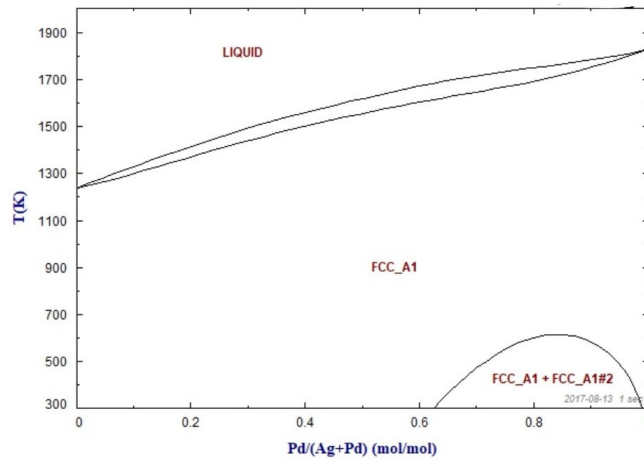
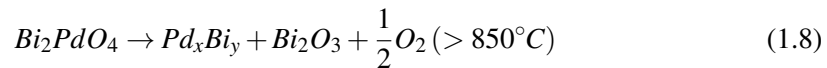
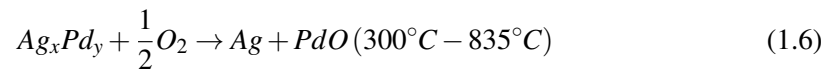


FIGURE 1.5: Phase diagram for Ag-Pd mixture (taken from: www.crct.polymtl.ca/fact/documentation/FS_All_PD.s.htm).

temperature of the electrode should be slightly higher than the sintering temperature. So the maximum sintering temperature for alloys of Ag and Pd is between 960 and 1150°C (see Fig. 1.5). Moreover, the thermal expansion coefficient of both materials should be similar, to avoid lamination failures. The thermal expansion coefficient of the Ag-Pd alloy for different Ag quantities is presented in Fig. 1.6.

Finally, a special attention should be paid for Bi-containing ceramics, since they can react with the Pd of the electrode, creating defects such as cracks or lamination on the MLCCs. The reactions between the Bi and Pd are:



Industrial experience shows that at least 30% of Ag should be added to the Pd for the Bi-containing materials in MLCC, to avoid the reactions between Bi and Pd. So, analyzing Fig. 1.5, the maximum sintering temperature for Bi-containing ceramics used in MLCCs is 1150°C

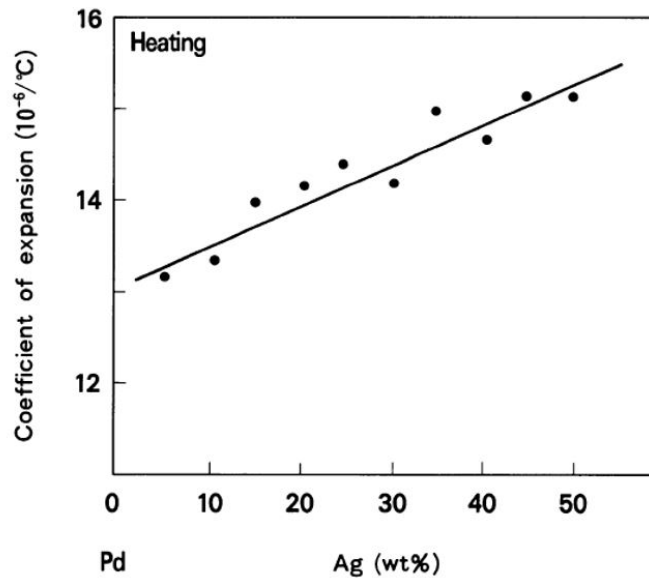


FIGURE 1.6: Thermal expansion coefficient of the Ag-Pd alloy with different compositions. [3]

1.3.2.1 Composition

Price limitations

The use of scandium (Sc) is not possible, because of its cost (4200 US\$ / kg). For comparison some expensive minerals used industrially are the Nb, with a price of approximately 50 US\$ / kg and the Ta, with a price of 100 US\$ / kg. Due to the production of tantalum capacitors and doping with Nb in BaTiO₃ base ceramics, they are widely used.

Legal limitations

The ceramic used cannot contain lead (Pb), cadmium (Cd) or other heavy metals as specified in the RoHS and REACH regulations (see 1.2.5.2).

Market limitations

Some elements with very few producers or with strategic industrial applications may be subjected to drastic price increase or suddenly become unavailable. They are therefore incompatible with the industrial MLCC production. Indium is an example of such element.

1.3.3 Conclusion and most important properties to choose the base material

After discussing with the Exxelia's head of R&D department, the most important properties to choose the base material are:

- the permittivity value of $1000 \leq \epsilon_r (1\text{kHz}) \leq 2000$ (the standard for comparing these values was chosen as 1kHz and 213°C)
- the similarity of the temperature range corresponding to a variation of 15% in the value of permittivity at 200°C and the desired operating temperature (from room temperature to 350°C)
- the dielectric losses in the temperature and the similarity between the temperature range for having $\tan \delta \leq 2.5\%$ and the desired operating temperature (from room temperature to 350°C)

- the insulation resistance at 300°C higher than 10 ΩF
- the industrial feasibility (tape casting synthesis with PVB as the binder, traditional sintering without a sealed oven, Ag-Pd alloy electrode compatibility and price limitation with no expensive elements)

1.4 Choice of the base dielectric material

As mentioned in section 1.2.5.2, lead-based materials are not suitable. Therefore, only lead-free materials are considered. The three main families of lead-free materials are reviewed first: they are based on BT (section 1.4.1.1), NBT (section 1.4.1.3) and KNN (section 1.4.1.2). [80] Table 1.3 provides a synthetic comparison of their properties with regard to Exxelia's requirements. NBT and NBT-BT solid solutions, the base material of choice, are then reviewed in more depth.

1.4.1 Lead-free material families

There is a growing demand for the development of new lead-free dielectric materials that can be used for MLCC production within the ever-stricter environmental constraints. For this reason, several papers have been published in recent years to study different ceramic systems that have a high and constant permittivity above 200°C, while maintaining low dielectric losses.

In this context, three main families of lead-free materials can be used to obtain desirable dielectric properties and to increase the operating temperature limit when compared to conventional high-permittivity (class II) dielectrics, which were based on BaTiO₃ until now. [80]

The materials are analyzed hereafter taking into account their basic properties and their variation in temperature: relative permittivity, dielectric losses, and electrical resistivity. In addition to these parameters, the sintering temperature, the composition, and the production process are also analyzed with respect to their compatibility with industrial constraints and, more specifically, with Exxelia's requirements.

1.4.1.1 BaTiO₃-based materials

The BaTiO₃-based materials are the most commonly used materials in the industry. BaTiO₃ Curie temperature is around 130°C, which means that, for higher temperatures, the dielectric properties are rapidly degraded. It is then necessary to modify the chemical composition, in order to increase the Curie temperature and make it useful for the production of high temperature MLCC.

(1-x) BaTiO₃ - x Bi(Mg_{0.5}Ti_{0.5})O₃ (BT - x BMT)

The BT - x BMT [85] solid solution has a relaxor behavior for $x \geq 10\%$ and for $20\% \leq x \leq 60\%$ of BMT, the permittivity becomes stable in temperature.

For BMT percentages of $x = 10\%$ to 20% , the material has a average relative dielectric constant between 600 and 1000 from 25 to 400°C, but high dielectric losses with a $\tan \delta$ between 5 and 10%. For higher percentages of BMT, the permittivity value increases and the losses decreases, but ceramics become less stable in temperature compared to $x = 10\%$ and the temperature range for low losses remains limited. For $x = 60\%$ for example $\epsilon_r = 2200 \pm 15\%$ from 136 to 375°C (compared to the permittivity at 200°C) and $\tan \delta \leq 2\%$

from 197 to 400°C.

The sintering temperature of this solid solution is from 1100 to 1350°C, so it is compatible with the industrial demands, however the sintering should be done in a air tight furnaces.

(1-x) (0.8 BaTiO₃ - 0.2 CaTiO₃) - x BiMg_{0.5}Ti_{0.5}O₃ with possible NaNbO₃ addition (BCT - x BMT)

Substitution of 20% of barium by calcium in the BT-BMT [82] solid solution stabilizes the variation of the permittivity with temperature and decreases the dielectric losses. However, it also decreases considerably the permittivity values. Considering the values for the best BCT - x BMT composition, with 55% of BMT, the optimum composition of the BT - x BMT solid solution, the BCT-BMT has an average relative permittivity value of $\epsilon_r = 1000 \pm 15\%$ from 80 to 500°C, where the value of 1000 is measured at the permittivity peak. It gives it a very low temperature coefficient of 230 ppm / °C, but also a low permittivity value. Moreover, it has a relatively high insulation resistance, from approximately 10 seconds up to 350°C.

However, its dielectric losses are still high up to 160°C, with $\tan \delta \leq 2.5\%$ from 160 to 430°C (measured at 100Hz). So the decrease in dielectric losses is not sufficient to meet the MLCC requirements. In addition, a small variation in the percentage of BMT can significantly deteriorate the properties, which can be a risk for industrial repeatability. Sintering is done between 1050 and 1150°C, which is compatible with the Ag-Pd electrodes. The synthesis method is the solid-state reaction that is also compatible with the industrial production.

The addition of NaNbO₃ decreases the maximum permittivity temperature T_m from 160°C to 0°C. This changes the lower limit of variation of $\epsilon_r \pm 15\%$ of the relative permittivity (considering 200°C as the reference temperature) to negative temperatures, resulting in $\epsilon_r = 600 \pm 15\%$ from -70 to 500°C and $\tan \delta \leq 2\%$ from -20 to 400°C for 20% of NaNbO₃, for example. This composition also has an insulation resistance of 10s at 330°C, compatible with Exxelia's requirements. However, the value of relative permittivity is also decreased, which is not interesting for the production of MLCC type II. The sintering temperature is 1050 to 1150°C, which is compatible with Ag-Pd electrodes.

(1-x) (0.6 BaTiO₃ - 0.4 SrTiO₃ - 0.2 ZrTiO₃) - x Bi(Mg_{0.5}Ti_{0.5})O₃ (BSZT - x BMT)

The BSZT - x BMT [25] solid solution has a wide temperature range of stable permittivity and very low values of dielectric losses, since, for the optimal composition with 20% of BMT, the relative permittivity is $\epsilon_r = 500 \pm 15\%$ from -70 to 300°C and $\tan \delta \leq 1.5\%$ from -60 to 310°C. However, it has a very low permittivity (500) at 150°C and also a low value of insulation resistance, of 3.7s at 300°C. The sintering temperature is 1150°C, which is ideal for Ag-Pd electrodes and the synthesis method is solid-state reaction, compatible with the industrial production.

(1-x) BaTiO₃-BiZn_{0.5}Ti_{0.5}O₃ (BT - x BZT)

The BT - x BZT [72] is a solid solution that has a diffuse maximum of permittivity starting from x=5% of BZT and a frequency dispersion from 20% of BZT where it becomes a relaxor. Its dielectric properties are optimal for the composition x=20% BZT, where the relative permittivity and losses are $\epsilon_r = 1700 \pm 15\%$ from 80 to 310°C and $\tan \delta \leq 2\%$ from 87 to 350°C. The temperature range can be improved to 100 to 350°C by adding 2% barium vacancies, which also increases the insulation resistance to 1.6s at 300°C. However, to achieve these values, the ceramic must be sintered in an oxygen flow and hot pressed (5000 psi and 1100°C), which is not suitable for industrial production.

(1-x) (0.8 BaTiO₃ - 0.2 CaTiO₃) - x Bi(Zn_{0.5}Ti_{0.5})O₃ (BCT - x BZT)

The BCT - x BZT [81] is also a solid solution, which, for a percentage of 30% of BZT,

has an almost flat permittivity (that is, the variation of $\pm 15\%$ in the relative permittivity takes place in a larger temperature range), with $\epsilon_r = 1165 \pm 15\%$ from 25 to 425°C. For this composition ($x=30\%$), the material has low dielectric losses, since $\tan \delta \leq 2.5\%$ from 87 to 460°C and $\tan \delta \leq 1\%$ from 110 to 420°C. The insulation resistance value is also compatible with Exxelia's requirements (10s at 300°C). However, the average relative permittivity value of 1030 is low and the minimum temperature to have low losses (87°C) is high compared to the industrial demands.

The sintering temperature of this solid solution ranges from 1050 to 1400°C, so it could be compatible with the industrial demands; however, the sintering should be done in a sealed furnace, which would require new industrial furnaces.

(1-x) BaTiO₃ - x Bi(Zn_{0.5}Zr_{0.5})O₃ (BT - x BZZ)

The BT - x BZZ [73] solid solution presents a relaxor behavior for $10\% \leq x \leq 60\%$ of BZZ. However, the dielectric properties of this material have not been studied and detailed. The relative permittivity is $\epsilon_r = 1000 \pm 15\%$ from less than 200 to 350°C and the dielectric losses are $\tan \delta \leq 2.5\%$ from the ambient temperature to 250°C. However, there are no studies on the insulation resistance of the material.

The sintering temperature of this solid solution is from 1100 to 1290°C, so it is compatible with the industrial demands, however, similar to BCT - x BZT, the sintering should be done in a sealed furnace.

(1-x) BaTiO₃ - x Bi(Mg_{0.5}Zr_{0.5})O₃ (BT - x BMZ)

The BT - x BMZ [11] is a solid solution up to a percentage of 50% of BMZ. This solid solution has a core-shell structure for 3 to 6% of BMZ, but, in this case, the relative permittivity has a value of $\epsilon_r = 6200 \pm 15\%$ from 150 to 370°C. For higher percentages of BMZ (from 30% to 40%) it has a more stable temperature permittivity of $\epsilon_r = 570 \pm 15\%$ from -20 to 430°C with low losses ($\tan \delta \leq 2\%$ from 30 to 420°C). However, in this case, the average permittivity value is too low for the MLCC application.

(1-x) BaTiO₃ - x Bi(Mg_{0.67}Nb_{0.33})O₃ (BT - x BMN)

The BT - x BMN [48] solid solution exhibits a temperature-stable behavior for compositions from 20 to 60% of BMN. The composition with 20% BMN has a very low permittivity variation but very high dielectric losses for temperatures higher than 150°C. The compositions from 40 to 60% BMN have a greater variation in the permittivity, but much lower losses. For example, for 50% of BMN, the material has a relative permittivity of $\epsilon_r = 900 \pm 15\%$ from 25 to 550°C and dielectric losses of $\tan \delta \leq 2.5\%$ from 74 to 350°C. For this composition, the insulation resistance is approximately 2s at 250°C, which is not sufficient considering that the IR should be of at least 10s at 350°C. So, this ceramic does not have a sufficiently high permittivity and IR values for the manufacturing of MLCCs.

(1-x) BaTiO₃ - x BiMg_{0.67}Ta_{0.33}O₃ (BT - x BMTa)

The BT - x BMTa [41] solid solution exhibits a stable permittivity for different ranges of temperature for to the compositions from 8 to 60% of BMTa. However, for low percentages of BMTa, the temperature range is not high enough. For example, for 10% BMTa, $\epsilon_r = 1278 \pm 15\%$ from 30 to 150°C. For larger quantities of BMTa ($x > 10\%$), the permittivity is $\epsilon_r = 1800 \pm 15\%$ from 115 to 230°C and losses are high for temperatures larger than 263°C. For these reasons, this solid-solution is not ideal for the production of MLCC.

1.4.1.2 $\text{K}_{0.5}\text{Na}_{0.5}\text{NbO}_3$ -based materials

The KNN-based materials are, with the BT-based materials, among the most studied lead-free dielectrics. [80] They are promising candidates for the production of high-temperature MLCC, since KNN has a high Curie temperature between 350 and 420°C. [27] The dielectric properties of pure KNN vary significantly temperature, but they can be controlled by various composition changes.

However, KNN-based materials have some important disadvantages, such as the higher volatility of alkali components at high temperature (which makes the synthesis difficult and decreases the reliability of the material) and the very low sintered densities. This creates the need for doping and changing the sintering methods to obtain ceramics with interesting properties and hinders their use in the MLCC production, even though some interesting properties were reported in the literature.

(1-x) KNN - x Bi(Zn_{0.75}W_{0.25})O₃

The addition of BZW to KNN lead to a solid solution with widened orthorhombic - tetragonal and tetragonal - cubic transitions compared to KNN. [12] The optimal composition, with 10% BZW, has a relative permittivity of $\epsilon_r = 1300 \pm 15\%$ from 120 to 350°C. However, it has a limited temperature range of low dielectric losses, with $\tan \delta \leq 2.5\%$ from 210 to 420°C. This is not ideal for the production of MLCC as operating temperature must be extend at from below 100 to 350°C.

(1-x) KNN - x LiTaO₃

The KNN - LiTaO₃ [22] is a ferroelectric solid solution with a high Curie temperature of about 420°C and a stable permittivity in temperature. The addition of LiTaO₃ to KNN decreases the transition temperature from the orthorhombic to the tetragonal phases from 200°C in pure KNN to -50°C for composition with 10% of LiTaO₃. This composition has therefore a relative permittivity of $\epsilon_r = 480 \pm 15\%$ from -50 to 350°C. For x=5% of LiTaO₃, the relative permittivity increases to $\epsilon_r = 650 \pm 15\%$ from 0 to 380°C and the dielectric losses become $\tan \delta \leq 2.5\%$ from 150 to 200°C. However, this is not high enough for the production of ceramic capacitors.

(1-x) KNN - x LaFeO₃ (KNN - x LaFeO₃) with possible MnO₂ addition

KNN - x LaFeO₃ [13] is a solid solution where LaFeO₃ increases the maximum permittivity and decreases the variation of permittivity with temperature. Addition of MnO₂ improves the densification of the ceramic during sintering, which reduces dielectric losses. This doping also acts as an acceptor, increasing the maximum permittivity, decreasing the leakage current, therefore increasing the insulation resistance and making the dielectric harder. The optimal composition, which has the formula 0.98KNN - 0.02LaFeO₃ - 1.5mol%MnO₂ exhibits a permittivity of $\epsilon_r = 2000 \pm 15\%$ from 100 to 380°C. However, this composition has high dielectric losses, between 2.5 and 5% between 100 and 400°C. This is not interesting for the MLCC application.

1.4.1.3 $\text{Na}_{0.5}\text{Bi}_{0.5}\text{TiO}_3$ -based materials

Despite an intensive research effort, opened questions remain on its structures and dielectric properties, due to its high structural complexity. A more detailed literature review will be presented in section 1.4.2.1. However, it must be highlighted here that the NBT have a high Curie temperature, of around 400°C, and it has two anomalies on its permittivity in temperature: the first one corresponding to the depolarization temperature, T_d , around 200°C

and the second one corresponding to an broad permittivity maximum at T_m , around 300°C. These anomalies increase the permittivity stability compared to other ferroelectric ceramics, like BaTiO₃, creating an extended temperature range of low dielectric losses, going from the T_d to the T_m .

Moreover, its properties, like the T_C , the T_m , and the conductivity, can be controlled by adding various dopings and by forming solid-solutions, which makes it an interesting base material for the MLCC production.

(1-x) NBT - x NaNbO₃ (NBT - x NN)

The NBT - x NN [36, 74] is solid-solution. The temperature of the maximum permittivity (T_m) is shifted to lower temperatures and becomes wider with a relative percentage of 1 to 3% NN. The best properties are obtained for 20% NN, with a permittivity of $\epsilon_r = 1500 \pm 15\%$ from 0 to 400°C and dielectric losses of $\tan \delta \leq 2.5\%$ from 100 to 450°C. These properties can be further enhanced by adding dopings, such as manganese, cobalt, and copper oxides to "flatten" the permittivity and increase the insulation resistance. Strontium, calcium, and barium oxides dopings enable to control the temperature range of stable permittivity.

Due the NBT - x NN's good potential properties, there are some patents [31, 32] presenting similar compositions, exhibiting high permittivity, wide range of usage temperature, low dielectric losses, and high insulation resistance. The optimal composition described in the Bridger patent, 2007 (US 2008/0239627 A1), for example, has a high relative permittivity ($\epsilon_r \geq 1000$), low dielectric losses ($\tan \delta \leq 2\%$), high resistivity ($IR * C \geq 10s$), and low permittivity variation ($\pm 15\%$) over a wide range of temperatures: from -30 to 200, for the fabrication of capacitors operating between $150 \pm 100^\circ\text{C}$ and $350 \pm 100^\circ\text{C}$. However, these properties do not have the proper reliability for industrial production and need to be further improved. In any case, the NBT - x NN is good candidate for the production of MLCCs used at high temperatures.

(1-x) NBT - x KTaO₃ (NBT - x KTaO₃)

In the NBT - x KTaO₃ [35] solid solution, KTaO₃ increases the stability of the permittivity as a function of temperature. The presence of a heat treatment before sintering and after calcination greatly reduces the dielectric losses, which becomes of $\tan \delta \leq 2\%$ from 200 to 250°C. The best properties were found for 20% of KTaO₃ and for three heating pre-treatment stages, the first at 950°C and the next two at 1100°C. For this composition, the relative permittivity is $\epsilon_r = 1750 \pm 15\%$ from 0 to 300°C and the dielectric losses are $\tan \delta \leq 2\%$ from 50 to 320°C. These permittivity values are close to the ones required by Exxelia for the high-temperature MLCCs. However, there is no study on the insulation resistance and on the variation of permittivity with time.

NBT - (K_{0.5}Na_{0.5}Nb)O₃ - (K_{0.5}Bi_{0.5})TiO₃

NBT - KNN - KBT [87] is a ternary solid solution and its most interesting compositions are (1-x) [0.6NBT-0.4KBT] - x KNN or (1-x) [0.84NBT-0.16KBT] - x KNN. Both solid solutions have a large temperature range of stable permittivity. The optimal composition has 12% of KNN and 16% of KBT and its relative permittivity is $\epsilon_r = 2000 \pm 15\%$ from 54 to 400°C. However, the low dielectric losses (limited to a small temperature range) are $\tan \delta \leq 2.5\%$ from 70 to 230°C. This is not ideal for the MLCC production.

From this survey of potentially interesting materials for MLCC production, a comparison of their properties with Exxelia's requirements can be made. This summary is presented in Table 1.3. It can be seen that none of the presented compositions have the required properties presented in sections 1.3.3 and 1.3.

Base material	ϵ_r at $200 \pm 50^\circ\text{C}$	$\epsilon_r(200^\circ\text{C}) \pm 15\%$		$\tan \delta$ (1)	$\tan \delta \leq (1)$		Industrial feasibility	IR at 250 to 300°C
		T_{min} ($^\circ\text{C}$)	T_{max} ($^\circ\text{C}$)		T_{min} ($^\circ\text{C}$)	T_{max} ($^\circ\text{C}$)		
BT-60%BMT	2200	136	375	2.0%	197	400	Sealed furnace	no info.
BCT-55%BMT	1000	80	500	2.5%	160	430	ok	85s at 250°C
BSZT-20%BMT	500	-70	300	1.5%	-60	310	ok	5.1s at 300°C
BT-20%BZT	1700	80	310	2.5%	87	460	Sintering with O_2 and pressure	1.6s at 300°C
BCT-30%BZT	1165	25	425	1.8%	97	440	Sealed furnace	10s at 300°C
BT-60%BZZ	1000	100	350	2.5%	25	250	Sealed furnace	no info
BT-40%BMZ	570	-20	430	2.0%	30	420	Sealed furnace	5.4s at 250°C
BT-10%BMTa	1828	115	233	2.0%	115	263	Sealed furnace	no info
KNN-10%BZW	1300	120	345	2.5%	210	420	Sealed furnace	no info
KNN-5%LiTaO ₃	650	0	380	2.5%	150	200	ok	no info
KNN-2%LaFeO ₃	2000	100	373	4.0%	100	400	Sealed furnace	no info
KNN-BSBT	2000	108	420	2.5%	87	305	Sealed furnace	no info
NBT-20%NN	1500	25	450	2%	100	400	ok	no info
NBT-20%KTaO ₃	1750	0	300	2.0%	50	320	Sealed furnace	no info

TABLE 1.3: Main properties of base material candidates. The references for each value are given in the text.

1.4.2 NBT and NBT-BT solid solution

1.4.2.1 Pure NBT

Even though pure NBT is known since the 1960's, there is still some discussions about its structure and its actual transition temperatures. It had long been agreed that pure NBT is rhombohedral ($R3c$ space group) at room temperature, where the Na^+ and Bi^{3+} ions are disordered, sharing the A-site, and that it does not go through structure change up to 200°C at least. However, recent studies indicate that the average structure is actually monoclinic (Cc space group) [37, 44].

NBT was originally considered as a ferroelectric at room temperature but, recently, some studies showed that it is actually a non-ergodic relaxor (e.g. [24]). This conclusion was taking into base on its hysteresis loop, dielectric and structural properties and their changes in temperature.

On heating, the first phase transition starts at around 200°C (depolarization temperature), when the ferroelectric domains starts to disappear. This transition can be described briefly as the formation of orthorhombic sheets ($Pnma$ space group) within the $R3c$ matrix, forming a modulated phase. [15] These sheets develop between 200 and 300°C by a micro-twinning process.

The modulated phase can explain another important discussion related to the NBT properties: the double hysteresis loop between 200 and 300°C , characteristics of anti-ferroelectric materials. The reason for this double loop was that two successive $R3c$ domains present anti-parallel vectors in a plane perpendicular to the modulation direction, giving rise to the anti-ferroelectric-like properties (see in Fig. 1.7).

This first phase transition was also explained in terms of a transition from a non-ergodic

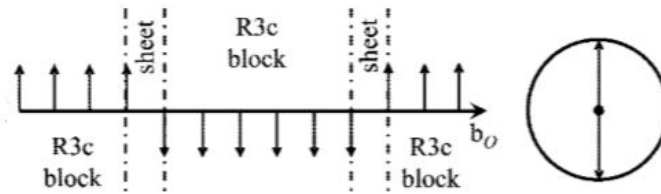


FIGURE 1.7: Schematic representation of the modulated phase present in NBT from 200 to 300°C , responsible for the anti-ferroelectric-like behaviour.[15]

to ergodic relaxor [24]. Above the T_d , the polar nano-regions or PNR (rhombohedral structure) are small and poorly correlated and the material behaves as an ergodic relaxor. At temperatures close to the T_d , when an electric field is applied to the material, the PNRs grow and the material becomes polarized. When this electric field is then reduced, the poled structure remains stable until it reaches a threshold, when material polarization decreases rapidly. This gives rise to the anti-ferroelectric-like behaviour. As the temperature increases further (over T_d), the stability of the poled structure decreases until some PNR start to return to the initial polarization continuously as the field is reduced, forming the thin polarization loop typical of relaxors. Decreasing the temperature below the T_d , the PNR grow in size and their correlation increase until it starts behaving like a non-ergodic relaxor, with a similar polarization property as a typical ferroelectric.

Both explanations about the first phase transition agree with each other, since the development of a modulated phase can explain change in behaviour from non-ergodic to ergodic relaxor behaviour on NBT.

The second phase transition, from the orthorhombic phase ($Pnma$ space group) to the

tetragonal centrosymmetric one ($P4/mbm$ space group), happens at about 320°C . The material is then paraelectric.[16]

From 400°C , there is a local $P4_2/mnm$ local structure that can be detected in the global tetragonal $P4/mbm$ one. [16] The Curie-Weiss law is valid for temperatures higher than 400°C , so this can be considered as the pure NBT Curie temperature, T_c . [37]

Finally, the last phase transition happens at 520°C , from the global tetragonal $P4/mbm$ phase to the cubic $Pm\bar{3}m$ phase [16].

Fig.1.8 presents a schematic representation of the structure and their microscopic electric properties.

The structure of pure NBT explains the dielectric properties of this material. The per-

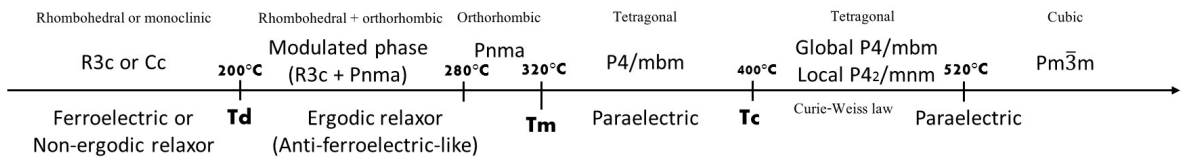


FIGURE 1.8: Schematic representation summarizing structural characteristics of pure NBT - the stable phases and their macroscopic electric properties.

mittivity and the dielectric losses in temperature goes through two anomalies[37]:

- The first one (around 200°C) is a frequency dependent transition (it shifts to higher temperatures with increasing frequency), since the NBT becomes an ergodic relaxor. It is observed as a shoulder in the permittivity at the depolarization temperature T_d around 200°C , and it corresponds to the first phase transition described in details in section 1.4.2.1. It can also be identified as the imaginary permittivity maximum.
- The second one at higher temperature is the broad permittivity maximum at T_m around 320°C and it corresponds to the second phase transition.

The dielectric losses are initially high, between 6 and 8%, for the temperatures lower than T_d . After the first phase transition they decrease and remain low, between 3 and 6%, up to about 300°C , when the losses increase again, due to the increase of the conductivity of the material. [54]

An example of typical dielectric properties for pure NBT is presented in the Fig. 1.9.

1.4.2.2 NBT-BT solid solution

NBT and BT form the most-studied solid solution based on NBT. The rhombohedral NBT-rich side of the NBT-BT solid solution is separated from the BT-rich tetragonal one by a morphotopic phase boundary (MPB).

The first unpoled NBT - x BT phase diagram [43, 44] in Fig. 1.10 shows an MPB at $x=0.06-0.07$ where the NBT-rich side of the MPB has a rhombohedral structure with the space group ($R3c$) at room temperature, as for pure NBT. The BT rich side has a tetragonal ($P4mm$) structure at room temperature also like the pure BT. However, for pure NBT and for NBT-rich compositions, the room temperature structure could also be the monoclinic (Cc) (see section ??).

In fact, adding barium to NBT creates a local strain in the crystal lattice, favouring the formation of tetragonal domains, depending on the percentage of Ba^{2+} that is added. [44] The barium decreases the interaction between the PNRs and increases the crystalline disorder. These changes give rise to an interesting MPB, where the solid solution presents the maximum piezoelectric and dielectric responses.

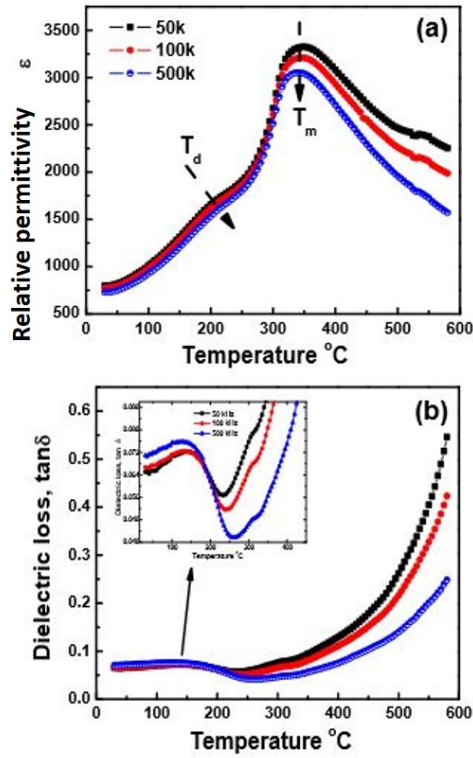


FIGURE 1.9: Typical dielectric properties of pure NBT [54]

There are still some discussions about the MPB structure at room temperature and its compositional range. It was often described as having a cubic or pseudo-cubic structure with possible small tetragonal and rhombohedral distortions. However, other studies described this composition range as having single-structures such as $R3m$, $R3c$, $P4bm$, or different structures, such as $Cc+Pm-3m$. [44] For the compositional range, there are also disagreements, but it is generally reported to be in between 4 and 8% of BT. So, the definition of the MPB in this solid solution is difficult, due to its complex structure. However, all the MPB studies describe it as having a nearly cubic structure, which agrees with the relaxor character found in the unpoled compositions of the MPB, similarly to the relaxor characters of the pure NBT also presented in section 1.4.2 [37].

Since there are no consensus on the NBT-BT structure at the MPB, there are still discussions about the origin of the PNR at room temperature for this composition. Many studies attribute the PNRs to a coexistence of rhombohedral and tetragonal domains, as for the pure NBT close to T_d (where the tetragonal $P4bm$ nano-domains result in anti-ferroelectric-like ordering)[16, 37], while a few others argue for local monoclinic distortions[37, 44]. In the first case, the competition between AFE and FE domains at the MPB would be the reason for its relaxor behaviour. [37]

The XRD measurement [37] on the NBT-rich (rhombohedral) phase are characterized by the splitting of the pseudocubic (111)pc peak around 2θ at $39-41^\circ$ and by the single (200)pc peak around $2\theta = 46 - 47.50^\circ$. The measurement on the BT rich (tetragonal) phase are characterized by a single (111)pc peak at around 40° and by the splitting of the (200)pc peak around $45 - 47.50^\circ$. The XRD in function of the percentage of BT is presented in the Fig 1.11.

The change in structure is visible from 5% of BT and it intensifies from 7% of BT, indicating the MPB composition range for this reference.

As for the pure NBT, the NBT-BT with $x \leq 0.15$ presents two dielectric anomalies in

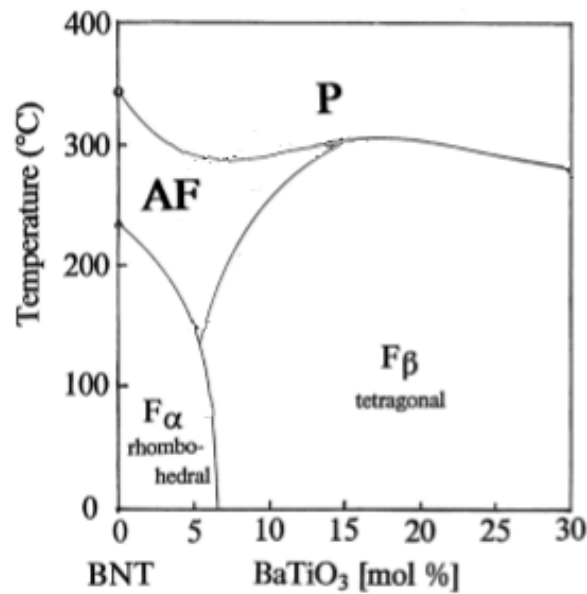


FIGURE 1.10: Original NBT-BT phase diagram with crystalline structure and ferroelectric characters. F, AF and P stand respectively for FE, AFE and paraelectric. [44]

temperature below 400°C. [43, 44] The first one at around 120°C (T_d) represents the transition from ferroelectric (or relaxor, as explained before) to anti-ferroelectric-like structure (or ergodic relaxor, as explained for the pure NBT in section 1.4.2.1). The second one is at around 300°C (T_m) and corresponds to the transition to the paraelectric cubic structure, also like the pure NBT compound [44].

The comparison between the permittivities in function of temperature pure NBT, NBT-BT with 6.5% of Ba and 7% of Ba are presented in Fig. 1.12. It can be seen that, for NBT-rich compositions, BT decreases the depolarization temperature T_d , and it also decreases the maximum permittivity temperature T_m . It increases the mean value of the permittivity, decreases its variation in temperature, and increases its variation in frequency. This analysis suggests that substitution with low barium levels (up to 7 mol%) favors rhombohedral (ferroelectric) transition to a tetragonal (paraelectric) phase [37].

When the BT content is greater than 7 mol% (BT-rich solid solution), the permittivity shows a frequency dispersion, the T_m is shifted to high temperatures, and the variation of the permittivity with temperature increases, as it can be seen in Fig 1.12.

For all compositions, the dielectric losses increase rapidly when the temperature is higher than 300°C, due to the increase the electrical conductivity[37].

Typical properties for NBT-BT at the MPB and choice of BT percentage

As it was mentioned before, the MPB improves the dielectric properties of the NBT-BT solid solution. Comparing the dielectric properties of various percentages of barium in the NBT-BT composition, the advantages of the MPB appear as:

- Low depolarization temperature, since the dielectric losses are lower for the ergodic relaxor temperature range,
- Higher permittivity value, in order to produce higher capacitance MLCC,

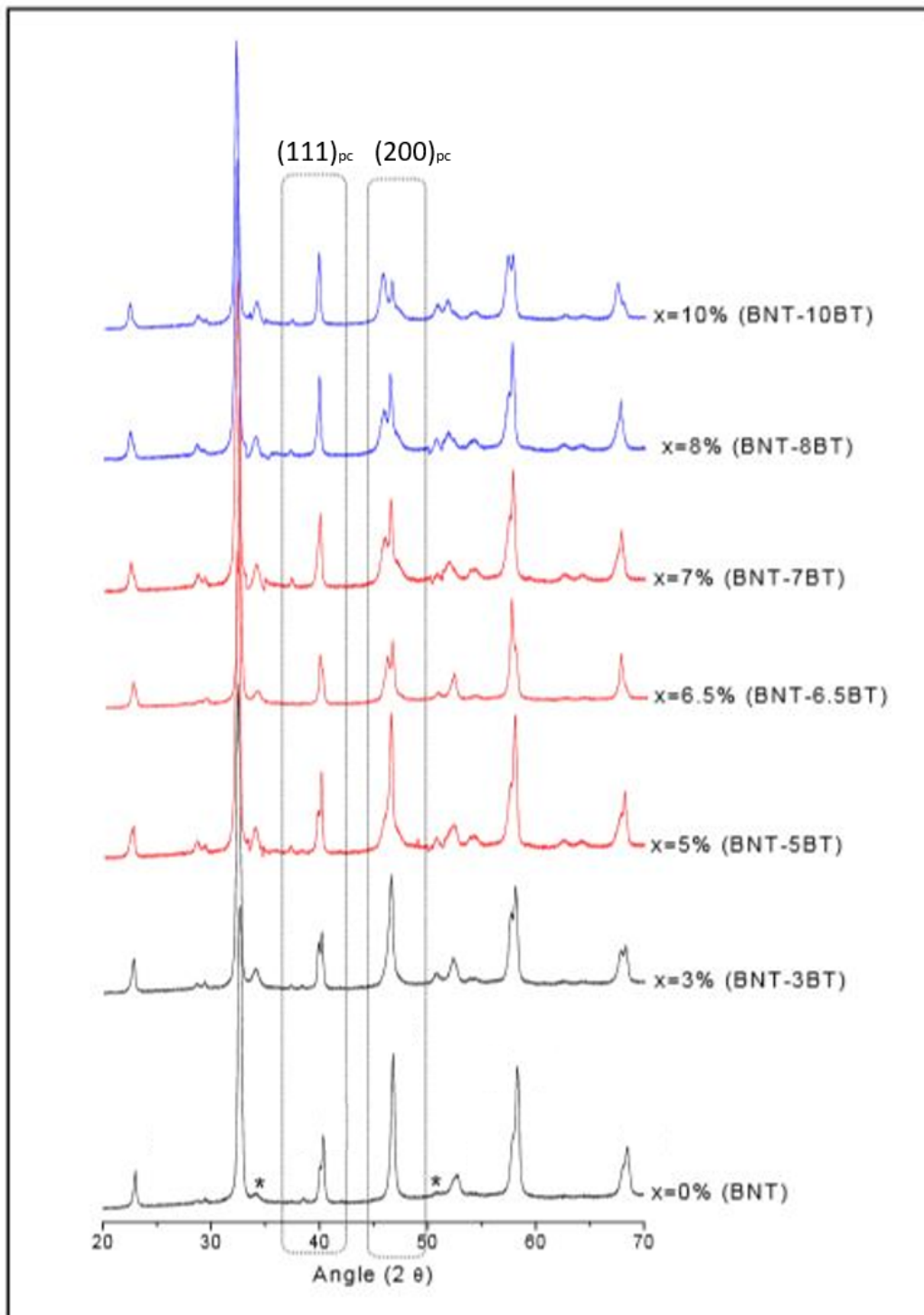


FIGURE 1.11: XRD patterns for different BT percentages in NBT-BT solid solution showing that the MPB is between 6.5 and 7% of BT. [37]

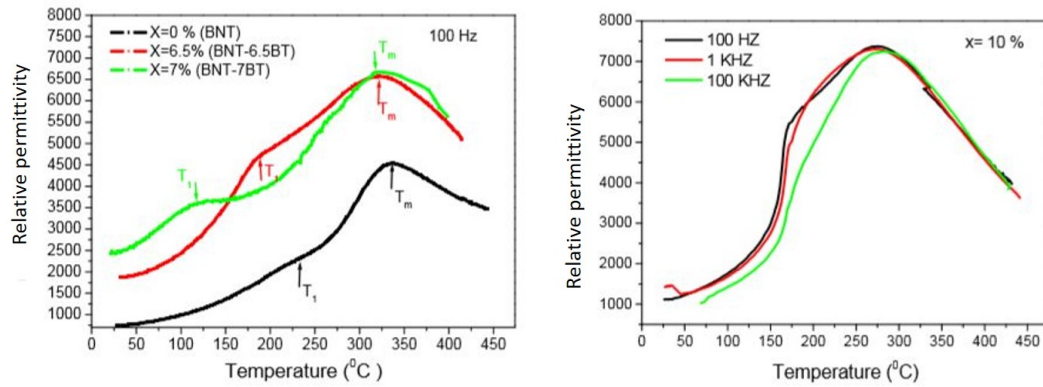


FIGURE 1.12: Relative permittivity as a function of temperature for a) NBT-BT with 0%, 6.5% and 7% of BT and b) NBT-BT with 10% of BT [37]

- Lower variation of the permittivity in temperature, in order to produce MLCC with more stable capacitance

The expected dielectric properties for the NBT-BT solid solution with 6% of BT can be seen in Fig 1.13.

It should be noted that the dielectric measurements of poled samples are different from the unpoled ones, since there is an abrupt transition at the depolarization temperature. Below this temperature, the frequency dispersion of the poled samples disappears and the material has a ferroelectric behaviour. This shows also the interest of having a low depolarization temperature for the MLCC production. [43, 44]

Finally, it will be presented in the chapter 4 that the reported dielectric properties of NBT-BT at the MPB are not necessarily compatible among them, due to differences in the synthesis parameters and with the stoichiometry. So the properties presented in Fig. 1.13 are only an illustration of possible properties at the MPB.

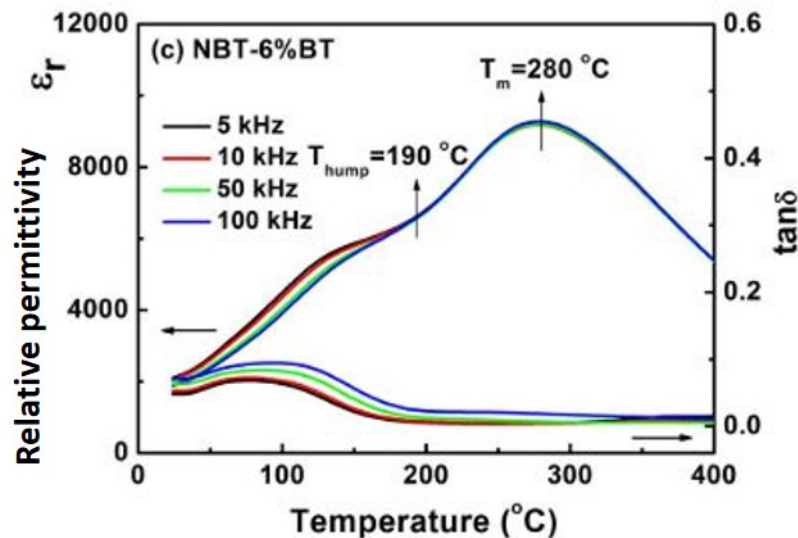


FIGURE 1.13: Dielectric properties (relative permittivity and dielectric losses) in function of the temperature for the NBT-BT solid solution with 6% of BT (at the MPB)

1.4.2.3 Possible NBT-BT solid solutions with $K_{0.5}Na_{0.5}NbO_3$ (KNN) and $Bi_{0.2}Sr_{0.7}TiO_3$

(SBT) The NBT-BT solid solution can be further improved thanks to the formation of new solid solutions with KNN and SBT.

NBT-BT-KNN [87] is a ternary solid solution also based on NBT. The compositions studied are $(1-x) [0.94NBT-0.06BT] -x$ KNN, since the morphotropic phase boundary of the NBT-BT is at 6% of BT. As with other complex solid solutions based on NBT, this material has a stable of permittivity within a specific temperature range. The optimal KNN composition range is from 12 to 18%. For 12% KNN, the ceramic has a high relative permittivity of $\epsilon_r = 2988 \pm 15\%$ from 75 to 325°C, average dielectric losses of $\tan \delta \leq 2.5\%$ from 100 to 350°C, insulation resistance of 17s at 250°C and, therefore, a wide operating temperature range from about 100 to at least 250°C. For 18%KNN, the relative permittivity is also high ($\epsilon_r = 2151 \pm 15\%$ from 40 to 350°C), dielectric losses increase rapidly, with $\tan \delta \leq 2.5\%$ from 70 to 250°C and a low resistivity of 2s at 250°C. This composition therefore has a limited temperature range from 70 to less than 250°C.

Due to its good electrical characteristics, compositions similar to NBT-BT-12%KNN with different percentages of BT and dopants, such as oxides of zinc, manganese and niobium, have been patented by MRA laboratories (US 8,076,257 B1). In the patented optimal composition, the percentage of BT is 6% and a total of about 1.6wt% of dopants (manganese oxide, niobium, zinc, silicon and neodymium) has been added. The resulting material exhibits a relative permittivity of about $\epsilon_r = 3600 \pm 15\%$ from 150 to 350°C, dielectric losses of $\tan \delta \leq 2.5\%$ from 150 to 350°C and a high insulation resistance of about 200s at 200°C, but that does not have the necessary reliability for industrial production, since there are no studies on the change in its relative permittivity and its dielectric losses over time. Moreover, no studies were done in a scale larger than a laboratory one, to test the properties variation from sample to sample. These ceramics are, therefore, excellent candidates for the production of MLCCs used at high temperatures, but they must be studied and improved with respect to the temperature range and the reliability. Finally, the final material should not be in conflict with the composition and the method in the published patent.

NBT-BT-Bi_{0.2}Sr_{0.7}TiO₃ [63] is a ternary solid solution with 10% of structural strontium vacancies, to ensure electrical neutrality. Its most studied composition is based on the composition of the morphotropic phase boundary of the NBT-BT solid solution (6% BT). It has been studied for several percentages of introduced bismuth vacancies. These vacancies decrease dielectric losses and greatly increase the permittivity in the stable permittivity temperature range, but they also increase the variation of the permittivity outside this range. The optimal composition contains 7% bismuth vacancies and 26% of SBT. This composition gives a very high relative permittivity with little variation in temperature ($\epsilon_r = 4884 \pm 1.5\%$ from 73 to 230°C and $\epsilon_r = 4884 \pm 15\%$ from 50 to 290°C), a relatively low dielectric loss of $\tan \delta \leq 2\%$ from 100 to 300°C, and a insulation resistance of 5.96s at 250°C.

Due to its good electrical characteristics, a composition similar to this ceramic, composed of a solid solution of 0.94NBT-0.06BT with oxides of manganese and niobium as doping has also been patented by MRA laboratories (US 8,076,257 B1). In the patented optimal composition, a total of about 1.6% (molar) of doping was added. This created a material with a relative permittivity of about $\epsilon_r = 1900 \pm 15\%$ from 150 to over 200°C, dielectric losses of about $\tan \delta \leq 2.5\%$ from 150 to over 200°C, and resistivity of about 10s at 200°C. This material has good dielectric properties, but it does not have the insulation resistance necessary for industrial MLCC production. As for the NBT-BT-KNN, there are no studies on the change in the relative permittivity and the dielectric losses of NBT-BT-SBT over time and from sample to sample.

The described dielectric properties of the NBT-BT-based solid solutions can be summarized in the Table 1.4.

Base material	ϵ_r at $200 \pm 50^\circ\text{C}$	$\epsilon_r(200^\circ\text{C}) \pm 15\%$		$\tan \delta$ (1)	$\tan \delta \leq (1)$		Industrial feasibility	IR at 250 to 300°C
		T_{min} ($^\circ\text{C}$)	T_{max} ($^\circ\text{C}$)		T_{min} ($^\circ\text{C}$)	T_{max} ($^\circ\text{C}$)		
NBT-BT-12%KNN	2900	75	325	2.5%	100	350	Sealed furnace	17s at 250°C
NBT-BT-26%BST	4645	50	290	2.0%	100	300	Sealed furnace	6s at 300°C

TABLE 1.4: Main properties of NBT-BT-based materials. The references for each value are given in the text.

1.4.2.4 NBT-6%BT choice

As it was presented in the section 1.4.2.2, the NBT-BT at its MPB is a good candidate for the MLCC production, due to its phase transitions that give it a relatively high and stable permittivity in temperature. Moreover, the NBT-BT present a relatively low dielectric loss when some additives are used.

For the undoped NBT-BT the best properties reported in the literature are $\epsilon_r=2700\pm 15\%$ from 60 to more than 450°C , $\tan \delta \leq 2.5\%$ from 100 to 350°C and a thin double hysteresis loop at room temperature, when an excess of bismuth and a deficiency of sodium are used. [23] This stoichiometry will be detailed in section 2.3.2.6.

Comparing these properties with the ones from the other base material candidates shown in Table 1.3 p. 24, it can be seen that the pure NBT-BT material in the MPB shows the highest relative permittivity value at the reference temperature, with a small variation in temperature (only BCT-BZT, BT-BMZ, KNN-LiTaO₃ and NBT-NN show a more stable relative permittivity within Exxelia's requirements). It also shows a large temperature range for having low dielectric losses (only the BT-BZT and BT-BMZ show a larger temperature range within Exxelia's requirements). Finally, it does not require any change in the industrial synthesis method or in the furnaces industrially used, unlike almost all the other candidates, except for the BCT-BMT, BSZT-BMT and KNN-LiTaO₃.

Moreover, other NBT-BT-base materials can be done, as shown in the Table 1.4 p. 32 and in the section 1.4.2.3, to improve its properties. It can be seen that the NBT-BT-KNN solid solution has good dielectric properties with $\epsilon_r=2900\pm 15\%$ from 75 to 325°C , $\tan \delta \leq 2.5\%$ from 100 to 350°C and IR of 17s at 250°C .

Finally, the NBT-BT-SBT in its optimal composition has a high and stable permittivity with $\epsilon_r = 4884 \pm 1.5\%$ from 73 to 230°C and $\epsilon_r = 4884 \pm 15\%$ from 50 to 290°C , a low dielectric loss of $\tan \delta \leq 0.02$ from 100 to 300°C , and a relatively high insulation resistance of 5.96s to 250°C .

So, the BT-BMZ is the only base material candidate having the relative permittivity stability and the low dielectric losses temperature range better than the NBT-BT within Exxelia's requirements. However, this material shows a low insulation resistance at high temperatures, contrary to the NBT-BT-based materials, that can have an insulation resistance more than twice as large.

In conclusion, the NBT-BT solid solution at the MPB was chosen as the base dielectric material, since it has interesting properties that could be used for the MLCC production.

Firstly, it presents two dielectric anomalies: the first at T_d is a frequency-dependent shoulder and the second at T_m is a permittivity maximum. These phase transitions give the NBT-BT a more stable permittivity in temperature when compared to most lead-free base material candidates.

Moreover, the MPB with 6% BT, which has both rhombohedral and tetragonal crystalline structures, improves the relative permittivity values, giving the NBT-BT the highest value in the reference temperature compared to other base material candidates. The MPB also improves the relative permittivity variation in temperature when compared to most base material candidates. The NBT-BT also has a double hysteresis loop between 200°C and 300°C, even though it is actually an ergodic-relaxor. This makes it interesting for energy storage applications. Finally, its composition can be changed by adding other lead-free ceramics, to change and improve its dielectric properties, depending on the requirements of the final MLCC.

1.4.2.5 Other possible dopants in NBT-BT

NBT-6% BT can be improved when using other dopants and additives:

- **KTaO₃ [35]:** It forms a solid solution with pure NBT, as shown in section 1.4.1, stabilizing the permittivity in temperature. The solid solution with NBT-BT was not studied, but the KTaO₃ could be a candidate to be used together with a heat treatment to increase the temperature range of stable permittivity.
- **Isovalent doping [78]:** A good example of isovalent doping is the K⁺ substitution of Na⁺, or Y³⁺ and La³⁺ substitution of Bi³⁺, and Zr²⁺ substitution of Ti²⁺. These dopants decrease the oxide-ion conductivity in pure NBT, which comes from high mobility oxygen vacancies created by the Bi₂O₃ loss during sintering. The decrease in the conductivity can be explained either by compositional variations (higher volatility of K), higher bond strength with oxygen or lower polarisability of the Bi substitutes. So isovalent doping can be useful for the MLCC production, since it significantly decreases the electrical conductivity.
- **Acceptor doping [78]:** normally used to increase the ionic conductivity of NBT, by inducing the formation of oxygen vacancies or p-type (hole) conduction. So, this type of doping is not interesting for the MLCC production, even if it can be useful for other applications.
- **Donor doping [78]:** A frequently used donor dopant is the Nb⁵⁺ substitution of Ti²⁺ (for example, using NaNbO₃). Contrarily to the electronic compensation effect of the Nb substitution of BT (that increases the conductivity), the compensation effect on NBT is the ionic one that reduces significantly the conductivity, even in low doping percentages. Other than changing the NBT-BT conductivity, the NaNbO₃ doping can also help to stabilize the permittivity in temperature, as it was shown in section 1.4.1. For this reason, the NaNbO₃ doping could be used to increase temperature range of stable permittivity.
- **Co₃O₄ and CoO [21, 69]:** It is an industrially used interstitial additive in BT ceramics. In NBT or NBT-BT-KBT, the Co is incorporated in the crystal lattice, substituting the Ti⁴⁺ ions. In pure NBT 0.3wt% of CoO addition acts as a sintering aid, increasing the grain growth and the density. It also increases the temperature of the maximum permittivity to 663°C, decreases the tan δ and stabilizes ε_r for temperatures lower than 400°C. In the solid solution NBT-BT-KBT with 4wt% of NBT and KBT, it also acts

as a sintering aid when the percentage of Co_3O_4 is $\leq 0,4\%$. In this case, the Co doping increases the depolarization temperature T_d , decreases $\tan \delta$ at temperatures lower than the T_d and increase $\tan \delta$ and ϵ_r dispersion at higher temperatures. This indicates that doping with Co increases the conduction at high temperatures. However, it might be an interesting doping, since the properties at moderate temperatures are improved.

- **MnCO_3** [17]: It is another industrial interstitial additive used in low quantities ($\leq 0.8\%$). In this case, Mn acts as a sintering aid, increasing the density and the grain growth and decreasing the sintering temperature. The maximal density is reached for 0.1wt% and the minimum dielectric losses are obtained for 0,8wt% of MnCO_3 addition. The permittivity always decreases with increasing Mn content. When it is added at higher quantities, Mn form precipitates and it creates air holes at the grain boundaries, decreasing the density and deteriorating the NBT-BT properties.

1.5 Conclusion

This chapter discussed the context and the problematic of the thesis, to explain the industrial specifications and limitations that apply to the choice of the base material for the multilayer ceramic capacitors (MLCC) used for high temperature electronics.

The MLCCs are the most consumed capacitor type in the world, due to their high volumetric efficiency, good reliability, and frequency features. The annual MLCC production is more than 100 billion units and its market grew around 20% each year since the beginning of the decade. One of the key factors contributing to this is the increase of the electronics production and its use in high-technology fields, such as controlling systems for transportation, aerospace, and military applications.

However, the environmental demands for the industrial production are increasing nowadays. In this context, the REACH and RoHS regulations are especially important for the MLCC production since the use of lead in the MLCC production will be soon forbidden for non-military or aerospace applications. This creates the need to develop new lead-free materials that can meet the environmental expectations.

Moreover, new MLCC applications and industrial demands are being created everyday. In this context, the high temperature electronics demands are growing, due to new applications such as the deep oil drilling, the use in train and airplane breaks, and also the creation of a new electric airplanes. Moreover, the MLCC miniaturization trend also intensifies to the need to develop new high-temperature capacitors. It is estimated that the electronic systems should be capable to work at a maximum temperature of 300 to 350°C.

Today, the high-temperature MLCC production are limited to capacitors that can operate in temperatures up to 200-250°C. *It is therefore imperative to bring out new lead-free materials capable of meeting the expectations of electronics at around 300-350°C.*

The MLCC production process in Exxelia is based on the tape casting of a ceramic slurry composed of a ceramic powder, a solvent, a binder and other additives, to improve the final properties of the ceramic tapes. The "green" ceramic tapes are screen printed with a Ag-Pd electrode and the blocks of alternated layers of ceramic and metal is co-sintered between 1000 and 1300°C. Sintering is done in industrial furnaces, where the sintering atmosphere and the pressure cannot be controlled.

The compatibility with the current production method in the MLCC industry and, more specifically, in Exxelia is an important limitation, since ideally no major changes should be done to the process, for the new dielectric to be useful for industrial production with reduced costs. Some important industrial limitations include the use of a tape casting slurry, the sintering process in a furnace without the possibility of controlling the atmosphere, the pressure or other heating sources (such as electric current and microwaves), the compatibility with the

Ag-Pd electrodes and the price and market limitations on the ceramic composition.

Considering these industrial limitations and the new high-temperature electronics demands, a specification document was created to sum up the specific requirements for the dielectric material studied in this thesis, taking into account its future lead-free high-temperature MLCC application.

The main objectives of this work include an operation temperature range from 25°C to 300-350°C, an operation frequency range from 400Hz to 100MHz with a standard measurement frequency of 1kHz, a relative permittivity between 1000 and 2000 at 1kHz, a permittivity variation of $\pm 15\%$ in the operating temperature range when compared to a reference temperature within this range, a maximum loss value of $\tan \delta < 2.5\%$ at 1 kHz, an insulation resistance of 10s from 250 to 300°C and 1s from 300 to 350°C, a layer thickness between 5 to 20 μm or less, a grain size of the ceramics of 0.3 to 0.5 μm before sintering and 0.5 to 2 μm after sintering and a dielectric strength of 25 to 60 V/ μm .

To achieve these objectives and considering the industrial and environmental restrictions, an extensive study of the main available lead-free dielectric families was carried-out. The choice of the final material was done considering the permittivity value, the dielectric losses and relative permittivity values, the similarity between the the desired operating temperature range and the temperature range to have $\tan \delta \leq 2.5\%$ and a variation of 15% in the relative permittivity, the insulation resistance at 300°C, and the industrial feasibility.

In this context, three families of lead-free materials were reviewed: the BaTiO₃-based materials, the K_{0.5}Na_{0.5}NbO₃-based materials and the Na_{0.5}Bi_{0.5}TiO₃-based materials.

The NBT-BT solid solution at the MPB was chosen as the base dielectric material, since it has interesting properties that could be used for the MLCC production. Firstly, it presents two dielectric anomalies: the first at the depolarization temperature T_d is a frequency dependent shoulder and the second at the maximum relative permittivity temperature T_m is a permittivity maximum. These phase transitions give the NBT-BT a more stable permittivity in temperature when compared with BT. It also shows low dielectric losses from T_d to T_m .

For the undoped NBT-BT the best properties reported in the literature are $\epsilon_r = 2700 \pm 15\%$ from 60 to more than 450°C, $\tan \delta \leq 2.5\%$ from 100 to 350°C and a thin double hysteresis loop at room temperature, when an excess of bismuth and a deficiency of sodium are used.[23]

Moreover, the MPB between 6% and 7%BT, which has both rhombohedral and tetragonal crystalline symmetry, improves the permittivity values and its variation in temperature when compared to pure BT. Finally, the NBT-BT has a double hysteresis loop between 200°C and 300°C, even though it is actually an ergodic-relaxor. This makes it interesting for energy storage applications.

The NBT-BT solid solution may also be further improved through the formation of new solid solutions with KNN and SBT. Other useful dopants and additives may be used, such as isovalent doping (K⁺ substitution of Na⁺ or Y³⁺ and La³⁺ substitution of Bi³⁺, and Zr²⁺ substitution of Ti²⁺) to decrease the oxide-ion conductivity, donor doping (Nb⁵⁺ substitution of Ti²⁺) to decrease the conductivity and stabilize the permittivity in temperature and addition of Co and Mn in small quantities to increase the final density and decrease the dielectric losses.

Chapter 2

Synthesis method

The objective of this chapter is to develop a synthesis method that is compatible with industrial production and enables to obtain samples matching Exxelia's specifications.

The main synthesis methods are first reviewed, before their respective industrial limitations are presented. The solid-state synthesis was chosen for this thesis, but it had to be improved to meet Exxelia's requirements. The way several parameters have been studied and optimized is therefore presented.

Before the existence and afterwards the influence of secondary phases is reported, leading to an optimized synthesis route for the NBT-6%BT meeting Exxelia's requirements.

2.1 Choice of the synthesis method

The synthesis method is composed of the method used to obtain the NBT-BT powder and of the sintering method.

Currently, solid-state reaction is the most used synthesis method in industries and the one used for MLCC production in Exxelia. Different synthesis methods used for the NBT-BT synthesis are reviewed, in order to choose the most adapted one for Exxelia's specifications.

2.1.1 Sol-gel [9, 45, 64]

The sol-gel synthesis method is used because it is based on a simple reaction that only requires mild temperatures to form the gel and the properties of the materials can be easily modified. This method uses salts of A and B cations of the perovskite and involves a series of hydrolysis and condensation reactions. [64]

For NBT-BT, Mercadelli *et al.*(2009) [45] and Cernea *et al.*(2010) [9] use the sol-gel synthesis with sodium, barium and bismuth acetate in water and acetic acid solutions or bismuth nitrate in nitric acid [9, 45]. Titanium is then added by Titanium IV isopropoxide in 2-propanol and isopropanol, or by titanium acetate in nitric acid. The solutions are mixed drop-wise to produce a Bi-Na-Ba-Ti complex solution (sol). After stirring under mild heating, the gel is formed, dried, and the resulting powder is heated at temperatures around 200 and 500°C to obtain the desired single-phase powder.

Once optimized and after sintering at 1150°C for one hour in air, this synthesis method gives a single phase material and a uniform microstructure. However, the density of the ceramics obtained from sol-gel powders is usually lower than for the ones obtained by solid-state reaction. The dielectric properties of the material are similar to those obtained by solid-state reaction and Spark-plasma sintering (see section 2.1.2). The ceramics obtained [9] have a permittivity of around 1200 at room temperature, a frequency dispersion for high temperatures, and an increase in ϵ'' for temperatures higher than 280°C, which indicates an increase in the conductivity of the material (see Fig 2.1).

So, even if the sol-gel synthesis method is based on a simple and easy to change

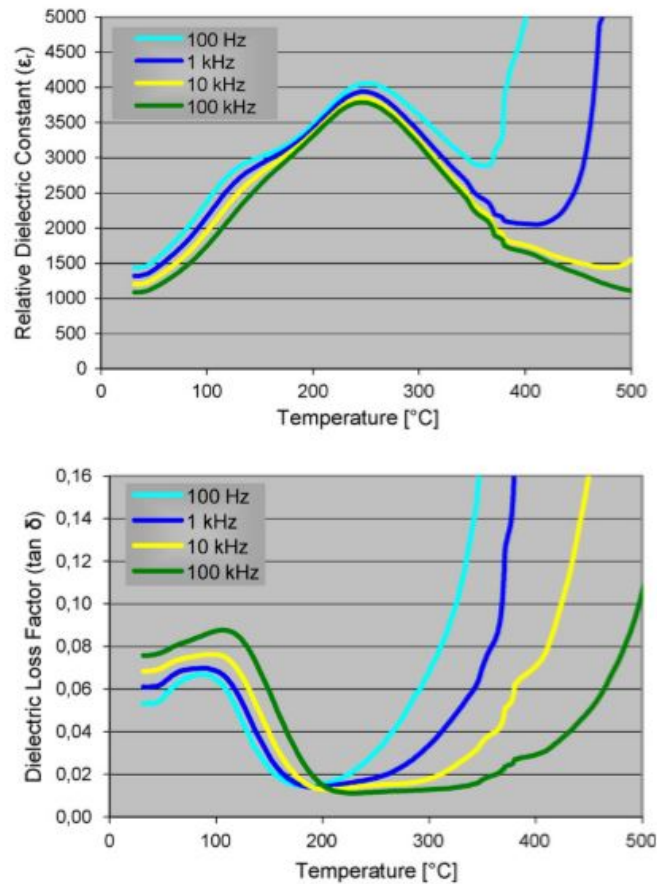


FIGURE 2.1: Temperature and frequency dependence of relative permittivity (ϵ_r) and dielectric losses ($\tan \delta$) of NBT-BT synthesized via sol-gel method and sintered at 1150°C for one hour in air. [9]

chemical reaction, using powder from sol-gel method does not enable to obtain ceramics exhibiting superior properties. Moreover, this synthesis method would completely change Exxelia's production of MLCC, that is now based on the solid-state reaction and on the tape casting. So there would be no reason to adopt this synthesis method instead of the industrially used solid-state reaction.

In conclusion, the sol-gel synthesis method is not the ideal one for the industrial production of MLCC at Exxelia.

2.1.2 Solid-state reaction

The solid-state reaction is the most common synthesis method used for poly-crystalline materials, for example, in the industrial production of ceramic-based products, such as MLCC, as described in the section 1.3.

It consists in mixing "starting" powders hence "solid state", which are generally carbonates and oxides and then heating (calcinating) at high temperature, in order to induce the reaction. The calcinated powders are then pressed into a green body, followed by sintering to get a ceramic.

The solid-state synthesis of the NBT-BT uses TiO_2 , Bi_2O_3 , NaCO_3 and BaCO_3 as starting powders. These powders are weighed according to the NBT-BT stoichiometric composition and then they are mixed by ball milling during one hour [37, 66] or by vibratory milling using ethanol as a milling solvent during 8 hours [79]. After the mixing, the powders are dried at 80°C .

The calcination step varies depending on the study. For Yusong *et al.* [79], the calcination is done at 900°C for 2h, but no more details on calcination atmosphere or state of the powders is given. For Lidjici [37], the calcination was done at 825°C for 4h in air, with a heating ramp of $3^\circ\text{C}/\text{min}$ and the cooling done in air. Finally, for Spreitzer *et al.* [66], the calcination using a uniaxially-pressed NBT-BT powder (100 MPa) is done in two steps. The first one at 800°C for 5h and the second one at 850°C for 5h with intermediate cooling and grinding step between the two calcinations. The uniaxial pressuring of the powders can decrease the loss of the volatile oxides (bismuth and sodium oxides).

After the calcination, the NBT-BT powder is either directly uniaxially pressed into pellets, or ball milled again. Finally, the pellets are uniaxially pressed with or without the use of a polymer, such as PVA, as a binder to improve the casting ability, before being sintered. [37, 66, 79]

The sintering can be done using different methods to decrease the bismuth and sodium evaporation and the consequent formation of oxygen vacancies.

So, the solid-state method is the one that has been chosen for this thesis, taking into account the resulting powders and Exxelia's requirements.

2.1.3 Sintering

The second stage of the synthesis method is the sintering of the powder to obtain a ceramic. The main sintering techniques are revised below.

2.1.3.1 "Traditional" sintering in an atmosphere

Because of the volatility of Na and Bi, it is necessary to create a Na and Bi-rich atmosphere in the crucible during synthesis, to limit the loss through evaporation of the volatile species. The created vacancies may alter the material's properties. In the case of NBT-BT, as it will be shown in the section 3.2.1.1, the bismuth evaporation and the oxygen vacancies created, drastically increase the material conductivity, which is detrimental for the MLCC properties.

A customary method to prevent the creation of vacancies of volatile elements is to cover the sample with the same composition powder. In the case of the NBT-BT ceramics, [37] the sintering is done in a covered alumina crucible at temperatures between 1100°C and 1200°C .

In this study, the same "traditional" sintering atmosphere was done. Properties of the as-obtained ceramics will be presented in section 2.3.4.4.

However, after the sintering, it is necessary to cut the samples with a circular-saw and then to polish it, to remove the NBT-BT powder used as an atmosphere that adhered to the ceramics. This would not be possible (either technically or economically) for the MLCC production, so the use of an NBT-BT powder was not considered ideal for the MLCC production (see section 2.3.4.4) and required an alternative that will be presented in section 2.2.1.1.

2.1.3.2 Spark Plasma Sintering sintering

The Spark Plasma Sintering (SPS) technique is normally used to get dense ceramics in a short time and with nanosized grains. It consists in loading the powder in a graphite die and passing a high AC or DC current through the graphite die and the sample, while applying a uniaxial pressure. The SPS requires a reducing atmosphere, due to the need of using the graphite dies. The heat created by Joule effect densifies the ceramics and nearly 100% relative densities can be achieved at relatively low temperature and short time (25 minutes and 727°C[4, 47]) when compared to the traditional sintering methods, since the heating comes from an internal source.

In the case of pure NBT, this sintering method was used to decrease the sintering temperature and reduce the evaporation of sodium and bismuth. The sintering temperature of pure NBT could be decreased by 300°C (from 1150 to 850°C), obtaining a final relative density close to 100%.[47] The relative permittivity at 100Hz of pure NBT sintered by SPS method was 1550 at room temperature and 6400 at its maximum value. The depolarization temperature was decreased to 180°C (compared to 200°C for traditionally sintered pure NBT).[47]

In the NBT-BT 8% case, the spark-plasma-sintered material showed some frequency dispersion, low relative permittivity, of about $\epsilon_r = 750$ at room temperature, and high conduction above 200°C. The conduction is due to the formation of oxygen vacancies (the sintering is done in reducing atmosphere) and the formation of defects and cracks during sintering. [4]

So, for the NBT-BT, the SPS does not have the expected advantages of this method (lower oxygen vacancies due to lower bismuth evaporation, leading to lower dielectric losses and conductivity). Moreover, the SPS is an expensive and energy-consuming sintering method and it requires reducing atmosphere (due to graphite die and vacuum atmosphere), which increases the vacancy formation in the final ceramics. Finally, it requires furnaces that allow the internal atmosphere control and the application of an electric current into the graphite die and, through the sample. For these reasons, this was not considered ideal for the MLCC synthesis at Exxelia.

2.1.3.3 Microwave sintering method

For the microwave sintering, [55] the green bodies of pure NBT were prepared using PVA as a binder and uniaxial pressure. The temperature inside the microwave furnace was controlled and the sintering was done at 950°C for 30 minutes, with an effective heating rate of 100°C/min, much faster than for solid-state sintering.

A more uniform grain size was obtained, compared to the traditional sintering method, as shown in [55]. The room temperature relative permittivity was also higher: $\epsilon_r = 798$ vs 720 for traditional method. Moreover, the dielectric losses decrease remarkably, from 4% for the traditional sintering to 2% for the microwave sintering at 250°C.

However, this sintering method would require a change in industrial furnaces and it would not allow the co-sintering of the ceramics with the electrodes. So it is not possible to use microwave sintering for MLCC production.

As a consequence, none of the current sintering technique is suitable for industrial production of MLCCs. The "traditional" sintering using the same composition powder (NBT-BT) involves the removal of the NBT-BT powder that has amalgamated to the ceramic using a circular-saw. The SPS is expensive, would require a change of furnace, and results in a leaky material. The microwave sintering would also require a change of furnace and would not allow the co-sintering with the electrodes. So, a new sintering method or way to create a sintering atmosphere should be studied, in order to allow the use of NBT-BT for the

MLCC production in a technically and economically applicable way, avoiding the formation of oxygen vacancies and minimizing conductivity.

2.1.4 Films, tape casting, and MLCC

The tape casting synthesis method is widely used for the synthesis of ceramic films and multilayer devices. The advantage of this method is that it allows the fast synthesis of thin and flat ceramic layers. [46]

In this synthesis method, the ceramic suspension (slurry) is kept in a reservoir behind the doctor blade, through which the carrier (support where the films are casted) passes. The film thickness is controlled by the gap between the blade and the carrier. Section 1.2.6 shows how this method is applied in Exxelia for the MLCC production.

The slurry composition and synthesis method are a key point to obtain homogeneous films with good mechanical properties before sintering and high density after sintering. It is normally composed of a mixture of a ceramic powder, a solvent, a dispersing agent, a binder and a plasticizer. The function of each is explained in section 1.2.6.1.

The different proportions and the properties of each component material of the slurry affect its rheological properties and the properties of the final ceramic film obtained after sintering. So the optimization of the slurry is essential to obtain the adapted final material properties.

Most of the rare studies on NBT-BT films or multilayer devices prepared by tape casting are focused on piezoelectric applications. Some examples are:

- Kimura *et al.* synthesized NBT-BT by templated grain growth (tape casting of NBT-BT with platelet grains) to create textured material used for piezoelectric applications. [33, 65] Even though textured materials can improve the piezoelectric properties, they are not interesting for the MLCC production, since an excessive increase in the piezoelectric coefficient may be a problem to practical capacitor applications.
- Zhang *et al.* synthesized NBT-BT by tape casting and sol-gel methods for piezoelectric application devices. The structure, ferroelectric and piezoelectric properties were measured. But no information is given on the dielectric properties. [84]
- Yan *et al.* synthesized pure NBT films by sol-gel method and measured its ferroelectric properties for transducer application in high frequency piezoelectric devices. But again no information is given on the dielectric properties of the material. [77]

Groh *et al.* published the only study on NBT-BT prepared by tape casting for MLCC applications. [20] The material studied was NBT-6%BT-xKNN with $x = 12, 18,$ and 24 sintered with CuO as a sintering aid. The dielectric, structural and conductivity properties of the material were measured. The best obtained properties were a stable relative permittivity from 40 to 225°C, low dielectric losses from 100 to 300°C, and a high insulation resistance of 300s at 150°C.

Even if the material's properties are promising, they still do not correspond to the industrial requirements of this work, since the usage temperature range is not sufficiently high as required by Exxelia.

In conclusion, tape casting is a simple method for synthesizing ceramic layers and multilayer devices with adequate properties. It is widely used in the industry, including in Exxelia's MLCC production. However, a slurry composition and synthesis method optimization step is fundamental to obtain the desired final properties.

For NBT-BT, this synthesis method was mainly studied for the development of piezo-electric devices and the results cannot be used for the MLCC applications. Only one study was published on NBT-BT prepared by tape casting for MLCC applications. However, the achieved results do not correspond the Exxelia's requirements.

2.2 Industrial limitations for each synthesis method

The industrial production and, more specifically, Exxelia's MLCC production imposes some limitations, specially due to the process and equipment available. A special attention has to be paid to the co-sintering of the dielectric and electrode layers, since this is a key point to obtain good quality MLCCs.

In this section, the industrial limitations for the synthesis method will be presented, to validate the synthesis method choice.

The production of the perovskite powder should be done with a simple synthesis method that can be carried out with the available equipment and material at Exxelia (horizontal and planetary ball-milling with different ball diameters, regulated-temperature furnace up to 1300°C, high-temperature-resistant crucibles, blade stirrer, ZrO₂ powder to be used in high temperature processes, and slurry preparation products).

As it was shown in section 2.1.1, the sol-gel route does not present advantages, when compared to the traditional solid-state-reaction synthesis method and it is not compatible with the industrial equipment and materials. So, the only possible synthesis route for the NBT-BT-based MLCC is the solid-state route.

The production of the ceramic sheets needs to be done by tape casting of a slurry over Millard sheet, without the use of a substrate. So the templated grain growth cannot be used and show no technical interest for the production of MLCC, since low piezoelectric properties and low texture are preferable in capacitors, in order to avoid cracks.

2.2.1 Industrial compatibility of the sintering process

The MLCC have to be co-sintered with the electrodes in a controlled temperature furnace that can reach 1300°C, as presented in the section 1.3. It is not possible to apply or control other parameters during the sintering, such as applying pressure and running an electric current through the sample, as in SPS. Moreover, the industrial furnaces cannot have their atmosphere controlled, since they are not sealed. Ideally, one should not have to separate the sample from the powder used to create the sintering atmosphere, even though minor surface contamination is not an issue as a polishing step is carried out after the sintering. This rules out the use of NBT-BT powder to create the sintering atmosphere.

As explained in section 2.1.2, the only sintering method that can be used for the MLCC production is the traditional sintering, using an appropriate atmosphere, to decrease the volatile species evaporation. Since the NBT-BT powder cannot be used, it is necessary to develop a new sintering method or atmosphere, in order to allow the use of NBT-BT for the MLCC, avoiding the increase of the material conductivity.

2.2.1.1 Sintering atmosphere

In this work, the sintering was done without the use of controlled atmosphere and using the NBT powder, as reported in [37], to create the atmosphere during sintering. The results,

presented in section 2.3.4.4, were used to demonstrate the need of creating a new method to control the sintering atmosphere for the NBT-BT industrial applications.

The atmosphere created from inert ZrO_2 powder was used. This powder covers the sample, thereby confining it and creating a Bi and Na saturated atmosphere around and close to the NBT-BT sample. The zirconium oxide was chosen as an inert powder due to its high melting and sintering temperatures and since it is often used in the industry, either to avoid volatile evaporation or to apply a mechanical force over the MLCC during sintering, avoiding the horizontal deformation of the capacitors. The results of using ZrO_2 to avoid volatilization will be presented in section 2.3.4.4.

In conclusion, the obvious and only choice for the synthesis method of the ceramic sheets is the tape casting with the pure perovskite powder synthesized by solid-state reaction.

Moreover, for both massive and layer NBT-BT, adding ZrO_2 powder in the crucible and covering the green body during sintering was tested to obtain NBT-BT perovskite ceramics that do not require post processing apart from polishing.

2.3 Solid-state reaction and improvements in this thesis

This section presents the synthesis method used for the NBT-BT synthesis, the improvements in the synthesis parameters studied in this thesis, and the influence of each parameter on the sample's structure, phase separation, and properties.

As it was explained in section 2.1, the solid-state reaction route was chosen as the synthesis method for NBT-BT powder. It consists in mixing oxides and/or carbonates through ball-milling, calcinating them, and sintering the samples by the traditional sintering method.

The mixing step creates an homogeneous reactant powder mixture while the calcination step promotes a solid-state reaction, forming the perovskite. For NBT-BT, this is an important step that should be done in a controlled atmosphere, to avoid evaporation of volatile species. A schematic representation of the closed crucibles and calcination atmosphere is shown in Fig. 2.2, where the atmosphere powder is composed of 50wt% of ZrO_2 , 25wt% of Bi_2O_3 and 25wt% of Na_2CO_3 . The role of the ZrO_2 on the atmosphere is to work as an inert high-melting-point powder, facilitating the withdrawal of the NBT-BT powder from the crucibles.

All calcinations were done at $900^\circ C$ for two hours, as discussed in section 2.1.2 and in

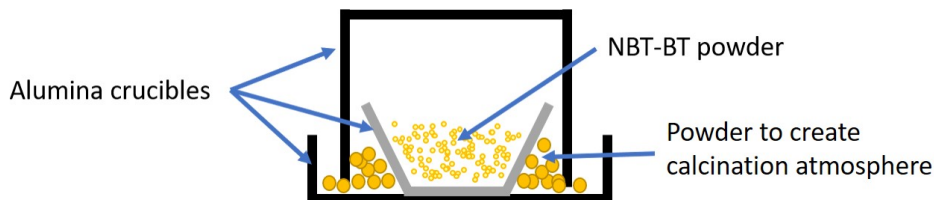


FIGURE 2.2: Schematic representation of the closed crucibles and calcination atmosphere

agreement with reference [79].

The sintering step increases the material's density and forms the final ceramics through solid-state diffusion. This step should also be done in a controlled atmosphere, to avoid the loss of volatile. In this thesis, the sintered samples are covered by a powder to create a sintering atmosphere and obtain ceramics without the need of post processing.

Finally, for the ceramic sheets used in the MLCC, tape casting was used for shaping the

layers.

Once the synthesis method is chosen, several parameters remain to be considered. The parameters analyzed and optimized in this thesis for the NBT-BT synthesis were: the weighing and drying of the reactants, the material of the ball-milling jars and balls, the size of the ball-milling balls, the ball-milling speed, time and solvent, the grain size of the starting powders, the reactants stoichiometry (or nominal stoichiometry), the use of a second ball milling after calcination, the shaping of the bulk samples (uniaxial or isostatic pressure with different values), the powder used to create the sintering atmosphere and the sintering temperature program for the ceramic samples, and the slurry composition and sintering conditions for the tape-casted samples.

2.3.1 Reactants weighing and drying

The first part of the synthesis consists in weighing the reactants, either in stoichiometric proportions or with an excess of volatile elements to compensate losses during calcination and sintering.

For the stoichiometric proportions and for the synthesis of 5g of powder, the weights are presented in Table 2.1.

Na_2CO_3 and Bi_2O_3 are hygroscopic powders, which means that they absorb the air mois-

Reactants	Weight (g)
Bi_2O_3	2.5689
Na_2CO_3	0.5843
TiO_2	1.8737
BaCO_3	0.2778

TABLE 2.1: Weight of reactants corresponding to 5g of nominal stoichiometric NBT-BT 6%.

ture, specially after being stored for a long time. The absorbed water does not change the appearance of the powders, however, its weight is taken into account when during weighting.

Mahajan *et al.* (2017) showed that NBT-BT prepared with dried reactants have a larger polar phase (R3c) percentage when compared to the same material prepared with the un-dried powders. Moreover, NBT-BT prepared from un-dried powders present a larger Na deficiency, which leads to a lower depolarization temperature. Finally, the presence of more point defects in the NBT-BT prepared from un-dried powders increases the frequency dispersion and the dielectric losses at high temperature compared to the samples prepared from dried powders. [42] This suggests that the drying of the reactants has a great influence on the final dielectric properties and should be evaluated in the present study.

To evaluate the average water quantity absorbed by Na_2CO_3 and Bi_2O_3 powders and its effect on the final material, both powders were dried during 24 hours at 400°C. [42]

Initially, the weight variation during drying of Na_2CO_3 and Bi_2O_3 powders was evaluated. For the Bi_2O_3 powder, the mass variation was 0.4% and for Na_2CO_3 powder it was 2.5%. This is responsible for the Na and Bi non-stoichiometries, resulting in the change of the NBT-BT phase separation and on the dielectric properties (see section 2.3.2.6).

The influence of drying the hygroscopic reactants on the NBT-BT phase separation and its effects on the dielectric properties will be discussed on details in section 3.2.1.2. The best adapted synthesis method will, then, be defined based on Exxelia's specifications for the high temperature MLCCs.

2.3.2 Mixture of the reactants

2.3.2.1 Ball milling of the reactants

After weighing, the mixture is carried-out by planetary ball-milling using an yttrium-stabilized zirconia (YSZ) jar or a tungsten carbide (WC) jar.

The ball-milling was done either at 250 rpm during 4 hours (less energetic) or at 350 rpm during 8 hours (more energetic option). The ball-milling energy was changed to improve the homogeneity of the samples and decrease the phase separation (see sections 2.3.2.5 and 3.2.1.2). The solvent used for ball milling was either ethanol (as in [37, 66, 79]) or a mixture of ethanol and methyl-ethyl-ketone, as normally used in Exxelia.

Ten-millimeter-diameter balls were used for the first ball millings and no problem on the powder composition, color, or size was observed. More details on the influence of the ball-milling energy, the composition of the jar, and the solvent will be given in sections 2.3.2.2 and 3.2.1.3.

The main objective of this stage is to mix the initial powders homogeneously. However, it can result in some mechanical synthesis (that is, the formation of the product: NBT-BT) depending on the ball-milling parameters and in a decrease in the grain size of the reactant powders.

The use of a dispersing agent during ball-milling was also tested. The function of the dispersing agent is to keep particles apart from each other in the solvent (see section 1.2.6.1). During ball-milling, this improves the dispersion of the grains, affecting the final material properties, as shown in section 3.2.1.3. A commercial product called Borchigen-911, with a polymeric base, was used as a dispersing agent, since it is widely used industrially (including in Exxelia's MLCC production) and it does not react with the NBT-BT powder.

XRD of the ball-milled powder (250 rpm during 4h, using the dispersing agent) of sample "H" is compared with the same powder after calcination in Fig. 2.3, to check the presence of mechanical synthesis.

The partial mechanical synthesis of NBT-BT is evident on the X-ray diffractograms through the presence of some small characteristic peaks corresponding to the pseudocubic (110), the (200), the (211), and the (111) peaks of the NBT-BT (see Fig. 2.3). However, as it can be seen from the peaks intensity of the NBT-BT when compared to the peaks of the starting powders that the formation (mecosynthesis) of NBT-BT during the first ball milling is minimal and this synthesis step can be considered mainly as a mixing step.

Moreover, no peak split can be observed in the calcined NBT-BT diffraction pattern in Fig. 2.3. This is because, as explained in section 1.4.2.1, NBT-BT is a non-ergodic relaxor at room temperature. So, when it is not polarized, as in the calcined powder, its average structure is cubic.

2.3.2.2 Influence of the jar and balls material

The jar and ball material has also a strong influence on the final properties of the sample, since the ball-milling energy (mechanical energy of the shock of the balls against the walls of the jar) is larger in the WC jar and balls, because the material is denser than the YSZ. Moreover, a possible contamination of the final material has to be taken into account.

Tungsten carbide (WC)

The effect of using the WC jar and balls for NBT-BT synthesis is evaluated by the "U-WC" sample properties. Table 2.11 p. 79 shows the synthesis conditions of "U-WC" sample (ball milling in WC jar before and after calcination for 8 hours at 350 rpm and sintered under ZrO₂ atmosphere powder for 3 hours at 1050 °C).

Formation of five different phases in the "U-WC" sample surface are observed in Fig. 2.4

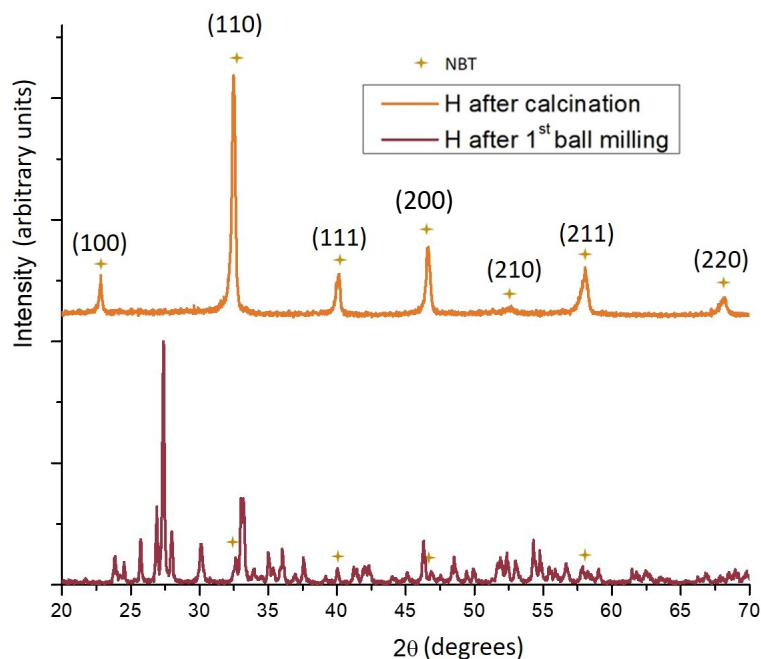


FIGURE 2.3: Comparison between the X-ray diffractograms of the ball-milled powder (250 rpm during 4h, using the dispersing agent) and of the same powder after calcination, for sample "H".

and their composition, as determined by EDS, are reported in Table 2.2.

The results confirm the important contamination of the NBT-BT by the jar material.

It also shows a separation of the barium from the NBT to form secondary Ba-containing phase. This secondary phase does not result from the jar material, since it is also present in the NBT-BT milled in the YSZ jar.

Moreover, the measurements of the dielectric properties (Fig. 2.5) and the insulation resistance of this sample (0.06s at 200 °C) show that the tungsten contamination has a strong influence on the dielectric properties of the final material, decreasing the resistivity, increasing the dielectric losses, and increasing the frequency dispersion compared to the same sample prepared in the YSZ jar (sample "U" in Fig. 3.14).

Phase	O	Na	Si	Ti	Ba	Bi	Zr	W
NBT phase 1	2.48	0.51	-	1.00	-	0.55	-	-
NBT phase 2	2.01	0.14	-	1.00	-	0.20	-	-
W phase 1	2.56	-	-	0.04	1.04	-	-	1.00
W phase 2	28.77	1.58	-	10.74	-	7.8	-	1.00
Secondary Ba-containing phases	19.70	0.23	-	9	3.91	-	-	-

TABLE 2.2: Phases composition for the "U-WC" sample, prepared in the WC jar.

In conclusion, the WC jar and balls are not ideal for the MLCC production, since the tungsten contamination degrades the dielectric properties of the material.

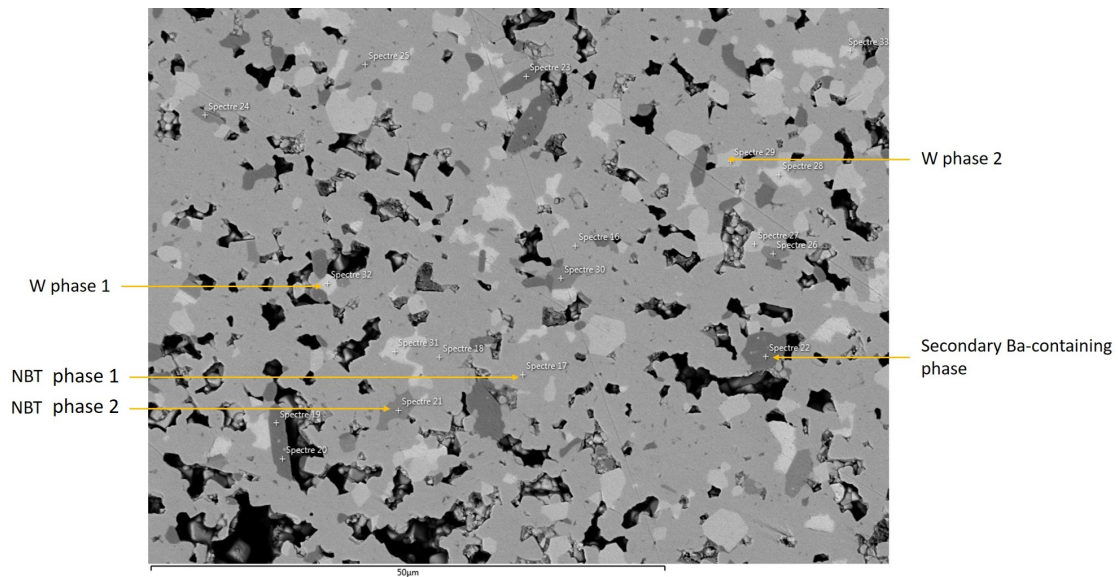


FIGURE 2.4: SEM backscattered electrons image of the "U-WC" sample, ball milled in the WC jar showing the formation of five different phases.

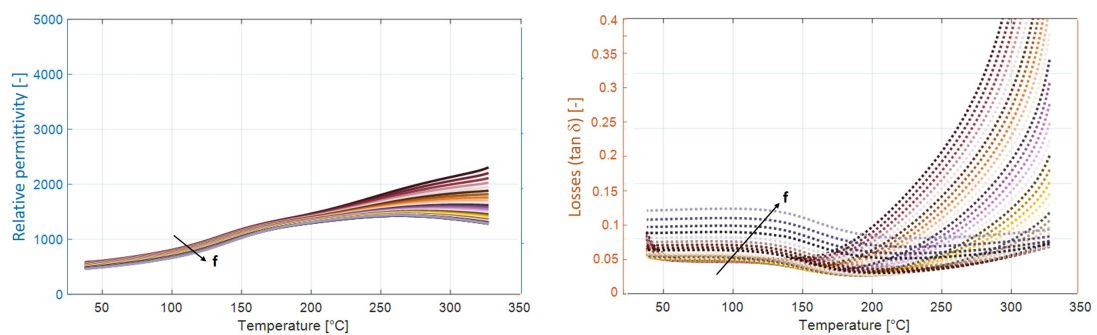


FIGURE 2.5: Dielectric properties of the sample "U-WC", ball-milled in the WC jar from frequencies from 1kHz to 1MHz.

The grain size and the structure differences between samples "*U-WC*", ball milled in the WC jar, and "*U*", ball milled in YSZ jar, are also interesting to compare. The SEM images (Fig. 2.6) of those samples indicate that the grain size of the ceramic ball-milled in the YSZ jar is around $0.8 \pm 0.05 \mu\text{m}$ and the one milled in the WC jar is around $1.5 \pm 0.05 \mu\text{m}$.

This difference in grain size is due to differences in the ball-milling energy. For both ball-millings, the same mass ratio between the balls and the powder was used, the ball mass being 10 times the powder mass. However, since the density of the WC balls are higher than that of the YZS balls, more YZS balls were used and the ball-milling energy is also higher.

The X-ray diffraction of the as-sintered samples and samples after polishing and thermal

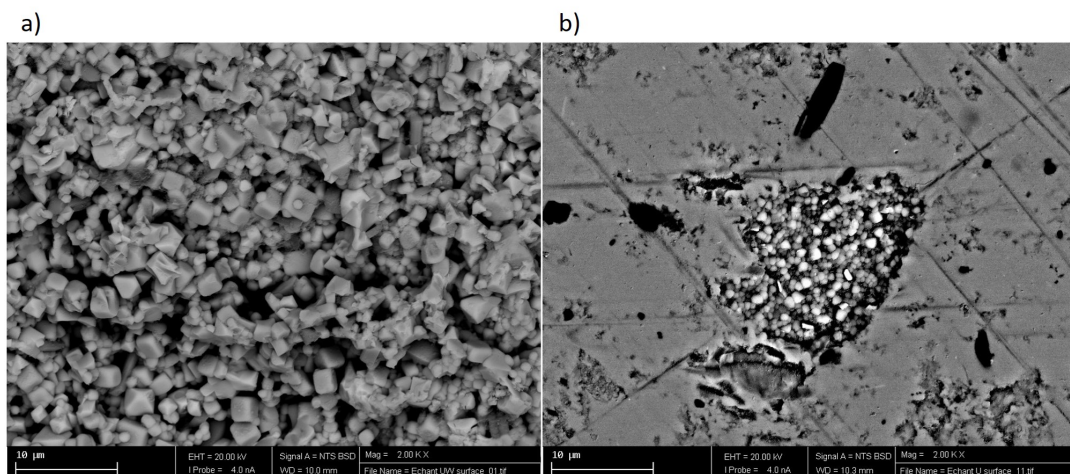


FIGURE 2.6: SEM image at the same scale for grain size comparison of the samples a) "*U-WC*" ball-milled in the WC jar b) "*U*" ball-milled in the YSZ jar

treatment at 400°C for 1 hour are marked by differences (see Fig 2.7) p. 50. Namely:

- In the X-ray diffractograms of the sample ball-milled in the WC jar ("*U WC*"), the peaks are narrow and there is no change in the peak widths after polishing and relaxing strain compared to the X-ray diffractograms of the as-sintered sample (sintered samples before polishing and strain relaxing). There is also no peak splitting in both diagrams, which indicates that both samples present a pseudo-cubic structure, as expected for unpoled non-ergodic relaxors. However, both diagrams present extra peaks related to the Ba-rich and W-rich phases present in the sample surface and core.
- As-sintered samples ball-milled in the YSZ jar have narrow and more symmetrical XRD peaks when compared to the polished and strain-relaxed ones that have larger and asymmetric peaks. The as-sintered sample also show no XRD peak splitting, indicating a pseudo-cubic structure. However, polished and strain-relaxed samples present the same pseudo-cubic related peaks with the addition of a shoulder on the lower-angle side.

Kong *et al.* showed very recently the existence of a skin effect in NBT-BT. They claimed that due to stress differences between the sample surface (plane stress) and core (tri-axial stress), there is a lattice expansion normal to the surface. This is responsible for a stress-induced transformation that creates a phase coexistence of pseudo-cubic, rhombohedral, and

tetragonal phases in the skin. [34]

Other factors, such as the increased concentration of oxygen and bismuth vacancies at the surface, may also induce a chemical pressure and a phase coexistence, with an increase of the lattice parameter. Finally, the larger concentration of Ba and its resulting lattice deformation can also induce the same phase coexistence. [34]

This phase coexistence may, then, be responsible for the low-angle-side shoulder peaks, reflecting a skin effect on NBT-BT. Since the effect may be due to stress differences between the core and the surface, it is always present, even after polishing. [34]

For my NBT-BT samples prepared in the YSZ jar, the XRD presents low-angle-side shoulder peaks for the polished and strain-relaxed samples, as expected for the sample surface, due to skin effect. However, thin single peaks are observed in the as-sintered sample, contrary to what would be expected.

Detailed investigation is needed to explain why the skin effect is not present in the as-sintered samples. However, one hypothesis is that the variation of the local Ba concentration in the NBT-BT lattice may prevent the skin effect on the as-sintered samples. This hypothesis takes into account that the surface of the as-sintered samples show higher Na evaporation compared to Bi. So, there is an intense secondary Ba-containing phase separation in the surface of these samples (see section 2.4). This decreases the local Ba concentration in the lattice of the NBT matrix phase, creating a gradient of local Ba concentration in the A-site of the matrix phase. Finally, the internal chemical pressure and lattice deformation on the matrix phase is lower in the as-sintered sample's surface compared to their core, inhibiting the skin effect.

In conclusion, the presence of the low-angle-side peaks in the XRD of the polished and strain-relaxed-samples is due to the skin effect and phase coexistence at the surface of these samples. The as-sintered samples do not show the same effect probably due to the effect of the decreased local Ba-concentration in the NBT-matrix phase owing to the increased secondary Ba-containing phases at the sample's surfaces.

ZrO₂

The "U" sample was used to evaluate the effect of using the YSZ jar and balls for the NBT-BT synthesis. Table 2.11 p. 79 shows the synthesis parameters of this sample (ball milling in YSZ jar before and after calcination for 8 hours at 350 rpm and sintering under an atmosphere created by ZrO₂ powder for 3 hours at 1050 °C).

Separation of the barium from the NBT to secondary Ba-containing phases is illustrated in Fig. 2.8. The material of the jar is not an important factor for this phase separation, since the secondary Ba-containing phases is also seen in other samples, including the one prepared in the WC jar. Details on the secondary Ba-containing phases stoichiometries and formation are given in section 2.4.

For this specific sample, where a Bi excess and a Na deficiency are added to the reactants in order to get the nominal (reactants) stoichiometry of Na_{0.44}Bi_{0.48}Ba_{0.06}TiO₃, there is a separation of the Bi excess, forming a third Bi-rich phase (see Table 2.3).

Fig. 2.8 also shows a small contamination with ZrO₂, mainly on the secondary Ba-containing phases (see Table 2.3), but there is no phase formation with Zr as a main compound, contrary to the case of the "U-WC" sample. The ZrO₂ contamination on the secondary Ba-containing phases is probably due to the contact between the sample's surface and the ZrO₂ powder during sintering (see section 2.4).

The ZrO₂ used to create the sintering atmosphere is also observed on the XRD diagrams in Fig.2.7 p. 50. It is, then, necessary to polish the sample after sintering to eliminate this ZrO₂ contamination. As the polishing is already a planned stage during the MLCC production, (see section 1.2.6), this is not a problem for industrial processing.

After polishing, the ZrO₂ peaks are not present anymore, but the diffraction peaks of the

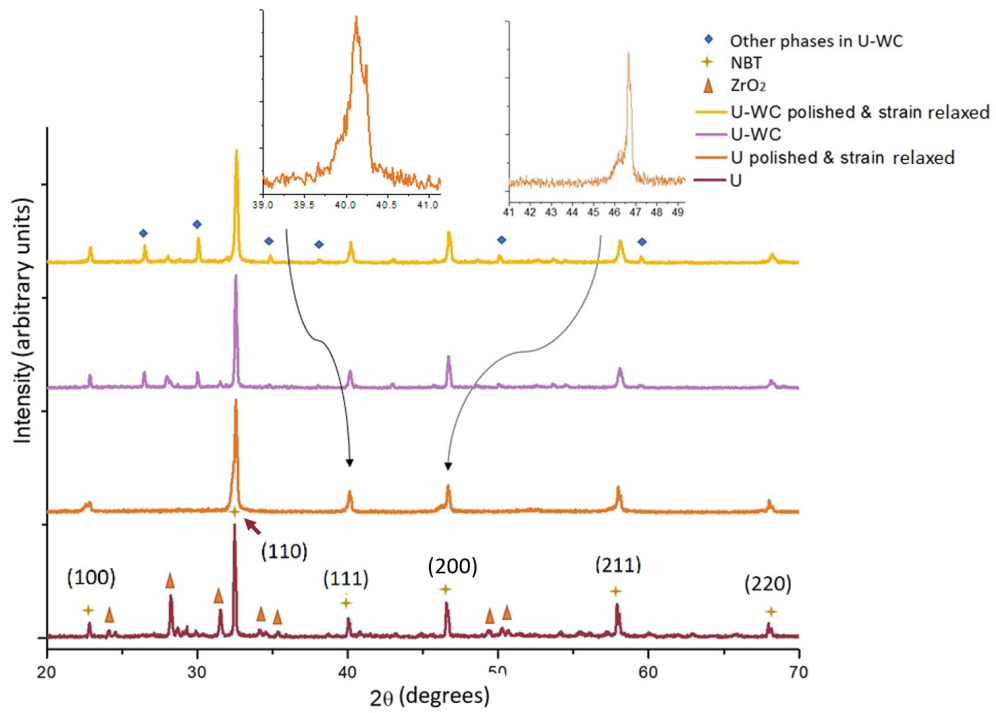


FIGURE 2.7: XRD diagrams of the samples "U" (ball milled in YSZ jar) and "U-WC" (ball milled in WC jar) after sintering and after polishing and strain relaxation and NBT, ZrO_2 , and W-rich phases identification

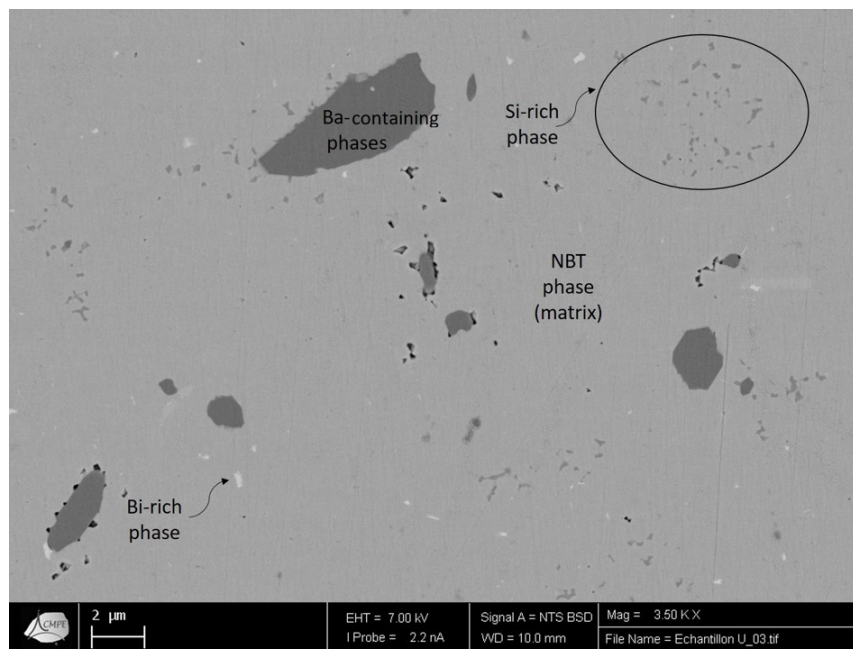


FIGURE 2.8: SEM image of the polished surface of the "U" sample (ball milled in the YSZ jar)

Phase	O	Na	Si	Ti	Ba	Bi	Zr
NBT	2.9 (0.1)	0.42 (0.02)	-	1.0	-	0.49 (0.01)	-
secondary Ba-containing	18.8 (0.5)	-	-	9.0	3.56 (0.25)	-	0.03 (0.01)
Si-rich	8.4	0.70	1.0	1.9	2.10	1.10	-
Bi-rich	3.2 (0.1)	0.18 (0.12)	-	1.0	-	0.95 (0.15)	-

TABLE 2.3: Composition of each phase present in the "U" sample (ball milled in YSZ jar) measured by EDS. The values in brackets are the measurements uncertainties.

NBT-BT are large and asymmetric, due to the skin effect that induces a phase coexistence in the sample's surface (see section 2.3.2.2). Moreover, a strain is introduced during polishing, so a strain relaxation step is also needed. Details on strain relaxation will be given in section 4.2.2.1.

Finally, Fig. 2.8 p. 50 also reveals a limited silicium contamination in the form of small grains. However, this Si-rich phase, coming from the polishing sand paper, is negligible for the sample structure and properties, due to its low quantity.

As a conclusion, the ball milling in the YSZ jar and balls is the best option for the NBT-BT synthesis for applications in MLCC.

The influence of the other synthesis parameters (the drying of the reactants, the ball-milling solvent, speed and time, the use of a dispersing agent during ball-milling, the grain size of the Na_2CO_3 reactant, the strain relaxation and the powder used to create a sintering atmosphere) and the sample stoichiometry on the dielectric properties will be discussed in Chapter 3.

2.3.2.3 Influence of the solvent

Two different solvents were used during the ball milling: ethanol, the most commonly used ball-milling solvent for NBT-BT synthesis [37, 66, 79] (see section 2.3.2.1), and a mixture of 29.7wt% of ethanol and 70.3wt% of methyl-ethyl-ketone (MEK), as used in the MLCC production at Exxelia.

The influence of the solvent on the secondary Ba-containing phases separation (size and concentration) was analyzed based on SEM images of the polished surface of two different samples: "V" and "N". The synthesis parameters of each sample is presented in Table 2.11 p. 79 and they are the same, except for the solvent (ethanol and MEK) for sample "N" vs ethanol for sample "V".

Table 2.4 shows the size and percentage of secondary Ba-containing phases in each sample. Considering a 95% confidence interval, the average size and concentration (percentage of area) of the secondary Ba-containing phases for the two samples are similar. This implies that the solvent does not have an influence on the phase separation in the NBT-BT samples.

The structure of samples "V" and "N" can also be compared via XRD measurements,

Sample	Average size (μm^2)	Error	% area	Error
V (ethanol)	1.71	1.58	1.56	0.92
N (ethanol and MEK)	0,89	0.36	2.35	0.04

TABLE 2.4: Secondary Ba-containing phases (SEM) characterization for samples "V" (ethanol) and "N" (ethanol+MEK).

shown in Fig 2.9.

The diffraction patterns of the two samples are similar. The extra peaks in the as-sintered samples are due to the ZrO_2 powder used to create the sintering atmosphere and have no influence on the bulk material structure (see section 2.3.2.1).

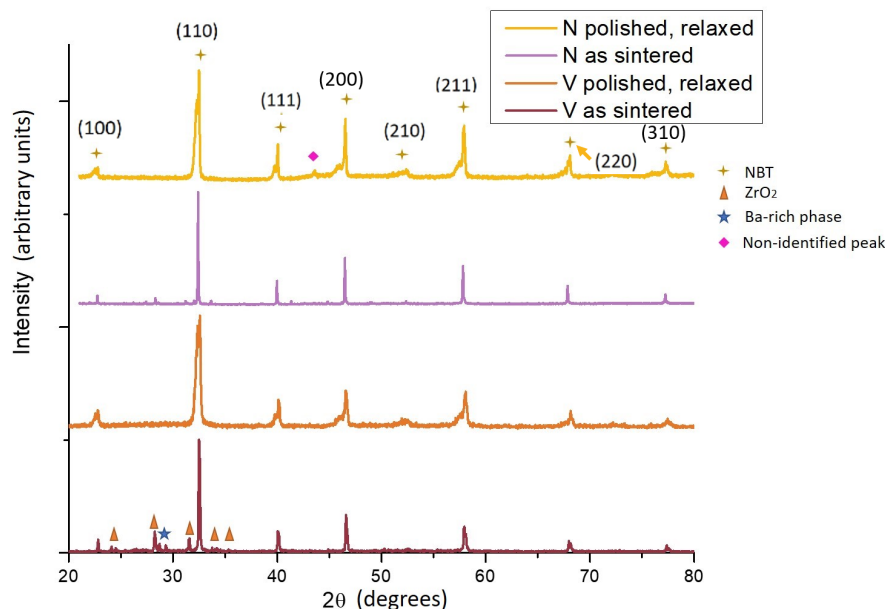


FIGURE 2.9: XRD measurements of samples "V" and "N" with phase identification

To sum up, the change in the solvent from pure ethanol to the ethanol and MEK mixture does not change the phase separation nor the structure of the NBT-BT.

2.3.2.4 Influence of the grain size of the reactants

Two different Na_2CO_3 grain sizes were used for the initial powders: the "granular" Na_2CO_3 that has an average grain size of $380\mu\text{m}$ and the "powder" Na_2CO_3 , with an average grain size of $0.9\mu\text{m}$.

Two samples were prepared with un-dried initial powders, 250 rpm ball milling for 4 hours, using ethanol as a solvent and a dispersing agent during the ball milling. The "H" sample used "granular" Na_2CO_3 while the "V" sample used "powder" Na_2CO_3 (see Table 2.11 p. 79). Table 2.5 shows that the grain size of Na_2CO_3 does not affect the secondary Ba-containing phases separation.

Analyzing the differences in structure from the XRD measurements presented in Figure

Sample	Average size (μm^2)	Error	% area	Error
H (granular Na_2CO_3)	3.35	2.35	1.51	0.24
V (powder Na_2CO_3)	1.71	1.58	1.56	0.92

TABLE 2.5: Secondary Ba-containing phases SEM characterization for samples H ("granular" Na_2CO_3) and V ("powder" Na_2CO_3)

2.10, it can be concluded that both grain sizes give rise to the same NBT-BT structure. Both

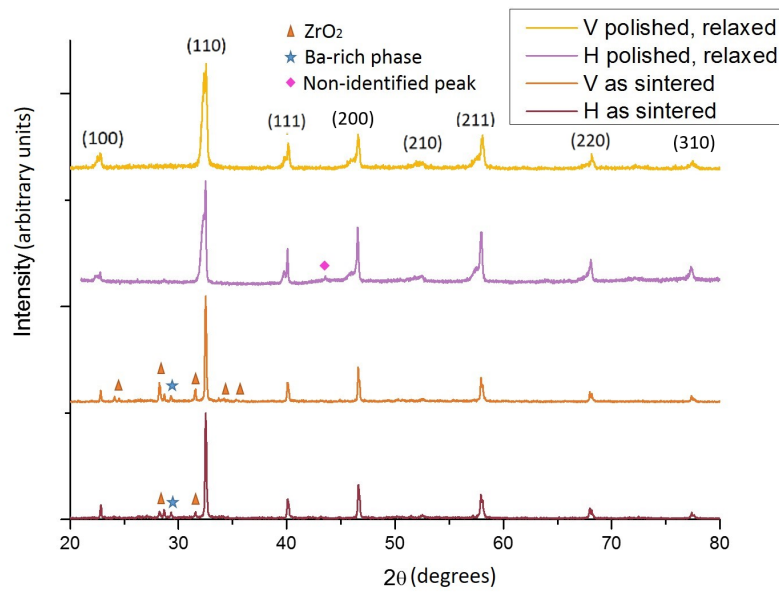


FIGURE 2.10: XRD measurements of samples "V" and "H" with phase identification

as-sintered samples present thin pseudo-cubic NBT-BT peaks and peaks coming from the ZrO_2 atmosphere powder and from the secondary Ba-containing phases. Both polished and strain-relaxed samples show no peaks related to the secondary Ba-containing phases or to the ZrO_2 , even though the widths of the peaks for the "V" sample ("powder" Na_2CO_3) are larger than for the "H" sample ("granular" Na_2CO_3), due to the skin effect (see section 2.3.2.2).

In conclusion, the grain size of the Na_2CO_3 initial powder does not affect the phase formation nor the structure of the NBT-BT.

2.3.2.5 Influence of the speed and duration of ball milling

The speed and duration of ball milling were initially chosen as 250 rpm and four hours. To verify the influence of the ball-milling energy and to increase the homogeneity of the final samples, new samples were synthesized with 350 rpm and 8 hours. The secondary Ba-containing phases separation and the structures were compared.

For the secondary Ba-containing phases separation, three different comparisons were done between the SEM images of the polished surface: "E" vs "B" samples, "I" vs "H" samples, and "P" vs "N" samples. The synthesis parameters of each sample are presented in Table 2.11 p. 79 and the parameters that vary between the samples are summarized in Table 2.6.

From Table 2.7, it can be seen that, in the case of the samples ball-milled without dispersing agent ("B" and "E" samples), the increase in the energy of ball milling decreases drastically the average size of the secondary Ba-containing phases, but it increases the proportion of this phase. In the case of the powders ball-milled with dispersing agent in the same solvent (ethanol - "H" and "I" samples), the change in the ball-milling energy does not affect the average grain surface and volume fraction of the secondary Ba-containing phases.

The structure differences between those samples were also analyzed via XRD measurements and are presented in Figures 2.11 (as-sintered) and 2.12 (after polishing and strain relaxation).

Sample	Dried reactants	Ball-millings	Solvent	Dispersing agent
"B"	Yes	250 rpm 4h - 250 rpm 4h	Ethanol	No
"E"	Yes	350 rpm 8h - 350 rpm 8h	Ethanol	No
"H"	No	250 rpm 4h - 250 rpm 4h	Ethanol	Yes
"I"	No	250 rpm 4h - 350 rpm 8h	Ethanol	Yes
"N"	No	250 rpm 4h - 250 rpm 4h	MEK + Ethanol	Yes
"P"	No	350 rpm 8h - 350 rpm 8h	MEK + Ethanol	Yes

TABLE 2.6: Synthesis parameters for NBT-BT samples "E", "B", "I", "H", "P" and "N". The "ball-millings" column present the speed and time for the first (before calcination) and second (after calcination) ball-milling.

Sample	Average size (μm^2)	Error	% area	Error
"E"	0.15	0.09	4.65	0.54
"B"	32.60	21.90	0.89	0.20
"I"	0.83	0.76	1.45	0.44
"H"	3.35	2.35	1.51	0.24
"P"	2.99	2.18	2.70	0.44
"N"	0.89	0.36	2.35	0.04

TABLE 2.7: Secondary Ba-containing phases characterization for samples "E" (dried reactants, high-energy ball-milling), "B" (dried reactants, low-energy ball-milling), "I" (un-dried reactants, ethanol as solvent, high-energy ball-milling), "H" (un-dried reactants, ethanol as solvent, low-energy ball-milling), "P" (un-dried reactants, ethanol+MEK as solvent, high-energy ball-milling) and "N" (un-dried reactants, ethanol+MEK as solvent, low-energy ball-milling).

It can be seen that, except for sample "N", all the as-sintered samples present NBT-BT pseudo-cubic structure with some peaks coming from the powder used to create a sintering atmosphere (ZrO_2) and some peaks coming from the secondary Ba-containing phases. The detailed Ba-rich peaks identification will be discussed in section 2.4. The as-sintered samples show pseudo-cubic structure in agreement with the relaxor character of the material (pseudo-cubic structure matrix with PNR of $R3c$ symmetry) before poling and with no induced stress or grain size peak deformation.[56, 62]

For the polished and strain-relaxed samples, peaks from the ZrO_2 and from the secondary Ba-containing phases disappear.

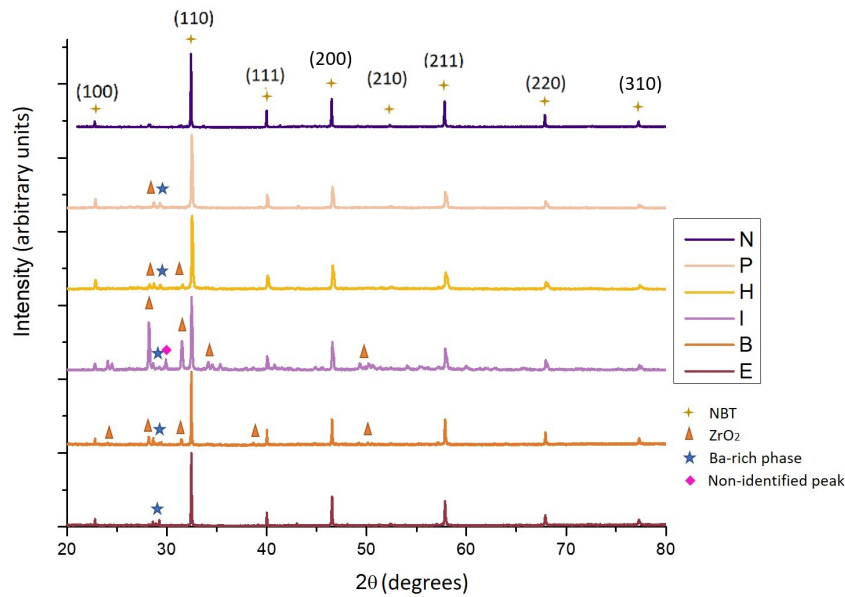


FIGURE 2.11: XRD measurements of as-sintered samples "P", "N", "H", "I" and "B" with phase identification.

2.3.2.6 Influence of the NBT-BT stoichiometry

The Bi^{3+} excess and/or the Na^+ deficiency in NBT-BT 6% have a great influence on the sample properties. This initially creates a pinched P-E loop, the pinching increasing with Bi-excess or Na-deficiency. Fig. 2.13 show the P-E loop of NBT-BT 7% with different Na and Bi nominal stoichiometries. Note that the behavior of NBT-BT 6% and NBT-BT 7% are similar, since both are on the morphotropic phase boundary of the NBT-BT solid solution. [44].

The pinched P-E loop with Bi-excess or Na-deficiency behaviour is attributed to the generation of "antiferroelectric-like" micro-regions in a macroscopic ferroelectric matrix through changes in the Na/Bi ratio. This is attributed to the appearance of orthorhombic $Pnma$ sheets within the rhombohedral $R3c$ matrix, similar to the modulated phase proposed to be the origin of "relaxor AFE" behavior in pure NBT. [23] An AFE-like to metastable FE reversible transition is induced by applying an external electric field, giving rise to the double P-E loop observed at room temperature for high bismuth excess and/or high sodium deficiency compositions.

The double hysteresis loop is desirable for energy storage materials, since it may increase the recoverable stored energy and it may decrease the energy losses when applying an

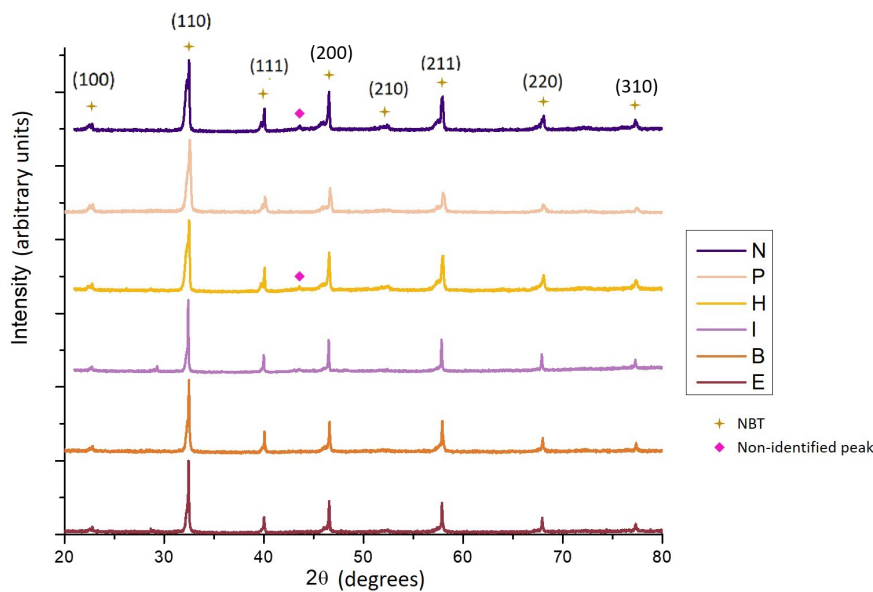


FIGURE 2.12: XRD measurements of polished and strain-relaxed samples "P", "N", "H", "I" and "B" with phase identification.

alternated external electric field. [53]

The effects of stoichiometry change can also be described by a decrease in the depolarization temperature, explained in section 1.4.2. As a consequence, the minimal temperature for having low dielectric losses ($T_{\tan \delta, \min}$ in Fig. 2.14) and low permittivity reduction on poled samples ($T_{\epsilon, \min}$ in Fig. 2.14) are displaced to lower temperatures and the material becomes useful for MLCC applications from room temperature.

Finally the decrease in the Na/Bi ratio decreases the DC conductivity of the NBT-BT

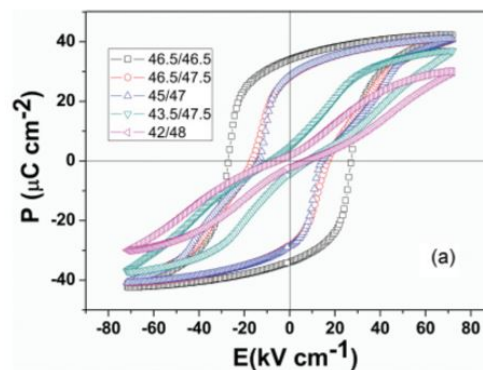


FIGURE 2.13: P-E loop for non-stoichiometric NBT-BT 7% ($\text{Na}_{x/100}\text{Bi}_{y/100}\text{Ba}_{0.07}\text{TiO}_3$) [23]

(see section 3.2.1.1) [78] increasing the insulation resistance of the material. This is also useful for the MLCC production, as presented in section 1.3.

Guo *et al.* measured the dielectric properties of the nominal (reactant) composition $\text{Na}_{0.44}\text{Bi}_{0.48}\text{Ba}_{0.06}\text{TiO}_3$ (see Fig. 2.15). A pinched P-E loop and no sharp anomaly on poled material, either for the permittivity or for the dielectric losses were also measured as the depolarization temperature lower than room temperature. [23] For this reason, the influence of the stoichiometry on the dielectric properties of NBT-BT were tested using this composition

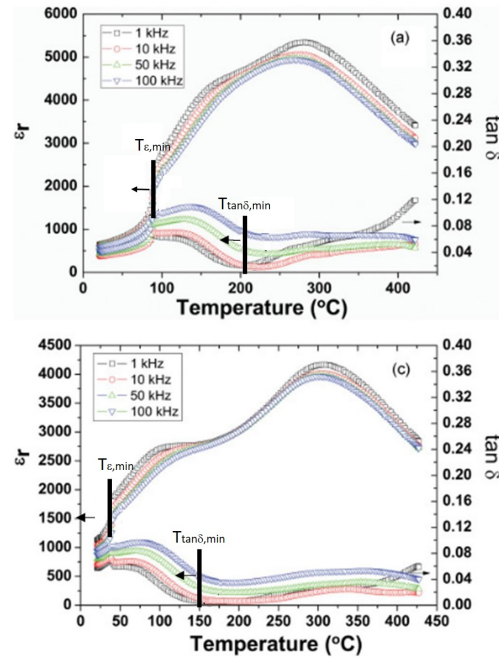


FIGURE 2.14: Relative permittivity and loss factor showing the stoichiometry effects on the depolarization temperature, and its useful consequences on the dielectric properties for MLCC applications. Vertical lines stand for the minimal temperature for having low dielectric losses ($T_{\tan \delta, \min}$) and permittivity reduction ($T_{\epsilon, \min}$). [23]

("U" sample).

The "U" sample ($\text{Na}_{0.44}\text{Bi}_{0.48}\text{Ba}_{0.06}\text{TiO}_3$ nominal composition) is composed of three main phases (see section 2.3.2.2) and one Si-rich phase, coming from the polishing paper and inert from a dielectric point of view, as observed in the SEM images of the polished surface and cross-section of this sample (Figures 2.8 p. 50 and 2.16 respectively). The composition of each phase was measured using EDS analysis and the results are presented in Table 2.3 p. 51.

The phases can be identified as secondary Ba-containing phases (also present in other samples), a Bi-rich phase (due to the non-stoichiometry of this composition) and a pure NBT phase (also present in other samples). The SEM image reveals the presence of the Bi-rich phase in the center of the sample, confirming the evaporation of bismuth oxide during sintering.

Comparing the volume fraction of the secondary Ba-containing phases of the "U" sample (complete synthesis parameters in Table 2.11 p. 79) with the sample synthesized using the same parameters, but a nominal NBT-BT 6% composition for the reactants ("P" sample), the larger bismuth concentration in the "U" sample decreases the percentage of secondary Ba-containing phases. The effect of this change in the dielectric properties of the material will be analyzed in section 2.4.

Two other samples were prepared after comparing the measured "U" sample composition with the nominal one "P": the "Y" sample, done using the same synthesis parameters as "U" but with an excess of 9.5% molar of sodium and 2.1% molar of bismuth, to obtain after sintering the nominal "U" composition (theoretical composition), the "Z" sample, with an excess of 16.9% molar of sodium, to obtain nominal NBT-BT composition after sintering.

These two samples were also observed using SEM and showed no phase separation. This implies that, not only the increase of bismuth concentration in the reactants, but also the

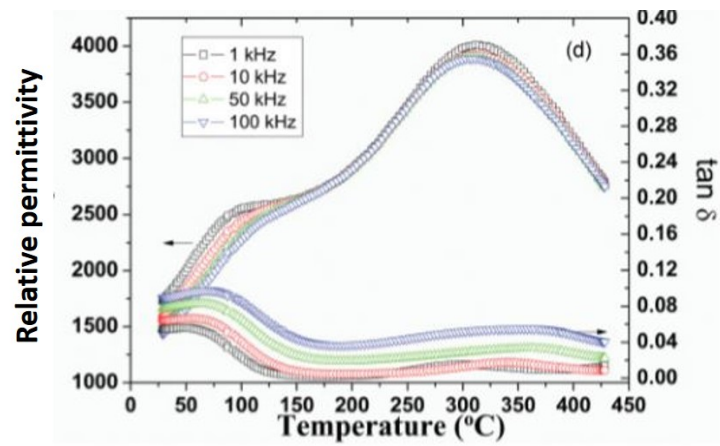


FIGURE 2.15: Relative permittivity and dielectric losses over temperature and frequency property for the poled $\text{Na}_{0.44}\text{Bi}_{0.48}\text{Ba}_{0.06}\text{TiO}_3$ composition [23]

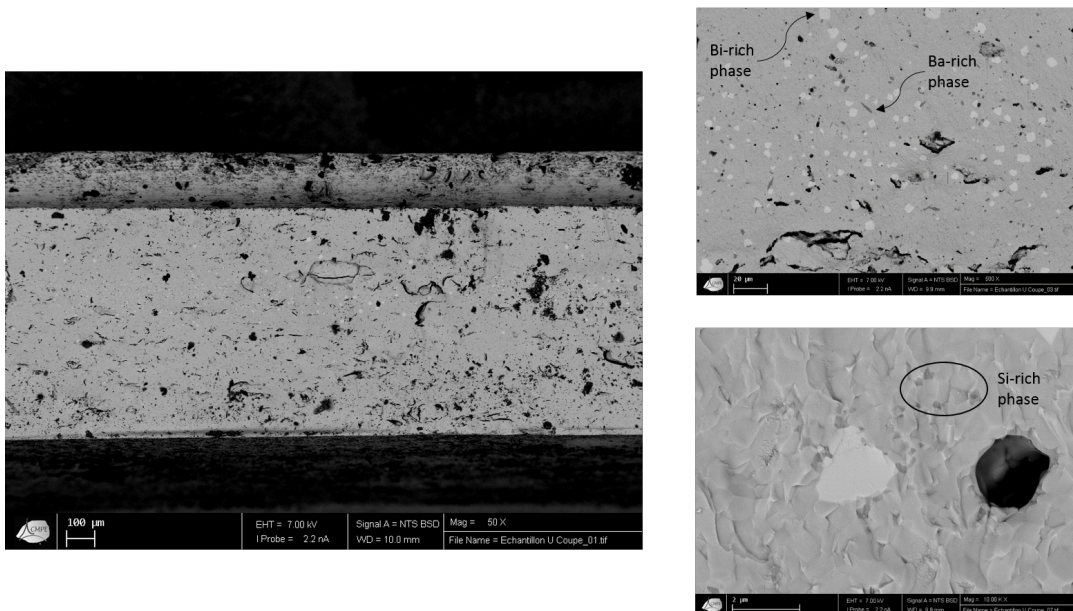


FIGURE 2.16: Cross-section SEM picture of the "U" sample ($\text{Na}_{0.44}\text{Bi}_{0.48}\text{Ba}_{0.06}\text{TiO}_3$ stoichiometry) showing three different magnifications and four different phases in the sample.

increase of sodium concentration result in lower volume fraction of secondary Ba-containing phases.

The XRD diagrams of the three nominally non-stoichiometric samples ("U", "Y" and "Z") were compared with the one of the nominal NBT-BT 6% synthesized under the same parameters (Figures 2.17 and 2.18). The four samples after sintering show a pseudo-cubic perovskite structure and extra peaks corresponding to the ZrO₂ powder used to create the sintering atmosphere and to the secondary Ba-containing phases. The polished and strain-relaxed samples show wide and asymmetric peaks, as explained in section 2.3.2.1, but they correspond well with each other. So, the change in bismuth and sodium stoichiometry in the reactants do not change the structure of the NBT-BT ceramics.

As a summary, the changes in the stoichiometry of the reactants do not affect the final material structure but the increase in bismuth and/or sodium concentrations decreases the secondary Ba-containing phases volume fraction. The increase in the Bi/Na ratio creates a partial separation of the bismuth excess in a Bi-rich phase.

2.3.3 Slurry preparation and tape casting

2.3.3.1 Introduction

Unlike NBT-BT ceramics, for the synthesis of tapes, the second ball milling is done together with the slurry preparation. The slurry is composed of a mixture of powdered ceramic, solvent, deflocculant, binder and plasticizer. The function of each component is explained in section 1.2.6. The slurry preparation is the most important factor to obtain a stable, resistant, and high-density ceramic tape.

After the slurry preparation, the tape-casting method is used to produce the ceramic tapes used in MLCC production.

Slurry composition

The initial slurry composition was defined taking into account the Exxelia's slurry compositions used in the organic MLCC production line and studies on the ideal concentration of binder, plasticizer and dispersing agent in X7R slurry. [38]

PVB was chosen as binder and PEG-400 (poly-ethylene-glycol with average molecular mass of 400 g/mol) was chosen as a plasticizer, since they are widely used in the industry and they do not react with NBT-BT. A commercial product called borchi-gen-911, with a polymeric base, was used as the dispersing agent, since it is also used in Exxelia and industrially for the MLCC production and since it does not react with the NBT-BT powder.

The stability of the slurry increases with increasing amounts of PVB (binder) and PEG (plasticizer) since they are responsible for the mechanical properties of the green tapes. However, an excess of these products can decrease the relative density of the ceramic tapes after sintering. The effect of the increase in concentration of the dispersing agent is not so clear. However, the slurry has better properties when it is added, even in low concentrations. [38]

The quality of the X7R slurry can be analyzed by its sheering properties, by the tensile diagram and micro-structure of the green tape and by the relative density of the sintered tapes. After analyzing different slurry compositions, Liu *et al.*(2012) concluded that the best one was as presented in the first column of the Table 2.8[38].

The slurry used in BT-based MLCC organic production line in Exxelia is presented in the second column of the Table 2.8.

Considering both compositions, the initial slurry composition in this study is as presented in the third column of the same table. The PVB, dispersing agent and PEG quantities added to the final slurry were taken from Liu *et al.*(2012) [38], since these parameters were

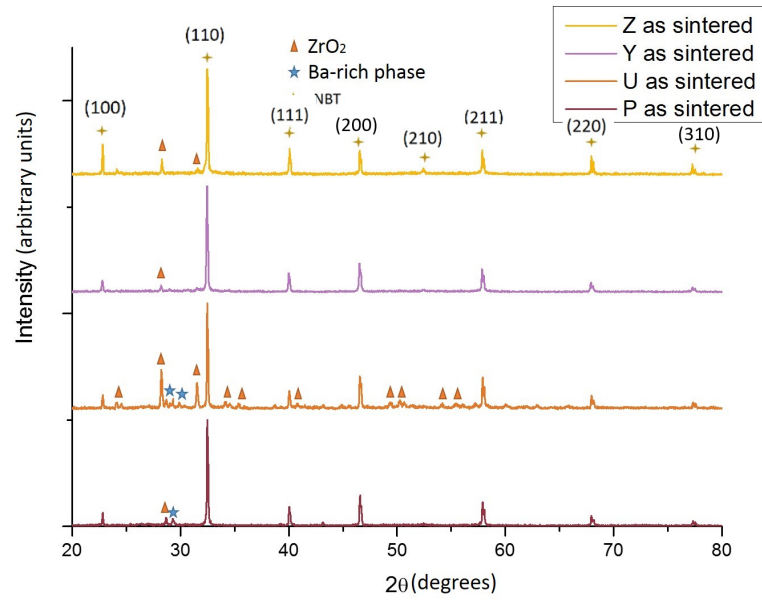


FIGURE 2.17: XRD diagrams of as-sintered "P", "U", "Y" and "Z" samples with phase identification.

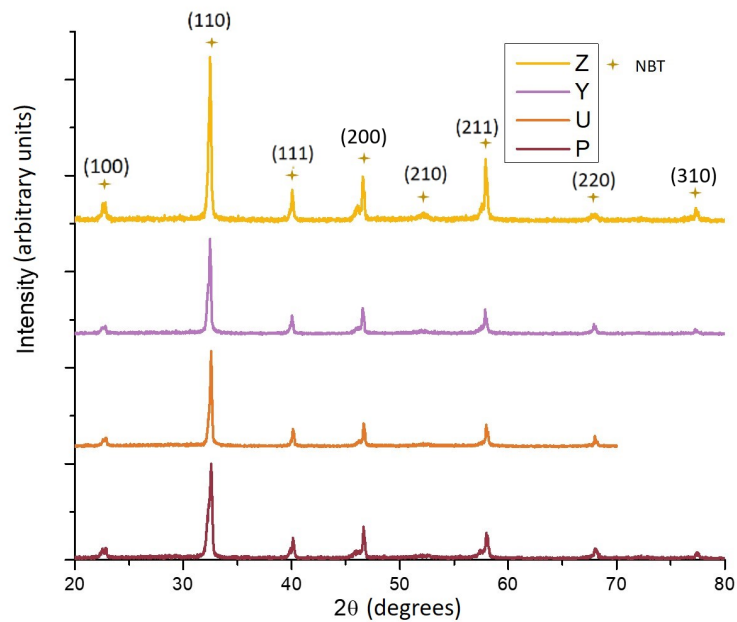


FIGURE 2.18: XRD diagrams of polished and strain-relaxed samples "P", "U", "Y" and "Z" samples with phase identification.

optimized. The NBT-BT powder and the solvent quantities were based on the slurry compositions used in Exxelia, to have a high density of the layers after sintering.

Component	Liu <i>et al.</i> (2012) [38]	Exxelia	Chosen composition
NBT-BT powder	68.9%	61.5%	60.6%
PEG	1.1%	1.5%	1.1%
MEK	11.5%	22.8%	22.7%
Ethanol	11.5%	9.6%	10.0%
PVB	4.5%	3.9%	4.5%
Dispersing agent	1.1%	0.6%	1.1%

TABLE 2.8: Slurry compositions based on Liu *et al.*[38], where the 1.1% missing is of butyl-benzyl-phthalate, not used in this study, on the MLCC slurries used by Exxelia and the initial slurry composition used in this work.

Ball-milling (mixing) conditions

The initial ball-milling conditions for the preparation of the slurry were based on the ZrO₂ tape-casting method and on the X7R slurry synthesis parameters.

For the X7R slurry preparation, the ceramic powder, the dispersing agent and the solvent are first mixed by stirring for four hours and, after the plasticizer and the binder are added, the slurry is mixed for 10 hours. [38] However, for the ZrO₂ tape casting method, the ceramic powder, the dispersing agent and the solvent are ball-milled at 300 rpm for 12 hours. Then PVB and PEG are added and the mixture is again ball-milled at 300 rpm for 2 hours.

Initially, the ZrO₂ synthesis method was adopted, since it is based on a ball milling in YSZ jar and balls.

2.3.4 Calcination and sintering

The second part of the synthesis consists in calcinating the ball-milled powders (to promote a solid-state reaction forming the perovskite) and of sintering the powders after calcination.

The sintering step is one of the most important for the NBT-BT production. During this step, the material is densified and the organic compounds are eliminated. The surface energy and the temperature are the driving forces for the solid-state mass exchange, responsible for the densification. So, the sintering can be controlled by the shaping of the samples (pressuring or tape casting), the grain size and the temperature of the sintering.

Due to the high volatility of the reactants, the sintering can significantly change the final properties of the NBT-BT. So the sintering atmosphere is crucial for improving it. The existing atmospheres used for the NBT-BT sintering are not ideal for the MLCC production (see section 2.1.2), so a new sintering method or atmosphere has been studied to allow the use of this material on MLCC production.

2.3.4.1 Density problem for ceramic samples

After calcinating and sintering of NBT-BT 6% ceramic at different sintering temperatures (sample "Density 1" in Table 2.11 p. 79) and without the second ball-milling step, the highest relative density was around $91.5\% \pm 2.5\%$ for the sintering temperature of 1150°C. The relative density of the sample sintered at 1050°C (the only temperature with no second phase peak in the XRD diagram of the as-sintered samples) was around $85\% \pm 2.5\%$. These densities are not compatible with Exxelia's requirements, since the ceramics used in MLCCs

should have a relative density of at least 95% to avoid interfacial defects and loss increase.

The density measurement were done using a caliper and a precision balance and the results are presented in Fig. 2.19 p. 62.

Ball milling and/or mechanical synthesis after calcination

To solve the density problem of NBT-BT ceramics, a second ball-milling step was added after calcination (see "Density 2" in Table 2.11 p. 79). Two sets of samples were done with the same synthesis parameters (presented in Table 2.11 p. 79) and different sintering temperatures during three hours and with a temperature ramp of 120°C/h in heating and 200°C/h in cooling. The second ball-milling, as the first one, was done in the YSZ jars, to avoid the contamination of the material with the W coming from the tungsten carbide jars (see section 2.3.2.2).

The relative densities (Fig. 2.19) show that the second ball-milling is useful to increase the final density of the samples. The maximum relative density after the second ball milling and after sintering is $93.5\% \pm 2.5\%$ at a sintering temperature of 1150°C and $91\% \pm 2.5\%$ at 1050°C. Considering the measurement uncertainty, the maximum density value for the NBT-BT after the second ball-milling and the sintering at 1150°C may be sufficient for the MLCC production. However, some sintering optimization should still be done in the layer synthesis, to further increase the density of the ceramics (see Chapter 5).

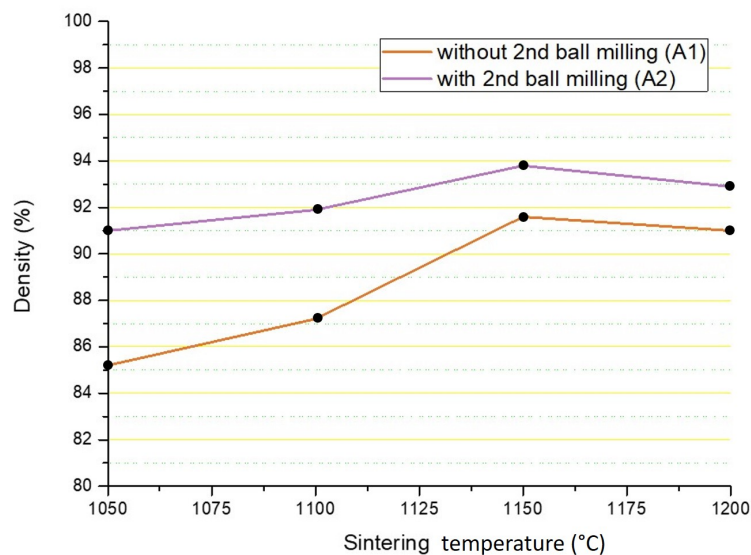


FIGURE 2.19: Relative density of samples without second ball milling and with second ball milling for different sintering temperatures (three hours sintering, 120°C/h in heating and 200°C/h in cooling).

Influence of the balls size

Two different ball sizes were used in the second ball milling: 10 mm-diameter YSZ balls and 1 mm-diameter YSZ balls.

For the 10 mm-diameter balls, the NBT-BT powders turned gray after ball milling. To understand the reason of this change, a new XRD measurement was done. No new phase could be identified when comparing the XRD of the powders after the ball milling with 10 mm-diameter balls (Fig. 2.20) with the powders before the second ball milling and after the ball milling with 1 mm-diameter balls for both 350 rpm - 8h and 250 rpm - 4h conditions

(Fig. 2.21). So the color change is not due to the formation of a new phase in the material.

Analyzing again Figures 2.20 and 2.21, a widening of the NBT-BT peaks of the pow-

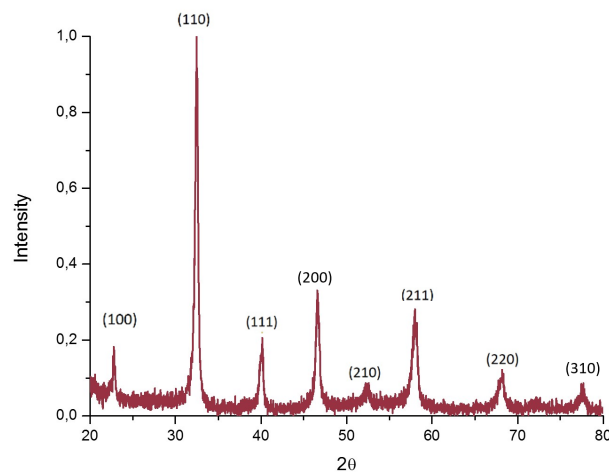


FIGURE 2.20: XRD measurement of the NBT-BT powder after the second ball-milling at 250 rpm during 4h using 10 mm-diameter balls.

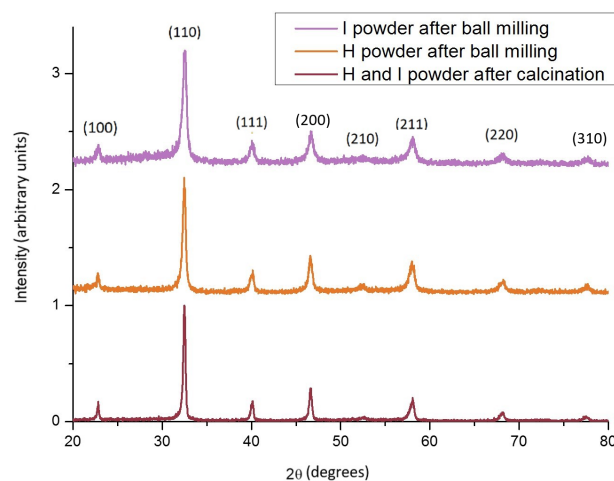


FIGURE 2.21: XRD diagram of the NBT-BT powder after the second ball-milling at 250 rpm during 4h (sample "H"), at 350 rpm during 8h (sample "I") using 1 mm-diameter balls.

ders is noticed for all of the measurements carried out after the second ball-milling. This indicates a decrease in the grain size during the ball milling and also with increasing ball-milling energy as the full width at half maximum (FWHM) of the peaks from sample "H" before ball-milling is 0.56 degrees vs 0.67 degrees for sample "H" after 250 rpm and 4h ball-milling vs 0.79 degrees for sample "I" after 350 rpm and 8h ball-milling.

The powders ball-milled after calcination with the 10mm-diameter balls were then heated at 400°C for five hours in air, in order to oxidize the oxygen vacancies and relax any strain introduced during the second ball milling. The temperature choice of 400°C was done to avoid sodium or bismuth evaporation, as it will be detailed in section 3.2.1.4. After this thermal treatment, the powder color was again white.

The oxygen vacancies cannot be easily detected in the XRD analysis [68] as they may

increase the lattice parameter but they can change the color of an oxide, even at really low concentrations. [71] So, the results indicate that the second ball milling with the 10 mm-diameter YSZ balls create oxygen vacancies in the NBT-BT that could have a negative effect in the MLCC productions, since it can result in a lower DC resistivity. [78]

A Raman analysis was also done using an excitation laser with 633 nm wavelength. The ball-milled powder was measured, since a high concentration of oxygen vacancies decreases the wave number and increases the intensity of the 650-950 cm^{-1} ("D") band, as observed in Fig. 2.22 [68]. The Raman spectra at different positions for the sample before the second ball-milling (Fig. 2.23), after the second ball-milling (Fig. 2.24), and after thermal treatment (Fig. 2.25) are presented. The fit was done for bands C and D (see Fig. 2.22), using three peaks for each. [68] The mean peak position and intensities of each fit peak is shown in Table 2.9.

The fit for the heat-treated sample is presented in Fig. 2.26 as an example.

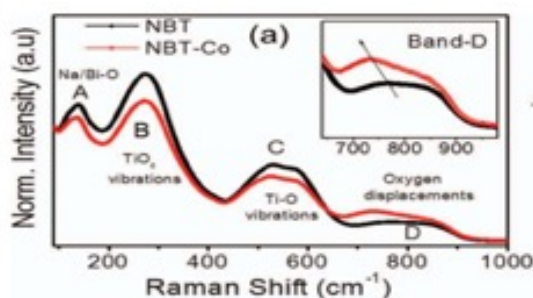


FIGURE 2.22: Raman reference spectra of NBT and NBT-Co (with oxygen vacancies). [68]

Peak center value	Before ball-milling		After ball-milling		After heat treatment		Reference [68]
	Wavenumber (cm^{-1})	Height (a.u)	Wavenumber (cm^{-1})	Height (a.u)	Wavenumber (cm^{-1})	Height (a.u)	Wavenumber (cm^{-1})
D3	869	1051	872	575	870	680	868.2
D2	819	1517	815	910	818	1116	815.8
D1	749	1287	750	450	749	671	759.6
C3	596	2492	599	1096	597	1684	578.3
C2	555	4517	554	2571	555	3022	518
C1	512	3715	511	2010	513	2961	477.7

TABLE 2.9: Mean position and intensities of each fitted peak for the Raman spectra of NBT samples before second ball-milling, after second ball-milling and after thermal treatment at 400°C for five hours in air. The C- and D-bands each consists in three peaks

By analyzing the peaks position, it can be seen that the difference in wavenumber between the three powders (their displacement) is not significant, since the greatest difference between the wavenumbers is 4 cm^{-1} . Moreover, the peaks height analysis also shows that the differences are not significant. It is concluded, therefore, that all the measurements before and after ball milling are similar. This implies that both samples are homogeneous (so the first ball-milling is enough to guarantee an homogeneity of the powders) and that the oxygen vacancies supposedly created during ball milling are not detectable by Raman, probably due to their low concentration.

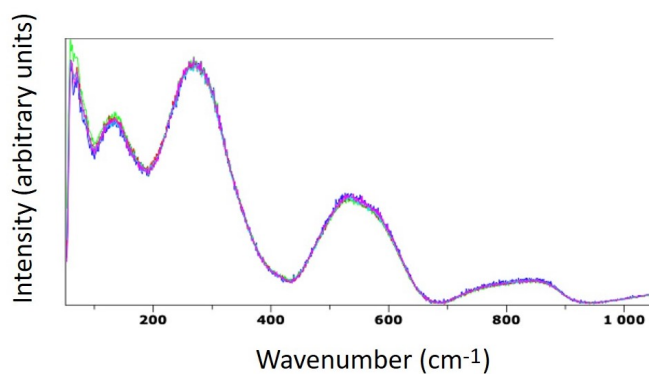


FIGURE 2.23: Raman spectra measured on different points for the NBT powder before the second ball-milling showing the homogeneity of the Raman signal.

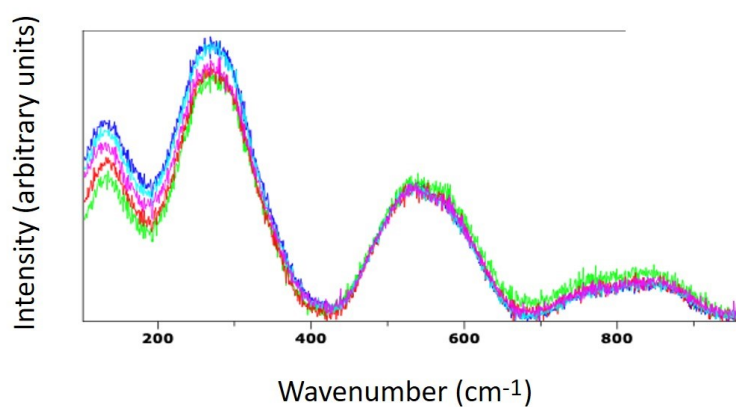


FIGURE 2.24: Raman spectra measured at different points for the NBT powder after the second ball-milling. Same variations of the intensity exist for low wavenumbers, but the C and D-bands have more uniform intensities.

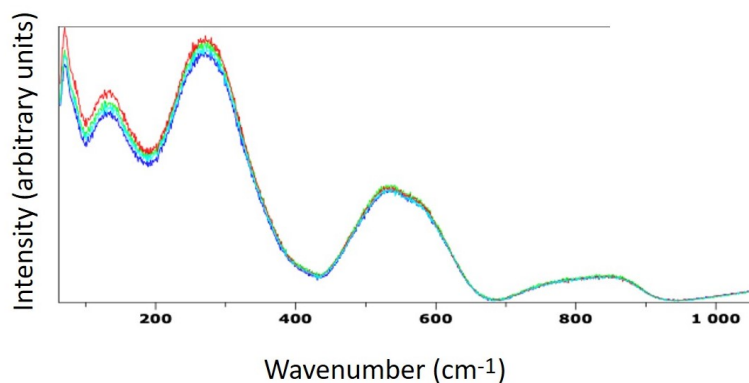


FIGURE 2.25: Raman spectra measured at different points for the NBT powder after thermal treatment at 400°C for five hours in air showing the homogeneity of the Raman signal, especially for the C and D bands.

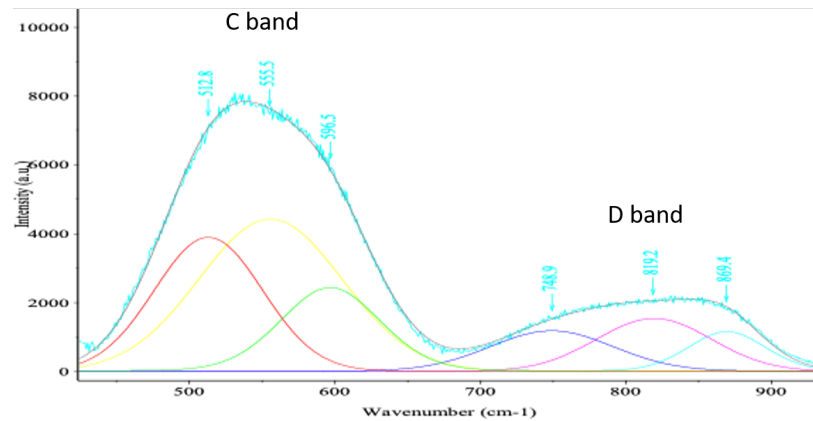


FIGURE 2.26: Fitting for bands C ($450 - 680\text{cm}^{-1}$) and D ($650 - 950\text{cm}^{-1}$) of the Raman spectra of the NBT sample after thermal treatment using three base peaks.

For the 1 mm-diameter balls, the NBT-BT powders did not change color after the second ball milling. Moreover, like for powders ball-milled with the 10 mm-diameter balls, no difference was noticed when comparing the XRD and SEM before and after ball milling (see Fig. 2.27). This indicates that there is no phase formation due to the second ball milling and that no oxygen vacancies are introduced when the powder is ball-milled using the smaller YSZ balls.

As a conclusion, the second ball milling with 1mm YSZ balls was chosen for the final

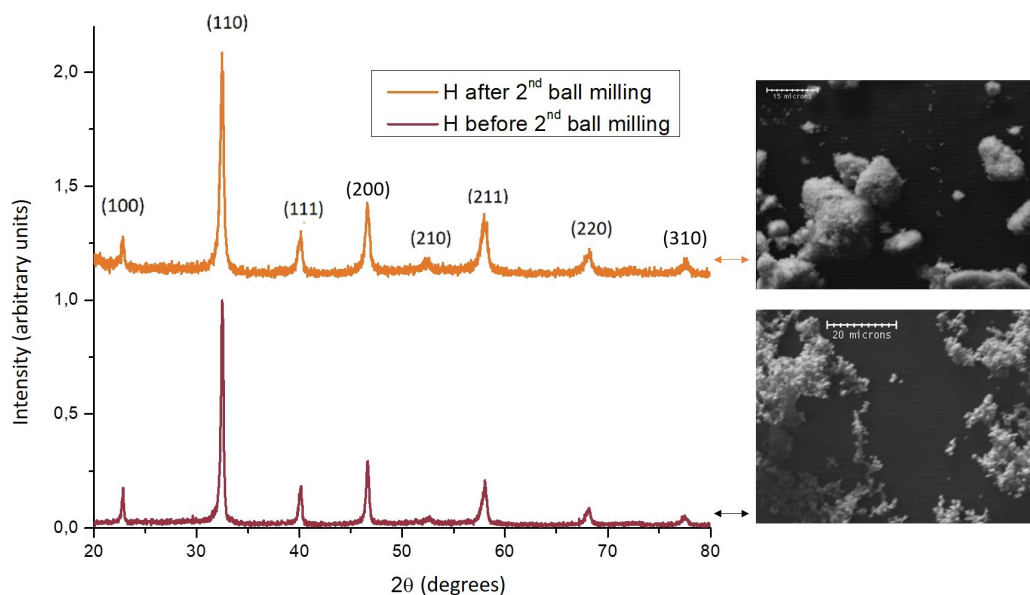


FIGURE 2.27: XRD and SEM analysis before and after the second ball milling with the 1mm-diameter balls (using dispersing agent, ethanol as a solvent and 250 rpm during four hours).

synthesis method, since it increases the final relative density of the samples without changing the micro-structure, nor the phase separation nor introducing oxygen vacancies that could have a negative effect on the material properties.

2.3.4.2 Influence of the pressure before sintering

The shaping of bulk ceramic samples is done by pressing the ball-milled powders into a pellet ("green body") in an 8 mm-diameter mold using a uniaxial oil press. About 8% of PVA has to be added as a binder, to avoid cracks during the pressing.

The applied uniaxial pressure was of two or three tons. After the first uniaxial press, an isostatic press was also used to increase the density of the green body samples. Following Exxelia's MLCC pressing parameters, the isostatic press was done at 40 MPa for five minutes, with a preheating at 65°C and a pressure ramp of 8 MPa/min.

The density of the samples "B", "C" and "D" the first one pressed uniaxially with two tons, the second one with three tons, and the third isostatically pressed were compared. The measured densities after sintering using ZrO₂ powder for three hours at 1050°C were 92%, 91.3%, and 92.6% respectively (the uncertainty is of 2.4%). So the increase in pressure during shaping does not increase significantly the relative density of the sintered sample. The two-ton pressure is sufficient to obtain the highest possible density after standard sintering.

In summary, the uniaxial shaping pressure of two tons was chosen because it is sufficient to obtain the highest possible density after standard sintering.

2.3.4.3 Influence of the sintering temperature

The influence of the sintering temperature on the final relative density is usually done using dilatometry. However, since the sintering of the NBT-BT requires a powder to create the sintering atmosphere to avoid evaporation of volatiles, (see 2.2.1.1), the dilatometry measurement is not appropriate.

The analysis of sintering temperature was done using different NBT-BT samples prepared from the same powder A (nominally stoichiometric, un-dried reactants, 250 rpm and 4 hours ball-millings, no dispersing agent, ethanol as solvent and coarse Na₂CO₃ reactant powder) and sintered at different temperatures.

The initial heating rate was 200°C/h and the initial cooling rate was 300°C/h. However,

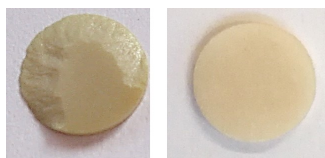


FIGURE 2.28: Crack on NBT-BT sample sintered at a heating rate of 200°C/h and a cooling rate of 300°C/h (left) and no crack on NBT-BT sample sintered at a heating rate of 120°C/h and a cooling rate of 200°C/h (right).

the samples sintered with those rates presented cracks, due to the fast temperature change (see Fig. 2.28). The heating rate was then changed to 120°C/h and the cooling rate to 200°C/h. The samples did not present cracks with those temperature rates, adopted for all the following sintering.

During the sintering heating, a 30-minute plateau at 800°C was used to eliminate the PVA added during pressing, other possibly present organic compounds and to guarantee the complete reaction (degradation of carbonates and formation of NBT-BT) [37].

The sintering temperature enabling a maximum density (of 94%) is 1150°C (see Fig. 2.19 p. 62). Comparing the XRD of those samples (see Fig. 2.29), reveals that the sample sintered at 1050°C (91% density) shows lower-intensity second-phase peaks compared to the

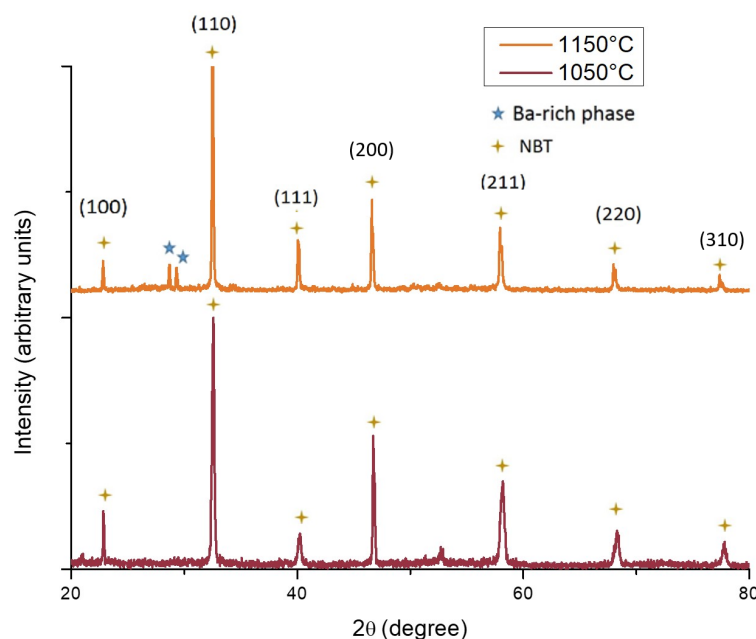


FIGURE 2.29: XRD diagram of the NBT-BT samples sintered on ZrO_2 for 3h at 1050 and 1150°C

sample sintered at 1050°C. This is because less second phases are formed in samples sintered at lower temperature, since the Na evaporation is decreased with decreasing sintering temperature.

In conclusion, the chosen temperature rates were 120°C/h for the heating, with a 30-minute plateau at 800°C to eliminate organics and complete the reaction, and 200°C/h for the cooling. The best sintering temperature in term of final relative density is 1150°C, but in terms of purity it is 1050°C. The temperature of 1050°C was chosen for the bulk NBT-BT samples.

2.3.4.4 Sintering atmosphere influence

The study of a new sintering atmosphere is crucial to allow the use of the NBT-BT in the industrial MLCC production (as explained in 2.2.1.1). In this work, three different sintering atmospheres were tested:

Open crucible

In order to verify the need of an atmosphere during traditional sintering, a sample was sintered in an open crucible for three hours at 1050°C. It was prepared with the following synthesis conditions : un-dried reactants, 250 rpm, and four hours for the first ball milling, no second ball milling, ethanol as a solvent, a nominal stoichiometric sample.

After sintering, crystal structure was characterized by XRD (Fig. 2.30).

There is only a minor NBT-BT formation in this sample. The major formed phase could not be identified. Hence, it is not ideal for NBT-BT synthesis.

Analyzing the dielectric properties of this sample (see Fig. 2.31), a relative permittivity of 340 and the dielectric losses of 44% were measured at 1MHz. This is also not ideal for the MLCC production due to the high dielectric losses compared to NBT-BT sintered in an atmosphere and to the industrial requirements (see section 1.3).

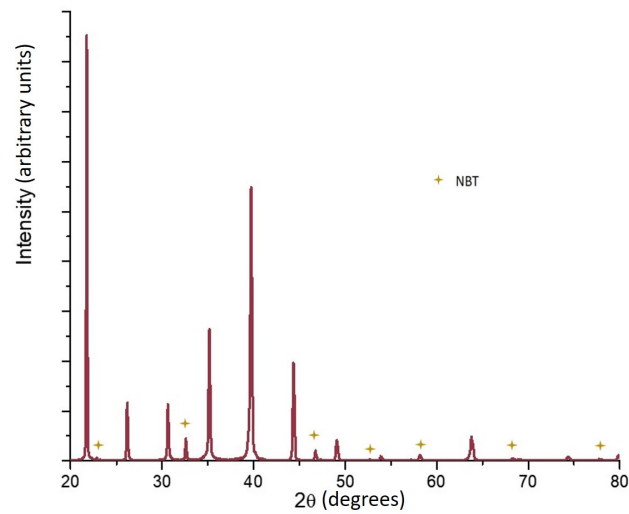


FIGURE 2.30: XRD diagram of the sample sintered in an opened crucible for 3h at 1050°C

The high dielectric losses and frequency dispersion can be explained by the bismuth and sodium evaporation that leads to the formation of a new non-identified, low permittivity, and high dielectric losses phase.

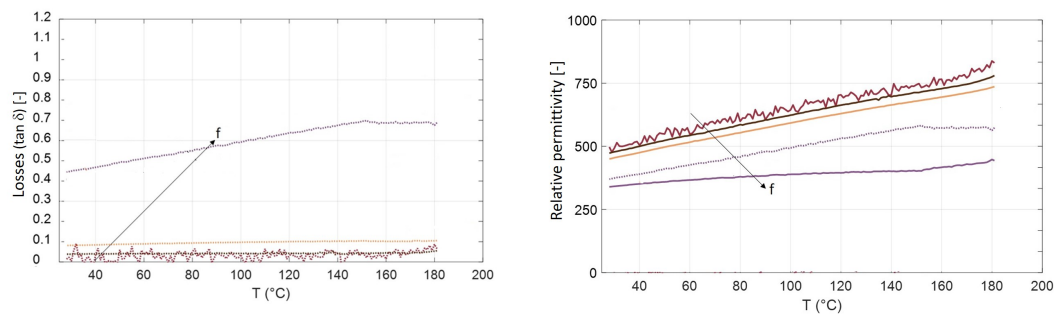


FIGURE 2.31: Dielectric properties of the NBT-BT sample sintered in an open crucible (left: $\tan \delta$, right: relative permittivity).

In conclusion, the use of an atmosphere powder during sintering is necessary for the NBT-BT formation.

BiO₂ + Na₂CO₃ and NBT

As explained in section 2.2.1.1, the sintering with the sample with the same composition powder (NBT-BT) is the most commonly used for the NBT-BT synthesis, due to the volatility of its components. However, there is a reaction between the sample and the powders used to create an atmosphere during sintering and slicing of the sample is necessary to obtain a clean surface. [37]

In order to test this sintering-atmosphere-creation method, an NBT sample was prepared with the same synthesis parameter as the sample sintered in an open crucible (un-dried reactants, 250 rpm and 4h for the first ball milling, no second ball milling, ethanol as a solvent and nominal stoichiometric).

Identical samples were sintered on pure NBT + ZrO₂ powder or on reactants mixture + ZrO₂ powders.

Only one ceramic could be recovered after sintering and without slicing off the surface, due to the reaction between the powder used to create the sintering atmosphere and the sample surface. Fig. 2.32 shows the inhomogeneous aspect of the inhomogeneous as-sintered sample.

The XRD measurement of this sample was done and is shown in Fig. 2.33 together with



FIGURE 2.32: Reaction between the sample surface and the atmosphere powder in NBT-BT sample sintered using NBT + ZrO₂ powder to create the sintering atmosphere at 1050°C resulting in an inhomogeneous sample surface.

the measurements of samples sintered on ZrO₂ and on open crucible NBT. Differently from sample sintered on open crucible, for the one sintered on NBT + ZrO₂, only peaks related to NBT-BT can be identified in the XRD, since the powder used to create the sintering atmosphere has a similar composition as the sample and the concentration of the second phase, if formed, is lower than the detection limit of the diffraction measurements.

Even though the XRD measurements indicate pure NBT-BT composition, the dielectric characterization of the sample could not be performed, due to the surface inhomogeneity.

Finally, creating a saturated atmosphere for sintering with powder of the same compo-

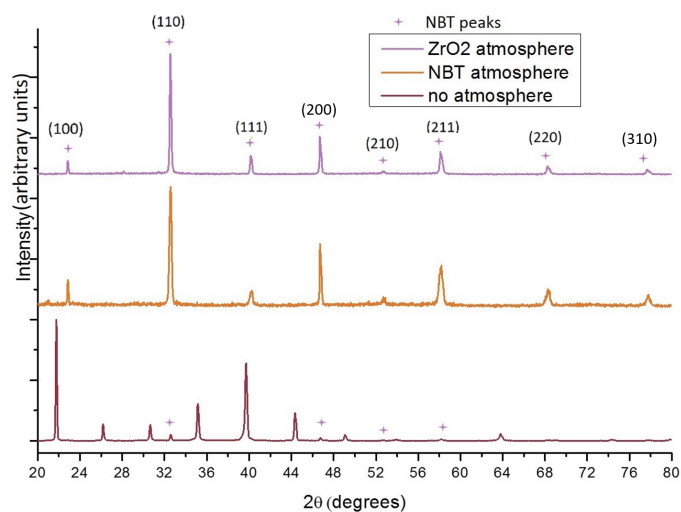


FIGURE 2.33: XRD diagram for the NBT-BT samples sintered at 1050°C during 3 hours using to create the sintering atmosphere: pure ZrO₂ powder, NBT + ZrO₂ powder and in open crucible.

sition as the green body would not be suitable for industrial MLCC production. The need to slice each sample would increase the production costs and would generate residues that are not ideal for the industry. Moreover, it would require the use of dedicated furnaces and crucibles, due to the high volatile concentrations during sintering. This would also imply higher production costs.

To summarize, it would not be practically possible to use a circular-saw to separate the sintered products, like in [37], during MLCC production. Moreover, this sintering atmosphere method would represent a cost increase for the industrial production. So, the sintering using an atmosphere created with powder of the same composition as the green body or with the reactants powder cannot be used industrially for the MLCC production and a new sintering atmosphere has to be devised.

ZrO₂

As explained in section 2.2.1.1, since the BiO₂ + Na₂CO₃ and NBT-BT powders cannot be used to create the sintering atmosphere and since the sintering in an opened crucible does not allow to obtain NBT or NBT-BT, a new sintering atmosphere had to be used, in order to obtain NBT-BT with low vacancies concentration and using an industrially adapted method.

The ZrO₂ powder was chosen to create the sintering atmosphere, since it is widely used in the industry and it is already used by Exxelia during sintering, due to its high melting point and low reactivity with other ceramic materials. So it can cover the sample, confining it, with little, if any, chemical influence.

The sintering using ZrO₂ powder was done and promising results were obtained, as explained by the dielectric properties of the material (see section 3.2.2.1), specially for sample "U".

The influence of the ZrO₂ powder on the formation and on the composition of the secondary Ba-containing phases is explained in section 2.4.

The XRD measurement of the sample "H" is presented as an example in Fig. 2.34. It can be seen that the as-sintered material presents extra peaks coming from the secondary Ba-containing phases and from the ZrO₂ powder. However, the peaks from the secondary Ba-containing phases and from the ZrO₂ powder disappear in the polished and strain-relaxed sample. Both show a pseudo-cubic phase, characteristic of unpoled relaxors. Finally, a skin effect is responsible for the peak enlargement on the poled and strain-relaxed samples (see section 2.3.2.2). However, it does not affect the dielectric properties.

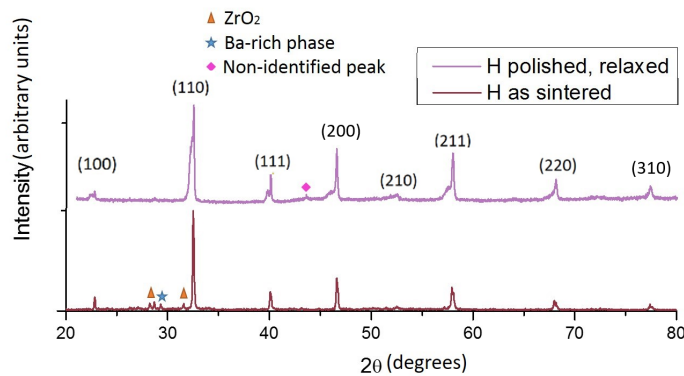


FIGURE 2.34: XRD measurement of sample "H" as-sintered and after polishing and strain relaxation (same data as in Fig. 2.10)

In conclusion, even if the use of a ZrO_2 powder to create the sintering atmosphere increases the formation of the secondary Ba-containing phases at the surface, the final samples sintered using this atmosphere present promising dielectric properties for high-temperature MLCCs. The samples present a pseudo-cubic structure, with no ZrO_2 or secondary Ba-containing phases peaks after polishing. A skin effect is responsible for the enlargement of the XRD peaks of the poled and strain-relaxed samples, but it does not affect the final ceramic sample properties.

2.4 Phase separation and secondary Ba-containing phases formation

The secondary Ba-containing phases separation is present in almost every sample of Table 2.11 p. 79, except for samples "Y", "Z", "Open crucible" and "NBT atm". These secondary phases can be considered as a conducting phase in an insulating matrix. For this reason, they affect considerably the dielectric properties of the samples (see section 3.2.1.2).

This section explains the secondary Ba-containing phases formation and it identifies the phase compositions. Details on the synthesis parameters affecting the phase formation (average grain surface and volume fraction) and the corresponding effects on the dielectric properties will be shown in section 3.2.1.2.

2.4.1 Phase formation and identification

Yang *et al.* showed that, contrary to the Bi evaporation that is compensated through the formation of defects, the Na evaporation creates secondary Ba-containing phases in the case of the NBT-BT (see section 3.2.1.1). [78] So the secondary Ba-containing phases formation is due to the Na evaporation during synthesis.

A similar phase separation is reported by Otoničar *et al.* (2010) for samples of $(Na_{1-x}K_x)_{0.5}Bi_{0.5}TiO_3$, where the secondary phase is composed of $K_2Ti_6O_{13}$. [50]

Pure NBT also has a phase separation that can be observed by the XRD of the as-sintered samples (Fig. 2.35). Similarly to NBT-BT, the phase separation in pure NBT is due to the Na evaporation. However, differently from the secondary Ba-containing phases formed in NBT-BT, the formed phase in pure NBT is a Ti-rich phase without Ba. The XRD analysis indicates that the formed Ti-rich phase in pure NBT is TiO_2 .

Fig. 2.23 p. 65 and 2.24 p. 65 show the Raman spectra of the pure NBT powder after calcination and after second ball-milling. Since no difference was found between the multiple Raman measurements, it can be concluded that the powders are homogeneous and, so, that there is no phase separation during calcination. This indicates that the Ti-rich phase separation and the Na and Bi evaporation happen during sintering for the pure NBT. It can be assumed that the same happens for NBT-BT and that the secondary Ba-containing phases separation takes place during sintering as well.

To identify the secondary Ba-containing phases, XRD and EDS analyses were performed on all samples. Figures 2.36 and 2.37 present the XRD measurements for the as-sintered samples "H" and "U" with the peak identification detail. For all samples, three possible secondary Ba-containing phases were identified: Ba_2TiO_4 , $Ba_2Ti_9O_{20}$ and $Ba_2Ti_9O_{20} \cdot 2BaO \cdot TiO_2$. Table 2.10 presents the EDS measurement results for the average Ba-containing phases. The stoichiometry is close to $Ba_2Ti_9O_{20}$, with extra Ba. This indicates that the main secondary Ba-containing phase formed is $Ba_2Ti_9O_{20}$. However, there is a decomposition of this phase to Ba_2TiO_4 and $2BaO \cdot TiO_2$, increasing the Ba/Ti ratio in the average secondary Ba-containing

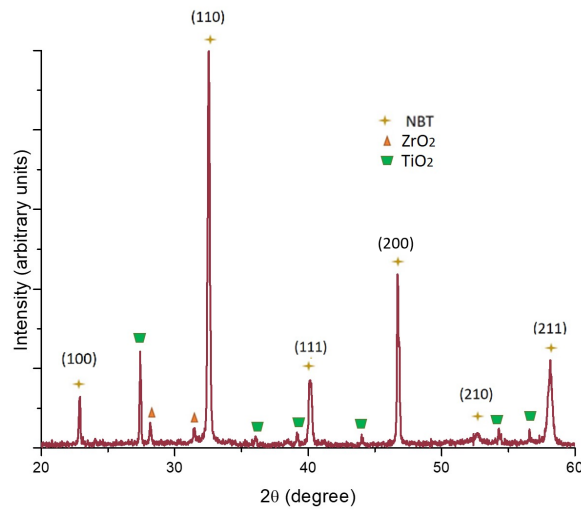


FIGURE 2.35: XRD analysis of the as-sintered pure NBT sample, indicating a TiO_2 phase separation.

phases.

Sample	O	Na	Ti	Ba	Bi	Zr
"E"	18.74 (1.87)	0.22 (0.02)	9.0	3.32 (0.33)	0.02 (<0.01)	0.28 (0.01)
"G"	20.64 (2.06)	0.02 (<0.01)	9.0	4.18 (0.42)	0.01 (<0.01)	0.03 (<0.01)
"I"	18.43 (1.84)	-	9.0	3.41 (0.34)	-	-
"P"	18.05 (1.80)	0.02 (<0.01)	9.0	3.38 (0.34)	0.01 (<0.01)	0.16 (0.01)
"U"	18.59 (1.86)	-	9.0	3.49 (0.35)	-	0.02 (<0.01)

TABLE 2.10: Secondary Ba-containing phases average composition measured via EDS considering a 9.0 stoichiometry for the Ti for samples "E", "G", "I", "P" and "U". The uncertainties are indicated in brackets.

2.4.1.1 ZrO_2 influence in secondary Ba-containing phases formation

The secondary Ba-containing phases formation is more pronounced at the sample's surface when compared to its core (up to a thickness of 20 to $30\mu\text{m}$). This means that the volume fraction and the grain surface of the secondary Ba-containing phases are larger at the surface. This can be observed in Fig. 2.38. This can be explained by the Na evaporation being more important at the surface, when compared to the core of a sample.

However, there is another factor affecting the secondary Ba-containing phases formation apart from the Na evaporation. Figures 2.39 and 2.40 show the secondary Ba-containing phases formation and concentration close to a YSZ (Y-doped ZrO_2) 1mm-diameter ball attached to the sample's surface and sintered together with this sample. The secondary Ba-containing phases average grain surface and concentration are larger close to the interface between the sample and the YSZ ball. This indicates that the ZrO_2 from the YSZ ball favours the secondary Ba-containing phases formation. The same effect should also be observed for interface between the ZrO_2 powder (used to create the sintering atmosphere) and the sample's surface. So, the contact between the ZrO_2 powder used to create the sintering atmosphere and the sample's surface as well as the Na evaporation are responsible for the second phase formation and for its higher concentration on the sample's surface compared to the core, as

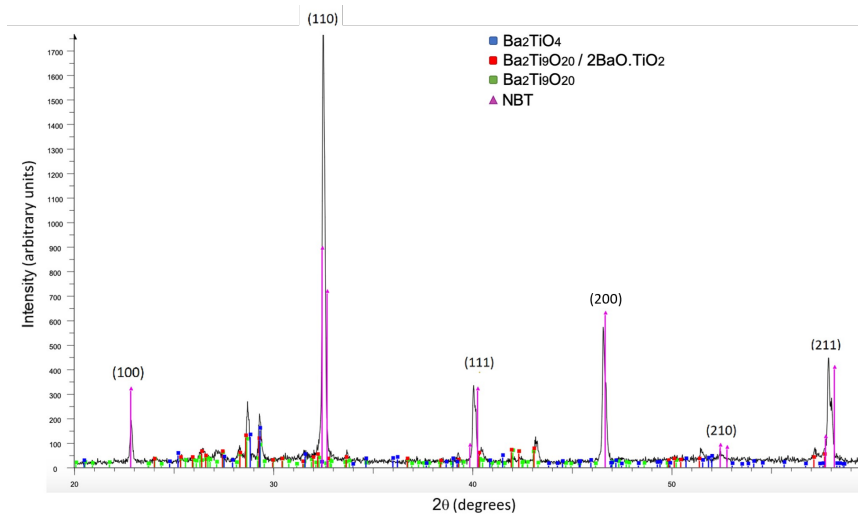


FIGURE 2.36: XRD measurement of the as-sintered sample "H" with the peaks identification details.

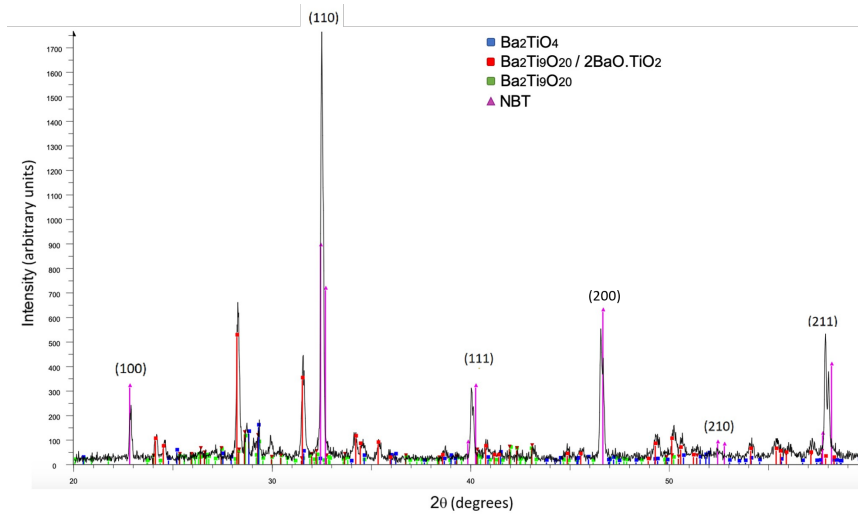


FIGURE 2.37: XRD measurement of the as-sintered sample "U" with the peaks identification details.

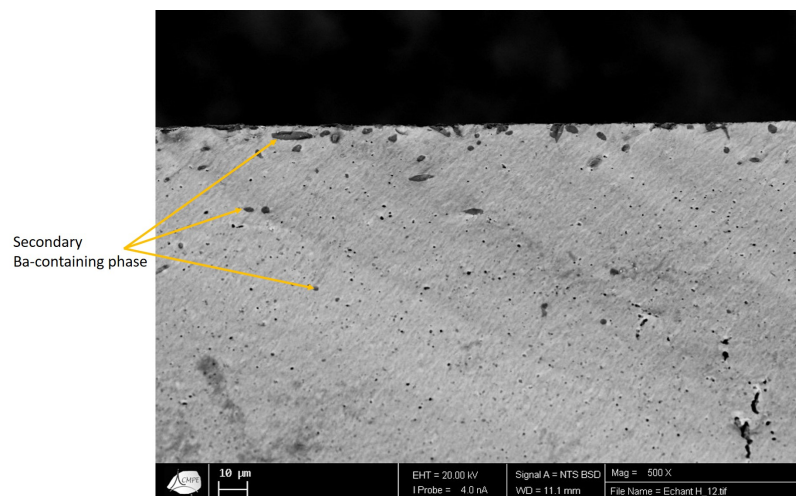


FIGURE 2.38: SEM cross-section image of the sample "H" showing the secondary Ba-containing phases concentration at the sample's surface.

seen in Fig. 2.38 p. 74

Formation of pure $\text{Ba}_2\text{Ti}_9\text{O}_{20}$ is difficult, since stress accumulates during phase growth.

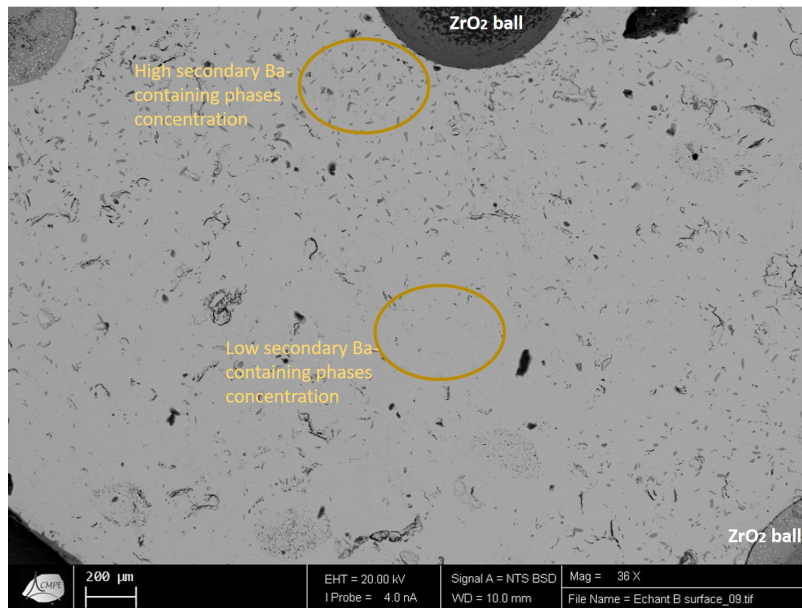


FIGURE 2.39: SEM image of the secondary Ba-containing phases concentration close to a YSZ 1 mm diameter ball attached to the "B" sample surface during sintering (YSZ ball not removed before measurement).

This stress results in a high potential-energy barrier. Zhou *et al.* showed that ZrO_2 doping can create defects, decreasing the stress and favouring the $\text{Ba}_2\text{Ti}_9\text{O}_{20}$ formation. [88]

Even though the $\text{Ba}_2\text{Ti}_9\text{O}_{20}$ phase is favoured by the contact with ZrO_2 (either from YSZ balls or from the ZrO_2 powder used to create the sintering atmosphere), the resulting secondary Ba-containing phases are not a single phase, as seen from the differences in stoichiometry measured by EDS (see Table 2.10 p. 73). $\text{Ba}_2\text{Ti}_9\text{O}_{20}$ can decompose into different Ba-Ti-O compositions with different stoichiometries, depending on the synthesis conditions, including Ba_2TiO_4 and $\text{Ba}_2\text{Ti}_9\text{O}_{20}/2\text{BaO}\cdot\text{TiO}_2$.

2.5 Conclusion and sample synthesis conditions

This chapter discussed different synthesis method and parameters, to determine the best synthesis conditions for the NBT-BT, considering Exxelia's requirements.

The synthesis methods is composed of the method used to obtain the NBT-BT powder and to shape and sinter the material.

Initially, two different syntheses of the NBT-BT powder were analyzed, the sol-gel and the solid-state synthesis. Considering the industrial limitations and the expected properties of the final material, the solid-state synthesis was chosen.

Three sintering methods were then analyzed: the microwave, the SPS, and the traditional sintering methods. The microwave sintering would require a change in the furnaces and it would not allow the co-sintering of the ceramics with the electrodes. The SPS sintering is an expensive and energy-consuming method and it requires reducing atmosphere, increasing the vacancy formation in the final ceramics. So the traditional sintering method was chosen.

However, the traditional synthesis uses a way to create a sintering atmosphere that is not compatible with industrial processing. So, a novel method had to be designed.

Finally, three different methods for controlling the atmosphere during sintering and

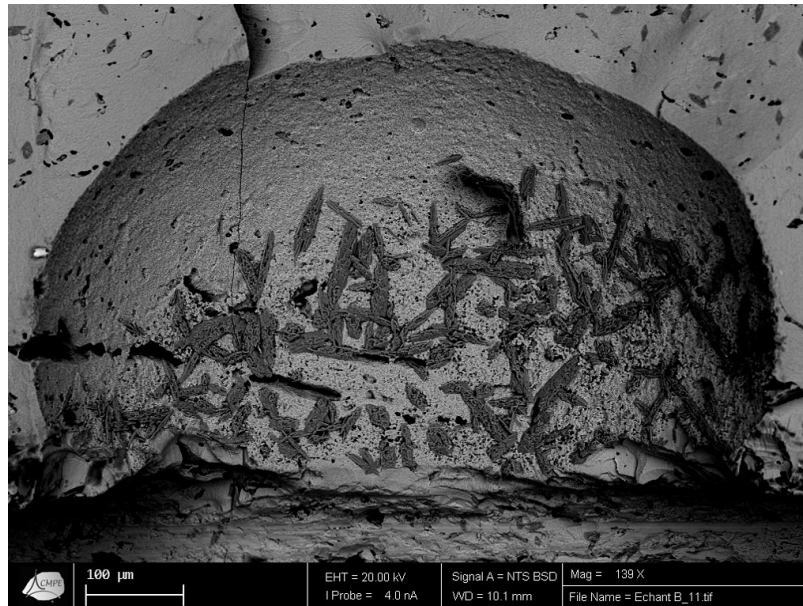


FIGURE 2.40: SEM image of the secondary Ba-containing phases concentration close to a YSZ 1 mm-diameter ball attached to the "B" sample surface during sintering (YSZ ball removed before measurement).

avoiding the evaporation of volatiles were analysed and tested: the sintering in air (atmosphere not controlled), the sintering using a powder of NBT or reactants + ZrO_2 to create the sintering atmosphere and the sintering using pure ZrO_2 powder. The first method resulted mainly in a material that is not NBT-BT and the second one needed post-sintering treatment other than polishing, to obtain a clean surface. So the sintering using ZrO_2 powder was chosen to control the sintering atmosphere.

The shaping of the ceramic layers was done through tape casting, since it is the only available method for Exxelia's synthesis of MLCCs.

Once the synthesis method is chosen, several parameters remain to be analyzed and optimized. In this study the considered parameters were:

- the weighing and drying of the reactants,
- the material of the ball-milling jars and balls,
- the size of the ball-milling balls,
- the ball-milling speed, time, and solvent,
- the grain size of the starting powders,
- the reactants stoichiometry (or nominal stoichiometry),
- the use of a second ball milling after calcination,
- the shaping of the bulk samples (uniaxial or isostatic pressure and their values),
- the powder used to create the sintering, atmosphere,
- the sintering temperature program for the bulk samples,
- the slurry composition and sintering conditions for the tape-casted samples.

The drying of the hygroscopic reactants intensifies the effects of the ball-milling energy, creating large grain surfaces of secondary Ba-containing phases for 250 rpm and 4h ball-milling and large volume fraction of small grain surface secondary Ba-containing phases for 350 rpm and 8h ball milling.

Two different ball-milling jars and balls material were tested: the tungsten carbide (WC) and the Yttrium-stabilized zirconia (YSZ). The ball milling with WC jars resulted in a contamination of the material with tungsten and in a high conductivity and dielectric losses. Using the YSZ jars and balls and the ZrO_2 powder to cover the sample during sintering, the final material showed some ZrO_2 contamination at the surface, that could be removed through polishing.

A skin effect at the sample's surface after polishing and strain relaxation was observed by the low-angle-side peaks on the XRD diagrams. This skin effect creates a phase coexistence (tetragonal, rhombohedral and cubic). It is not present in the as-sintered samples, due to the lower effect of the Ba at the surface (lower local concentration of Ba in the NBT lattice). This variation in the local concentration is due to the formation of secondary Ba-containing phases and concentration of these phases at the sample's surface.

All the samples showed the separation of secondary Ba-containing phases, due to the Na evaporation during sintering. These phases were identified as a mixture of Ba_2TiO_4 , the $Ba_2Ti_9O_{20}$, and the $Ba_2Ti_9O_{20} \cdot 2BaO \cdot TiO_2$. They concentrate in the sample's surface due the higher Na evaporation and also because the ZrO_2 favours the formation of $Ba_2Ti_9O_{20}$.

Two ball-milling solvents were also tested: pure ethanol and a mixture of ethanol and methyl-ethyl-ketone (MEK). However, the change in the solvent did not affected the structure and phase separation of the NBT-BT samples. A similar result is found when changing the Na_2CO_3 reactant grain size.

The speed and duration of ball-milling were also investigated with a ball-milling at 250 rpm for 4h and another at 350 rpm for 8h. The effects of ball milling were evident in the samples ball-milled without the use of dispersing agent, when the increase in the energy resulted in a smaller grain surface and higher volume fraction of the secondary Ba-containing phases. This effect is not observed for the samples ball-milled with the use of a dispersing agent.

Also, in relation to the ball-milling parameters, the use of a second ball-milling after calcination was tested as well, to increase the final density of the samples. The higher relative density for the samples with no second ball-milling was 91.5% vs 93.5% for the sample prepared with a second ball-milling. The maximum densities were achieved in both cases for the sintering at 1150°C for 3h. The temperature ramps used were 120°C/h for the heating and 200°C/h for the cooling, to avoid cracks during sintering.

Two ball sizes were tested for the second ball-milling: 1mm-diameter and 10mm-diameter balls. The 1mm-diameter balls were chosen, since it increases the relative density of the material without changing the micro-structure and phase separation, and without introducing oxygen vacancies.

Finally, the nominal (or reactant) stoichiometry changes of Na and Bi were also studied. The Na/Bi ratio proved having an important effect on the sample's final composition (after sintering) and properties, with no change in its structure. The increase in the Bi and Na concentrations decreased the secondary Ba-containing phases volume fraction and samples without phase separation could be obtained from samples with Na and Bi excess. The decrease in the Na/Bi ratio created a matrix with the 10% (atomic) of Bi, as expected for the stoichiometric NBT, and a separation of the bismuth excess in a Bi-rich phase concentrated in the sample's core. This resulted in important changes in the dielectric properties, reported in Chapter 3.

The last tested parameters were used for the tape casting of the NBT-BT. The second ball-milling parameters and the slurry compositions in this case were obtained by comparing

the ones used by Exxelia and a slurry optimization reported for the NBT-BT. However, further optimization should still be done.

A summary of the synthesis conditions of all the samples used for this study is shown in Table 2.11 p. 79 .

Sample	Dried reactants	Jar	First ball-milling	Solvent	Dispersing agent	Second ball-milling	Na ₂ CO ₃ grain size	Pressure and Sintering atmosphere	Sintering temperature (°C)	Stoichiometry of reactants
"Open crucible"	No	YSZ	250 rpm - 4h	Ethanol	No	-	Coarse	2t / -	1050	NBT - 6%BT stoichiometric
"NBT atm"	No	YSZ	250 rpm - 4h	Ethanol	No	-	Coarse	2t / NBT	1050	NBT - 6%BT stoichiometric
"Density 1"	No	YSZ	250 rpm - 4h	Ethanol	No	-	Coarse	2t / ZrO ₂	1050 to 1200	NBT - 6%BT stoichiometric
"Density 2"	No	YSZ	250 rpm - 4h	Ethanol	No	250 rpm - 4h	Coarse	2t / ZrO ₂	1050 to 1200	NBT - 6%BT stoichiometric
"B"	Yes	YSZ	250 rpm - 4h	Ethanol	No	250 rpm - 4h	Coarse	2t / ZrO ₂	1050	NBT - 6%BT stoichiometric
"C"	Yes	YSZ	250 rpm - 4h	Ethanol	No	250 rpm - 4h	Coarse	3t / ZrO ₂	1050	NBT - 6%BT stoichiometric
"D"	Yes	YSZ	250 rpm - 4h	Ethanol	No	250 rpm - 4h	Coarse	isostatic 40 MPa / ZrO ₂	1050	NBT - 6%BT stoichiometric
"E"	Yes	YSZ	350 rpm - 8h	Ethanol	No	350 rpm - 8h	Coarse	2t / ZrO ₂	1050	NBT - 6%BT stoichiometric
"G"	Yes	YSZ	250 rpm - 4h	Ethanol	Yes	250 rpm - 4h	Coarse	2t / ZrO ₂	1050	NBT - 6%BT stoichiometric
"H"	No	YSZ	250 rpm - 4h	Ethanol	Yes	250 rpm - 4h	Coarse	2t / ZrO ₂	1050	NBT - 6%BT stoichiometric
"I"	No	YSZ	250 rpm - 4h	Ethanol	Yes	250 rpm - 4h	Coarse	2t / ZrO ₂	1050	NBT - 6%BT stoichiometric
"N"	No	YSZ	250 rpm - 4h	MEK+Ethanol	Yes	250 rpm - 4h	Fin	2t / ZrO ₂	1050	NBT - 6%BT stoichiometric
"P"	No	YSZ	350 rpm - 8h	MEK+Ethanol	Yes	350 rpm - 8h	Fin	2t / ZrO ₂	1050	NBT - 6%BT stoichiometric
"U"	No	YSZ	350 rpm - 8h	MEK+Ethanol	Yes	350 rpm - 8h	Fin	2t / ZrO ₂	1050	Na _{0.44} Bi _{0.48} Ba _{0.06} TiO ₃
"U WC"	No	WC	350 rpm - 8h	MEK+Ethanol	Yes	350 rpm - 8h	Fin	2t / ZrO ₂	1050	Na _{0.44} Bi _{0.48} Ba _{0.06} TiO ₃
"V"	No	YSZ	250 rpm - 4h	Ethanol	Yes	250 rpm - 4h	Fin	2t / ZrO ₂	1050	NBT - 6%BT stoichiometric
"X"	No	YSZ	250 rpm - 4h	MEK+Ethanol / Ethanol	Yes	250 rpm - 4h	Fin	2t / ZrO ₂	1050	NBT - 6%BT stoichiometric
"Y"	No	YSZ	350 rpm - 8h	MEK+Ethanol	Yes	350 rpm - 8h	Fin	2t / ZrO ₂	1050	Na _{0.489} Bi _{0.489} Ba _{0.06} TiO ₃
"Z"	No	YSZ	350 rpm - 8h	MEK+Ethanol	Yes	350 rpm - 8h	Fin	2t / ZrO ₂	1050	Na _{0.56} Bi _{0.48} Ba _{0.06} TiO ₃

TABLE 2.11: Synthesis parameters for selected bulk ceramic samples.

Chapter 3

Dielectric characterization and compatibility with industrial requirements

The objective of this chapter is to present the results of the dielectric characterizations and to compare them with Exxelia's specifications. Together with Chapter 2, the results presented here enable to determine the synthesis parameters needed to obtain a material meeting these specifications.

In the first part, the experimental setups, the model to calculate the complex permittivity, and the associated uncertainties will be presented.

The second part will show the dielectric and insulation properties in temperature and discuss the influence of the various synthesis parameters, and the secondary Ba-containing phases formation in these properties. The compatibility of the properties with Exxelia's requirements will be presented afterwards.

The third part will present the dielectric spectroscopy results for the various samples and the influence of the secondary Ba-containing phases, the relaxor character and the conductivity on the dielectric properties.

Finally, the influence of small additions of Co and Mn on the dielectric properties will be discussed.

3.1 Models for dielectric properties calculations and uncertainties

In this section, the measurement setup, the properties estimation model, the temperature corrections, and the measurement uncertainties will be presented.

It is important to know the details of the measurement setup, since they can influence the measured temperatures and increase the uncertainties in the impedance measurements. For this reason, error estimations are also needed to guarantee better result interpretations.

3.1.1 Description of electrical measurements: impedance spectroscopy and insulation resistance

The dielectric (impedance) measurements were carried out on unpoled, polished and strain-relaxed samples, with an impedancemeter connected to a temperature controlled Linkam THMS600 operating in a temperature range between -196°C and 600°C. In this Linkam, the temperature control is accomplished by heating or cooling a platinum support under the sample that is grounded electrically. The electric insulation of the sample from the heating device

is done using a thin glass plate. Finally, the temperature is measured by a thermocouple installed close to the heating device. The picture of the measurement device is presented in Fig. 3.1.

The measurements give the complex impedance (norm and argument) as a function



FIGURE 3.1: Picture of the impedance measurement device (Linkam).

of temperature and were done using a Hioki 3570 impedancemeter operating in a frequency range between 5Hz and 5MHz and capable of measuring impedance between 100mΩ and 100MΩ. A RC model was adopted and will be further explained, in order to obtain the real and imaginary permittivity values.

The insulation resistance measurements were done *after* the permittivity measurements, to perform the latter on unpoled samples. Industrial standards were used, so the measurements were carried out using direct current by applying a direct voltage of 50V and by measuring the bulk sample resistance initially for 30 seconds. Since the 30s-measurement was not enough to saturate the sample, the DC was re-applied during 30 seconds and the resistance measurement and the insulation resistance calculations were done. So the presented values correspond to the insulation resistance at one minute.

The performed measurement gives a set of internal resistance vs temperature values for each sample. This measured resistance represents the ratio between the applied voltage and the leakage current after a fixed time when a DC is applied. The value of the fixed time should be higher than to charging time of the capacitor, so that only the leakage current is measured.[7]

Using this resistance value, the resistivity of the sample can be calculated from equation 3.1. The insulation resistance corresponds to the product of the calculated resistivity by its corresponding permittivity at the same temperature (or to the product of the resistance and the capacitance), as shown in equation 3.2. So the insulation resistance represents the time constant of the capacitor, which is the time that a charged capacitor in an opened circuit will take to drop to the value of 1/e of its initial charge (around 36.8% of it) through the internal resistance. [6]

$$\rho = R_{internal} \cdot \frac{A}{e} \quad (3.1)$$

$$IR = \rho(T) \cdot \epsilon_r(T) \cdot \epsilon_0 = R_{internal}(T) \cdot C(T) \quad (3.2)$$

where $R_{internal}$ is the internal resistance measured, A in the sample's surface, e is the sample's thickness, IR is the insulation resistance and ρ is the resistivity. Due to equipment restrictions, the measurements were performed up to a maximum temperature of 200°C. For the higher temperature values, the curve was extrapolated supposing an exponential decrease, as it normally happens for dielectric materials at high temperature.

3.1.2 RC model for permittivity and dielectric losses

The parallel RC model was used to estimate the real and imaginary parts of the permittivity, as represented in Fig. 3.2. Since the material is a dielectric with losses, the permittivity is:

$$\epsilon_r^*(f) = \epsilon_r' - j \cdot \epsilon_r'' \quad (3.3)$$

In this model, the real and imaginary parts of the permittivity read:

$$\epsilon_r'(f) = \frac{1}{\epsilon_0} \cdot \frac{\text{Im}\left(\frac{1}{Z^*(f)}\right)}{2\pi f} \cdot \frac{e}{A} \quad (3.4)$$

$$\epsilon_r''(f) = \frac{\text{Re}\left(\frac{1}{Z^*(f)}\right)}{2\pi f} \cdot \frac{e}{A} \quad (3.5)$$

$$\tan \delta(f) = \frac{\epsilon_r''(f)}{\epsilon_r'(f)} \quad (3.6)$$

$$C^*(f) = \frac{(\epsilon_r'(f) - j \cdot \epsilon_r''(f)) \cdot A \cdot \epsilon_0}{e} \quad (3.7)$$

$$\text{Re}(\sigma^*) = \sigma(f) = \text{Re}\left(\frac{1}{Z^*(f)}\right) \cdot \frac{e}{A} = \omega \cdot \epsilon_r''(f) \quad (3.8)$$

where σ is the sample resistivity, C^* is the sample complex capacitance, f is the fre-

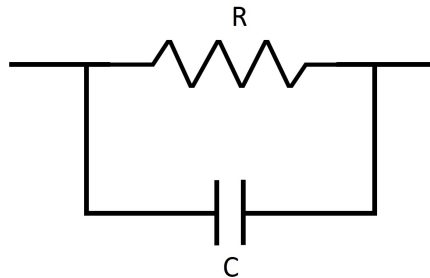


FIGURE 3.2: RC model used for the permittivity calculation from the measured system impedance

quency of the AC applied during measurement, e is the sample thickness, A is the sample surface, ϵ_0 is the vacuum permittivity, Z^* is the complex impedance, Re is the real part of the

complex number and Im is the imaginary part of the complex number.

3.1.2.1 RC model validation

Graphic impedance

In order to verify that this model is adapted for our measurements and to confirm that the cables and the measurement device do not influence significantly the measurements after calibration, the impedance versus the frequency (f) are plotted in Fig. 3.4 and 3.5.

From a more general the RC model like the one shown in Fig. 3.3 that takes into account the resistance and the capacitance of the cables and the setup, the impedance reads:

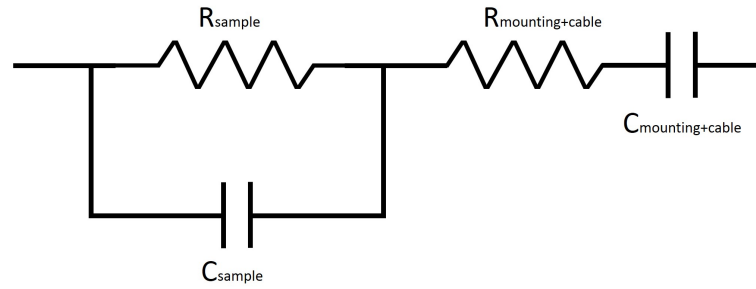


FIGURE 3.3: RC model circuit considering the influence of the cables and the setup to calculate the dielectric properties from the measured impedance

$$Z^* = \frac{R_{sample}}{1 + R_{sample} \cdot j \cdot 2\pi f \cdot C_{sample}} + R_{setup} + j \cdot 2\pi f \cdot C_{setup} \quad (3.9)$$

So, for high frequencies in a system where the setup affects the measurements results, the $\lim_{f \rightarrow \infty} Z^*(2\pi f)$ is $R_{setup} + j \cdot 2\pi f \cdot C_{setup}$, so the imaginary part of the impedance tends to infinite if there is an effect of the setup capacitance. For low frequencies in the same systems, the $\lim_{f \rightarrow 0} Z^*(2\pi f)$ is $R_{sample} + R_{setup}$. So, for systems where the setup resistance affects the measurements, the value of $Re(Z^*)$ for high frequencies should be negligible compared to the value of $Re(Z^*)$ for low frequencies.

Analyzing Figures 3.4 and 3.5 that shows the real and imaginary part of the complex impedance $Re(Z^*)$ for sample "H" respectively, it can be seen that, for high frequencies, the $Im(Z^*)$ values tend toward zero and the value of $Re(Z^*)$ tends to a constant value lower than 250Ω , a lot smaller than the $Re(Z^*)$ in low frequencies. This means that C_{setup} is negligible and R_{setup} is small when compared to the R_{sample} , seen in the Z value when $f \rightarrow 0$ (over $30k\Omega$). A similar behaviour is found for the other NBT-BT samples. So the RC model adopted is valid for these measurements.

3.1.3 Bruggeman model [2, 28]

Since the NBT-BT samples have different values of relative density (see section 2.3.4.1), being all significantly lower than the fully dense material, it is interesting to consider a model that can take the density effects into account. This is important to be able to compare better the intrinsic properties of the materials, regardless of their relative density.

Bruggeman's model was developed to determine the properties of 3-0 composites from

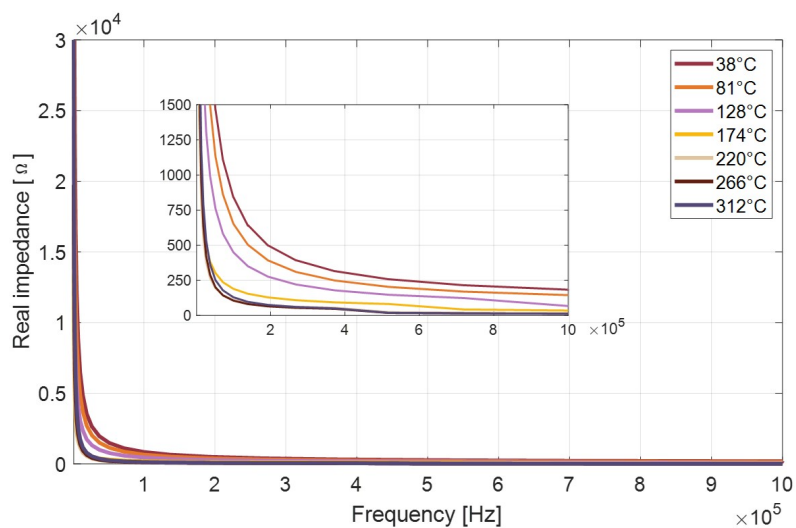


FIGURE 3.4: Real part of the complex impedance module $\text{Re}(Z^*)$ vs frequency for sample "H". The inset shows the low impedance values.

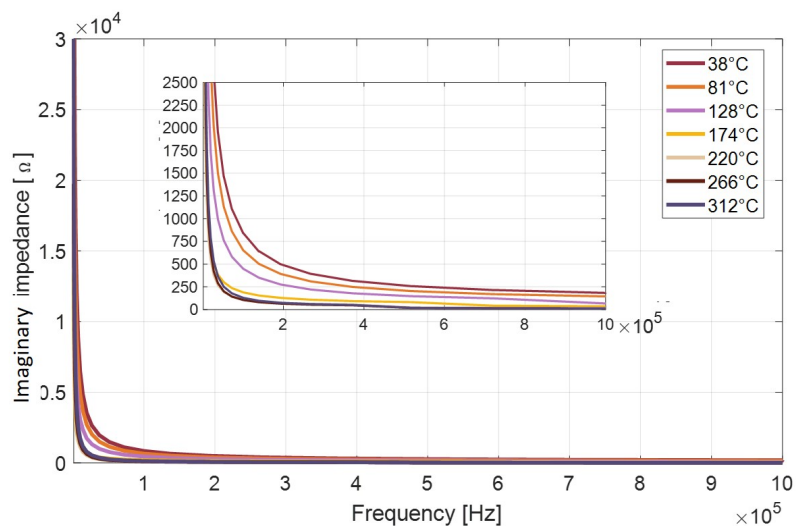


FIGURE 3.5: Imaginary part of the complex impedance module $\text{Im}(Z^*)$ vs frequency for sample "H". The inset shows the low impedance values.

the properties of their constituents and their proportions (see section 3.2.1.2). As a single-phase ceramic but with a density less than 100% can be considered as a ceramic-air composite, the Bruggeman model can be used to estimate the permittivity and the dielectric losses for theoretical samples having 100% density. This would be important for comparing the dielectric properties of samples without taking into account the density effect in the dielectric properties.

The complex permittivity for the 100% density material can be calculated as[2]:

$$\varepsilon_i^* = \frac{2\varepsilon_{eff}^* \cdot \frac{1-f}{f} \cdot \frac{\varepsilon_e^* - \varepsilon_{eff}^*}{\varepsilon_e^* + 2\varepsilon_{eff}^*} + \varepsilon_{eff}^*}{1 + \left(\frac{\varepsilon_e^* - \varepsilon_{eff}^*}{\varepsilon_e^* + 2\varepsilon_{eff}^*} \cdot \frac{1-f}{f} \right)} \quad (3.10)$$

where ε_i^* is the complex permittivity of the 100% density material, ε_{eff}^* is the effective (measured) complex permittivity, f is the volume fraction of ceramic in the material (relative density) and ε_e^* is permittivity of the air ($1.0006 \cdot \varepsilon_0$).

The relative permittivity for fully-dense material can be calculated from the real part of $\varepsilon_i^*/\varepsilon_0$ and the dielectric losses can be calculated from the imaginary part of $\varepsilon_i^*/\varepsilon_0$ divided by its real part.

However, this model supposes an isotropic and homogeneous medium and spherical particles of both phases of the composite (in this approximation, spherical ceramic grains and spherical pores) with a size of the "inclusions" larger than the distance between them. [28]

As it can be seen in Fig. 2.8 p. 50, for example, these conditions are not met by my NBT-BT samples. So the values estimated for samples with a 100% density would not be reliable. Moreover, for the MLCC production, the most interesting properties are the ones directly measured in the prepared samples (ε_{eff}) and not the theoretical 100% density material properties. So the Bruggeman model and the 100% density properties were not used to compare the dielectric properties of the samples in this study.

3.1.4 Estimation of measurement uncertainties

The uncertainties and the measurement noise estimations are necessary to guarantee a better interpretation of the measured dielectric properties. In the impedance measurement, variations may be created by the faulty electric contacts due to the cables linking the Linkam to the impedance measurement setup.

The measurement noise was estimated from the "U" sample measurements, with the synthesis parameters specified in Table 2.11 p. 79. Two measurements were performed at different times for this sample. For the first one, the permittivity and the dielectric losses ($\tan \delta$) values at room temperature and at T_m are indicated in Table 3.1. For the second one, the measurement values follow two different curves "jumping" from one to the other as temperature is changed, depending on the electric contact between the Linkam and the impedance measurement setup. The permittivity and the dielectric losses values of both curves for the second measurement are indicated in Table 3.1 (as curve 1 and curve 2).

These "jumps" were used to evaluate the noise on the dielectric measurement.

The relative permittivity value for this sample can be described as $\varepsilon_r = 1300 \pm 160$ at 50°C and $\varepsilon_r = 2700 \pm 550$ at T_m . So the noise on the measured relative permittivity value is around 12% at 50°C and 13% at T_m . So a 13% noise estimation was taken for the relative permittivity for all the samples.

The dielectric losses values for this sample are $\tan \delta = 10.7 \pm 0.9\%$ at 50°C and $\tan \delta = 3.4 \pm 0.5\%$ at T_m . So the noise on the dielectric losses value is around 7.5% at 50°C and 14% at T_m . So a 14% noise estimation was taken for the dielectric losses for all the samples.

Fig. 3.6 shows the permittivity and the dielectric losses for the "U" sample and for the two consecutive measurements, the second one following two different curves, as mentioned before, depending on the electric contact.

To compare the noise estimation with the uncertainty of the dielectric properties, a

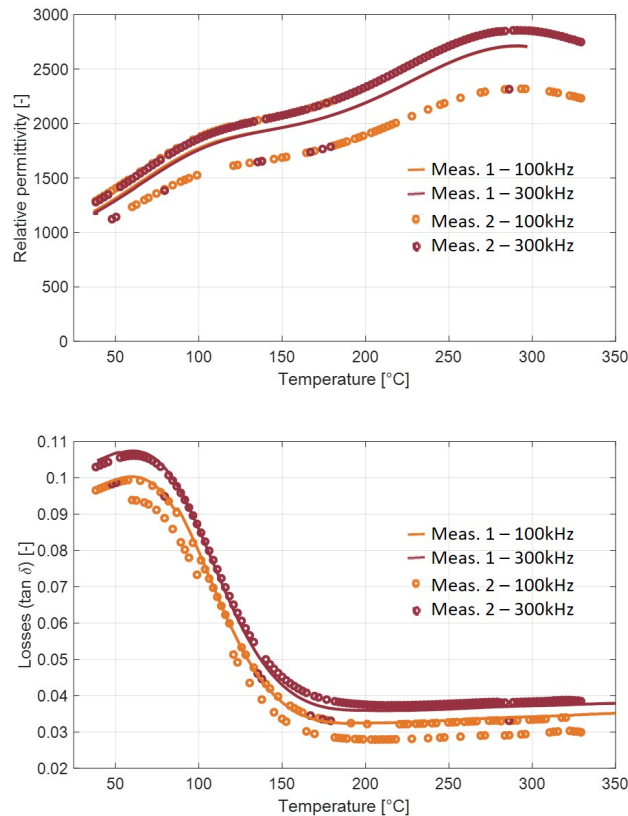


FIGURE 3.6: Relative permittivity (top) and the dielectric losses $\tan \delta$ (bottom) for "U" sample over two consecutive measurements. The first (continuous line) represents the measurement that is typical for "U" sample (see Fig. ??). The second measurement (dots) either fall on the continuous line or on another evolution, shifted from the first measurement, depending on the temperature.

second sample "X" (synthesis parameters in Table 2.11 p. 79) was also measured twice and the values of permittivity and dielectric losses of this sample on the first and the second measurements are presented in Fig. 3.7. There are no "jumps" on the measurements of the sample "X", and the maximum variation between the first and the second measurement is 2.4% for the relative permittivity and of 14% for the dielectric losses ($\tan \delta$) for temperatures lower than 200°C and 25% for higher temperatures. The permittivity and the low temperature dielectric losses variations from one stable measurement to another are lower than the uncertainties. This shows that the main contribution for the measurement variability comes from the measurement noise and not from the uncertainties on the sample's properties. So, the estimations of the measurement noise were associated with the measurement uncertainties.

It will be shown in chapter 4 that, for some samples, the dielectric losses at high temperatures can increase when the measurements are carried out over multiple heating and cooling cycles, depending on the sample, on the electrode, and on the maximum temperature. Those dielectric-losses increases do not come from the measurement uncertainties but from an actual change of property in the samples and electrodes.

Property	Measurement at 50°C	Measurement at T_m
ϵ_r meas. 1	1300	2700
$\tan \delta$ meas. 1	10.7%	3.4%
ϵ_r meas. 2 - curve 1	1140	2350
$\tan \delta$ meas. 2 - curve 1	9.8%	2.9%
ϵ_r meas. 2 - curve 2	1400	2850
$\tan \delta$ meas. 2 - curve 2	10.5%	3.2%

TABLE 3.1: Relative permittivity and the dielectric losses ($\tan \delta$) values at 50°C and at T_m for "U" sample in two consecutive measurements. Curve 1 and 2 correspond to two different trends in the second measurement, depending on the electric contact.

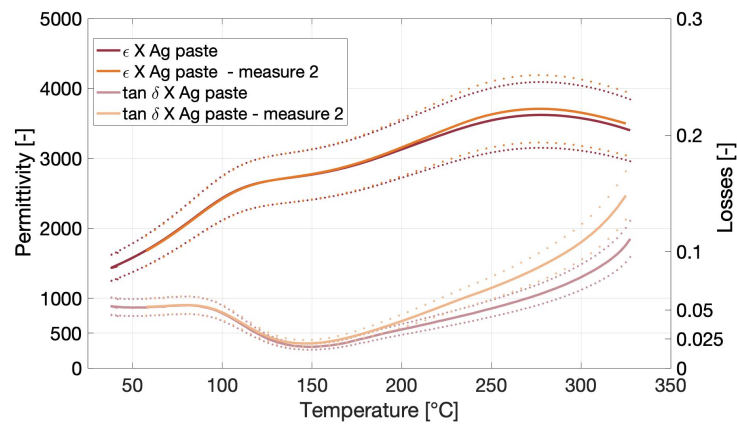


FIGURE 3.7: Permittivity and dielectric losses of NBT-BT sample "X" measured at two different times with the same electrodes (silver paste). The solid lines indicate the measured values and the dotted lines indicate the uncertainties lines of $\pm 14\%$ for the permittivity and $\pm 13\%$ for the dielectric losses (see section 3.1.4).

3.1.5 Temperature drift and corrections

3.1.5.1 Wire fixing method

The Linkam temperature control system is based on the heating or cooling of the platinum support separated from the sample by a glass plate. For this reason, the way the wire is fixed to the bottom of the sample can create a gap between the sample and the heating system, increasing the heat transfer resistance. So, the way the wire is fixed can disturb the temperature measurement, potentially contributing to the uncertainty.

Two methods to fix the wire to the bottom electrode were tested and are discussed here after.

3.1.5.2 Silver paste on sample surface and temperature correction

The simplest method used to fix the wires was to use a silver paste drop over the wire and the bottom surface of the sample (see Fig. 3.8). This silver paste is then heated before measurement for two hours at 200°C, as indicated in the product instructions.

Even if this method is the simplest one to implement, it can create significant tempera-

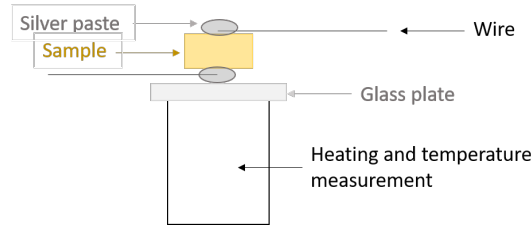


FIGURE 3.8: Wire fixing method based on silver paste over the sample surface

ture drifts in the measurements. The distance between the heating source (platinum) and the sample bottom surface, due to the presence of the silver paste drop, causes the temperature of the ceramic to always be lower than the temperature measured by thermocouple located close to the heating element.

In order to correct that, a reference BaTiO_3 sample was measured using the same fixing method and this measurement was compared to the reference sample properties. The measurement and the known sample properties are shown in Fig. 3.9. Two points were taken as a reference to fit a correction by the straight line. The first one was the Curie temperature and the second one was the room temperature, considered to be correctly measured as both the heating element and the sample are thermalized at room temperature (30°C , in that case).

Two different wires were used: a type-K thermocouple wire (Nickel-Chromium / Nickel-

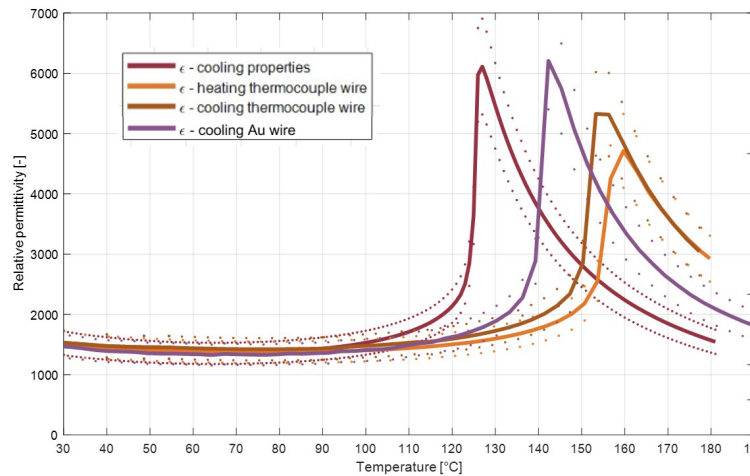


FIGURE 3.9: Relative permittivity of a reference BaTiO_3 sample (purple curve, cooling only - data courtesy of C. Bogicevic) and measurement of the same sample using the simple Ag-paste fixation of a type-K thermocouple wire (yellow: heating, brown: cooling) and Au wire (blue: cooling only) on the bottom of the sample .

Alumel) with 0.20mm diameter and a gold wire with 0.05mm diameter.

For the thermocouple wire, it can be seen in Fig. 3.9 that the measured Curie temperature was 154°C , contrary to the known sample Curie temperature of 127°C . Considering the room temperature of 30°C to be correct, a linear temperature correction reads:

$$T_{corrected} = T_{meas} \cdot 0.81 + 5.50 \quad (3.11)$$

For the gold wire, the measured Curie temperature was 142°C . Considering the room temperature to be correct, the linear temperature correction reads:

$$T_{corrected} = T_{meas} \cdot 0.87 + 4.02 \quad (3.12)$$

The fact that $T_{\epsilon,max}$ for the gold wire is closer to the reference than $T_{\epsilon,max}$ for the thermocouple wire confirms the hypothesis that the thicker the wire the larger the thermal resistances and, hence, the temperature shift in the measurements.

BaTiO_3 undergoes a first order transition. So, there is an expected difference in the temperature of the maximum permittivity, as shown in Fig. 3.10. [70] From T_0 to T_c , the ferroelectric phase is stable and the paraelectric phase is meta-stable, from T_c to T_1 , the ferroelectric phase is meta-stable and the paraelectric phase is stable. So the maximum permittivity temperature in cooling is T_0 and the maximum permittivity temperature in heating is T_1 . The difference between T_0 and T_1 for BaTiO_3 is, then, 3°C , as illustrated in Fig. 3.10.

To analyze if there is a temperature gradient in the samples measured with the simple Ag-paste method to fix the wires on the bottom of the samples, the same BaTiO_3 sample measurements in heating and cooling were compared. If a temperature gradient is present in the sample, a greater difference in the maximum permittivity temperature is observed after comparing the heating and the cooling.

The heating and cooling measurements for the BaTiO_3 show a difference of the maximum permittivity temperature of 3°C for the gold wire (with the smaller diameter) and 6°C for the thermocouple wire (with the larger diameter). So, there is no significant temperature gradient in the sample (especially for thinner wire) and no significant difference between the heating and cooling temperature correction.

The following measurement results carried out with this method to fix the wires will therefore be presented with corrected temperatures.

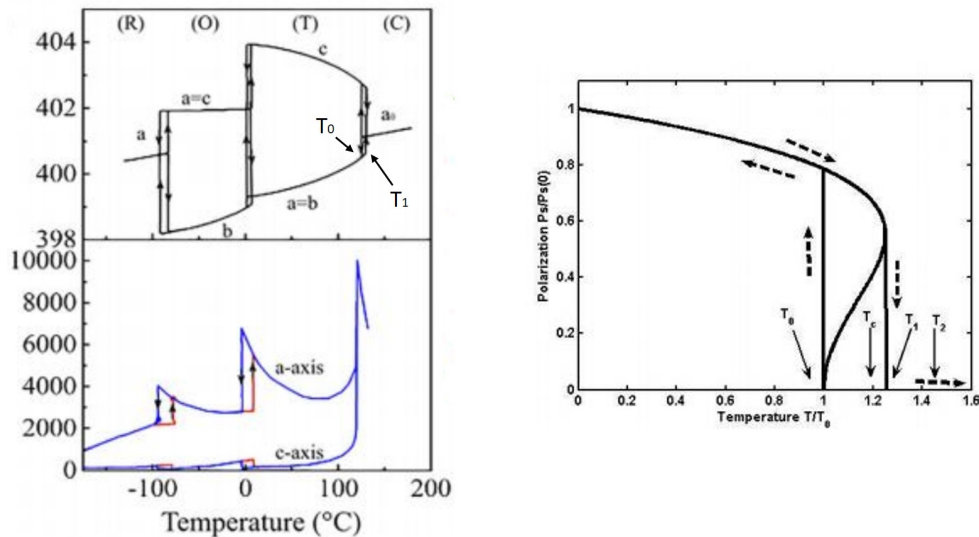


FIGURE 3.10: Lattice parameter (top) in the rhomboedral (R), orthorhombic (O), tetragonal (T) and cubic (C) phases and relative permittivity (bottom) along a- and c-axis (left) [1] and polarization in the first order phase transition from ferroelectric to paraelectric phase in BaTiO_3 (right) [70]

3.1.5.3 Simplified electric contact and temperature corrections

To further verify the temperature correction for the first method (when silver paste is used to fix the wires on the samples surface), its corrected temperatures were compared to other measurements using a displaced electric contact method (silver paste on copper plate).

In this method, the Cr-Au electrodes are deposited by sputtering on the sample's surfaces (see section 4.2.2.2) over the sample. Then, a copper plate is fixed to the bottom electrode of the sample with a small amount of silver paste. The wire is then fixed on the plate also with a drop of silver paste, as shown in Fig. 3.11. This creates a better thermal contact between the sample and the heating source (platinum). So the temperature correction should no longer be necessary.

The comparison was done on the T_m and the T_d measurements of a NBT-BT sample "N" (synthesis parameters in Table 2.11 p. 79). The simplified Ag-paste electric contact temperatures were measured and corrected using equation 3.11. These values were then compared to the measurements using a displaced electric contact method (silver paste on copper plate).

This comparison between the first method after temperature correction and the method

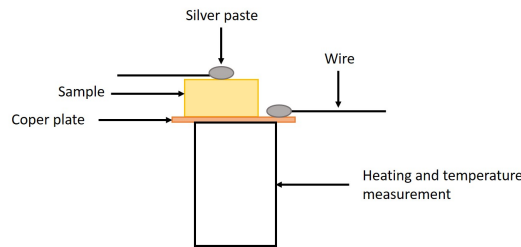


FIGURE 3.11: Wire fixing method based on Cr-Au sputtering and a shifted wire contact (silver paste on copper plate).

described in this paragraph, can be used then to verify the validity of the temperature correction and to estimate the temperature measurement uncertainty in temperature. The T_d and T_m measured at 10kHz for both methods are presented in Table 3.2.

Considering T_d and T_m as being $T_d = 112 \pm 4^\circ\text{C}$ and $T_d = 271 \pm 8.5^\circ\text{C}$, the uncertainty

Wire fixing method	T_d ($^\circ\text{C}$)	T_m ($^\circ\text{C}$)
Silver paste over sample	116	280
Shifted electric contact	108	263

TABLE 3.2: Measured T_d and T_m for sample "H", at 10kHz for the two methods to contact the bottom electrode.

in the measurements of temperature can be estimated as being 3.5%.

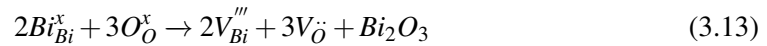
3.2 Dielectric properties with temperature

The dielectric properties vs temperature are the most important properties for the ML-CCs. In this section, the influence of synthesis parameters, second phase, polishing, and stoichiometry on these properties were studied, in order to optimize the NBT-BT properties according to Exxelia's specifications.

3.2.1 Influence of stoichiometry, secondary Ba-containing phases, synthesis parameters and polishing and strain relaxation on the dielectric properties vs temperature

3.2.1.1 Stoichiometry

The stoichiometry is specially important for NBT-BT, since bismuth and sodium can evaporate during calcination and sintering. The Bi_2O_3 loss during ceramic processing is a source of oxygen vacancies with high mobility in the final material:



where Bi_{Bi}^x is a bismuth ion sitting on a bismuth lattice site with neutral charge, O_{O}^x is an oxygen ion sitting on an oxygen lattice site with neutral charge, V_{Bi}''' is a bismuth vacancy with triple negative charge and $\text{V}_{\text{O}}^{\bullet\bullet}$ is an oxygen vacancy with double positive charge, as indicated by the Kröger–Vink notation.

It could be expected that the Na evaporation also happens via defect mechanism (like for the Bi case), creating oxygen vacancies and increasing conductivity. Actually, it creates a phase separation composed of TiO_2 for pure NBT and secondary Ba-containing phases for NBT-BT, making the matrix phase deficient in Na and Ti and therefore rich in Bi. On the other hand, the resulting Na excess forms a second phase and is not incorporated in the matrix phase. So, the Na excess cannot fill the Bi vacancies to compensate for oxygen vacancies even though they occupy the same site in the perovskite unit cell. Since, there is always a Bi evaporation during processing, the matrix composition is Bi-deficient and has high-mobility oxygen vacancies. [78]

In conclusion, the Na behaves contrarily to the Bi, with an increase in the conductivity for Na-rich samples and a decrease in conductivity for the Na-poor samples. So non-stoichiometry can be measured by the Na/Bi ratio, with a high conductivity when increasing the Na/Bi ratio. [78]

Slight changes in Na/Bi ratio can drastically affect the dielectric properties of NBT-BT,

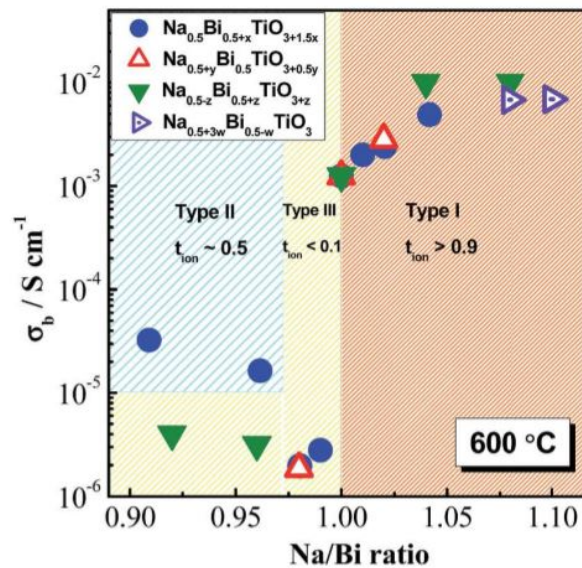


FIGURE 3.12: Bulk conductivity of pure NBT with different Na/Bi ratios at 600°C [78]

resulting in more than 3 orders of magnitude difference in the room temperature DC conductivity. This high conductivity created in the material is one of the most important hinderances to the use of NBT-BT in MLCCs, since it also results in an increase in the dielectric losses, when used in alternating current applications.

NBT-BT show three types of electrical conductivity: [78]

- Type I - the nominal stoichiometric NBT-BT exhibits a high oxide-ion DC conductivity due to the oxygen vacancies created through Bi_2O_3 loss and to their high mobility resulting from highly polarized Bi^{3+} ions and weak Bi–O bonds. The increase of the Na/Bi ratio increases the oxide-ion conductivity as shown in Fig. 3.12, owing to the generation of additional oxygen vacancies.
- Type III- the decrease in the nominal Na/Bi ratio to 0.98 drastically reduces the conductivity since the Bi excess can compensate for the loss during synthesis. The material exhibits electronic conduction.
- Type II - decreasing even more the nominal Na/Bi ratio to 0.96, the material shows mixed conduction (oxide-ion and electronic conduction) because of the increase of a space-charge effect due to the formation of a Bi-rich phase.

As shown in Fig.3.13, the changes in conductivity have a great impact on the dielectric losses (see section 3.1.2). Type I conductivity NBT-BT shows a sharp increase in the dielectric losses from 100°C. Type III conductivity NBT-BT exhibit low dielectric losses, with $\tan \delta \leq 2\%$ from 250 to 650°C. Finally, type II conduction NBT-BT have an intermediate behaviour, with $\tan \delta \leq 2\%$ from 300 to 500°C.

This effect can also be shown by analyzing equations 3.5 and 3.8 of the RC model adopted for the dielectric properties estimation, indeed $\varepsilon'' = \sigma' / \omega$. Since the dielectric losses are calculated by the ratio of the real to the imaginary part of the permittivity (equation 3.6), then the increase in conductivity induces the increase of the dielectric losses.

Other interesting effects of the stoichiometry change are the creation of a pinched P-E

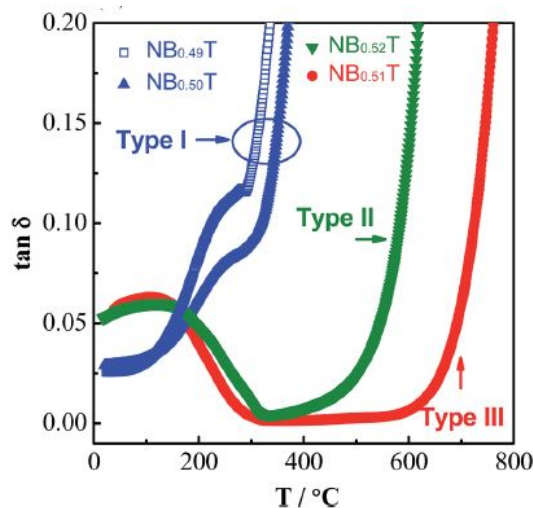


FIGURE 3.13: Dielectric losses with temperature for the three conductivity types NBT and NBT-BT [78]

loop and a decrease of the depolarization temperature T_d with decreasing Na/Bi ratio (see section 2.3.2.6). These changes are attributed to the decrease of the temperature of the FE to the "AFE-like" phase transition. However, the reason of this decrease is not well understood

yet. [23]

In this study, three non-stoichiometric samples were prepared with the same synthesis parameters (see Table 2.11 p. 79) and compared to sample "P". The "P" sample has a nominal stoichiometric composition (the reactants were weighted in stoichiometric proportions), the "U" sample has the nominal composition of $\text{Na}_{0.44}\text{Bi}_{0.48}\text{Ba}_{0.06}\text{TiO}_3$, i.e. with a 6.38% Na-deficiency and 2.12% Bi-excess, the "Y" sample has a nominal excess of 10.5% mol of sodium and 2.1% mol of bismuth when compared to sample "U", to obtain the nominal "U" composition ($\text{Na}_{0.44}\text{Bi}_{0.48}\text{Ba}_{0.06}\text{TiO}_3$) after sintering, and the "Z" sample has a nominal excess of 16.9% mol of sodium when compared to sample "U", to obtain nominal NBT-BT composition after sintering. The nominal and the EDS Na/BI ratios are presented in Table 3.3.

As sodium is a light element, the EDS measurements are less precise. The uncertainties can be considered as 5% for the heavy elements (Bi and Ti) and 10% for the light elements (Na and O). The Ba measurement also has a higher uncertainty (10%), since its measurement has to be done from the M series or from the Lb series, which have lower intensity than the La series.[51]

Analyzing the differences between the nominal composition and the final one analyzed

Sample	Nominal composition	Nominal Na/Bi	EDs measured Na/Bi	EDS measured composition of matrix
"P"	$\text{Na}_{0.47}\text{Bi}_{0.47}\text{Ba}_{0.06}\text{TiO}_3$	1.0	0.88 ± 0.13	$\text{Na}_{0.430}\text{Bi}_{0.486}\text{TiO}_{2.70}$
"U"	$\text{Na}_{0.44}\text{Bi}_{0.48}\text{Ba}_{0.06}\text{TiO}_3$	0.92	0.85 ± 0.13	$\text{Na}_{0.437}\text{Bi}_{0.500}\text{TiO}_{2.70}$
"Y"	$\text{Na}_{0.49}\text{Bi}_{0.49}\text{Ba}_{0.06}\text{TiO}_3$	1.0	0.90 ± 0.14	$\text{Na}_{0.460}\text{Bi}_{0.510}\text{TiO}_{2.60}$
"Z"	$\text{Na}_{0.56}\text{Bi}_{0.48}\text{Ba}_{0.06}\text{TiO}_3$	1.06	0.91 ± 0.14	$\text{Na}_{0.457}\text{Bi}_{0.500}\text{TiO}_{2.36}$

TABLE 3.3: Nominal composition of samples "P", "U", "Y" and "Z", their nominal and EDS measured Na/BI ratios, and the average final composition of the matrix phase for samples "P" and "U" and of the only phase for samples "Y" and "Z" measured by EDS. The EDS uncertainties for the Bi and Ti are 5% and for the Ba, Na and O is 10%.

by EDS, all samples have a lower Na/BI ratio in the final composition when compared to the nominal one. This indicates that the Na losses are more important than the Bi ones, since it is more volatile.

Table 3.3 shows the nominal composition of each sample and the average final composition of the matrix phase measured by EDS (where the measurement uncertainties are 5% for Bi and Ti and 10% for Na).

It can be observed that the matrix phase does not show a Ba concentration that can be measured by EDS. Since the L series of Ba and Ti are close to each other, the Ba concentration measurement has to be done from the M or the Lb series, as explained earlier in this section. This means that the detection limit is higher when compared to the other elements. However, the EDS analysis show that the majority of the Ba is in the secondary Ba-containing phases. The composition of the secondary Ba-containing phases was detailed in section 2.4 and the secondary Ba-containing phases average grain surface and fraction will be detailed in section 3.2.1.2.

The Na and Bi losses estimation for all the samples is difficult, since a part of the Ti is present on the secondary Ba-containing phases for samples "P" and "U". However, samples "Y" and "Z" do not have any phase separation, so they can be used for estimating the losses of volatile species. Analyzing Table 3.3 p. 94 and considering that no titanium is lost during the synthesis, the sodium losses average is $17\% \pm 9\%$ and the average Bi losses are $2\% \pm 0.03\%$. As explained before, the Na losses are responsible for the secondary Ba-containing phases separation in the NBT-BT materials. The Bi losses are responsible for the creation of

oxygen vacancies that increase the conductivity of the sample. So adding Bi to the reactants to compensate for its evaporation, as done for sample "U", and the study of the secondary Ba-containing phases effects in the NBT-BT properties, as presented in section 3.2.1.2 are the key to understand and control the dielectric properties of NBT-BT, to achieve an adapted material for the MLCC production.

Comparing now the SEM images of samples "P" and "U", it can be observed that the relative excess of Bi compensates for evaporation during synthesis (see Table 3.3) and a second Bi-rich phase is formed in the sample's core (see Fig. 2.16 p. 58).

The dielectric properties and the insulation resistance of samples "P", "U", "Y" and "Z" are presented in Figures 3.14, 3.15 and 3.16.

Comparing again samples "P" and "U", the decrease of the Na/Bi ratio in the sample "U" through Na-excess and Bi-deficiency and the consequent oxygen vacancies compensation do not decrease the dielectric losses, as it would be expected (see figures 3.14 and 3.15). This indicates that the higher evaporation of Na in sample "P" compared to the Bi evaporation, owing its Na/Bi measured ratio to be 0.88 (see Table 3.3) is sufficient to change the conduction type from type I to type II, with low dielectric losses ($\tan \delta \leq 2.5\%$) up to 300°C.

The permittivity of the "U" sample when compared with the "P" sample is lower, but still complaint with Exxelia's specifications, and it is also more stable in temperature, so this material is more adapted to the MLCC application. The reason for this is related to the presence of a secondary Ba-containing phase and will be discussed in section 3.2.1.2.

Finally, another important difference between the "U" and the "P" samples is the depolarization temperature, around 105°C at 10kHz for the "P" sample and around 65°C at 10kHz for the "U" sample. This is another reason why the non-stoichiometric material is more adapted for the MLCC production. This decrease of the depolarization temperature is due to the modulated phase being more stable at lower temperature. [23]

Comparing now the samples "Y" and "U", the increase of the Na content inhibits the secondary Ba-containing phases separation, increasing the Ba and Ti content in the matrix and decreasing the relative Bi content. This can be seen comparing their respective SEM images (Fig. 3.17 and Fig. 2.8 p. 50), where no second phase was detected in samples "Y" and "Z".

So, the increase of the Na content and of the Na/Bi ratio in these samples enhance the dielectric losses and change the conduction type back to type I, as expected. This can be confirmed by the increase in the dielectric losses of the samples from 200°C shown in Fig. 3.14 and by the high conductivity, specially for sample "Z" shown in Fig. 3.16.

The measured permittivity is also increased with increasing Na/Bi nominal ratio, as reported in [23]. This can be observed by comparing the relative permittivity of samples "Z" and "P" in Fig. 3.14, for example.

The increase in the DC conductivity can be seen by the decrease in the insulation resistance of both "Y" (47s at 200°C) and "Z" (0.3s at 200°C) samples in Fig. 3.16.

The depolarization temperature increases from 65°C in sample "U" to 115°C in sample "Y", for the same reason (cf. [23]) as for sample "P".

Finally, comparing the samples "Y" and "Z", similar effects on the permittivity, dielectric losses, insulation resistance, and depolarization temperature are observed: an increase in the permittivity and in the dielectric losses, a decrease in the insulation resistance of the sample "Z" when compared to the sample "Y", and an increase in the depolarization temperature, from 115°C in sample "Y" to 145°C in sample "Z", due to the increase of the Na/Bi ratio.

In conclusion, the sample "U", with the lower Na/Bi ratio is the most adapted for the MLCC production due to its higher resistivity that satisfy Exxelia's requirements and lower dielectric losses, when compared to the samples "Y" and "Z". Moreover, this sample has a lower variation of permittivity with temperature when compared to the other ones.

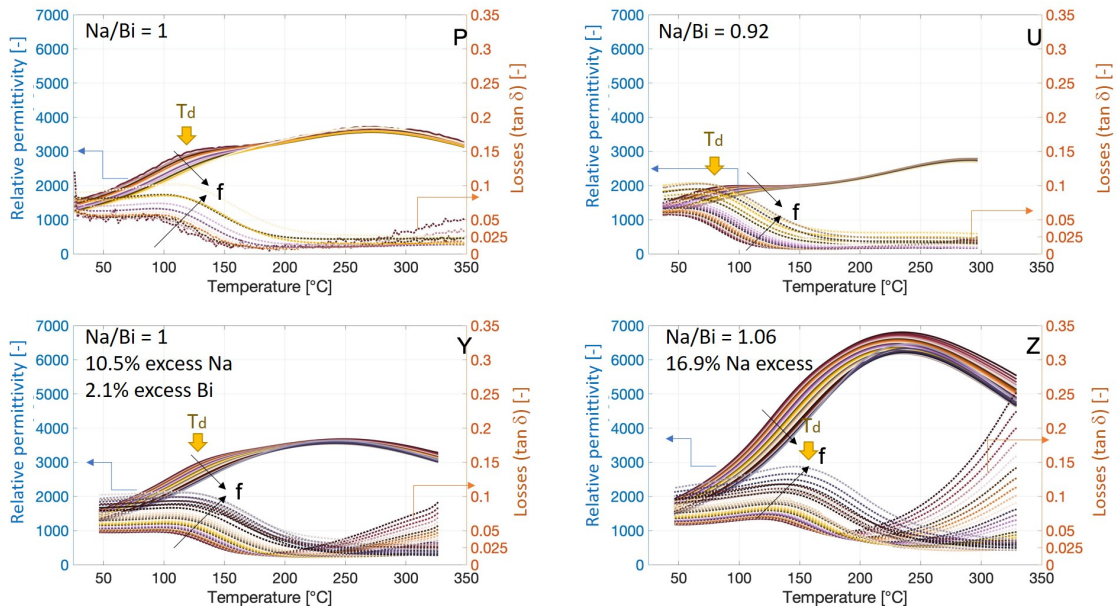


FIGURE 3.14: Relative permittivity and dielectric losses versus temperature from 1kHz to 1MHz for samples "P", "U", "Y" and "Z".

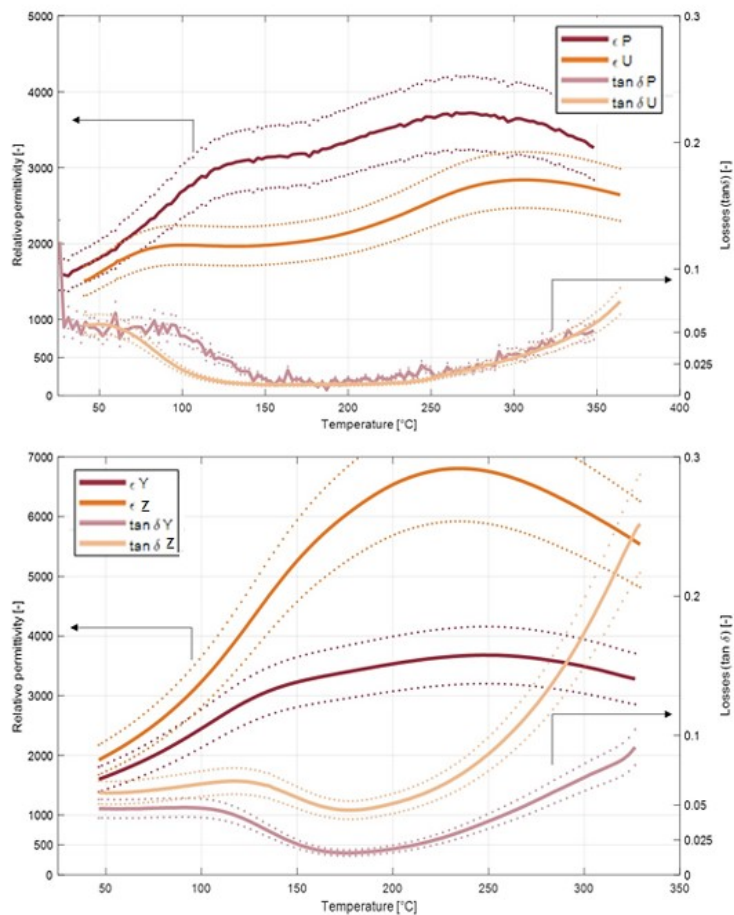


FIGURE 3.15: Comparison of relative permittivities and dielectric losses versus temperature measured at 1kHz for samples "P", "U", "Y" and "Z" having different stoichiometries. The solid lines indicates the measured values and the dotted lines indicate the uncertainty lines of $\pm 14\%$ for the permittivity and $\pm 13\%$ for the dielectric losses (see section 3.1.4)

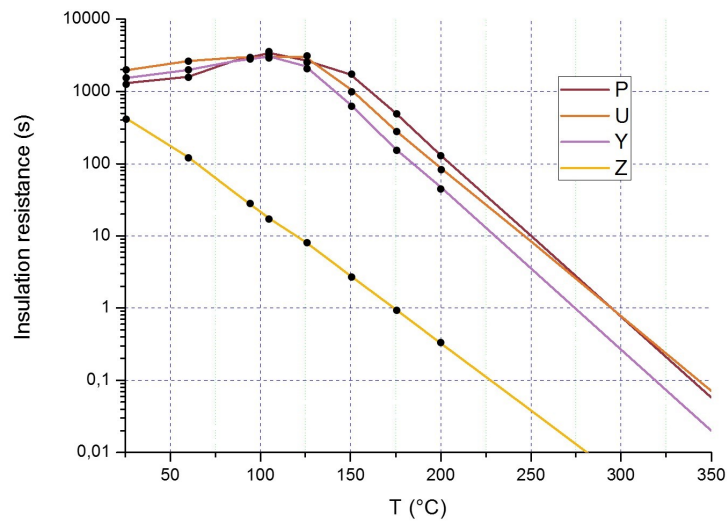


FIGURE 3.16: Insulation resistance versus temperature of samples "P" (nominal Na/Bi = 1), "U" (nominal Na/Bi = 0.92), "Y" (nominal Na/Bi = 1, 10.5% Na excess and 2.1% Bi excess compared to "U") and "Z" (nominal Na/Bi = 1.06, 16.9% Na excess compared to "U") with different stoichiometries (logarithme scale).

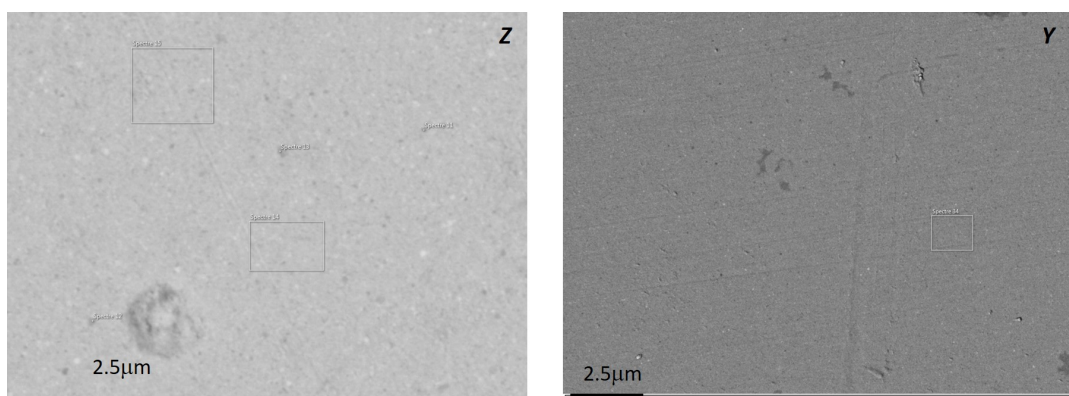


FIGURE 3.17: SEM image of samples "Y" and "Z" surface showing no secondary Ba-containing phases separation

Furthermore, the increase in Na content inhibits the phase separation and, as a consequence, decreases the relative Bi content in the main phase (increases the conductivity). So, to obtain a sample with no phase separation but without increasing the conductivity, Bi and Na excess should be added, maintaining the same Na/Bi ration as sample "U", but with increased Na/Ti ratio. A suggested nominal composition would be $\text{Na}_{0.4818}\text{Bi}_{0.5256}\text{Ba}_{0.06}\text{TiO}_3$ (same Na/Ti ratio as sample "Y" and same Na/Bi ratio as sample "U".)

3.2.1.2 Secondary Ba-containing phases

The second phase formation explained in section 2.4 also has an important effect on the dielectric properties and on the insulation resistance of the samples.

The samples can be analyzed as a composite, since the secondary Ba-containing phases is a conducting phase and the matrix (mostly NBT) can be considered as an insulating ferroelectric phase (see section 3.3.1).

The classical models used to estimate the effective dielectric properties of composites (Maxwell Garnett, Bruggeman Symmetric, Bruggeman Non-symmetric, Sen-Scala-Cohen, Looyenga and Lichtenecker) consider the hypothesis of spherical and isotropic particles, [29] which is not the case for the secondary Ba-containing phases (see Fig. 2.40) p. 76. Moreover, these models assume that the materials of the composite are linear, which means that the induced dipole moments depend linearly on the electric field. [29] This is also not the case for NBT-BT, since the NBT matrix is a ferroelectric relaxor material. Finally, they assume that the distance between particles is larger than the particle size, which is not necessarily the case for all the samples in this study.

A correction of the Maxwell Garnett (MG) and Bruggeman Symmetric (BS) models

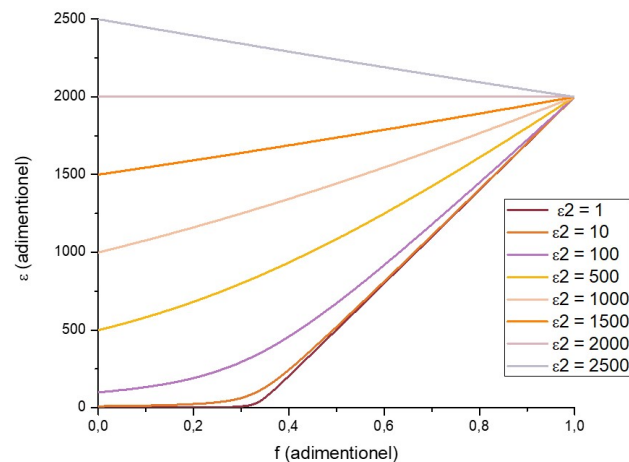


FIGURE 3.18: Evolution of effective permittivity ($\epsilon - eff$) with the matrix volume fraction (f) for different values of particle permittivities (ϵ_2 or ϵ_e from 1 to 2500) and a matrix permittivity of $\epsilon_i = 2000$, considering the Bruggeman Symmetric model

considers ellipsoidal particles. However, this correction assumes a specific particle orientation (long axis either parallel or orthogonal to the electric field), which is also not the case for this study, since the secondary Ba-containing phases are randomly oriented. Moreover, even after correction, the MG and BS models are still restricted to linear composites. [29]

For the classical composite models, the increase in volume fraction of the secondary Ba-containing phases would increase the interface surface between the conductive and the non-conductive phases, increasing the electric field in the bulk material. This would increase the permittivity, the conductivity, and the dielectric losses of the sample.[75] Fig. 3.18 shows the expected evolution of the effective (measured) permittivity with the matrix volume fraction for different values of inclusion permittivities, considering the BS model. It can be seen that the permittivity presents a monotonic evolution with the matrix volume fraction, regardless of the matrix and particle permittivity values. This is not the case for the samples in this study (see Fig. 3.19), proving that the classical models cannot be used. The secondary Ba-containing phases volume fraction and average grain surface estimations will be presented in section 3.2.1.2.

The average inter-particle distance and the average particle size also have an important

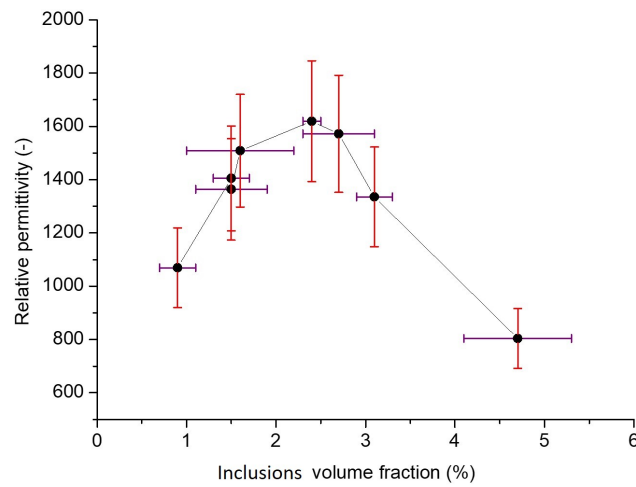


FIGURE 3.19: Relative permittivity at 10kHz and room temperature vs volume fraction of inclusions for the NBT-BT samples.

effect on the effective properties of composites. The decrease in the inter-particle separation requires a model that takes into account the interactions between particles.[30] Kaufman *et al.* modeled during the course of this PhD the effect of BaTiO₃ particle interactions in a polymeric insulating matrix. [30] The permittivity increases with decreasing particle separation when compared to all classical composite models estimations. Deepa *et al.* showed the effect of the conducting La_{1-x}Sr_xCoO_{3-y} particles size in an insulating polymeric matrix. [14] For fine grained particles, the increase in permittivity occurs for lower volume percentage of conducting phase when compared to the coarse-grained ones (Fig. 3.20). This is because, for a given volume percentage, smaller particle creates a larger interface and higher density of accumulated charges, resulting in a greater dipole moment. So, a higher permittivity can be obtained for composites with lower average grain surface. Moreover, the overlapping of interfaces occurs at lower concentrations for composites with lower average grain surface, proving the need of a model that takes this into account.

Finally, the effect of the increase in average particle size is possibly not the same depending on the studied system, since it would decrease the interface surface and increase the electric field in the material, having competing effects on the permittivity.

In conclusion, there is no classical composite model that can take into account the

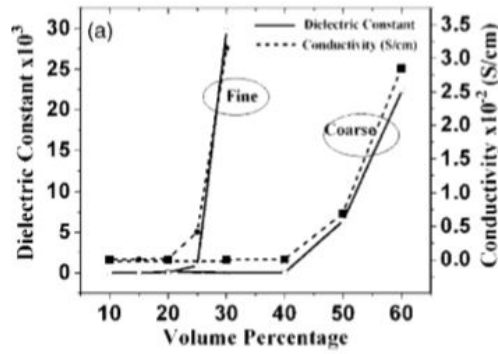


FIGURE 3.20: Permittivity evolution with concentration of LSCO conducting phase in the composite in a polymeric matrix for fine and coarse grained particles [14]

non-spherical shape of the secondary Ba-containing phases particles that are randomly oriented, the interactions between particles, the non-linear ferroelectric character of the NBT-BT, and the different average grain surfaces of the secondary Ba-containing phases at the same time. A new model could be created, for example using finite element method, as in [30]. However, this was not the main aim of this work.

The effects of the secondary Ba-containing phases volume fraction have been, then, evaluated qualitatively.

Sample	Average grain surface (μm^2)	Volume fraction (%)	Dried reactants	Ball-milling	Solvent	Dispersing agent	Na ₂ CO ₃ grain size
"B"	32 ± 22	0.9 ± 0.2	Yes	250 rpm - 250 rpm	Ethanol	No	Coarse
"E"	0.10 ± 0.05	4.7 ± 0.6	Yes	350 rpm - 350 rpm	Ethanol	No	Fine
"G"	1.2 ± 0.3	3.1 ± 0.2	Yes	250 rpm - 250 rpm	Ethanol	Yes	Coarse
"H"	3.4 ± 2.3	1.5 ± 0.2	No	250 rpm - 250 rpm	Ethanol	Yes	Coarse
"I"	0.9 ± 0.6	1.5 ± 0.4	No	250 rpm - 350 rpm	Ethanol	Yes	Coarse
"V"	1.7 ± 1.1	1.6 ± 0.6	No	250 rpm - 250 rpm	Ethanol	Yes	Fine
"P"	3.0 ± 2.1	2.7 ± 0.4	No	350 rpm - 350 rpm	MEK + Ethanol	Yes	Fine
"N"	0.9 ± 0.3	2.4 ± 0.1	No	250 rpm - 250 rpm	MEK + Ethanol	Yes	Fine

TABLE 3.4: Secondary Ba-containing phases average grain surface, volume fraction, and synthesis parameters for NBT-BT samples considering a confidence interval of 95% or two time the standard deviation. The two ball-milling speeds correspond to the first and second ball-milling conditions.

Effects of the secondary phase on the permittivity and dielectric losses

In order to analyze the effects of the volume fraction and grain surface of the secondary Ba-containing phases on the permittivity and on the dielectric losses, samples with different synthesis parameters affecting the secondary Ba-containing phases formation were analyzed: the drying of the reactants, the grain size of Na_2CO_3 , the ball-milling energy (speed and duration), the ball-milling solvent, the use of a dispersing agent, and the nominal stoichiometry.

The estimation of the secondary Ba-containing phases volume fraction and average grain surface was done using the SEM images of the polished samples surface. Using different color threshold for the image analysis, the average grain surface, the surface fraction and their uncertainties were estimated.

Sample "E" can be used to show an example of the image processing used to estimate the average volume fraction and grain surface of the secondary Ba-containing phases in this sample. All the image processing were done using "ImageJ" software. Fig. 3.21 shows the polished surface of the "E" sample before image processing, after a high threshold processing, after a low threshold processing and after a high threshold processing and an elimination of small "dots" with a binary "erode" and "dilate" treatments. For low threshold, light color particles and large particle's borders may be neglected, with high threshold, images imperfections may be considered as particles and for the binary treatment, small particles and imperfections are eliminated, but borders are kept. Table 3.5 show the average volume fraction and grain surface for the three image processing methods. The average grain surface and volume fraction considered are a mean of the values obtained by the three methods, and the uncertainties related to them.

It was considered that the volume fraction of the core is equal to the surface fraction of

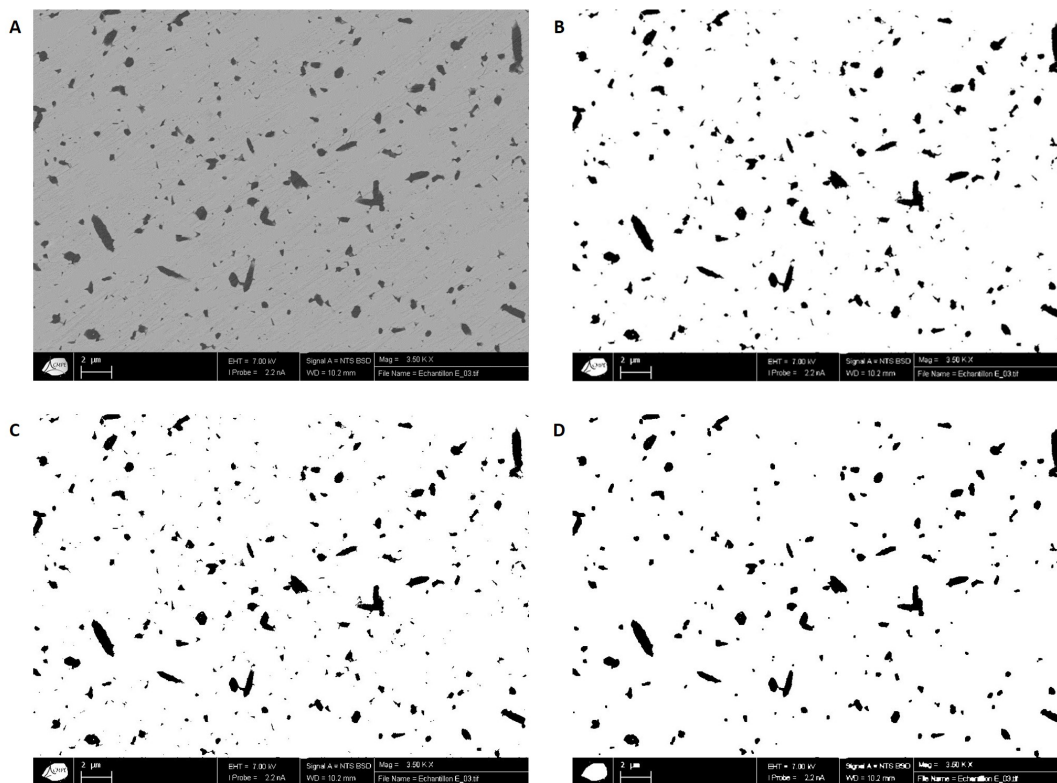


FIGURE 3.21: SEM image of the polished surface of sample "E" A - before image processing, B - after a low threshold processing, C - after a high threshold processing and D - after a high threshold processing and an elimination of small "dots" with a binary "erode" and "dilate" treatments.

ImageJ processing	Average grain surface (μm^2)	Volume fraction (%)
Low threshold	0.850	3.156
High threshold	0.747	6.562
High threshold + Binary	1.029	5.881

TABLE 3.5: Average grain surface and volume fraction of the secondary Ba-containing phases of sample "E" after a low threshold processing, a high threshold processing and a high threshold processing and a binary "erode" and "dilate" treatments.

the *polished* surface. Finally, for the uncertainties, the value of two standard variations was considered (or a confidence interval of 95%).

The size and volume fraction of the secondary Ba-containing phases are presented in Table 3.4 p. 100. The two ball-milling speeds correspond to the first and second ball-milling conditions. All the 250 rpm ball-millings had a 4h duration and all the 350 rpm ball-millings had a 8h duration.

Fig. 3.22 presents the relative permittivity of each sample at T_m and the dielectric losses at 300°C, both measured at 10kHz, versus the secondary Ba-containing phases volume fraction. Average secondary Ba-containing phases grain surfaces are indicated by the labels on this Figure. The 10kHz frequency was chosen since it is a stable measurement (not at the limit of the device calibration), the permittivity was measured at T_m to compare the maximum values of this property and the dielectric losses were measured at 300°C so all the sample's high temperature losses can be compared.

The increase in the secondary Ba-containing phases volume fraction initially increases

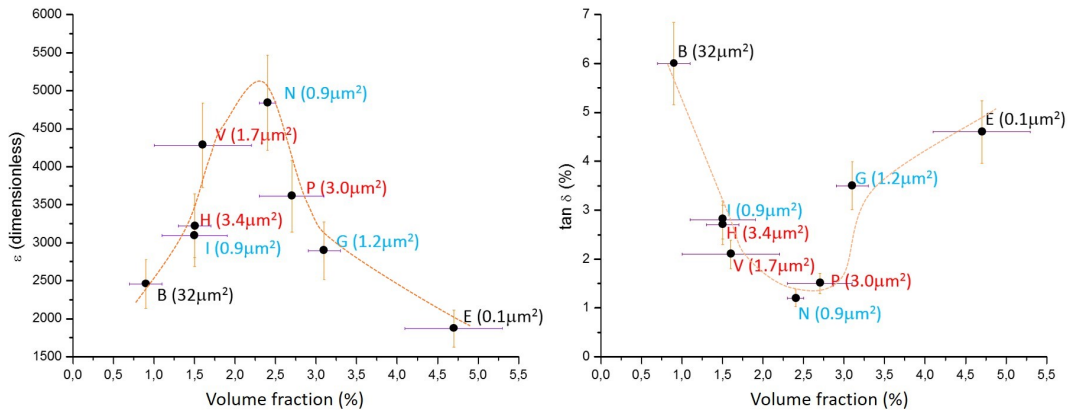


FIGURE 3.22: Relative permittivity at T_m measured at 10kHz (left) and dielectric losses at 300°C measured at 10kHz (right) versus secondary Ba-containing phases volume fraction for the NBT-BT samples with different synthesis parameters. Labels indicate each sample and its secondary Ba-containing average grain surface red and blue labels indicate groups with similar secondary Ba-containing average grain surface and black labels indicate the group with no dispersing agent used in ball-millings. Dotted lines are a guide for the eyes.

the relative permittivity and decreases the dielectric losses until $2.5 \pm 0.9\%$ of secondary Ba-containing phases volume fraction. For higher volume fractions the increase in the secondary

Ba-containing phases volume fraction decreases permittivity and increases dielectric losses. There is therefore an optimal volume fraction for dielectric properties around 2.5%.

Decreasing the Na_2CO_3 grain size changes neither the secondary Ba-containing phases volume fraction, nor the average secondary Ba-containing phases grain surface nor the dielectric losses of NBT-BT, as observed comparing samples "V" and "H". Considering the "H" and "V" sample's permittivities within their uncertainties in Fig. 3.27 p. 108, it can be concluded that the decrease in the Na_2CO_3 grain size may slightly increase the permittivity value of NBT-BT, specially for the temperatures between T_d and T_m . However, due to the relatively high value of the permittivity uncertainties, it is difficult to evaluate the effect of this synthesis parameters for the entire temperature range.

Increasing the energy of ball milling from 250 rpm - 4h to 350 rpm - 8h on NBT-BT samples ball-milled with the use of dispersing agent and without drying of the reactant, no difference is found in the secondary Ba-containing phases volume fraction, grain surface and on their dielectric properties, as it is observed from the comparison of samples "I" and "H". This indicates that, for these samples, the second ball-milling energy does not affect the secondary Ba-containing phases formation.

Comparing now the NBT-BT samples ball-milled at 250 rpm, for 4h using a dispersing agent and with or without dried reactants (samples "G" and "H" respectively), the only observed difference is in the secondary Ba-containing phases volume fraction (1.5% for "H" and 3.1% for "G"). This indicates that the samples with dried reactants have higher volume fraction of second phase.

Finally, when comparing samples ball-milled using a dispersing agent (with different ball-milling energies and drying of the raw powders) with their equivalents ball-milled without dispersing agent, it can be observed that the increasing ball-milling energy decreases drastically the grain surface and increases the volume fraction of the secondary Ba-containing phases phase, when no dispersing agent is used. This is clear from the large grains of secondary secondary Ba-containing phases containing phases in sample "B" (250 rpm - 4h) comparing to the smaller grains in sample E (350 rpm - 8h);

Moreover, the use of dispersing agent also decreases the dielectric losses and increases the permittivity. This can be observed when comparing samples "G" (250 rpm ball milling, drying of reactants and use of dispersing agent), "H" (250 rpm ball milling, no drying of reactants and use of dispersing agent) and "I" (350 rpm ball milling, no drying of reactants and use of dispersing agent) with samples "B" (250 rpm ball milling, drying of reactants and no use of dispersing agent) and "E" (350 rpm ball milling, drying of reactants and no use of dispersing agent) on figures 3.22 p. 102 and 3.23 p. 104.

To conclude, adding MEK to the solvent mixture, the only observed differences are the dielectric losses that are lower for the ball-milling with ethanol and MEK as solvents, and the second phase volume fraction that is lower for the ball-milling with pure ethanol as solvent. So, the addition of MEK as a solvent together with ethanol decreases the dielectric losses and increases the secondary Ba-containing phases volume fraction. This can be observed when comparing samples "V" (ethanol as solvent) and "N" (MEK+ethanol as solvent).

The relative permittivity and the dielectric losses of samples "N", "B" and "E" for the complete temperature range measured (from room temperature to 350°C) are shown in Fig. 3.23 p. 104. and they prove the same tendency of values showed in Fig. 3.22.

Dielectric properties of samples "H", "I" and "V" will be discussed in section 3.2.1.3.

As a summary, the increase in the secondary Ba-containing phases volume fraction initially increases the permittivity and decreases the dielectric losses until a $2.5 \pm 0.9\%$ volume fraction value. For higher percentages of second phase, the trend reverts.

No considerable changes are observed in secondary Ba-containing phases and in dielectric properties for different Na_2CO_3 grain sizes and for different ball-milling energies in

samples prepared with dispersing agent.

The use of dispersing agent decreases the dielectric losses, increases permittivity and mitigates the ball-milling effects on NBT-BT properties. Finally, adding MEK as a solvent decreases the dielectric losses and increases the secondary Ba-containing phases volume fraction.

Therefore, to obtain samples compliant with Exxelia requirements of high permittivity values (at least 2000) and low dielectric losses or $\tan \delta$ (lower than 2.5%), an intermediary volume fraction (2.5%) and average grain surface (0.9 to $3.0 \mu\text{m}^2$) on the secondary Ba-containing phases should be used.

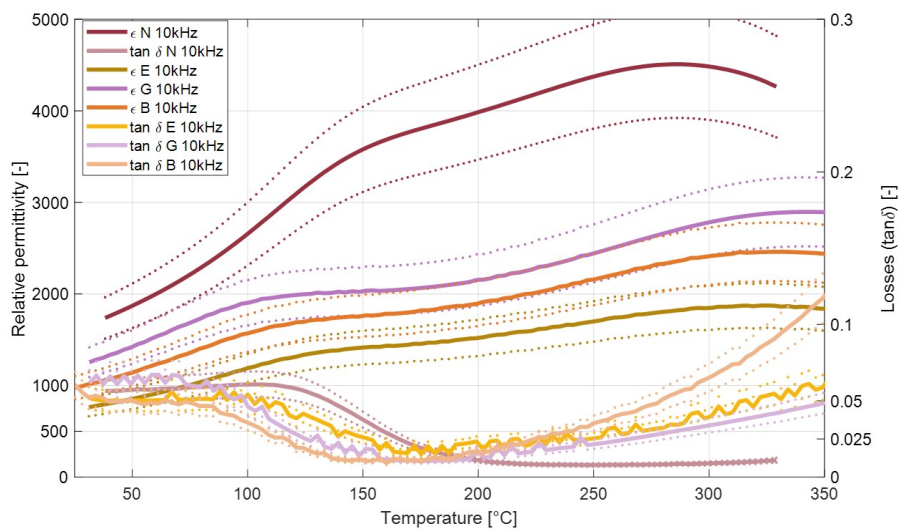


FIGURE 3.23: Comparison of permittivity and dielectric losses versus temperature measured at 1kHz for samples "N", "B", "E" and "G" with different secondary Ba-containing phases average size and volume fraction. The solid lines indicates the measured values and the dotted lines indicate the uncertainties lines of $\pm 14\%$ for the permittivity and 13% for the dielectric losses (see section 3.1.4).

Effects of the 2nd phase on the insulation resistance

Fig. 3.25 presents the evolution of the insulation resistance of sample "N", "B", "E", "G", "H", and "V" with temperature and Fig. 3.24 show the insulation resistance at 200°C (the highest measured temperature) versus the secondary Ba-containing phases volume fraction and average grain surface.

The increase in the secondary Ba-containing phases volume fraction and average grain surface initially increase the insulation resistance up to 2.5% and $3 \mu\text{m}^2$. Then, for higher volume fractions and grain surfaces, the insulation resistance decreases.

Decreasing the Na_2CO_3 grain size does not affect the secondary Ba-containing phases volume fraction and average grain surface (see section 3.2.1.2). The insulation resistance, however, decreases from 50 to 34s, as observed in samples "H" and "V" respectively. The difference in the insulation resistance between these samples is small, considering that the variation of this property in temperature is exponential. For example, for sample "V", the decrease from 50 to 34s in the insulation resistance corresponds to an increase in temperature from 193 to 200°C , so 3.9% with respect to the temperature range from room temperature (20°C) to 200°C , the temperature interval over which the insulation resistance is measured. So the decrease in the Na_2CO_3 grain size slightly decreases the insulation resistance value of

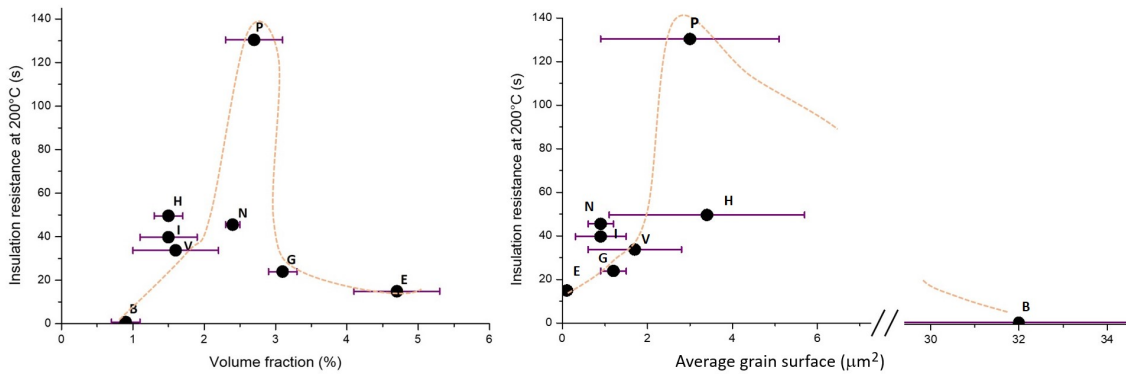


FIGURE 3.24: NBT-BT sample's insulation resistance at 200°C (the highest measured temperature) versus the secondary Ba-containing phases volume fraction and average grain surface.

NBT-BT.

No difference is found in the secondary Ba-containing phases volume fraction and grain surface when the energy of ball milling is increased from 250 rpm - 4h to 350 rpm - 8h on samples ball-milled with dispersing agent and without drying the reactants (see section 3.2.1.2). However, the insulation resistance decreases from 50 to 40s, as it is observed in samples "I" and "H". This insulation resistance variation corresponds to a temperature decrease of 2.5°C in sample "I" (from 200 to 197.5°C) or 1.4% of the temperature range of measurement. Considering the temperature measurement uncertainties of 3.5% presented in section 3.1.5.3, a variation of 2.5°C can be considered as being part of measurement uncertainty. This indicates that, for these samples, the second ball milling energy does not affect the insulation resistance.

The ball-milling energy drastically changes the grain surface and the volume fraction of the secondary Ba-containing phases when no dispersing agent is used (see section 3.2.1.2). Samples ball-milled without dispersing agent also show lower insulation resistance. An example is given by the comparison of sample "G" (250 rpm ball milling, dried reactants and use of dispersing agent) with sample "B" (250 rpm ball milling, dried reactants and no use of dispersing agent). The use of dispersing agent increases the insulation resistance at 200°C from 0.7 to 24s. This is equivalent to a temperature variation of 78°C for sample "B" or 43% of the temperature range measured. Significant insulation resistance differences are also present when comparing samples "G", "H" and "I" (with use of dispersing agent) with samples "B" and "E" (without use of dispersing agent).

Finally, the drying of the reactants for samples ball-milled at 250 rpm - 4h increases the secondary Ba-containing phases volume fraction from 1.5% to 3.1% (see samples "H" and "G"). This decreases the insulation resistance from 50 to 23s, corresponding to a temperature variation of 15°C for sample "G" (from 200 to 185°C) or 8.3% of the total temperature range measured. This indicates that the samples with dried reactants have significantly higher volume fraction of second phase and lower insulation resistance.

To conclude, adding MEK to the solvent mixture increases the second phase volume fraction (see 3.2.1.2). It also slightly increases the insulation resistance from 33 to 45s, being equivalent to a temperature decrease of 5°C for sample "V" (from 200 to 195°C) or 2.7% of the temperature range measured. This can be observed when comparing samples "V" (ethanol as solvent) and "N" (MEK+ethanol as solvent). Considering again the temperature measurement uncertainties of 3.5% a variation of 5°C can be considered as being part of measurement uncertainty.

In short, the increase in the secondary Ba-containing phases volume fraction and average grain surface initially increases the insulation resistance up to 2.5% and $3\mu\text{m}^2$. But, for higher volume fractions and grain surfaces, the trend reverts.

The decrease of the Na_2CO_3 grain size and the change in the ball-milling solvent do not affect the insulation resistance. No large change is observed in secondary Ba-containing phases and in insulation resistance for different ball-milling energies in samples prepared with dispersing agent.

Finally, the use of dispersing agent and of un-dried reactants increase the insulation resistance and mitigates the ball-milling effects on NBT-BT properties.

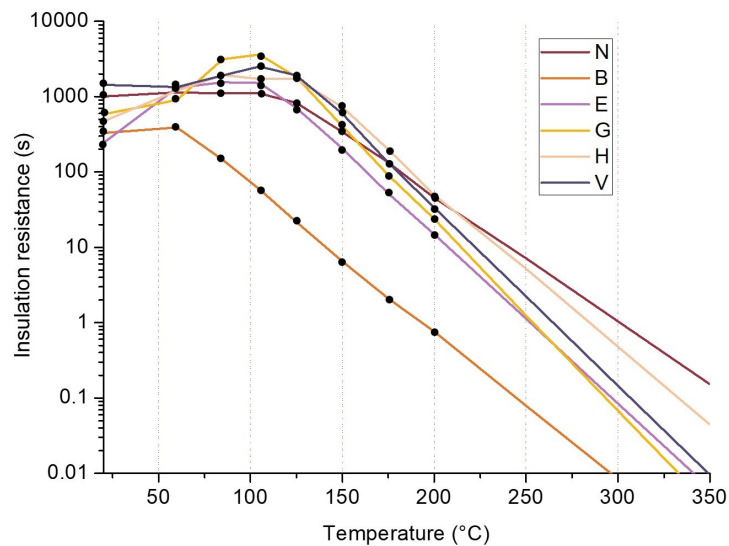


FIGURE 3.25: Insulation resistance versus temperature of samples "N", "B", "E", "G", "H" and "V" with different secondary Ba-containing phases average size and volume fraction (logarithme scale).

Ideal structure and 2nd phase state and relation with the synthesis parameters

Analysing the effect of the secondary Ba-containing phases volume fraction and average grain surface on the NBT-BT dielectric properties and insulation resistance it is possible to conclude that:

- A moderate volume fraction (2.5 to 3.0%) and average grain surface (0.9 to $3.0\mu\text{m}^2$) of the secondary Ba-containing phases is desirable to obtain high permittivity, low dielectric losses, and high insulation resistance.
- It is also important to use a dispersing agent during ball-milling, to obtain high permittivity, low dielectric losses, high insulation resistance, and to mitigate the ball milling energy effects on NBT-BT properties.
- The changes in the Na_2CO_3 grain size and in the ball milling energy when using a dispersing agent do not influence significantly the dielectric and insulation properties.
- The use of MEK and ethanol mixture of solvents also increases the insulation resistance and decreases the dielectric losses.

- The drying of the reactants is not recommended to obtain a higher insulation resistance.

Considering the dielectric and insulation properties of samples analyzed in this section ("*B*", "*E*", "*G*", "*H*", "*I*", "*N*", "*V*", and "*P*"), the influence of the secondary Ba-containing phases separation on these properties and Exxelia's requirements for the high temperature MLCCs, it is possible to conclude that samples "*P*", "*N*", and "*V*" are the most promising ones for the MLCC production, due to their high permittivity, low dielectric losses, high insulation resistance and moderate values of secondary Ba-containing phases volume fraction and average grain surface.

As shown in Fig. 3.15 p. 96 and in Fig. 3.16 p. 97, sample "*U*", synthesized with the same parameters of sample "*P*" but with different stoichiometry, show similar dielectric and insulation properties of sample "*P*". However, it shows a lower T_d and a more stable relative permittivity in temperature, even though the insulation resistance at 200°C of sample "*U*" (87s) is slightly smaller than "*P*" (130s), corresponding to a temperature decrease of 8° for sample "*U*". So, sample "*U*" is also one of the most promising samples for the MLCC production. The suitability of the properties for these samples will be detailed in section 3.2.2.

3.2.1.3 Synthesis parameters

As shown in section 3.2.1.2, the grain size of the Na_2CO_3 initial powder and the ball milling energy for the samples synthesized with dispersing agent do not affect the average grain surface and the volume fraction of the secondary Ba-containing phases. So, these synthesis parameters effects on the material properties can be analyzed independently of this phase.

Figures 3.26 and 3.27 compare the dielectric properties of the samples "*H*" and "*I*" (used to analyze the effect of the change in ball-milling energy) and the samples "*H*" and "*V*" (used to analyze the effect of the change in the Na_2CO_3 grain size).

It is possible to conclude that, the effects observed in section 3.2.1.2 on the dielectric properties due to the change in the ball-milling energy of samples prepared with dispersing agent are valid for the entire temperature range and frequency (i.e. it does not affect the dielectric properties of the NBT-BT as shown in Fig. 3.1.4). Additionally, the change in the grain size of the Na_2CO_3 increases moderately the permittivity between the T_d and the T_m and increasing the value of T_d for all frequency range (see Fig. 3.27).

As also mentioned in section 3.2.1.2, comparing the insulation resistance of samples "*H*", "*I*", and "*V*" in Fig. 3.28, the sample "*H*", synthesized with lower ball milling energy and larger Na_2CO_3 grain size has higher insulating resistance than the other samples for temperatures above 130°C. However, the maximum insulation resistance difference for the entire temperature range is 39%, a value lower than the difference between samples with different stoichiometry ("*U*" and "*Y*" have a 60% difference in insulation resistance at 200°C). So the effect of the Na_2CO_3 grain size and the ball milling energy on the insulation resistance is not as important as the stoichiometry effect.

3.2.1.4 Polishing and strain relaxation

The samples surfaces present a higher percentage of secondary Ba-containing phases and a zirconium oxide contamination from the sintering, contrary to the core (see sections 2.4 and 2.3.2.6). For this reason, a polishing step is necessary to guarantee a more homogeneous sample and to mitigate the effects of the ZrO_2 contamination. The polishing is done in four steps, using polishing papers with decreasing grain sizes, from #180 (average grain size of 82 μm), #800 (average grain size of 21.8 μm), #1200 (average grain size of 15.3 μm)

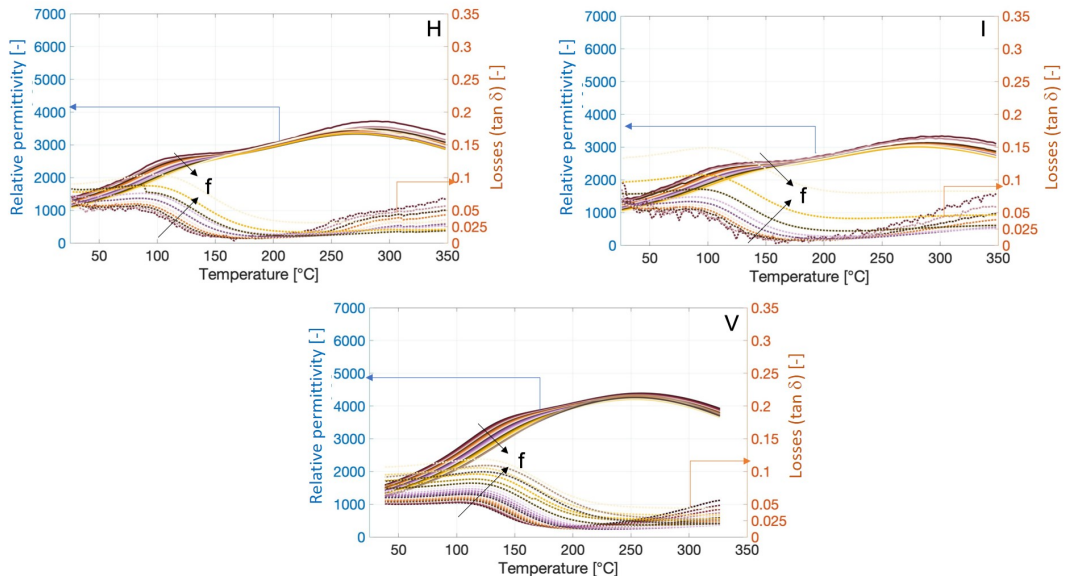


FIGURE 3.26: Relative permittivity and dielectric losses versus temperature from 1kHz to 1MHz for samples "H", "I" and "V" with the same secondary Ba-containing phases average size and volume fraction and different synthesis parameters.

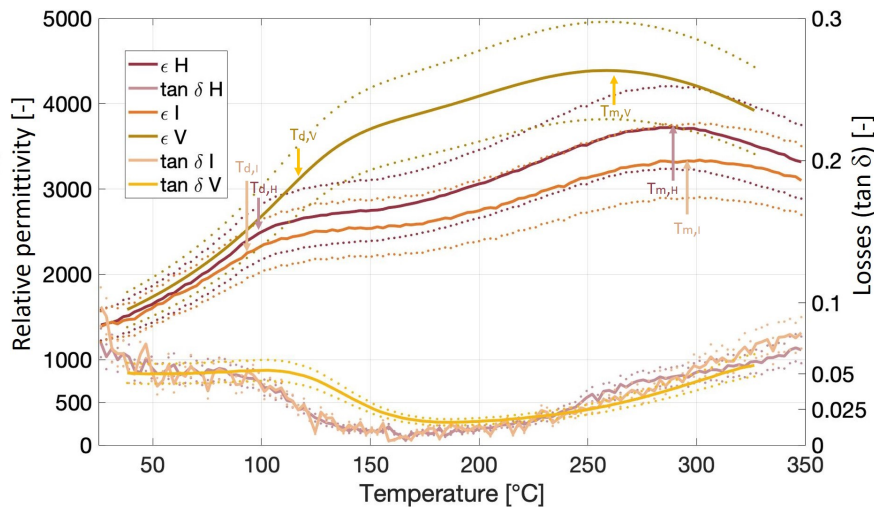


FIGURE 3.27: Comparison of permittivity and dielectric losses versus temperature measured at 1kHz for samples "H", "I" and "V" with the same secondary Ba-containing phases average size and volume fraction and different synthesis parameters. The solid lines indicates the measured values and the dotted lines indicate the uncertainty lines of $\pm 14\%$ for the permittivity and $\pm 13\%$ for the dielectric losses (see section 3.1.4).

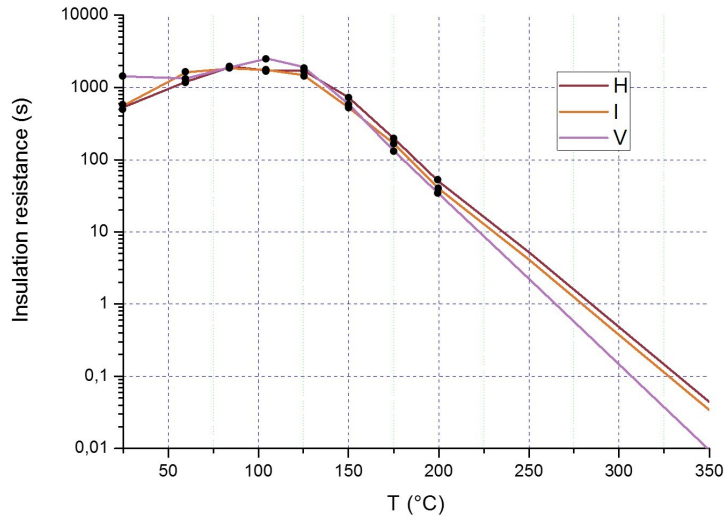


FIGURE 3.28: Insulation resistance versus temperature of samples "H", "I" and "V" with the same secondary Ba-containing phases average size and volume fraction and different synthesis parameters (logarithme scale).

to # 4000 (average grain size of $5\mu\text{m}$). The total thickness removed from the sample surface is $25\mu\text{m} \pm 0.1\mu\text{m}$.

XRD analysis of the polished sample compared to the as-sintered sample is presented in Fig. 3.29.

The low angle side shoulder peaks after polishing are due to the skin effect and the pseudo-cubic, rhombohedral and tetragonal phases coexistence, as described in section 2.3.2.2.

After polishing, a thermal treatment is done in order to relax the strain introduced during polishing. Fig. 3.29 shows the XRD of the samples treated for one hour at 400°C and 500°C . The maximum temperature to relax strain without needing to use a powder to create an atmosphere during the strain relaxation and without forming parasite phases is 400°C .

Two different polished samples ("H" and "N") were cut into four parts. Each part was thermally treated at 400°C for a different times, going from zero to three hours, to relax strain due to polishing. XRD analysis of these samples is shown in Fig. 3.30. In order to evaluate the effectiveness of the strain relaxation and to compare the different thermal treatment times, a Williamson-Hall analysis was carried out on each diffraction pattern.

In the Williamson-Hall analysis, it is assumed that the size and the strain-induced peak broadening vary differently with Bragg's angle. This method assumes that the peak width depends on the Bragg's angle 2θ as:

$$\beta \cdot \cos \theta = C\varepsilon \sin \theta + \frac{K\lambda}{D} \quad (3.14)$$

where β is the integral breadth of the Bragg peak in radians, θ is half of the Bragg's angle, λ is the X-ray wavelength, C is the dimensionless dislocation contrast factor, K is a dimensionless shape factor, D is the diffraction domain size and ε is the strain.

From the $\beta \cdot \cos \theta$ versus $\sin \theta$ plot of the XRD integral breadth fit of each sample, it is possible to estimate the $C\varepsilon$ (strain) and the $\frac{K}{D}$ (average diffraction domain size). The Williamson-Hall fit results for each sample with different strain relaxing times are presented in Figures 3.30 and 3.31. The fit were done using only the peaks corresponding to the pseudo-cubic phase (see section 2.3.2.2).

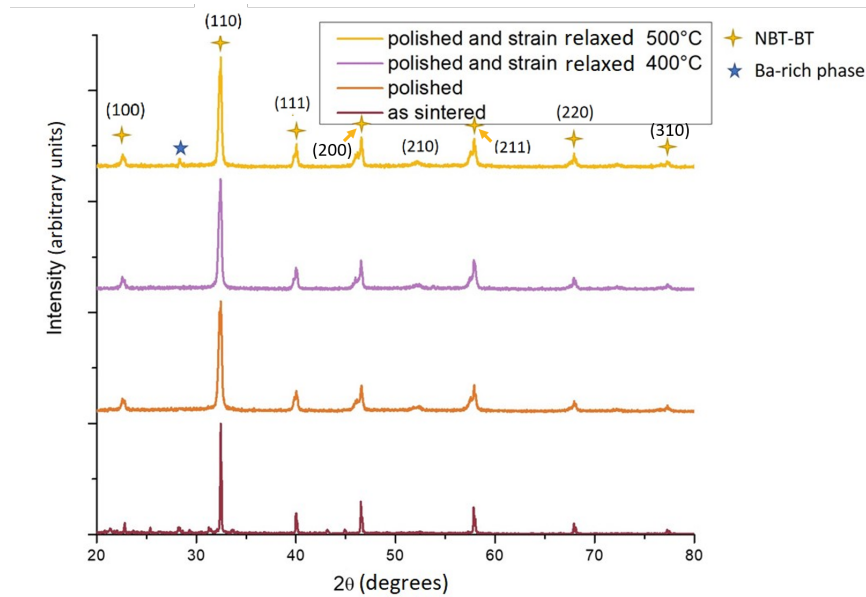


FIGURE 3.29: XRD analysis of NBT-BT samples as-sintered, polished, polished and strain relaxed for 1h at 400°C and polished and strain relaxed for 1h at 500°C.

For both samples, the angular coefficient and, so, strain increases after the polishing. The decrease in the angular coefficient with increasing strain relaxing time shows that the strain is relaxed during the thermal treatment. Moreover, the strain reaches a similar level of strain when compared to the as-sintered sample after three hours at 400°C to relax strains.

The diffraction domain size estimation in Williamson-Hall model is based on the Scherrer equation. When the grains are nanosized, they often contain a single diffraction domain, therefore the grain size can be estimated by the diffraction domain size. However, the average grain size of the NBT-BT samples are all around 1 μm . So the average grain size estimation via Williamson-Hall model cannot be done.

The influence of the internal strain on the dielectric properties was analyzed by measuring the permittivity and the dielectric losses for each sample after different thermal treatment times. The measurement results can be observed in Figures 3.32 and 3.33.

Taking into account the measurement uncertainties, there is no difference in the measured dielectric properties when comparing different strain-relaxing times (different internal strain levels).

In conclusion, the polishing and strain-relaxing steps are necessary to have a better homogeneity and a lower effect of the ZrO_2 contamination in the bulk sample, without introducing internal strains. The maximum temperature for relaxing strain is 400°C and the internal strains are relaxed after three hours. However, the internal strains do not markedly affect the dielectric properties of the final NBT-BT samples.

3.2.2 Comparison of the measured properties with Exxelia's specifications

Samples "U", "P", "V", "H", and "N" have the best dielectric properties and insulating resistance compared to Exxelia's specifications (see section 3.2.1). These samples will be analyzed in details in this section, to choose the best stoichiometry and the best synthesis method that will be used for the MLCC synthesis.

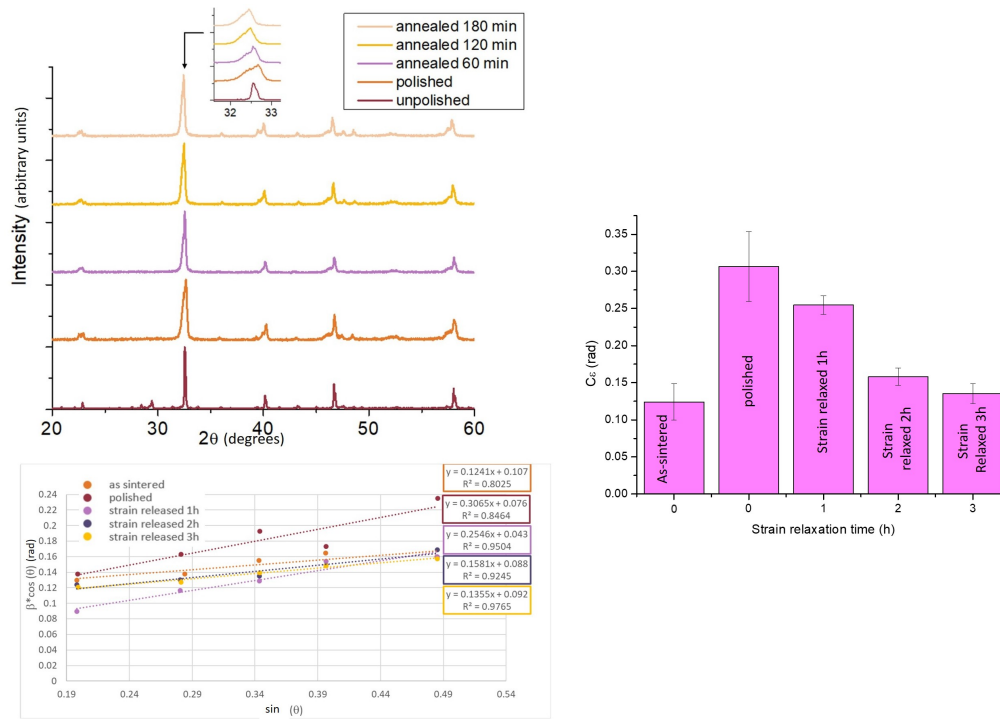


FIGURE 3.30: XRD measurements (top) and Williamson-Hall fits for sample "N" (bottom). The equations and the results of the fits are shown in the boxes. The color of the box indicates the corresponding fit.

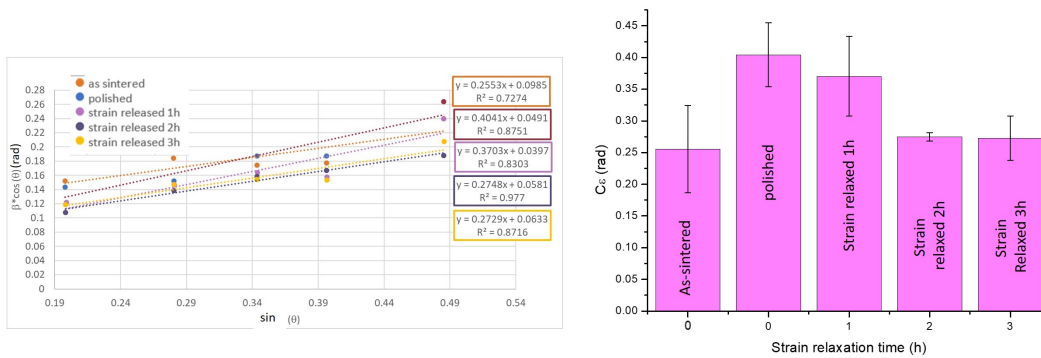


FIGURE 3.31: Williamson Hall fits for sample "H". The equations and the results of the fits are shown in the boxes. The color of the box indicates the corresponding fit.

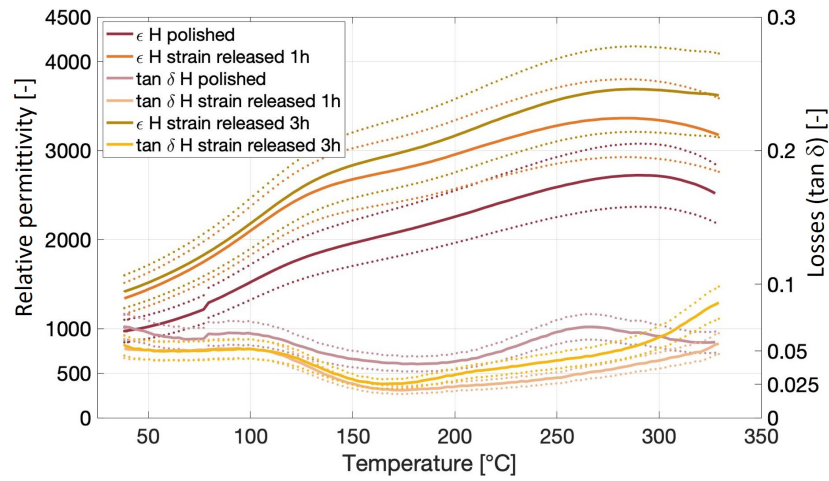


FIGURE 3.32: Comparison of relative permittivity and dielectric losses versus temperature measured at 1kHz for samples "H" polished, after 1h strain-relaxed at 400°C and after 3h strain-relaxed at 400°C. The solid lines indicates the measured values and the dotted lines indicate the uncertainties lines of $\pm 14\%$ for the permittivity and $\pm 13\%$ for the dielectric losses (see section 3.1.4).

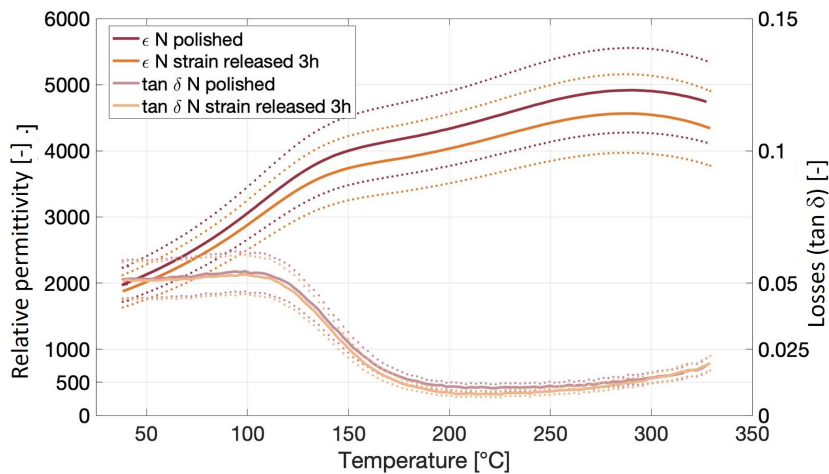


FIGURE 3.33: Comparison of the relative permittivity and dielectric losses versus temperature measured at 1kHz for samples "N" polished and strain-relaxed for 3h at 400°C. The solid lines indicates the measured values and the dotted lines indicate the uncertainties lines of $\pm 14\%$ for the permittivity and $\pm 13\%$ for the dielectric losses (see section 3.1.4)

3.2.2.1 Industrial layout graphics for permittivity, dielectric losses and RI versus temperature

The permittivity variation with temperature is shown in Fig. 3.34 for these samples. The chosen reference temperature is 213°C, since it is the mean temperature between the maximum operation temperature required (350°C) and the minimum average depolarization temperature for NBT-BT (75°C).

Sample "U" presents the most stable permittivity in temperature, since, considering the 1kHz frequency (industrial standard), the permittivity of this sample is $\epsilon_r = 2338 \pm 15\%$ (limits shown as dotted lines) from 90 to at least 300°C.

The evolution of the dielectric losses with temperature are shown in Fig. 3.34 for the same samples, with the industrial limit of 2.5% in the operation temperature range as dotted lines.

Sample "U" also presents the lower dielectric losses and, for the frequency of 1kHz, the losses are $\tan \delta \leq 2.5\%$ from 90 to at least 300°C.

Finally, the insulation resistances with temperature (logarithme scale) are shown in Fig. 3.35. The measurements were done to a maximum temperature of 200°C, due to equipment limitations (see section 3.1.1). The curves extrapolation were done through a exponential decrease in the insulation resistance in temperatures, as it is normally observed for MLCCs at high temperatures (see section 3.1.1).

Considering Exxelia's specifications for the insulation resistance (IR ≥ 10 s from 250 to 300°C and 1s from 300 to 350°C), none of the samples give an expected result. However, samples "N", "P" and "U" have the highest insulation resistances at high temperature, with IR ≥ 1 s up to 300°C.

To conclude, the dielectric properties and the insulation resistance of NBT-BT in temperature were analysed, to evaluate the effects of stoichiometry, structure, phase separation, synthesis parameters and internal strain.

The dielectric and insulation properties of the material are particularly sensitive to the stoichiometry and, more specifically, to the Na/Bi ratio. The increase in the Na content inhibits the secondary Ba-containing phases formation and increases the conductivity. The increase in the Bi content initially compensates for the oxygen vacancy formation (decreasing conductivity) and then forms a second phase, increasing again the conductivity.

Considering Exxelia's requirements for the high temperature MLCC, the stoichiometry of sample "U" is the most adapted one, due to its high insulation resistance and lower dielectric losses and permittivity variation in temperature when compared to others.

The phase separation and the secondary Ba-containing phases formation are due to the Na evaporation during sintering. The increase of volume fraction and in average grain surface of this phase initially increases the permittivity, decreases the dielectric losses and increases the insulation resistance, due to the elimination of oxygen vacancies, being beneficial to the MLCC applications. Above a critical fraction and grain surface for the secondary Ba-containing phases, the tendency reverts, due to the conducting character of this phase. So, an intermediary volume fraction (2.5 to 3.0%) and average grain surface (0.9 to 3.0 μm^2) of the secondary Ba-containing phases is desirable.

To obtain this intermediary average grain surface and volume fraction of secondary Ba-containing phases, the best dielectric and insulation properties, a dispersing agent should be used during ball milling in MEK and ethanol mixture and the reactants should not be dried before weighing. In this case, the average Na_2CO_3 grain surface and the energy of ball milling do not affect significantly the final bulk properties.

Considering Exxelia's requirements, samples "P" (un-dried reactants, ball-milled with

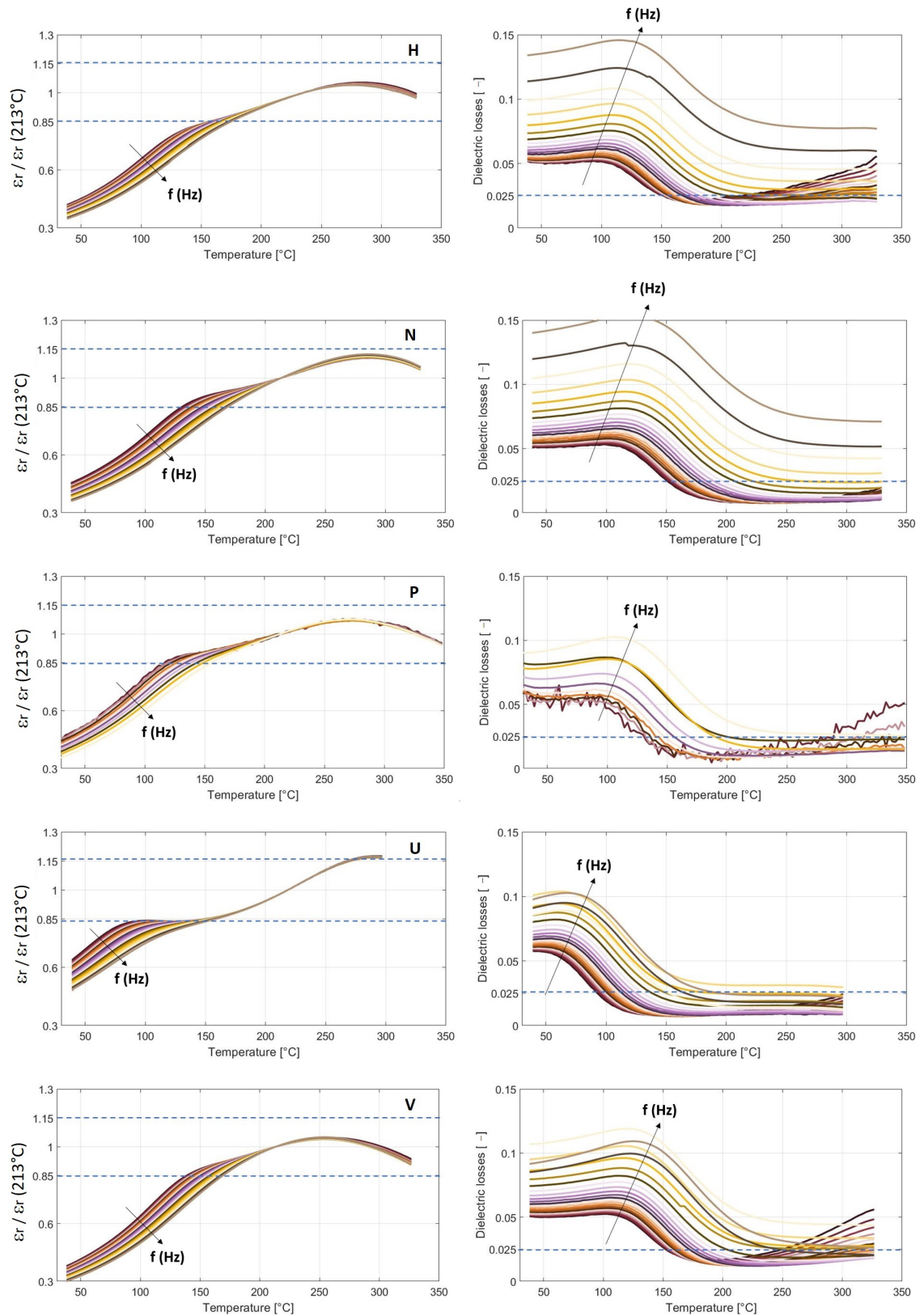


FIGURE 3.34: Variation of the relative permittivity with respect to the reference temperature (213°C) and dielectric losses from 1kHz to 1MHz for samples "H", "N", "P", "U" and "V" respectively and Exxelia's specifications for the high temperature MLCCs. The arrows show the increasing frequency curves. The dotted lines stand for Exxelia's requirements on relative permittivity variation in temperature, and on dielectric losses maximum value.

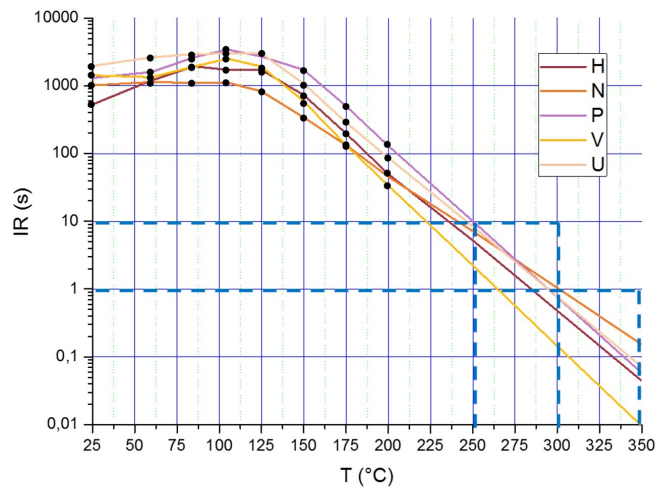


FIGURE 3.35: Insulation resistance to the reference temperature (213°C) and dielectric losses for samples "H", "N", "P", "U" and "V" and Exxelia's specifications for the high temperature MLCCs

dispersing agent in ethanol and MEK mixture during 8h at 350 rpm with fine Na_2CO_3 powder), "N" (un-dried reactants, ball-milled with dispersing agent in ethanol and MEK mixture during 4h at 250 rpm with fine Na_2CO_3 powder) and "U" (un-dried reactants, ball-milled with dispersing agent in ethanol and MEK mixture during 8h at 350 rpm with fine Na_2CO_3 powder and lower nominal Na/Bi ratio compared to samples "N" and "P") are the most adapted for the NBT-BT application in MLCCs in terms of synthesis parameters and secondary Ba-containing phases characteristics, confirming the synthesis parameters and phase separation analysis.

Finally, the polishing and strain relaxation are an important step to have a better homogeneity and a lower ZrO_2 contamination from the powder used to create sintering atmosphere. The thermal treatment should be done at 400°C during 3h to release the introduced strain. However, the internal strain does not affect drastically the NBT-BT dielectric properties.

Lastly, it is possible to conclude that the sample presenting the best stoichiometry, synthesis parameters, secondary Ba-containing phases average grain surface and volume fraction and strain level to obtain the most promising dielectric and insulation properties for the MLCC production is sample "U".

3.3 Dielectric spectroscopy

NBT-BT samples show a frequency dependent behaviour. Several models were considered to analyse this dependence: a composite model with a conducting phase in an insulating matrix (through the Maxwell-Wagner model, section 3.3.1), two parallel and frequency dependent RC circuits representing a grain core and grain boundary with different conductivity (through a Cole-Cole plot, section 3.3.1.1) and a relaxor behaviour (through the modified Curie-Weiss law, section 3.3.1.2).

3.3.1 Maxwell-Wagner model

The Maxwell-Wagner model is used to estimate the dielectric properties and the frequency dispersion of the permittivity when an external electric field is applied to a heterogeneous system of dielectrics. This model is applied to systems in which the ratio of permittivity to conductivity is different in the various phases, at least one of the phases having a conducting behaviour and in which the inhomogeneities are on a scale that is large compared to the size of the sample. So, it describes the properties of the accumulation of charges at the boundary between one dielectric phase and one conducting phase. For that reason, this model is also called the space-charge model. [5, 18]

In the case of the NBT-BT, it is possible to apply the model considering that the secondary Ba-containing phases are conducting and that they have large-scale randomly-dispersed grains in a less conducting NBT matrix phase. In this case, the Maxwell-Wagner model shows the influence of the secondary Ba-containing on the dielectric properties and, more specifically, on the frequency dispersion of the NBT-BT samples.

As mentioned before, in the Maxwell-Wagner systems there is an effect of charge accumulation at the interfaces in the material related to polarization discontinuity. [49] So the system can be modeled by an equivalent circuit of two parallel RC circuits. The equations taken into account for the modeling are similar to the Debye relaxation. However, the Debye relaxation considers only the polarization relaxation, while the Maxwell-Wagner model takes into account the interfacial polarization due to the presence of a more conducting-phase particles. So the relative permittivity, imaginary permittivity and dielectric losses can be expressed as:

$$\epsilon'_r = \frac{1}{\epsilon_0} \cdot \left(\epsilon_\infty + \frac{\epsilon_0 - \epsilon_\infty}{1 + \omega^2 \tau^2} \right) \quad (3.15)$$

$$\epsilon'' = \frac{(\epsilon_s - \epsilon_\infty) \cdot \omega \tau}{1 + \omega^2 \tau^2} + \frac{1}{\omega C_0 (R_1 + R_2)} \quad (3.16)$$

$$\tan \delta = \frac{(\epsilon_s - \epsilon_\infty) \cdot \omega \tau}{\epsilon_s + \epsilon_\infty \omega^2 \tau^2} + \frac{\sigma}{\omega \epsilon_0} \cdot \frac{1}{\epsilon_0 + \frac{\epsilon_s - \epsilon_\infty}{1 + \omega^2 \tau^2}} \quad (3.17)$$

where ϵ_s and ϵ_∞ are the static and high frequency permittivities, τ is the relaxation time, ω is the angular frequency, C_0 is the empty cell parameter, R_1 and R_2 are the resistances of the two phases and σ is the conductivity of the material. [49]

The resulting permittivity and dielectric losses are shown in Fig. 3.36. [39].

In order to evaluate the Maxwell-Wagner fit for samples with different volume fractions of secondary Ba-containing phases, the permittivity and the dielectric losses versus frequency for different measurement temperatures were plotted for samples "H", "P" and "U". These plots are shown in Fig. 3.37.

Due to an internal auto-scale in the impedance measurement device, the raw dielectric vs frequency data (before correction) shown in Fig. 3.38 for sample "U", presents a discontinuity for the high frequency measurements. These discontinuities are present for most samples and they represent a shift on the high temperature dielectric losses for lower values, with a delta of between 0.5 to 2%.

For this reason, the dielectric properties in frequency shown in Fig. 3.37 corrected for these high-frequency dielectric-losses shift.

It can be observed that the relative permittivity decreases with frequency, but no permittivity plateau is observed. For low temperatures (lower than 180°C for sample "P", 132°C

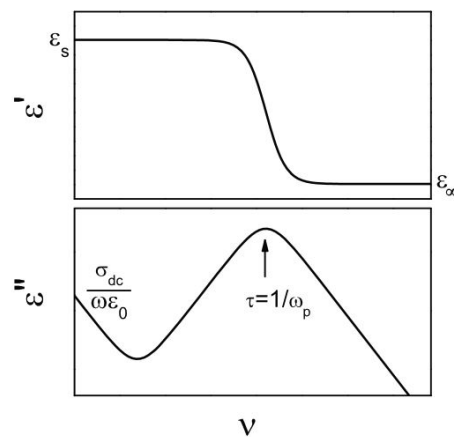


FIGURE 3.36: General behaviour of the real (ϵ') and imaginary (ϵ'') parts of the permittivity in the Maxwell-Wagner model as a function of frequency. The frequency ν is shown in logarithmic scale. [39]

for sample "H", and 207°C for sample "U"), the dielectric losses increase with frequency. For high temperatures, the losses first decrease then increase with frequency. This indicates that there may be a Maxwell-Wagner type relaxation, due to the presence of conducting secondary Ba-containing phases particles.

However, for the range of frequencies measured (1kHz to 1MHz), the only measured part of the Maxwell-Wagner relaxation curve is as indicated in Fig. 3.39 with the red lines for the case of a composite BaTiO₃-Cu composite.[49] So, the relaxation curve could not be entirely measured and the maximum losses could not be achieved.

All the NBT-BT samples presenting secondary Ba-containing phases have similar behaviour as the ones shown in Fig. 3.37.

Considering equations 3.15 and 3.17 and Fig. 3.36, it can be seen that the Maxwell-Wagner fit for measures that do not include at least ω_p or limits for low and high frequencies values would create huge uncertainties in its parameters. So the fit could not be done for the measurements shown here.

In conclusion, the Maxwell-Wagner model may be applied to explain the frequency dispersion of the dielectric properties of the samples. Even if the fit could not be done, due to a limited frequency range of measurements, the Maxwell-Wagner model is useful to confirm the hypothesis that the Ba-containing phases are more conducting than the NBT-matrix phase. So that the interfacial polarization due to the presence of this phase contributes to the increase of the dielectric properties of the material.

3.3.1.1 Nyquist analysis

The Nyquist plot is a graphic representation of the complex impedance Z^* . In this plot, the real and imaginary parts of the impedance are plotted in the complex plane, for different frequencies and a single temperature. Using the electrical-circuit-modeling approach, it is possible to estimate the contribution of different parts of the measured system (grain core, grain boundary and electrode, for example) for the effective properties measured, since it is possible to identify the kinetics of different steps involved in the effective properties.

In the case studied here, the Nyquist analysis could be useful to identify the contribution

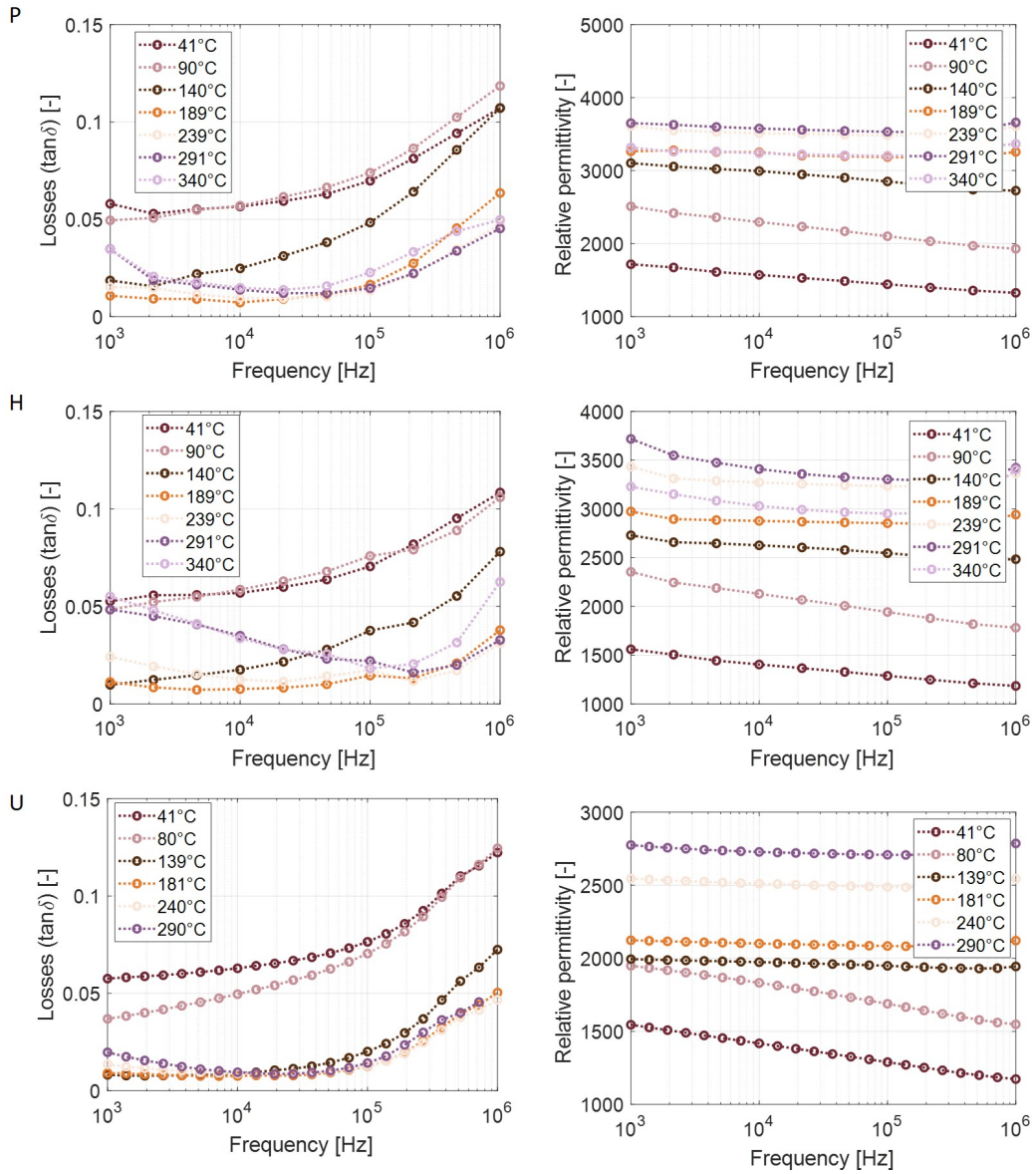


FIGURE 3.37: Relative permittivity and dielectric losses versus frequency for different temperatures and for samples "P", "H", and "U" (from the top to the bottom) with different volume fractions of secondary Ba-containing phases.

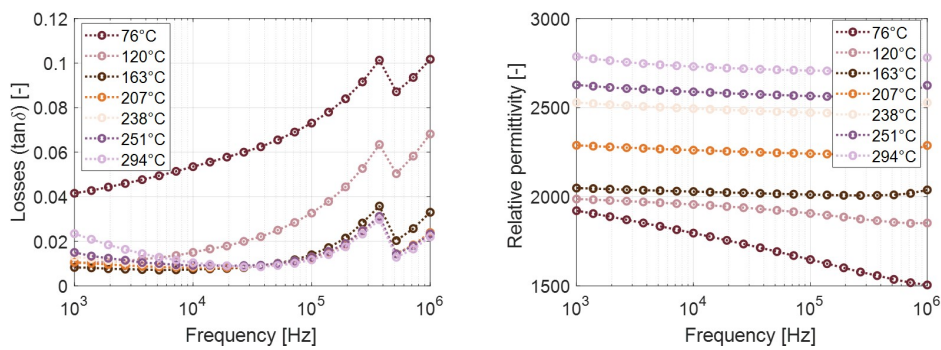


FIGURE 3.38: Raw relative permittivity (left) and dielectric losses (right) vs frequency data (before correction) shown for sample "U", showing a discontinuity for the high frequency measurements.

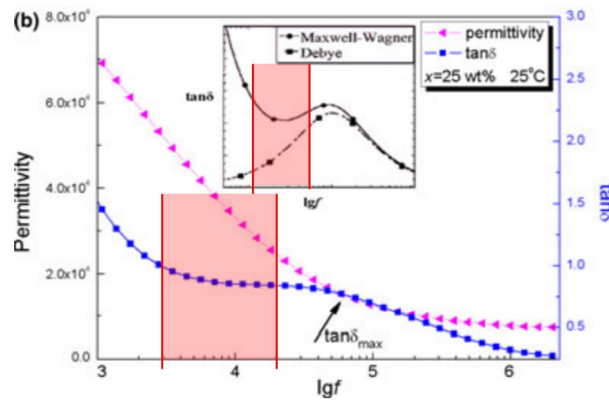


FIGURE 3.39: Permittivity and dielectric losses vs frequency (logarithmic scale) for the case of a composite BaTiO₃-Cu composite. [49] The red lines indicate a similar frequency range from the one measured for the NBT-BT samples.

of the samples (grain core and grain boundary) and of the electrodes to the measured dielectric properties (calculated from the impedance).

Fig. 3.40 shows the Nyquist plots for NBT-BT samples "P", "H", and "U". The scales in both axis are not the same so that the details of the curves can be observed.

The fit of the curves using an equivalent circuit cannot be done, due to the a frequency limitation (the range of frequencies used for these measurements go from 1kHz to 1MHz). So, to estimate the values of the material's properties and to separate the contributions from the grain core, grain boundary, and electrodes, a new measurement should be done including lower frequencies, as suggested in section 4.4 about future works.

For this reason, the Nyquist plots presented here will only be analyzed qualitatively.

Ning *et al.* showed a similar Z^* plot for BaTiO₃ - Cu composites, as shown in Fig. 3.41. [49] They adopted an equivalent circuit of two parallel RC circuits, the first one related to the grains (core) and the second one related to the grain boundaries. In this case, the impedance can be calculated as:

$$Z' = \frac{R_g}{1 + (\omega R_g C_g)^2} + \frac{R_{gb}}{1 + (\omega R_{gb} C_{gb})^2} \quad (3.18)$$

$$Z'' = R_g \left(\frac{\omega R_g C_g}{1 + (\omega R_g C_g)^2} \right) + R_{gb} \left(\frac{\omega R_{gb} C_{gb}}{1 + (\omega R_{gb} C_{gb})^2} \right) \quad (3.19)$$

where (R_g, R_{gb}) and (C_g, C_{gb}) are the resistance and capacitance of grains and grain boundaries, respectively. [49]

For those composites, the R_{gb} contribution to the Z'' peak is much higher than the R_g . This can be seen by the 25% Cu curve in Fig. 3.41, where the diameter of the semi-circle associated with the grain boundaries (left) is much higher than the one associated with the grains (right). So the composite is composed of conducting grains with resistive grain boundaries.

For the NBT-BT samples analysed here, one hypothesis to describe the Nyquist plot behaviour would be that, for the low temperature plots shown in the right side of Fig. 3.40 (up to 140°C for sample "U", and up to 180°C for samples "H" and "P"), the resistance associated with the grain boundaries is much higher than the one associated with the grain

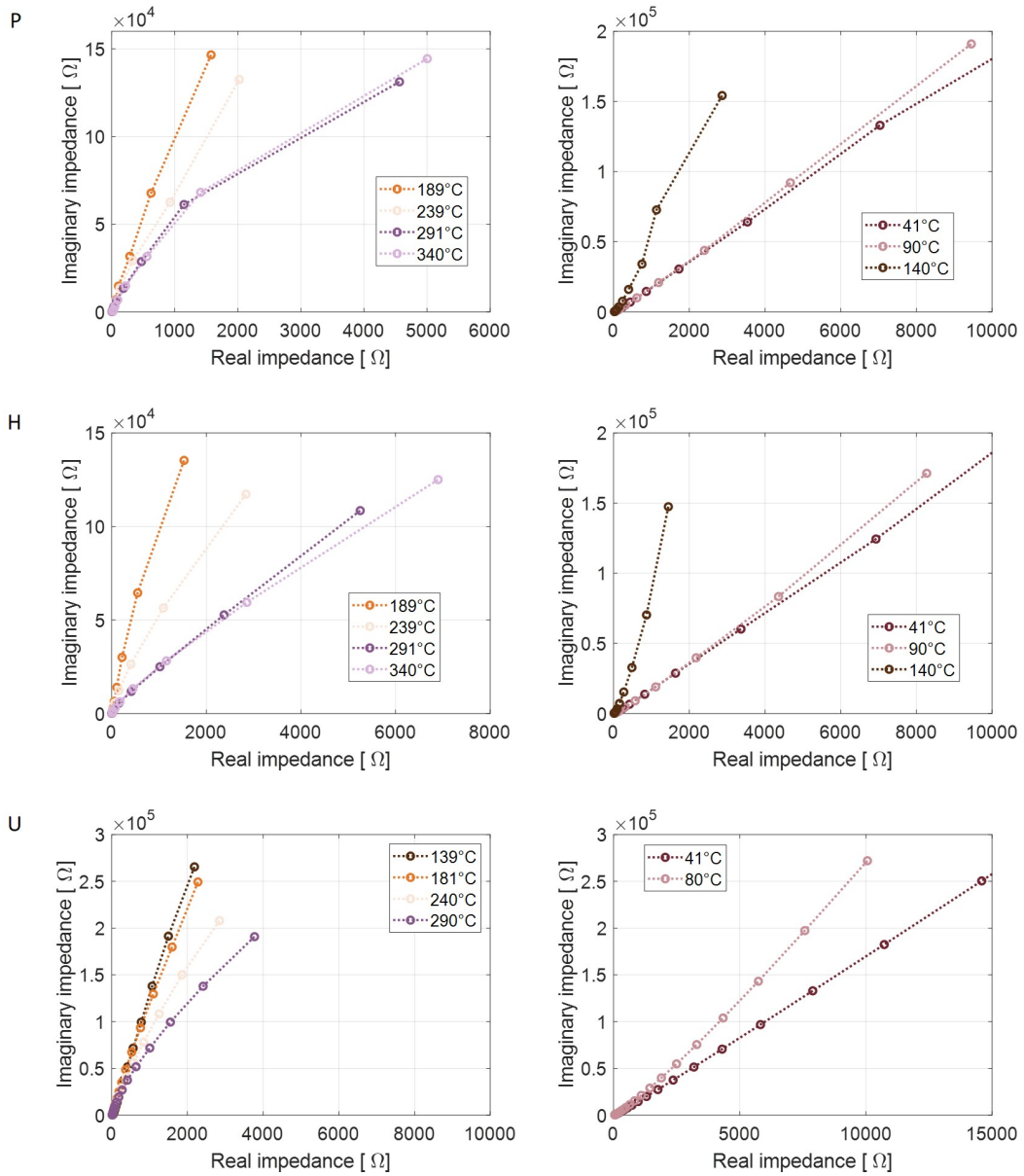


FIGURE 3.40: Nyquist plots for NBT-BT samples "P", "H" and "U" (from top to bottom) for the high temperature (left) and low temperatures (right).

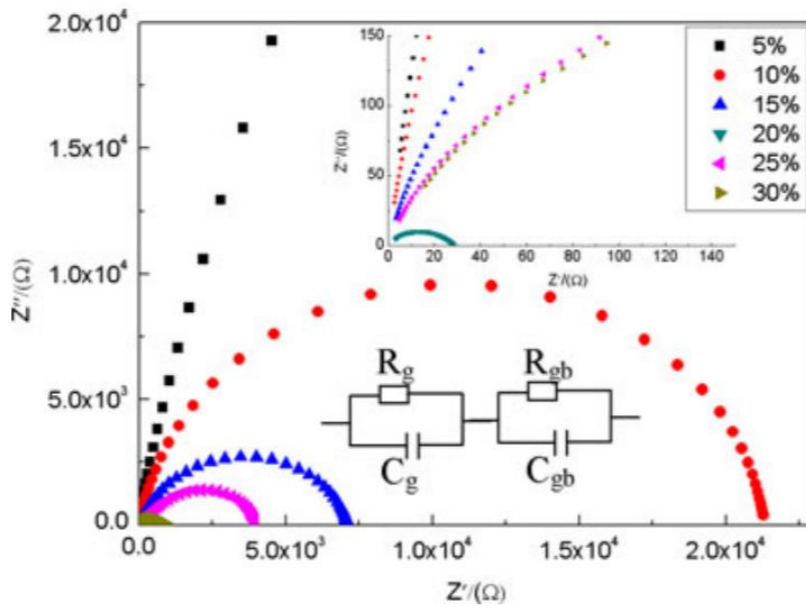


FIGURE 3.41: Nyquist plot for BaTiO₃ - Cu composites with different Cu fractions. [49]

cores. Besides that, this grain boundary resistance increases with increasing temperature until a critical temperature is reached. Then the resistance of the grain boundaries decreases with increasing temperature, creating the high temperature plots shown in the left side of Fig. 3.40.

As mentioned before, in order to confirm this hypothesis, a measurement including lower frequencies should be done.

Once the lower frequency measurement is included and the entire Nyquist plot can be analyzed, the effects of the secondary Ba-containing phases should be taken into account. This could potentially be done using a third RC series component representing the secondary phase grains effect, with low R values.

In conclusion, the Nyquist plot model may be applied for the NBT-BT samples. It indicates that a two parallel RC circuits associated with the grain cores and the grain boundaries could be used. In this case, the resistance associated with the grain boundaries is larger than the one associated with the grain cores and it increases with temperature up to a critical temperature, where the tendency reverts. However, a new measurement including lower frequencies should be performed to confirm this hypothesis.

3.3.1.2 Relaxor character

The frequency dispersion of the real part of the relative permittivity is described for relaxors by the modified Curie-Weiss law (equation 3.20):

$$\frac{1}{\epsilon_r} - \frac{1}{\epsilon_{r,m}} = \frac{(T - T_m)^\gamma}{C} \quad (3.20)$$

where $\epsilon_{r,m}$ is the maximum relative permittivity value, T_m is the temperature of the maximum relative permittivity, ϵ_r is the permittivity for temperatures higher than T_m , T is the temperature of where ϵ_r is measured, C is the Curie-Weiss constant and γ is the constant used to indicate if the material is a ferroelectric or a relaxor.

This law predicts the permittivity behaviour for ferroelectric materials for temperatures above the paraelectric transition. Classic ferroelectrics have $\gamma = 1$ while relaxor materials have $\gamma = 2$. [26]

In order to evaluate the effects of the stoichiometry and of the secondary Ba-containing phases size and volume fraction on the relaxor character of the material, samples "U", "P", "G", "H", "B", "E" and "I" were evaluated by the modified Curies-Weiss law. The relaxor characteristics for samples "N" and "V" were also evaluated, since they are part of the best candidates for the MLCC production (see section 3.2.2).

The fit was done using the linear regression for the equation:

$$\ln\left(\frac{1}{\epsilon_r} - \frac{1}{\epsilon_{r,m}}\right) = \gamma \cdot \ln(T - T_m) - \ln C \quad (3.21)$$

Sample "H" is used as an example to show the plot of $\ln\left(\frac{1}{\epsilon_r} - \frac{1}{\epsilon_{r,m}}\right)$ versus $\ln(T - T_m)$ for different frequencies and the evolution of the C and γ estimations with increasing frequency ranges. From Fig. 3.42 it is possible to see that the low frequencies have a less precise estimations, when using the modified Curie-Weiss law.

The estimated C and γ values for the frequency range of 1 kHz to 1 MHz for each sample are presented in Fig. 3.43.

Except for sample "E", all other samples present a relaxor character, with γ close to 2. The mixed character of sample "E" between a relaxor and a ferroelectric shows that a high volume fraction of small-sized secondary Ba-containing phases grains affects the effective properties of the sample. This also shows that the second phase and the interaction between neighbouring grains can tune the relaxor behaviour in NBT-BT material. [52]

A slight increase in the gamma value is observed for the sample "U" that could mean that the stoichiometry and the decrease in the Na/Bi ratio are a good way to tune the relaxor behaviour in NBT-BT material. For sample "Z", even though the Na/Bi ratio is higher than for the "U" sample, there is no second phase to decrease the relaxor character of the material, showing that the second phase effect on the relaxor properties is more important than the stoichiometric one.

In conclusion, the three frequency dispersion models for the dielectric dispersion can possibly be applied to the NBT-BT samples, to explain the frequency scattering.

The Maxwell-Wagner model fit could not be done, due to a limited frequency range of measurements. However, it was useful to confirm the hypothesis that the Ba-containing phases are more conducting than the NBT-matrix phase and that an interfacial polarization contributes to the dielectric properties of the material.

The Nyquist plot fit could not be done, also due to a limited frequency range of measurements. However, this model indicates that two circuits associated with the grain cores and the grain boundaries could be used. In this case, the resistance associated with the grain boundaries is larger and it increases with temperature up to a critical temperature.

Finally, the modified Curie-Weiss model fit could be done and it indicated that the all NBT-BT samples present a relaxor character, except for sample "E". This indicates that the secondary Ba-containing phases and the interaction between neighbouring grains can tune the relaxor behaviour in NBT-BT.

Even though the Maxwell-Wagner and Nyquist plot fits could not be done, it is not a problem for this study, since the frequency dispersion is not a part of the main requirements for the MLCC applications.

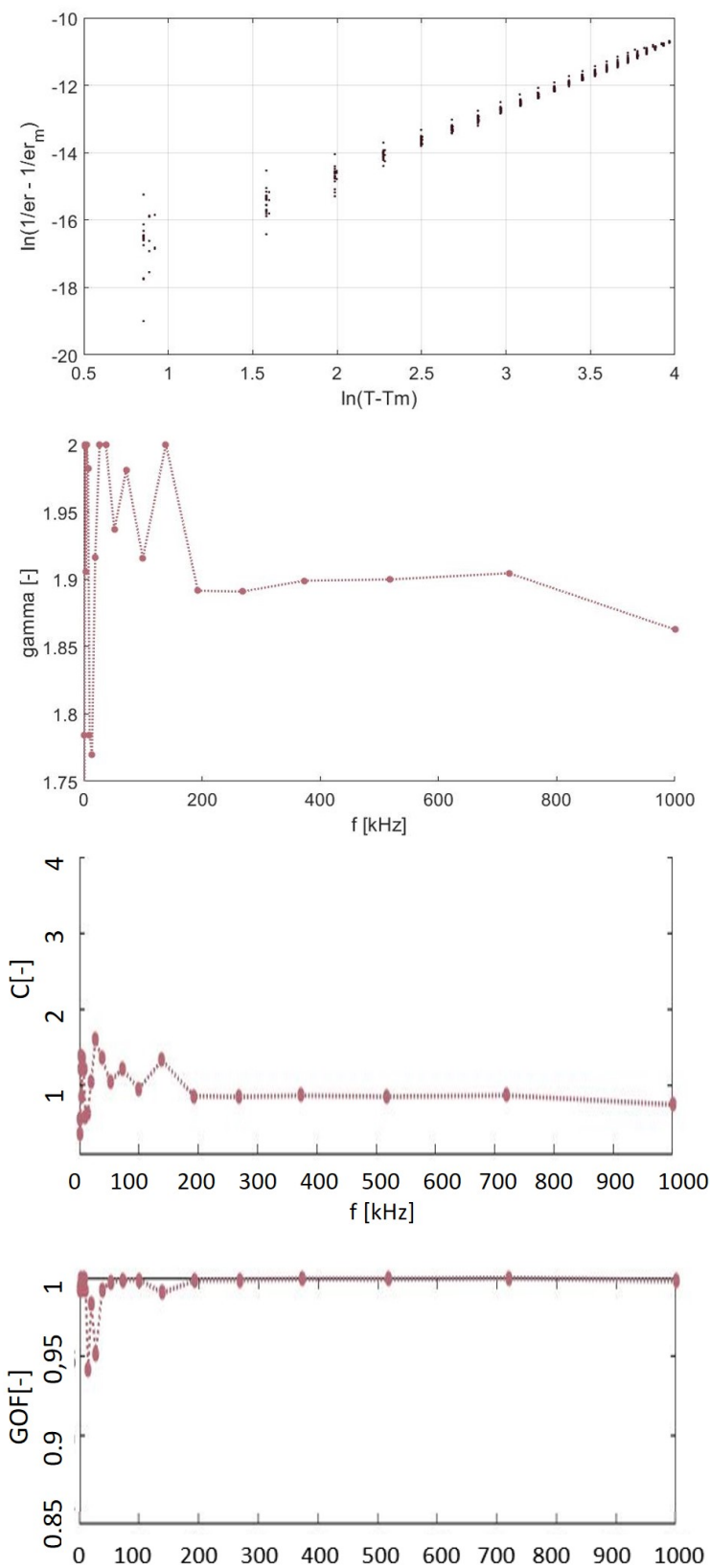


FIGURE 3.42: Curie-Weiss law with increasing frequency for different frequencies and evolution of the C and γ estimations in frequency for sample "H"

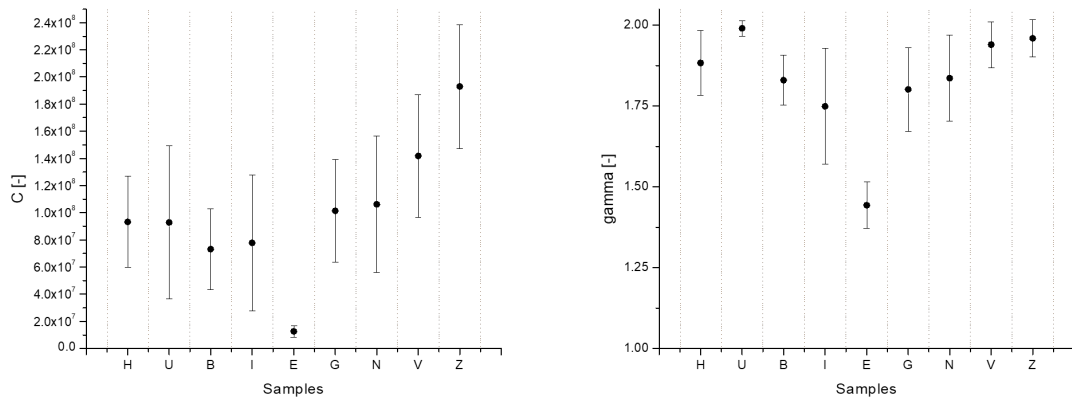


FIGURE 3.43: Estimated C and γ values for the frequency range of 1 kHz to 1 MHz for samples "U", "P", "G", "H", "B", "E", "N", and "V"

3.4 Co and Mn additions and properties improvement

In order to try to improve the dielectric properties of the NBT-BT, specially to decrease the dielectric losses and to increase the insulation resistance, some samples were sintered with addition of Mn and Co oxides and characterized.

3.4.1 Co_3O_4

Adding Co_3O_4 was chosen, since it can act as a sintering aid and it can increase the temperature of the maximum permittivity, decrease the dielectric losses and stabilize permittivity for temperatures lower than 400°C (see section 1.4.2.5). Moreover, it is an additive use intensively for industrial applications and at Exxelia.

For NBT [69] and NBT-BT-KBT, [21] the percentage of Co_3O_4 added varies from 0.3 to 0.8 mol%. For the pure NBT, sample with 0.3 mol% of Co-addition showed good dielectric properties, with low dielectric losses and stable permittivity in temperature. [69] For the NBT-BT-KBT, samples with 0.2 and 0.4 mol% of added-Co showed good dielectric and ferroelectric properties. [21]

In this study, two different Co_3O_4 percentages were tested: 0.5 and 5 wt% corresponding to 0.4 and 4.4 mol%, respectively. Samples were prepared with 250 rpm for 4 hours ball-milling with dispersing agent, with un-dried reactants, and with sintering at 1050°C for three hours under ZrO_2 . The Co_3O_4 was added before the second ball-milling.

3.4.1.1 Phase separation

Initially, the structure and phase separation of the samples were analyzed. Figures 3.44, 3.45 and 3.46 show the SEM and XRD measurement of samples with 0.4 and 4.4% of Co_3O_4 .

The SEM measurements in Fig. 3.44 show that the sample with 0.4% of Co_3O_4 have a similar phase separation as the NBT-BT samples, with a secondary Ba-containing phases separation and a NBT matrix. However, the 4.4 mol%-Co-addition sample does not have secondary Ba-containing phases separation, but the excess of Co forms a new Co-rich phase. The composition of each phase could not be measured with sufficient precision, however, it can be considered that the phase separation takes place similarly to the pure NBT-BT material

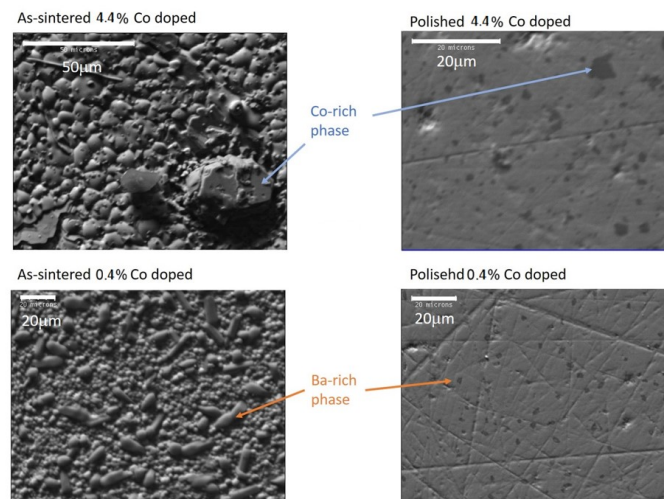


FIGURE 3.44: SEM images of the as-sintered (left) and the polished and strain relaxed (right) samples with 0.4mol% (bottom) and 4.4mol% (top) Co_3O_4 .

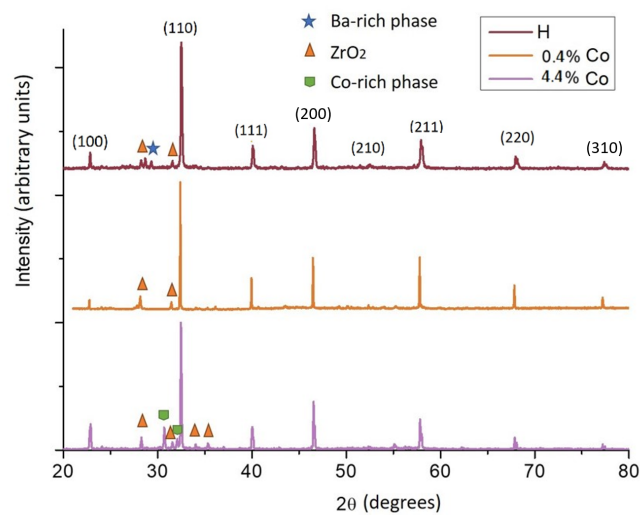


FIGURE 3.45: XRD measurement of as-sintered samples with 0.4mol% and 4.4mol% of Co_3O_4 and comparison with the pure NBT-BT sample ("H").

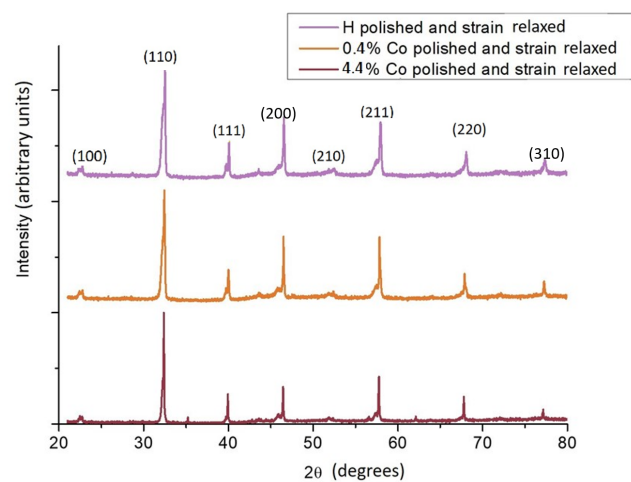


FIGURE 3.46: XRD measurement of the polished and strain-relaxed samples with 0.4mol% and 4.4mol% Co_3O_4 and comparison with the pure NBT-BT sample ("H").

for the 0.4mol%-Co-addition sample with a slightly higher concentration of Co on the secondary Ba-containing phases. The EDS cartography of the Co-addition as-sintered samples shows the Co separation in the 4.4mol%-Co-addition sample and the slightly higher concentration of Co on the secondary Ba-containing phases in the 0.4mol%-Co-addition sample. (see Fig. 3.47).

The XRD measurements in Fig. 3.45 show no phase separation for the 0.4% of Co_3O_4 -

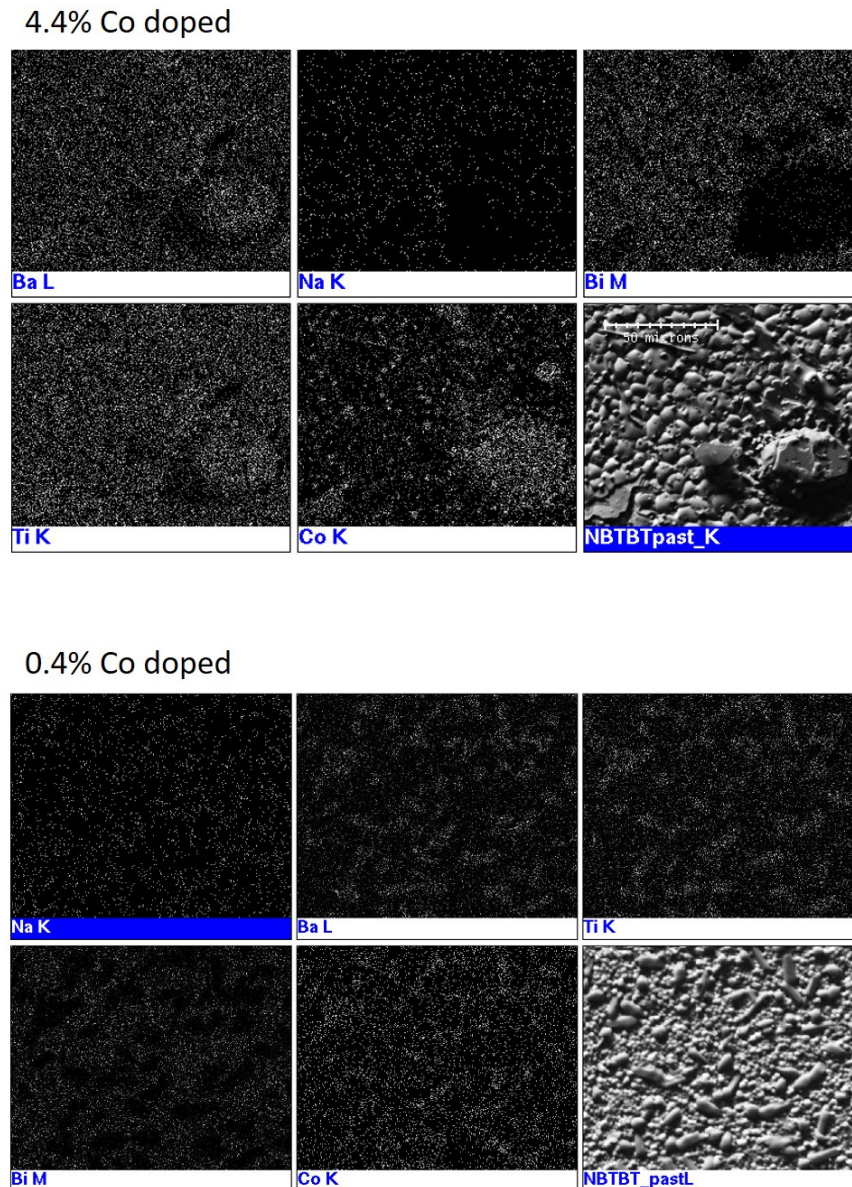


FIGURE 3.47: EDS cartography of the 4.4mol%-Co-addition as-sintered sample (top) and the 0.4%-Co-addition as-sintered sample(bottom).

addition sample. For the the as-sintered 4mol%-Co-addition sample, however, it is possible to identify peaks from a new unidentified phase. Even if the stoichiometry and structure of this phase were not identified, by comparing the XRD and SEM results, it is possible to conclude that they correspond to the Co-rich phase. After polishing and relaxing strain of the 4.4mol%-Co-addition sample (Fig. 3.46), no extra peak was identified, but SEM images still indicate the presence of some Co-rich phase. This indicates that the Co excess and second

phase are mostly concentrated at the sample's surface.

3.4.1.2 Dielectric properties in temperature

Finally, the comparison of the dielectric properties of the Co-addition samples with the equivalent pure NBT-BT (sample "H") is presented in Fig. 3.48.

For the 4.4mol%-Co-addition sample, a clear increase in the dielectric losses is ob-

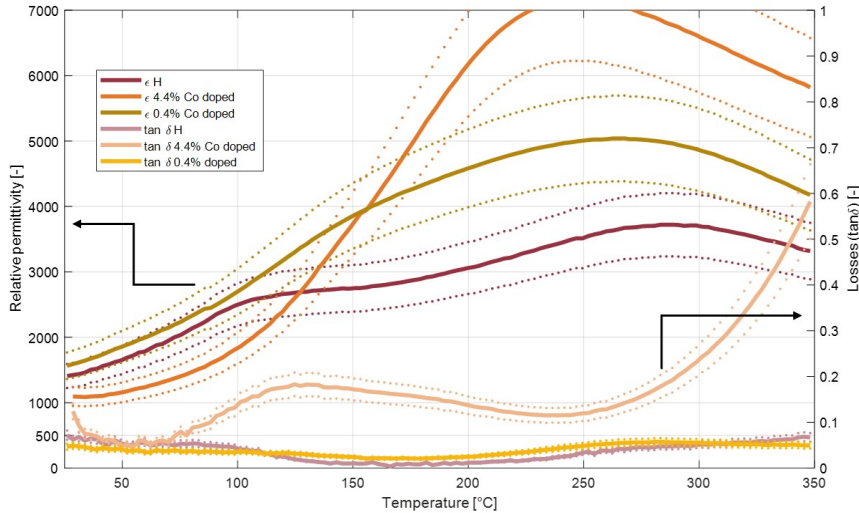


FIGURE 3.48: Comparison of relative permittivity and dielectric losses versus temperature measured at 1kHz for pure NBT-BT (sample "H"), 0.4mol%-Co-addition, and 4.4mol%-Co-addition samples. The solid lines indicate the measured values and the dotted lines indicate the uncertainty lines of $\pm 14\%$ for the permittivity and $\pm 13\%$ for the dielectric losses.

served, together with an increase in the relative permittivity. This indicates an increase in the sample's conductivity and the presence of a conducting second phase. The increase in the sample's conductivity is confirmed by the decrease of the insulation resistance, as observed in Fig. 3.49.

For the 0.4mol%-Co-addition sample, there is a slight decrease in dielectric losses for temperatures lower than the depolarization temperature T_d . However, the dielectric losses at high temperatures do not change significantly and for temperatures between T_d and T_m they slightly increase. The permittivity value and the conductivity also increase compared to the pure NBT-BT, as shown by the insulation resistance measurements in Fig. 3.49.

Comparing now the depolarization temperature T_d and the temperature of maximum permittivity T_m of the pure NBT-BT sample with the 4.4mol% and 0.4mol%-Co-addition ones in Table 3.6 and considering the temperature uncertainties of 3.5% (section 3.1.5.3), it is possible to conclude that the T_m is not significantly changed, while an important increase in T_d is observed with increasing Co concentration. This shows again that the Co-addition is not ideal for MLCC application of NBT-BT.

Finally, pure NBT-BT sample density was 90.1%, sample with 0.4mol%-Co addition density was 92.3%, and sample with 4.4mol%-Co addition density was 87.8%. So, it can be concluded that the Co addition act as a sintering aid when low quantities are added, even if the resulting dielectric properties do not meet the MLCCs requirements.

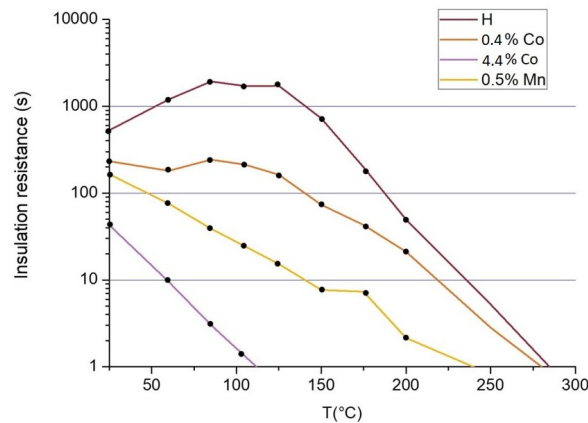


FIGURE 3.49: Insulation resistance for NBT-BT samples with 0.4mol% of Co, 4.4mol% of Co and 0.5wt% of Mn and comparison with the pure NBT-BT equivalent sample ("H").

Sample	T_d (°C) at 10kHz	T_m (°C) at 10kHz
pure NBT-BT	104	258
4.4mol%-Co-addition	undefined	260
0.4mol%-Co-addition	136	248

TABLE 3.6: Depolarization temperature T_d and temperature of the maximum relative permittivity T_m for the pure NBT-BT, the 4.4mol%-Co-addition, and the 0.4mol%-Co-addition samples.

In conclusion, the addition of Co on NBT-BT increased the NBT-BT conductivity and, for the 0.4mol%-Co-addition it did not affect significantly the dielectric losses, while, for the 4.4mol%-Co-addition increased losses are measured. So, the Co addition have not shown promising dielectric properties and it is not ideal for the MLCC production.

3.4.2 MnCO₃

Adding MnCO₃ was also investigated, since it is reported that it can also act as a sintering aid for NBT-BT.[17] For 0.1wt% Mn-addition the maximum density is achieved while for 0.8wt% Mn-addition the minimum dielectric losses are achieved. [17]

In this study, an intermediate MnCO₃ percentage was chosen: 0.5wt%. As for the Co₃O₄-added sample, the MnCO₃-added one was prepared with 250 rpm for 4 hours ball-milling with dispersing agent, with no un-dried reactants and with sintering at 1050°C for three hours using ZrO₂. The MnCO₃ was added before the second ball-milling.

3.4.2.1 Phase separation

Initially, the structure and phase separation of the sample were analyzed through SEM and XRD measurement. The results are shown in Figures 3.50 and 3.51.

The SEM measurements in Fig. 3.50 show that the 0.5wt%-Mn-addition sample has a similar phase separation as the NBT-BT samples, with a secondary Ba-containing phases separation and a NBT matrix. The composition of each phase could not be measured with sufficient precision, however, it can be considered that the phase separation takes place similarly to the pure NBT-BT material. Moreover, the EDS cartography of the Mn-addition

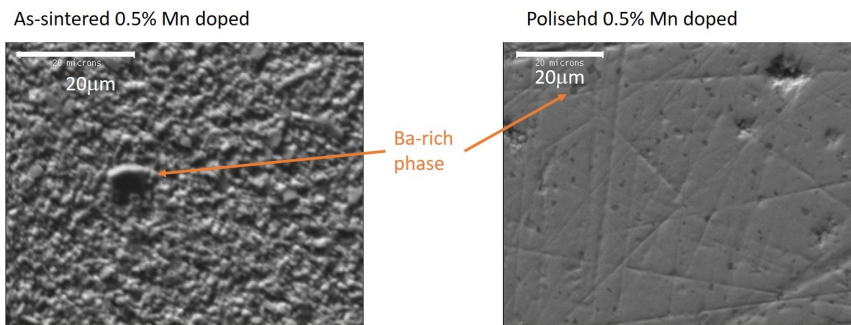


FIGURE 3.50: SEM measurements of the as-sintered (left) and the polished and strain relaxed (right) samples with 0.5wt% MnCO_3 .

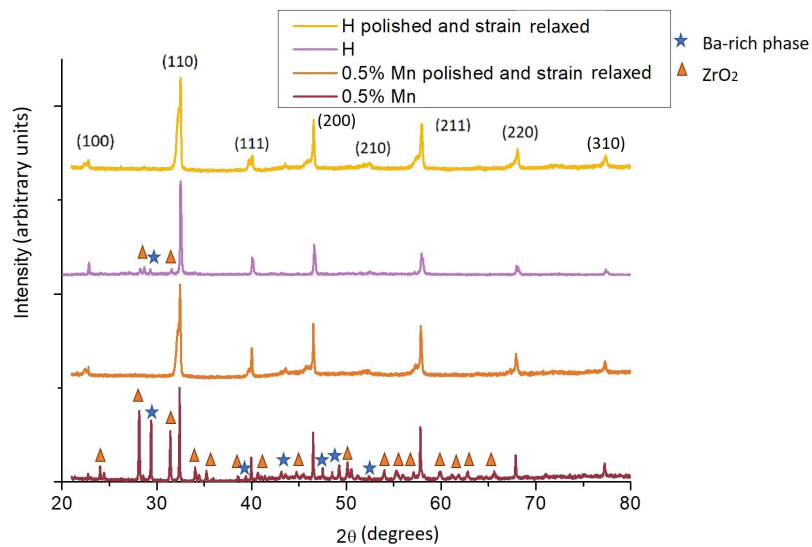


FIGURE 3.51: XRD measurement of as-sintered and polished and strain relaxed samples with 0.5wt% MnCO_3 and comparison with the pure NBT-BT sample ("H").

as-sintered sample shows a uniform concentration of Mn on both phases (see Fig. 3.52).

The XRD measurements in Fig.3.51 show a significant amount of secondary Ba-containing

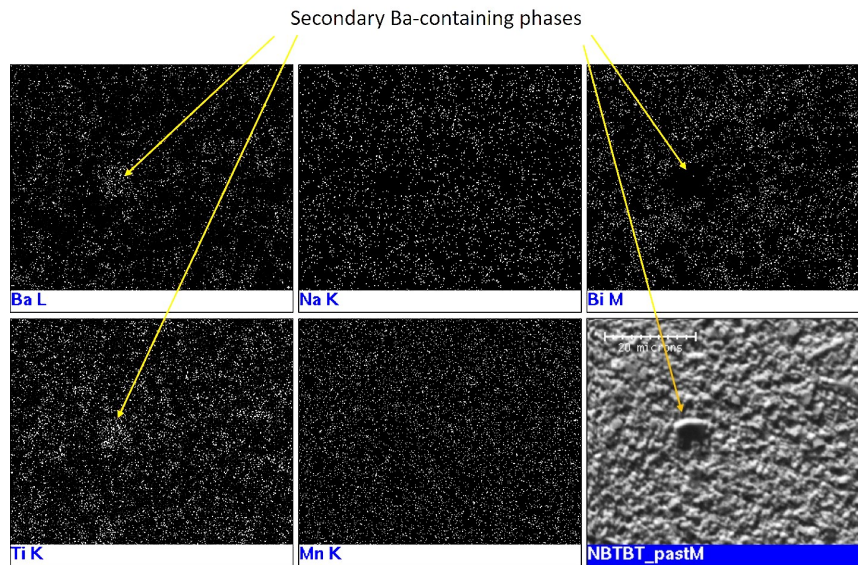


FIGURE 3.52: EDS cartography of the 0.5% Mn-addition as-sintered sample.

phases and ZrO_2 in the as-sintered sample. However, the polished and strain relaxed one show no extra peaks.

3.4.2.2 Dielectric properties in temperature

Finally, the comparison of the dielectric properties of the Mn added sample with the equivalent pure NBT-BT (sample "H") is presented in Fig. 3.53.

The dielectric losses also decrease for temperatures lower than the depolarization tem-

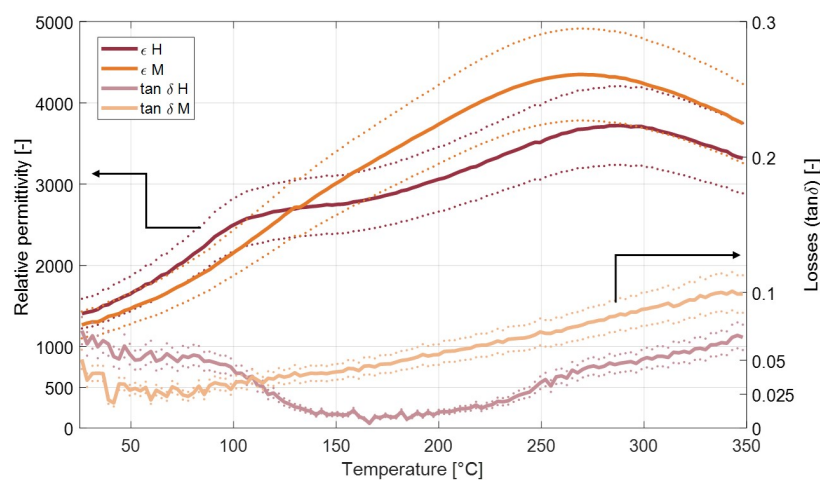


FIGURE 3.53: Comparison of relative permittivity and dielectric losses versus temperature measured at 1kHz for samples pure NBT-BT (sample "H") and for sample with 0.5wt% of Mn. The solid lines indicates the measured values and the dotted lines indicate the uncertainties lines of $\pm 14\%$ for the permittivity and $\pm 13\%$ for the dielectric losses

perature T_d . However, at temperatures higher than T_d , the dielectric losses increase when compared to pure NBT-BT. The permittivity value also increases compared to the pure NBT-BT, indicating an increase in the conductivity. This is again confirmed by the insulation resistance measurements in Fig. 3.49 p. 128.

Finally, pure NBT-BT sample density was 90.1%, sample with 0.5% Mn-addition density was 97.6%. So, it can be concluded that the Mn can act as a effective sintering aid, even if the resulting dielectric properties do not meet the MLCCs requirements.

In conclusion, the addition of Mn on NBT-BT increases the conductivity and the dielectric losses for temperature higher than T_d . So, the Mn-addition does not improve dielectric properties and it is not ideal for the MLCC production.

3.5 Other compatibilities with industrial requirements

Besides the dielectric and insulation properties and the restrictions concerning the synthesis method and parameters, other factors have to be taken into account to use a material in MLCC applications. These include the dielectric strength and the ability to co-sinter the material and the electrodes.

3.5.1 Dielectric strength

It is important to know the dielectric strength of the material, in order to characterize the maximum electric field that can be applied to the material and the application limits of the MLCC. The dielectric strength is a secondary parameter in the industrial requirements. However, the average measured values for BaTiO₃-based MLCC are between 25 and 30 V/ μ m for Class II capacitors (see section 1.3.1.8).

The dielectric strain was characterized for sample "P" as being 7.5 ± 0.5 kV/mm or V/ μ m. This value is lower than the average for the BT-based MLCC. However, it is possibly higher for "U" sample (the sample showing the best dielectric properties), since this sample shows lower conductivity when compared to sample "P". So a new "U" sample should be synthesized, to allow the breakdown voltage without making the existing sample unusable for further measurements.

In conclusion, the dielectric strength should be increased for the MLCC application. However, it is expected that sample "U" shows a dielectric strength higher than 7.5 V/ μ m.

3.5.2 Compatibility with the electrodes

The compatibility of the ceramics with the electrodes and the possibility of co-sintering are an important factor for the use of the materials in MLCC production.

The compatibility of NBT-BT with the Ag-Pd electrodes is specially important due to the possible reaction between the Bi and the Pd, forming Pd_xBi_y et Bi_2O_3 . This was tested for the 70% Ag - 30% Pd electrode by mixing the ceramic powders with the metal powder (prepared from the dried metallic ink) in an agathe mortar. The powders mixture was, then, sintered at 1050°C or 1200°C for three hours under ZrO₂ in the laboratory furnace. Another sample made with the same powder mixture was sintered at 1115°C following Exxelia's sintering temperature program in their furnace. The XRD of the sintered material and its comparison with the pure NBT-BT and the pure electrode powder diffraction patterns are presented in Fig. 3.54.

The XRD measurements show that there is no detectable formation of new phases,

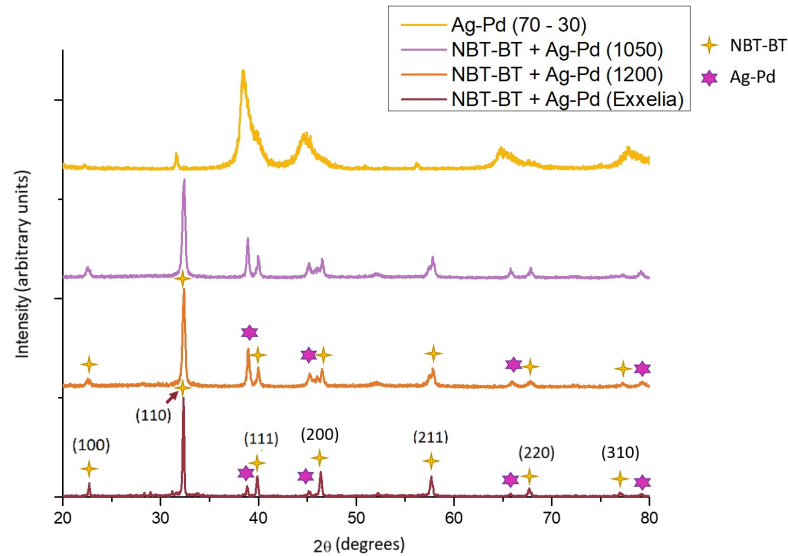


FIGURE 3.54: XRD of the sintered NBT-BT and Ag-Pd (70-30) powder mixtures sintered at 1050°C or 1200°C in the laboratory furnace and at 1115°C in Exxelia's furnace and comparison with XRD of the Ag-Pd (70-30) powder.

since the XRD of the sample prepared by the ceramic and electrode powder mix show only the peaks related to the NBT-BT and to the electrode phases.

An SEM and EDS measurement was also carried-out, to confirm that there is no reaction between the NBT-BT and the electrode and there is no defect formation on the interface between the two phases. The measurement results are presented in Fig. 3.55.

The measurement results show that there is no defect formation at the interface of the two phases. Moreover, there is also no phase formation, as can be observed in the concentration profile in Fig. 3.55. Finally, the EDS point analysis of the ceramic grains show no Pd presence and a small Ag concentration (1%), probably due to the migration from the electrode grains. So, there is no reaction between the ceramic material and the electrode during the co-sintering.

Concerning the sintering temperature, the best density for the NBT-BT samples was obtained after sintering at 1150°C and the best structure and phase separation characteristics was obtained after sintering at 1050°C (see section 2.3.4.3). These temperatures are compatible with the maximum co-sintering temperature of the 70% Ag - 30% Pd electrode of 1150°C (see section 1.3.2). So this does not represent a limitation for the use of NBT-BT in MLCCs.

In conclusion, the NBT-BT can be co-sintered with 70% Ag and 30% Pd electrodes, since there is no chemical reaction between the Bi and the Pd and since the sintering temperature is lower than the maximum co-sintering temperature for this electrode material.

3.6 Conclusion

This chapter discussed the dielectric properties of the NBT-BT samples and their comparison to Exxelia's specifications. The results allowed the determination of the synthesis parameters needed to obtain a material meeting these specifications.

Initially, the experimental setups, the model to calculate the complex permittivity, and

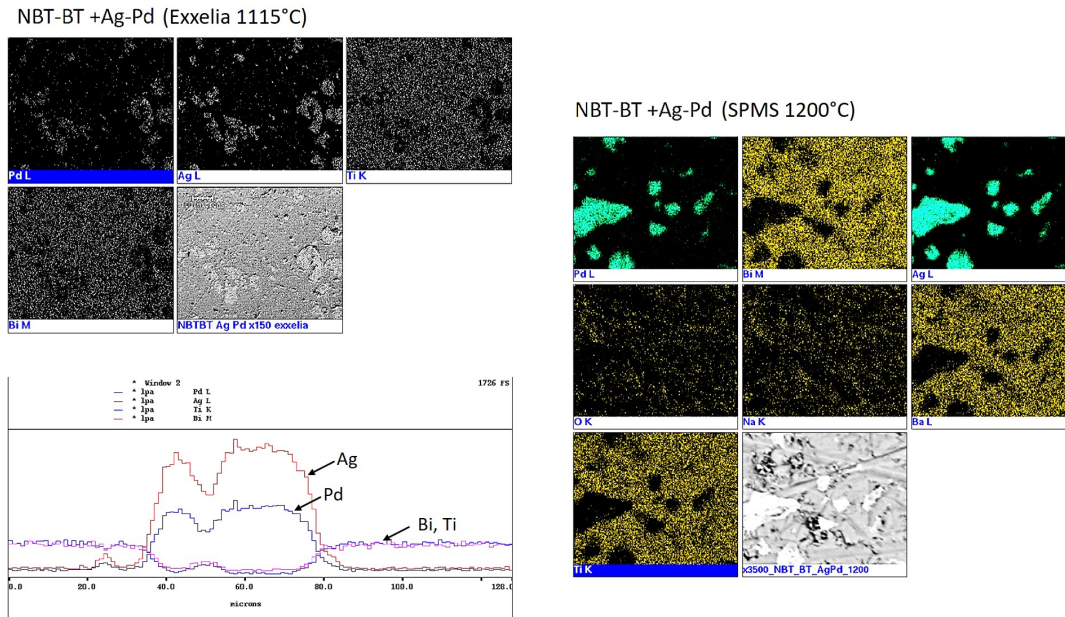


FIGURE 3.55: SEM measurements of the sintered NBT-BT and Ag-Pd (70-30) powder mixtures sintered at 1200°C on the laboratory furnace and at 1115°C on Exxelia's furnace and concentration profile of a Ag-Pd grain on sample sintered in Exxelia.

the associated uncertainties were presented.

After analyzing the variation of the complex impedance in frequency, it was possible to conclude that the resistance and the capacitance of the setup can be neglected. So, the RC model was used to calculate the complex permittivity from the impedance measurements.

Since the NBT-BT samples showed different relative densities, the use of the Bruggeman model was proposed to estimate the fully dense dielectric properties. However, due to the sample's microstructure, it was shown that this model cannot be used.

The dielectric properties (relative permittivity and dielectric losses) measurements uncertainties were estimated from the measurement of one sample that showed results compatible with two different curves. So a 13% uncertainty was taken for the relative permittivity and a 14% uncertainty was taken for the dielectric losses.

Due to the method initially used to fix the wires on the bottom of the samples (silver paste on the sample surface), a temperature shift correction was also done. The correction was done after measuring one reference BaTiO₃ sample with the same fixation method and comparing the measured properties with the known properties of the BT sample. Moreover, the shift in the Curie temperature in this sample comparing the heating and the cooling measurements showed that there is no significant temperature gradient in the samples.

Finally, a new method to fix the wires on the bottom of the samples was used (Cr-Au sputtering metallization and displaced fixation over a copper plate). These measurements were used to estimate a 3.5% uncertainty in the temperature measurements.

After defining the models to calculate the dielectric properties and estimating uncertainties, the dielectric properties and the insulation resistance of the NBT-BT ceramics in temperature were analyzed. The effects of the stoichiometry, structure, phase separation, synthesis parameters, and internal strain in these properties were analyzed.

The NBT-BT properties are particularly sensitive to the stoichiometry and, more specifically, to the Na/Bi ratio. The increase in Na content inhibits the secondary Ba-containing phases separation and decreases the relative Bi content in the main phase, increasing the sample's conductivity. On the other hand, the increase in the Bi content initially compensates for

the oxygen vacancy formation and decreases the conductivity before forming a second phase, increasing again the conductivity. So non-stoichiometry can be measured by the Na/Bi ratio, with a larger conductivity with increasing the Na/Bi ratio.

Considering Exxelia's requirements for the high-temperature MLCC, the stoichiometry of sample "U" is the most adapted one, due to its high insulation resistance, lower dielectric losses, and permittivity variation in temperature when compared to others.

Finally, to obtain a sample with no phase separation but without increasing the conductivity, Bi and Na excess should be added, maintaining the same Na/Bi ratio as sample "U". A suggested nominal composition would be $\text{Na}_{0.4818}\text{Bi}_{0.5256}\text{Ba}_{0.06}\text{TiO}_3$.

The phase separation and the secondary Ba-containing phases formation are due to the Na evaporation during sintering. The final material can be considered as a composite where the matrix phase is composed of non-stoichiometric NBT and the inclusions are composed of the secondary Ba-containing phases. However, due to the physical characteristics and the properties of the phases, there is no classical composite model that can be applied. So the effects of the secondary Ba-containing phases volume fraction were evaluated only qualitatively.

The increase of volume fraction and of average grain surface of this phase is initially beneficial to the MLCC application, since it increases the permittivity, decreases the dielectric losses, and increases the insulation resistance, due to the elimination of oxygen vacancies. Above a critical fraction and grain surface for the secondary Ba-containing phases, the tendency reverts, due to the conducting character of this phase. So, an intermediary volume fraction (2.5 to 3.0%) and average grain surface (0.9 to $3.0\mu\text{m}^2$) of the secondary Ba-containing phases is desirable.

For this reason, the effect of multiple synthesis parameters on the secondary Ba-containing phases average grain surface and volume fraction were studied, to control this phase formation and characteristics.

The Na_2CO_3 grain size showed no considerable effects on secondary Ba-containing phases and on sample's dielectric and insulating properties.

The use of dispersing agent and of un-dried reactants mitigated the ball-milling energy effects on the secondary Ba-containing phases (i.e. decreasing average grain surface and increasing volume fraction of the secondary phase with increasing ball-milling energy). Therefore, it decreases the dielectric losses and increases permittivity.

Finally, adding MEK as a solvent increases the secondary Ba-containing phases volume fraction and decreases the dielectric losses.

So, to obtain this intermediary average grain surface and volume fraction of secondary Ba-containing phases and the best dielectric and insulation properties, a dispersing agent should be used during ball milling in MEK and ethanol mixture and the reactants should not be dried before weighing. In this case, the average Na_2CO_3 grain size and the energy of ball milling do not affect significantly the final bulk properties.

Considering Exxelia's requirements, samples "P" (un-dried reactants, ball-milled with dispersing agent in ethanol and MEK mixture during 8h at 350 rpm with fine Na_2CO_3 powder), "N" (un-dried reactants, ball-milled with dispersing agent in ethanol and MEK mixture during 4h at 250 rpm with fine Na_2CO_3 powder) and "U" (un-dried reactants, ball-milled with dispersing agent in ethanol and MEK mixture during 8h at 350 rpm with fine Na_2CO_3 powder and lower nominal Na/Bi ratio compared to samples "N" and "P") are the most adapted for the NBT-BT application in MLCCs in terms of synthesis parameters and secondary Ba-containing phases characteristics, confirming the synthesis parameters and phase separation analysis.

Finally, the polishing and strain relaxation are important step to have a lower ZrO_2 contamination from the powder used to create the sintering atmosphere, without introducing internal strains. In this case, the thermal treatment should be done at 400°C during 3h to relax

the introduced strain, even if it does not drastically affect the NBT-BT dielectric properties.

Considering now the NBT-BT properties in frequency, several hypothesis were considered: a composite model with a conducting phase in an insulating matrix (Maxwell-Wagner model), two parallel and frequency-dependent RC circuits representing a grain core and grain boundary with different conductivity (Nyquist plot) and a relaxor behaviour (modified Curie-Weiss law).

The three frequency-dispersion model could be applied for the NBT-BT samples, even if the fits could not be done for the Maxwell-Wagner and the Nyquist plot models, due to a limited frequency range of measurement.

The Maxwell-Wagner confirmed the hypothesis that the Ba-containing phases are more conducting than the NBT-matrix phase and so an interfacial polarization contributes to increase the dielectric properties and the frequency dispersion of the material.

The Nyquist indicated that two circuits associated with the grain cores and the grain boundaries could be used. In this case, the resistance associated with the grain boundaries is larger and it increases with temperature up to a critical temperature.

Finally, the modified Curie-Weiss indicated all the samples, except for sample "E", showed a relaxor character, with γ close to 2. This indicated that the secondary Ba-containing phases and the interaction between its neighbouring grains can tune the relaxor behaviour in NBT-BT.

Lastly, Co_3O_4 and MnCO_3 were added to NBT-BT, to try to improve the dielectric properties of the samples and to act as a sintering aid. Both additions are often done in the MLCC industry. Even though an increase in density was measured with the addition of 0.4mol% of Co_3O_4 (from 90.1% to 92.3%) and 0.5wt% of MnCO_3 (from 90.1% to 97.6%), in both cases, the conductivity was increased. The dielectric losses were either unchanged or increased after adding Co or Mn. So, it did not improve dielectric properties and it is not ideal for the MLCC production.

Besides the dielectric and insulation properties, other factors were considered, including the dielectric strength and the ability to Co-sinter the material and the electrodes.

The dielectric strength was only measured for sample "P" and the result was 7.5 V/ μm . It should be increased for the MLCC application. However, it is expected that sample "U" shows a higher dielectric strength owing to its higher insulation resistance.

Finally, the NBT-BT can be co-sintered with 70% Ag and 30% Pd electrodes, since there is no chemical reaction between the Bi and the Pd and since the sintering temperature is lower than the maximum co-sintering temperature for this electrode material.

Chapter 4

Literature incompatibilities

The objective of this chapter is to identify the origin of the differences in the dielectric properties NBT-BT presented in the literature.

NBT-BT's dielectric properties are sensitive to variations in the stoichiometry, in the synthesis method and in the atmosphere used for sintering the material (see Chapter 3). These are some reasons that are responsible for the variety of measurements reported for this material.

In this chapter, some arguments and some other reasons for the incompatibilities among the reported results will be discussed and the importance of having a strict synthesis and measurement method will be presented.

4.1 Dielectric properties differences reported in the literature

Ge *et al.* reported the dielectric properties for NBT-BT 6% as presented in Fig. 4.1. Those properties are what we would expect when analyzing the material structure (see section 1.4.2.2). The first phase transition from non-ergodic to ergodic relaxor presents a frequency dispersion, due to the relaxor character of the material. This happens at a temperature of $T_d = 120^\circ\text{C}$. The maximum permittivity temperature $T_m = 280^\circ\text{C}$ represents the transition to the paraelectric structure, so no frequency dispersion is observed. For this sample, relative permittivity values are 2000 at room temperature and 9000 at T_m . [19]

Kumar *et al.* reported dielectric properties for NBT-BT 7% (still on the MPB of the NBT-BT solid solution) as presented in Fig. 4.2. For this report, NBT-BT presents a frequency dispersion in permittivity and in dielectric losses over the temperature range measured. Moreover, the transition temperatures are at $T_d = 80^\circ\text{C}$ and $T_m = 300^\circ\text{C}$, at odds with what would be expected from the material structure. [10] Finally, the permittivity at room temperature is 1000 and at T_m is 2500, lower than the values reported for Ge *et al.* (2014) and the dielectric losses are 5% on average over the temperature range of measurements, having a higher value when compared with the reported properties by Ge *et al.* (2014). The relative permittivity does not show a hump at T_d as would be expected from the relaxor phase transition. [10]

Finally, Zhang *et al.* also reported the dielectric properties of NBT-BT 6% as presented in Fig. 4.3. Relative permittivity values (2000 at room temperature and 6000 at T_m) and dielectric losses tendency (decrease of the losses for temperatures higher than T_d) are more similar to the results reported by Ge *et al.* (2014). However, the sample presents an increase in the dielectric losses at high temperatures, a frequency dispersion over the measured temperature range and no permittivity hump at T_d can be observed, as would be expected from the relaxor phase transition. [86]

These are representative examples of literature incompatibilities for the dielectric properties of the NBT-BT. To explain the differences in the relative permittivity values, in the dielectric losses values at low and high temperature, the frequency dispersion and the presence

of a hump at T_d , the influence of stoichiometry, phase separation, metallization, synthesis parameters, and polishing and strain relaxation on the material's dielectric properties were analyzed.

4.2 Differences in the measured sample dielectric properties

4.2.1 Influence of the stoichiometry on the dielectric properties

Stoichiometry is really important to define the dielectric properties of NBT-BT, since the presence of volatile species can significantly change the final material stoichiometry depending on the synthesis and on the sintering methods used. Moreover, slight changes in the stoichiometry of these elements can significantly affect the dielectric properties and the conductivity of the material (see section 3.2.1.1).

As mentioned in Chapter 3, the increase in Na content inhibits the secondary Ba-containing phases separation (decreases the relative Bi content in the main phase) while the increase in the Bi content initially compensates for the oxygen vacancy formation before forming a second phase. For these reasons, the increase of the nominal Na/Bi ratio increases the dielectric losses at high temperature and the conductivity of the NBT-BT. It also increases the frequency dispersion and the relative permittivity values, as observed in Fig. 3.14 p. 96.

The changes in stoichiometry can also have a large effect on the transition temperature (see section 3.2.1.1). Table 4.1 show the depolarization temperature T_d and the maximum permittivity temperature T_m for samples "P", "U", "Y", and "Z", with different Na/Bi ratio (see Table 3.3 p. 94). It can be concluded that the increase in the nominal Na/Bi ratio increases T_d and decreases T_m , due to the decrease in the stability of the "AFE-like" phase (see section 2.3.2.6). However, the reason of this decrease is not well understood yet. [23]

Finally, the increase in the nominal Na/Bi ratio also decreases the relative permittivity

Sample	T_d (°C)	T_m (°C)
"U"	65	294
"P"	105	272
"Y"	115	246
"Z"	145	230

TABLE 4.1: Depolarization temperature T_d and temperature of the maximum relative permittivity T_m for samples "U" (nominal Na/Bi ratio of 0.92), "P" (nominal Na/Bi ratio of 1), "Y" (nominal Na/Bi ratio of 1 and 10.5mol% Na and 2.2mol% Bi nominal excess compared to sample "U") and "Z" (nominal Na/Bi ratio of 1.06 and 16.9mol% Na nominal excess compared to sample "U").

change at T_d , making it less evident, due to the increase of the relative permittivity of the "AFE-like" phase. This can be observed in Fig. 3.15 p.96.

Therefore, the change in stoichiometry can have an important influence on the shape and values of the relative permittivity and dielectric losses vs temperature curves of the NBT-BT.

A comparison of the shape of the dielectric properties vs. temperature curves can be done, for example, between the samples "Z" and the one reported by Zhang *et al.*[86], and between the samples "P" and the one reported by Ge *et al.*[19], as shown in Fig. 4.4.

Due to the high nominal Na/Bi ratio of sample "Z", it shows increased dielectric losses, especially for high temperatures, a high frequency dispersion over the entire measured temperature range and no shoulder on the relative permittivity vs temperature curve at T_d . The same observations can be done for the results reported by Zhang *et al.*. Moreover, the reported

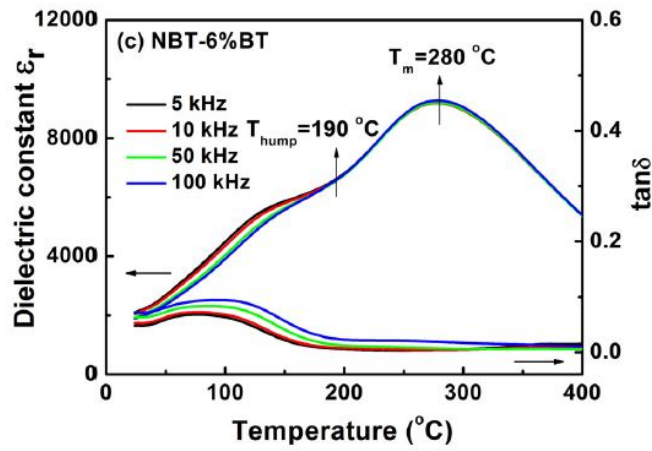


FIGURE 4.1: Dielectric properties of NBT-BT 6% reported by Ge *et al.*(2014) [19]

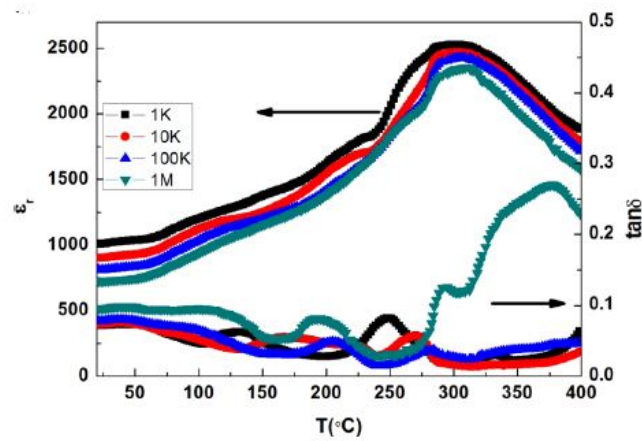


FIGURE 4.2: Dielectric properties of NBT-BT 7% reported by Kumar *et al.*(2015) [10]

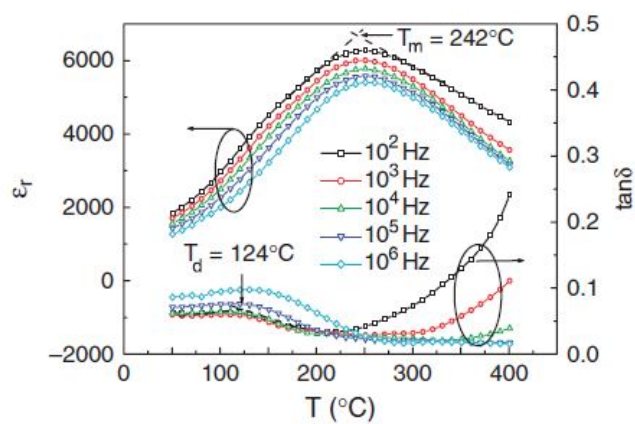


FIGURE 4.3: Dielectric properties of NBT-BT 6% reported by Zhang *et al.*(2008) [86]

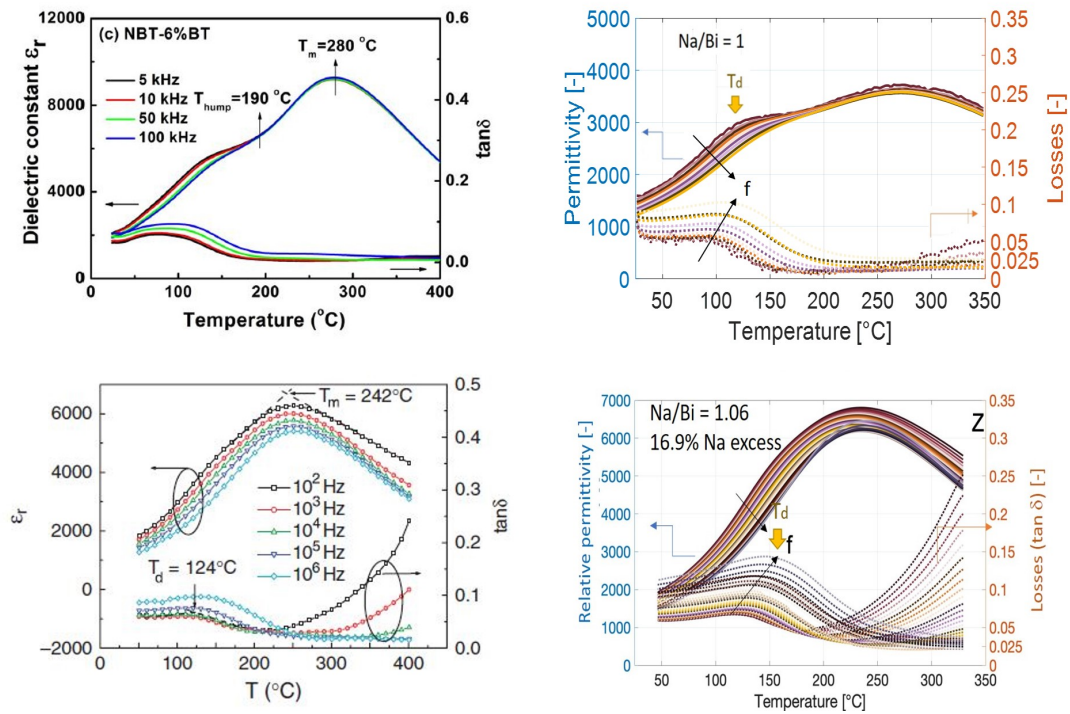


FIGURE 4.4: Dielectric properties vs. temperature curves reported by Ge *et al.*[19] (top left), and by Zhang *et al.*[86] (bottom left), and for samples "P" (top right), and "Z" (bottom right).

T_d (124°) is higher than the one of the nominal stoichiometric NBT-BT sample (105°C) and the reported T_m (242°C) is lower than the one of the nominal stoichiometric NBT-BT sample (272°C), also similar to sample "Z".

Conversely, sample "P" shows decreased dielectric losses, a frequency dispersion only for temperatures lower than T_d and a shoulder on the relative permittivity at T_d , due to its stoichiometric nominal Na/Bi ratio. The dielectric properties reported by Ge *et al.* show similar characteristics.

In conclusion, the stoichiometry has a crucial effect on the dielectric properties of the NBT-BT. The increase in the nominal Na/Bi ratio increases the conductivity, the relative permittivity, the dielectric losses over, and the frequency dispersion over the entire temperature range of the measurements (from room temperature to 350°C).

Moreover, the change in the stoichiometry also changes the shape of the relative permittivity and dielectric losses vs temperature curves, since the increase in the nominal Na/Bi ratio also increases T_d , decreases T_m , and decreases the relative permittivity change at T_d , making it less evident.

Finally, due to the volatile character of Na and Bi, the material's stoichiometry is sensitive to the synthesis and sintering methods used. This is one of the reasons that can explain the literature incompatibilities for the dielectric properties of NBT-BT.

4.2.2 Differences in the dielectric properties of over first heating measurement

All the dielectric measurements shown in Chapter 3 are over the first cooling of the sample. However, these measurements were carried out in two or three temperature cycles of

heating and cooling. An example of dielectric measurement vs temperature over two consecutive cycles is shown in Fig. 4.5 for sample "X" (synthesis parameters in Table 2.11 p. 79).

It can be observed that all the cycle measurements are similar, except during the first

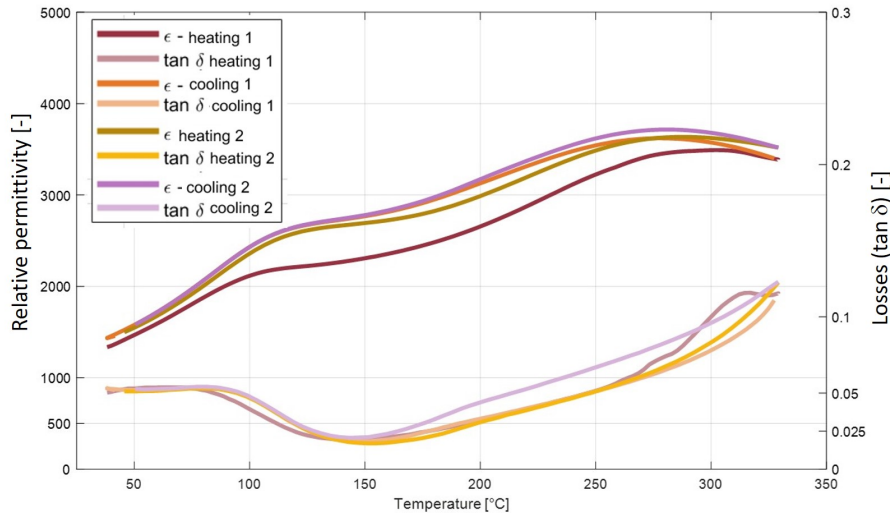


FIGURE 4.5: Dielectric properties of NBT-BT sample "X" measured in subsequent thermal cycles from 25 to 325°C.

heating. So an hysteresis is observed over the first heating/cooling cycle, decreasing the permittivity value, and often increasing the measurement noise.

To explain the reason of this temperature hysteresis, the influence of the structure and secondary Ba-containing phases, the synthesis parameters, the polishing, strain relaxation, and the metallization were studied.

4.2.2.1 Influence of the structure and secondary Ba-containing phases, the synthesis parameters and the polishing and strain relaxation on the temperature hysteresis

The first hypothesis tested to explain the hysteresis of the first cycle was that it came from intrinsic properties of the samples. In this case, differences either on the structure, composition, or synthesis methods would create samples with different properties and, consequently, could decrease or eliminate the hysteresis. To test this hypothesis that samples were measured in a sequence of thermal cycles, from room temperature to 350°C.

Analyzing in Fig. 4.6, the dielectric properties of samples "U", "Y", and "Z" with different stoichiometries (see Table 2.11 p. 79), it can be seen that a similar hysteresis on the first temperature cycle is observed for all of them. This indicates that the stoichiometry does not induce the temperature hysteresis.

Samples "B", "N", "H", and "Z" have different Na_2CO_3 grain size, ball-milling solvents and ball-milling energy (see Table 2.11 p. 79). Sample "B" has dried reactants and no dispersing agent was used during its synthesis. These differences result in different secondary Ba-containing phases average grain surface and volume fraction (see Table 2.11 p. 79) and, for the case of sample "Z", no phase separation. The dielectric properties of those samples were compared and are shown in Fig. 4.7. For each sample in this figure, the first heating measurement is different from all the other measurements in temperature cycles, showing lower relative permittivity. This also indicates that the synthesis parameters and the phase

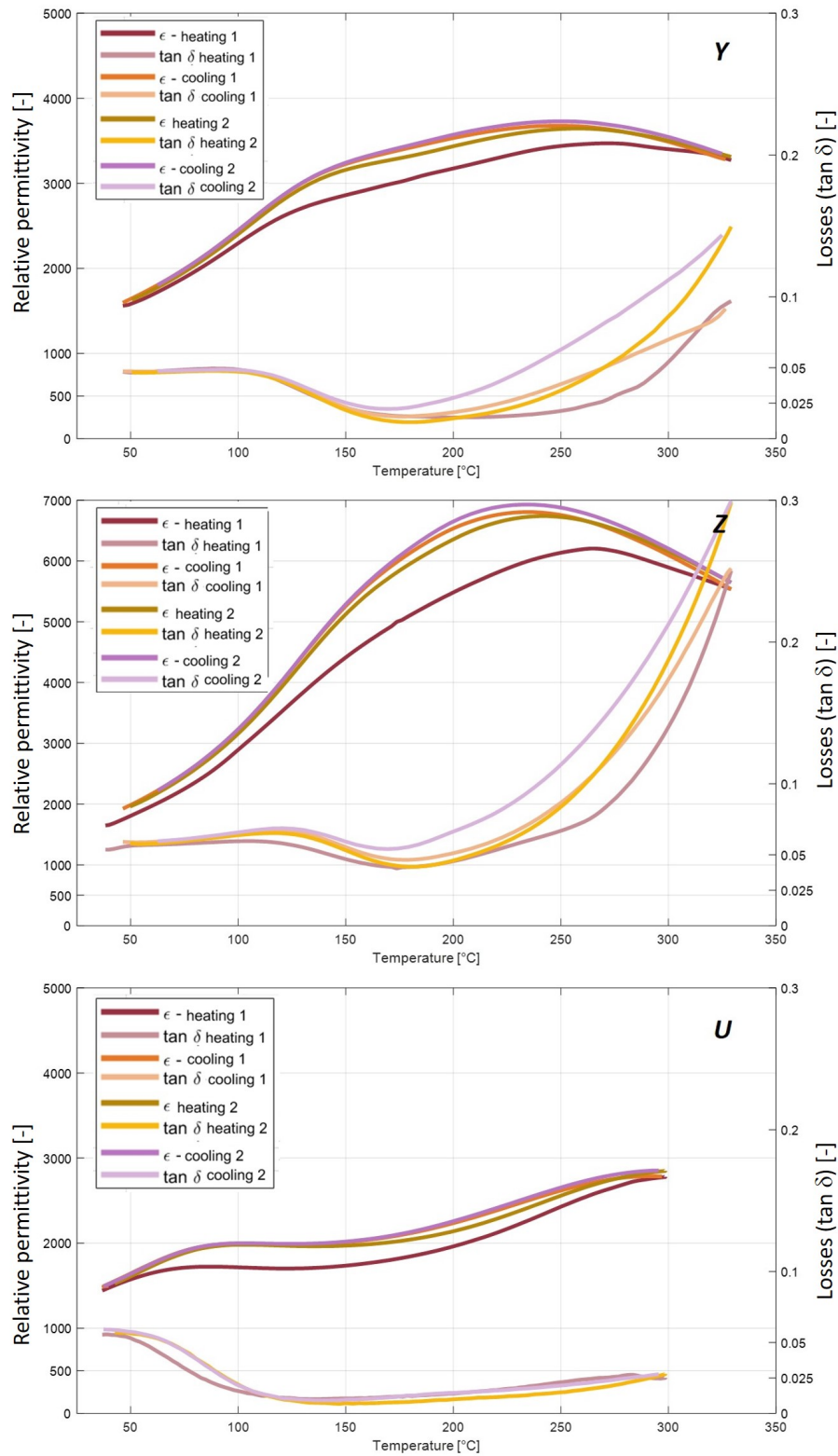


FIGURE 4.6: Dielectric properties of NBT-BT samples "Y", "Z" and "U", with different stoichiometries, measured in subsequent thermal cycles from 25 to 300 or 325°C.

separation on NBT-BT are not the reason for the first heating hysteresis of the dielectric properties.

Finally, sample "H" (synthesis parameters at Table 2.11 p. 79) was polished and

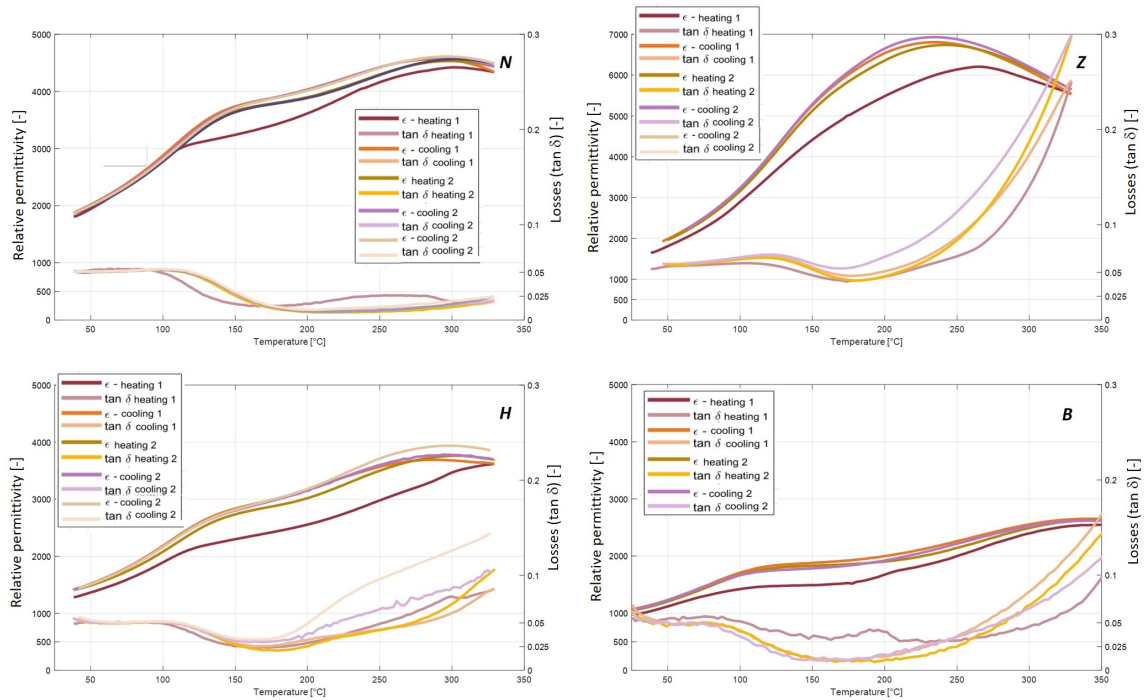


FIGURE 4.7: Dielectric properties of samples "B", "N", "H" and "Z" with different Na_2CO_3 grain size, ball-milling solvents and energy over thermal cycles from 25 to 325 or 350°C.

strain-relaxed at 400°C for different periods of time. As mentioned in section 3.2.1.4, the Williamson-Hall analysis show that the internal strain of the unpolished NBT-BT samples is similar to the ones in samples after polishing and strain-relaxing for three hours. So the sample relaxed for one hour still show internal strains introduced during polishing. The dielectric properties of the sample after one and three hours of thermal treatment for strain relaxing are shown in Fig. 4.8.

From Fig. 4.8, it can be seen that the samples present similar hysteresis over the first cycle of the dielectric properties, independently of the relaxing time. This indicates that the strain introduced by polishing is not the reason for this hysteresis.

In conclusion, the hysteresis of the dielectric properties of NBT-BT over the first cycle is neither due to the synthesis method, nor to the phase separation, nor to the strain level, nor to the stoichiometry of the material. So this hysteresis should not be an intrinsic characteristics of the material.

4.2.2.2 Influence of the metallization and electric contact on the temperature hysteresis

The hypothesis that the metallization and the electric contact method are the cause of the hysteresis over the first cycle was done after verifying that it is not due to an intrinsic characteristic of the material.

To verify this hypothesis, the simple method used to fix the wires with a silver paste drop directly onto the surface of the sample, used in section 3.1.5.1, was compared to a new metallization and electrical leads contact method, as described in section 3.1.5.3 p. 91. In the

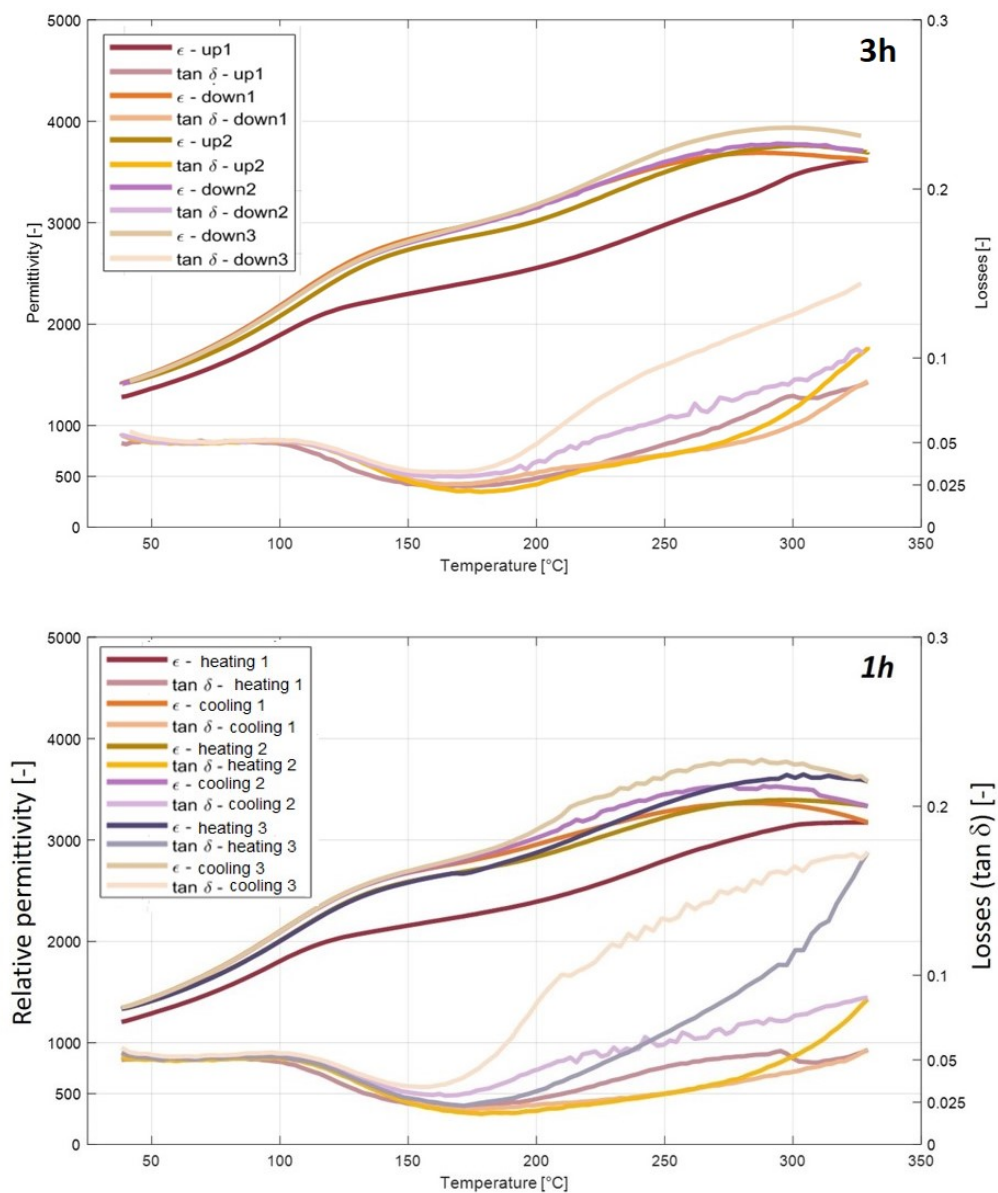


FIGURE 4.8: Dielectric properties of sample "H" after 1 and 3h strain relaxation at 400°C, measured over thermal cycles from 25 to 325°C.

first method, a silver paste drop is put over the wire and the sample's surface and both are heated for two hours at 200°C before measurement, as indicated in the product instructions. For the second method, the metallization is done by sputtering of Cr-Au. A copper plate is fixed to the bottom electrode of the sample with a small amount of silver paste, avoiding the drawbacks of having a direct contact of the wire underneath the sample and large silver paste thickness under the samples. Finally, the wire is fixed on the copper plate with a drop of silver paste.

The dielectric properties of two "H" samples (synthesis method in Table 2.11 p. 79) were measured. A new (never before measured) "H" sample polished and strain-relaxed during 3h at 400°C and a "H" sample also polished and strain-relaxed during 3h at 400°C first measured using Ag paste and subsequently using Cr-Au metallization method were compared. Fig. 4.9 show the dielectric properties of these samples measurements.

The comparison of the dielectric properties of the sample measured with silver paste and Cr-Au metallization methods in Fig. 4.9 (top and middle panels) indicates that the use of silver paste on metallization compared and wire fixing is the cause of the hysteresis over the first temperature cycle.

Moreover, a decrease from 3600 to 3000 in the relative permittivity value at 300°C is observed from the simple Ag paste metallization to the Cr-Au sputtering. This corresponds to a 16% difference in relation to the Ag paste metallization. Considering the uncertainties of 14%, it can be considered that the use of Cr-Au sputtering metallization slightly decreases the permittivity. This is not observed for the dielectric losses, since the measured values are similar.

To confirm that there is no effect of the sample's intrinsic properties due to the heating cycles, the dielectric properties of a new Cr-Au metallized "H" sample were measured. No temperature hysteresis over the first cycle is measured. This proves that the dielectric properties hysteresis is due to the use of silver paste on the metallization and the way the wire (electric lead) is fixed onto the sample.

Finally, the comparison between the two different "H" samples with the same Cr-Au metallization method (middle and bottom panels of Fig. 4.9) show that the variability from one sample to the other can be important. For the relative permittivity, this difference is of 390 (1440 for the sample first measured with Ag paste - middle panel - and 1830 for the "new" sample - bottom panel) at 50°C, being equivalent to 21% difference. For the dielectric losses, this difference is between 1.2% at the same temperature (4.85% for the sample first measured with Ag paste and 4.91% for the "new" sample). So the variability from sample to sample is also an important factor to explain the literature differences in the relative permittivity. However, there is no difference in the dielectric properties anomalies temperatures (T_d and T_m) due to the sample to sample variability. The dielectric losses behaviour is different for both samples, since the sample first measured with Ag paste show a higher dispersion and increase in the dielectric losses over consecutive measurement cycles. This behaviour change may be due to the presence of silver paste remains in the sample's surface, since the sample was not polished after removing the Ag paste electrode.

In conclusion, the use of silver paste for the metallization and the fixing of the electric wires can change the measured dielectric properties of the samples during the first temperature cycle. The measured permittivity is decreased and the measured dielectric losses noises are often increased compared to subsequent cooling/heating. Since the silver paste is a very common metallization method for research on dielectric materials and since the properties are normally reported over the first heating, the metallization and the method to contact the electric leads can also be held responsible for the literature incompatibilities of the dielectric properties of NBT-BT.

Furthermore, the variability in the measured dielectric properties from sample to sample

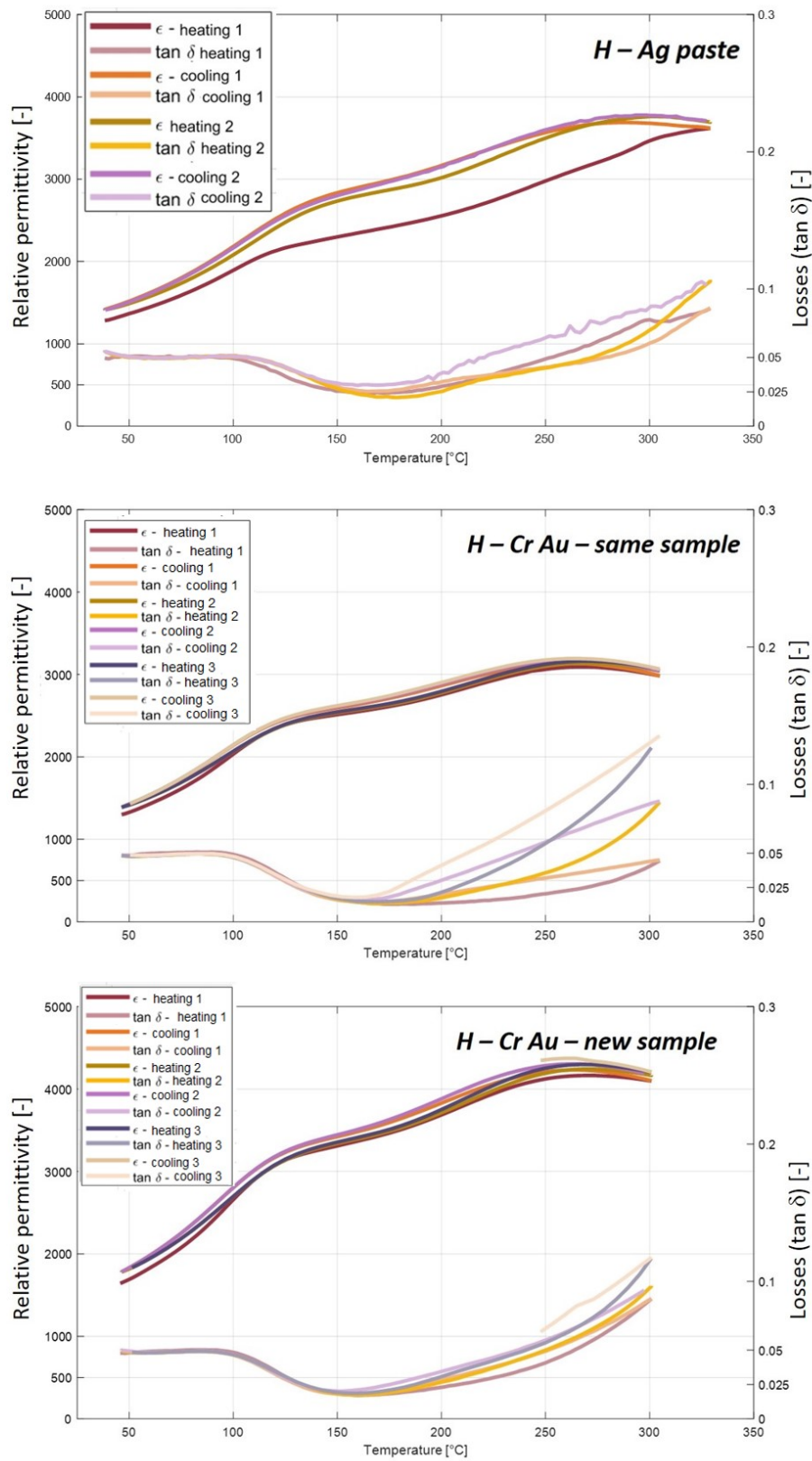


FIGURE 4.9: Dielectric properties of sample "H" with Ag paste metallization and of the same and a new "H" samples with Cr-Au metallization, measured over three consecutive thermal cycles from 25 to 325°C

is also an important factor to explain the differences observed in the literature.

4.2.2.3 Other dielectric properties changes during temperature cycle measurement

Other than the first cycle hysteresis, dielectric properties show other changes during measurements over temperature cycles. The middle panel of Fig. 4.9 shows the evolution of the permittivity and the dielectric losses of sample "H" with Cr-Au metallization method after three thermal cycles (from room temperature up to 325°C).

The permittivity is stable, but an increase in the dielectric losses can be clearly observed for temperatures higher than 160°C after each measurement cycle. Contrary to what was observed for the hysteresis over the first temperature cycle, this high-temperature dielectric losses increase is observed for all samples, regardless of the metallization and method to contact the electrical leads, the stoichiometry, the phase separation, the synthesis parameters, or the polishing and strain relaxation (see Figures 4.6 to 4.9).

Fig. 4.10 compares subsequent dielectric measurements for sample "U", both using the silver paste metallization method, the first for thermal cycles up to 300°C and the second for thermal cycles up to 360°C. It is possible to conclude that the increase of the dielectric losses over 300°C depends on the higher temperature reached. This indicates that a degradation takes place at high temperatures (over 300°C).

However, even after having been heated up to 360°C, the dielectric losses of sample "U" maintain a low value up to 260°C.

Two possibilities are considered to explain the thermal degradation of the NBT-BT. The first one is the presence of thermally activated phenomenon, such as defect movements at high temperatures. The second one is the change in the microstructure of the material that can be permanent or not.

Analyzing Fig. 4.9 p. 146, for sample "H", it can be seen that the dielectric losses increase after the first measurement with silver paste electrode. After removing this electrode and applying a new one by sputtering of Cr-Au, the dielectric losses return to low values (even lower than for the first measurement with silver paste). However, the same losses increase is observed during measurement over consecutive thermal cycles with Cr-Au electrodes. So, analyzing only this sample, it would be possible to make the hypothesis that a change in the sample microstructure takes place while heating. This change would not be permanent, but it would take a long time to be reverted (the measurements with the different electrodes were carried out three months apart).

However, analyzing now Fig. 4.11, for sample "X", it can be seen that the dielectric losses also increase during the first measurement with silver paste electrode. The second measurement is done on the same sample without removing the electrode. For this new measurement, the dielectric losses do not return to their original value and they continue to increase at each heating and cooling cycle. This may indicate that the high temperature dielectric losses increase is due to an electrode effect.

For all measurements, an increase in the dielectric losses is observed after each heating and cooling cycle. However, for samples where the electrode is removed and a new electrode is applied, the dielectric losses return to their original value. For samples that are remeasured with the same electrodes, the dielectric losses keep increasing over each heating and cooling cycle.

This can indicate that the electrodes influence the measured dielectric losses, increasing them by changes in the electrode's morphology during heating. In this case, the presence of uneven surface can result in just a few contact points between the electrode and the NBT-BT, which adds a series surface resistance to the equivalent electric circuit, increasing the dielectric losses, specially for the high frequencies.[76] However, it is also possible that there is a

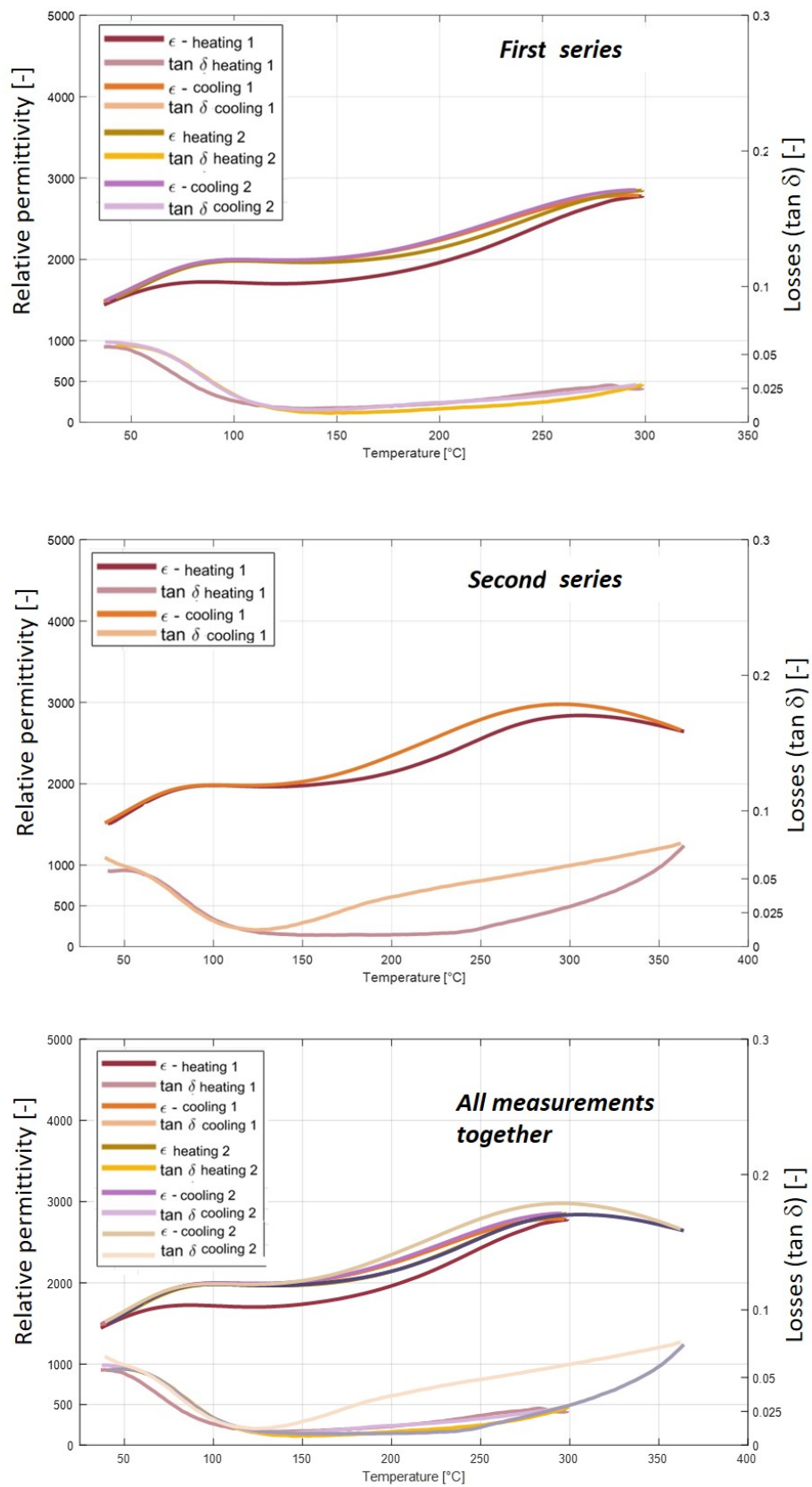


FIGURE 4.10: Dielectric properties of NBT-BT sample "U" with Ag paste metallization measured over consecutive thermal cycles from 25 to 300 (top) or 360°C (bottom).

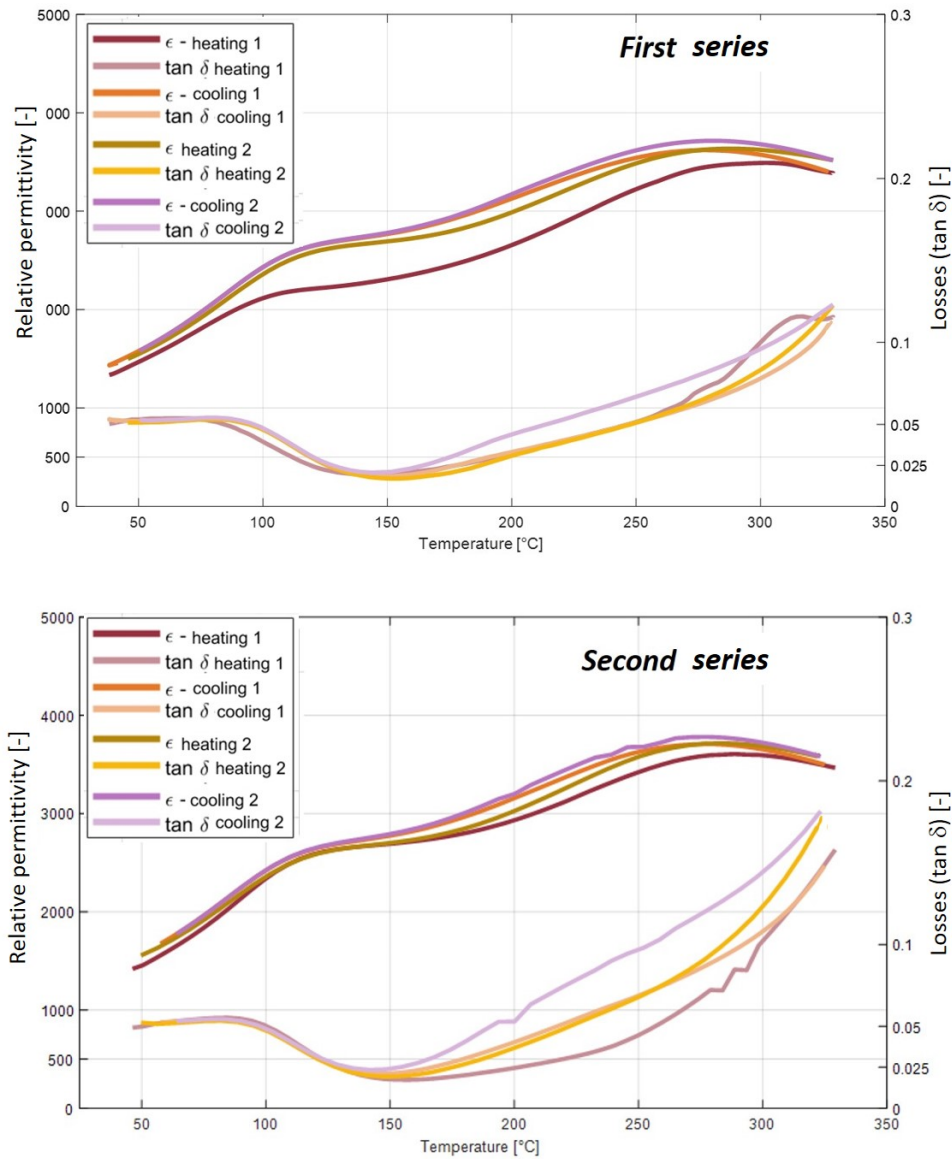


FIGURE 4.11: Dielectric properties of NBT-BT sample "X" with Ag paste metallization measured in thermal cycles from 25 to 325°C and in two different measurement series carried out three months apart.

change in the sample's microstructure influenced by the high temperature.

In order to identify the source of this increase in the dielectric losses after heating, a Cole-Cole analysis could be done. In this analysis, the electrode contribution to the permittivity and to the dielectric losses can be identified by the presence of a second semi-circle (see section 3.3.1.1). However, in order to obtain good results for this analysis, a less conductive sample is needed. Furthermore, to determine maximum temperature to avoid the dielectric losses increase, a stability of the dielectric properties over time for different temperatures should be tested (see section 4.4).

4.3 Conclusion

This chapter discussed the origin of the differences in the dielectric properties NBT-BT reported in the literature. Some arguments for these incompatibilities were discussed and the importance of having a strict synthesis and measurement method was presented.

Some examples of literature incompatibilities for the dielectric properties of the NBT-BT are: Ge *et al.* that reported the expected properties for stoichiometric NBT-BT with a frequency dispersion for temperatures lower than T_d , a shoulder in the relative permittivity vs temperature curve at T_d and low dielectric losses for temperatures higher than T_d ; [19] Kumar *et al.* that reported a frequency dispersion, no hump in permittivity at T_d , a different shape of the dielectric losses vs temperature curve, and higher values of $\tan \delta$ compared to Ge *et al.* (2014); [10] and Zhang *et al.* that reported an increase in the dielectric losses at high temperatures, a frequency dispersion, and no permittivity hump at T_d . [86]

To explain these differences the influence of stoichiometry, metallization, phase separation, synthesis parameters and polishing and strain relaxation on the material's dielectric properties were analyzed.

The stoichiometry has a crucial effect on the properties of NBT-BT. The increase in the nominal Na/Bi ratio and Na quantity increases the conductivity and the quantity of free charges. This increases the relative permittivity and the dielectric losses from room temperature to 350°C. It also increases the frequency dispersion for the entire temperature range. Finally, it also changes the shape of the relative permittivity and dielectric losses vs temperature curves. In addition to the effects on the relative permittivity and dielectric losses values, the increase in the nominal Na/Bi ratio decreases the relative permittivity change at T_d , making it less evident, increases T_d and decreases T_m .

Another important difference in the measured dielectric properties of NBT-BT samples is the temperature cycle measurement hysteresis. All the heating / cooling cycle measurements are similar, except for the first heating that shows a decreased permittivity value and may show an increased measurement noise. The hysteresis of the dielectric properties of NBT-BT over the first cycle is neither due to the synthesis method, nor to the phase separation, nor to the strain level, nor to the stoichiometry of the material. So this hysteresis should not be an intrinsic characteristics of the material.

The hypothesis that the first heating hysteresis is due to the metallization method was confirmed and it showed that it is due to the use of silver paste on metallization and electric wire fixing. Since the silver paste is a very common metallization method in research, the metallization and the method to contact the electric leads can also be held responsible for the literature incompatibilities of the dielectric properties of NBT-BT.

The variability in the measured dielectric properties from sample to sample is also an important factor to explain the differences observed in the literature depending on the heating / cooling cycle considered.

Finally, a change in the dielectric losses at high temperatures after each heating and cooling cycle is observed. Contrary to what was observed for hysteresis over the first heating, the high-temperature dielectric losses increase is observed regardless of the metallization and method to contact the electrical leads, the stoichiometry, the phase separation, the synthesis parameters, or the polishing and strain relaxation. Moreover, it is present for temperature cycles where the higher temperature reached is greater than 300°C and it increases with increasing maximum temperatures. This indicates that a thermally degradation takes place at high temperatures (over 300°C).

Two possibilities are considered to explain the thermal degradation of the NBT-BT. The first one is the presence of thermally activated phenomenon, such as defect movements at high temperatures. The second one is the change in the microstructure of the material that can be permanent or not.

Comparing samples with different metallization methods it was possible to conclude that the electrode influences the measured dielectric losses, increasing it by changes in its morphology during heating. However, it is also possible that there is a change in the sample's microstructure influenced by the high temperature. A new Cole-Cole analysis could be done with a less conductive sample and including lower frequencies.

4.4 Future works for bulk NBT-BT

Some synthesis improvements could still be studied, to further enhance the properties of the final material. One suggested modification that could be studied is the *change in the calcination parameters*, decreasing the temperature and increasing the time of calcination. Otoničar *et al.* used a two-step calcination with the first one at 750°C for 10h and the second one at 850°C for 10h with the reactant powder mixture pressed onto the crucible. [50] In this case, as the calcination is done in a temperature lower than the fusion temperature of Bi₂O₃, there is no liquid phase formation and potentially less Bi evaporation, improving the final material properties.

Another suggested modification that could be studied is the use of the reactants powder or the NBT powder around the sample in a sealed crucible to create a saturated sintering atmosphere, avoiding the volatile species evaporation. Differently from the studied method shown in section 2.1.3.1, the used powders would not touch the material's surface, eliminating the need of post-sintering treatment. However, as it was shown in Chapters 2 and 3, the sintering on ZrO₂ powder results in satisfying NBT-BT properties, with small Zr contamination in the sample's surface. Moreover, the sintering on ZrO₂ powder method is less costly than the one using the same composition or the reactants powder. So, it would be an academic rather than an industrial study.

In order to prove that the change in the NBT-BT powder color after the second ball-milling with the 10mm-diameter balls (section 2.3.4.1) is really due to the creation of oxygen vacancies, a *band gap measurement by UV-vis absorption* of the powders could be done. The change of the band gap for powders ball-milled with the 10-mm diameter balls compared to those ball-milled with the 1mm-diameter balls would confirm the presence of oxygen vacancies and therefore the inadequacy of using 10-mm diameter balls for the second ball-milling.

The increase of the dielectric losses, even if they can be temporary, represent a problem for the material application for the MLCC production. In order to identify the maximum temperature that the NBT-BT can be used and to characterize its behaviour at high temperatures, an analysis of the *stability of the dielectric properties in time for different temperatures* should be done, specially over 300°C.

The stability of the dielectric properties over time and depending on the temperature

would also be useful to estimate the *aging and lifetime* properties of this material. These are also important characteristics for the MLCC application (see section 1.3.1.6).

A *Nyquist plot analysis* would also be useful to identify the influence of the electrodes on the measured dielectric properties, as mentioned in section 4.2.2.3. However, this measurement requires a less conductive sample to enable the semi-circle identification. It also requires lower frequency measurements (around 1mHz), to be able to identify the semi-circle linked to the electrode's effect.

The *polarization vs electric field hysteresis cycle* measurements of the final NBT-BT material are also important to determine the energy storage properties of these samples. However, a less-conductive sample at high-electric fields should be obtained first, to enable the measurement of a saturated polarization vs electric-field cycle.

Finally, the measurement of the *dielectric properties under constant (bias) applied electric field* would also be interesting. In case the material presents stable or increasing permittivity with limited dielectric losses (lower than 2.5%) when a bias field is applied, it could be a good candidate for substituting the lead-based MLCC capacitors presenting the maximum capacitance for specific values of constant applied voltage.

Chapter 5

NBT-BT Layers

The objective of this chapter is to ensure the compatibility of the NBT-BT layers with the industrial specification and to compare the differences in structure and properties of the best samples in bulk in with the layers obtained from these powders.

5.1 Layer preparation

5.1.1 Best NBT-BT bulk sample

Chapters 3 and 4 analysed the dielectric and insulation properties of NBT-BT in temperature, frequency, and over thermal cycling.

The results show that the stoichiometry of sample "U" is the best one, due to its high insulation resistance, and low dielectric losses and permittivity variation in temperature. Moreover, the secondary Ba-containing phases formation with an intermediary volume fraction (2.5 to 3.0%) and average grain surface (0.9 to $3.0\mu\text{m}^2$) is beneficial for the properties.

To obtain this grain surface and volume fraction of the secondary Ba-containing phases, and the best dielectric and insulation properties, a dispersing agent should be used during ball milling in MEK and ethanol mixture and the raw powders should not be dried before weighing. In this case, the average Na_2CO_3 grain size and the energy of ball milling do not affect significantly the final bulk properties.

So, the synthesis parameters of sample "U" (nominal NBT-BT with un-dried raw powder, ball milled with dispersing agent on ethanol and MEK mixture during 8h at 350 rpm with fine Na_2CO_3 powder) are also the most adapted ones to meet Exxelia's requirements for MLCCs (as presented in section 1.3).

Finally, for the bulk ceramic samples, the polishing and strain relaxation at 400°C during 3h should be done to release the internal strain and to have no secondary Ba-containing phases or ZrO_2 powder concentration on the surface.

5.1.2 Monolayer synthesis and sintering improvements

The slurry synthesis consists in preparing a NBT-BT powder by solid-state synthesis (weighing, ball-milling, and calcination) using the synthesis parameters and the stoichiometry of the bulk "U" sample, as detailed in Chapter 2: initially the un-dried raw powders were weighed with the nominal composition of $\text{Na}_{0.44}\text{Bi}_{0.48}\text{Ba}_{0.06}\text{TiO}_3$. Then they were ball-milling during 8h at 350 rpm in an ethanol and MEK mixture with the addition of a dispersing agent. The milled powders were, then, calcinated during 2h at 900°C .

A second ball-milling is then carried-out giving rise the slurry. The synthesis parameters used in this second ball-milling were detailed in section 2.3.3.1 and are summarized here:

The slurry composition was 60.6wt% of NBT-BT powder, 1.1wt% of PEG (poly-ethylene-glycol), 22.7wt% of MEK (methyl-ethyl-ketone), 10wt% of ethanol, 4.5wt% of PVB (poly-vinyl-butyril) and 1.1wt% of dispersing agent (borchi-gen-911), as reported in Table 2.8 p. 61.

The slurry preparation was done by adding initially the solvents (ethanol + MEK), the dispersing agent and the NBT-BT powder, as for the "U" ceramic sample. The mixture was ball-milled at 300 rpm for 12 hours in an YSZ jar. Then PVB and PEG are added and the mixture is again ball-milled at 300 rpm for 2 hours (see section 2.3.3.1).

Finally, the slurry was deaerated by pumping its recipient that is, the air was removed from the slurry, to avoid defects on the tape. It was then tape casted using the setup shown in Fig. 5.1 with a thickness of the casted slurry set to 100 μ m.

The "green" tapes (before sintering) showed good mechanical resistance, no cracks and

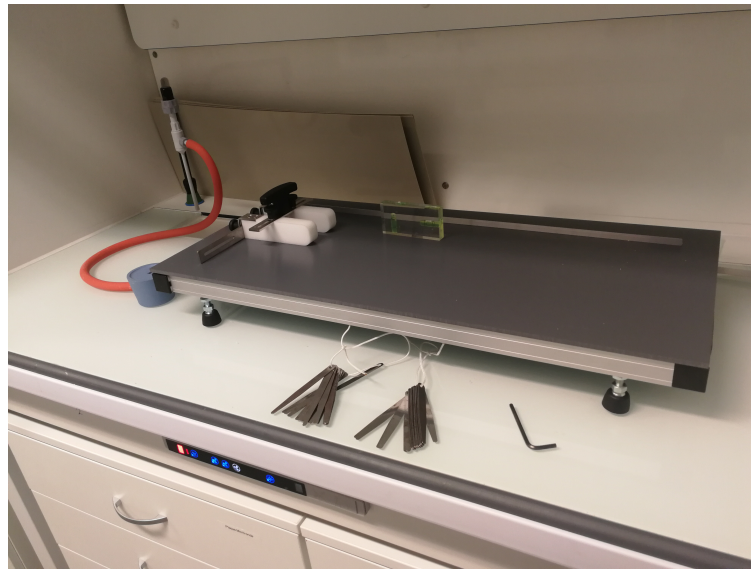


FIGURE 5.1: Tape casting setup.

a uniform thickness ($153 \pm 24\mu\text{m}$). This indicates that the slurry is well dispersed and stable.

Initially, the sintering of the monolayers was done following the same parameters as the ones used for the bulk "U" sample (sintering under ZrO_2 for 3h with a heating speed of 120°C/h and a cooling speed of 200°C/h). However, the as-sintered monolayers showed a low density of 58%. For this reason, the sintering parameters were optimized for the monolayer synthesis.

The first tested parameter was the sintering time that was increased to 6h and decreased to 1h. However, the density decreased to 47% for the 6h sintering and to 49% for the 1h sintering. So the initial sintering time of 3h was maintained.

The second parameter investigated was the sintering temperature. It was decreased to 1000°C and increased to 1150°C . As for the bulk, the NBT-BT monolayers presented the maximum density at 1150°C with a density of 62% while the sample sintered at 1000°C showed a lower density of 42%. However, the 62% density is still not enough for the MLCC application. Due to the limited time available and to the fact that the relative density decreased for the bulk NBT-BT samples sintered at temperatures higher than 1150°C , the maximum sintering temperature tested for monolayers was 1150°C .

Finally, the last parameter changed was the temperature steps during sintering. Salam *et al.* showed by thermogravimetric analysis that the oxidative breakdown of the PVB structure takes place between 400 and 500°C , achieving a complete burnout.[61] The minimum temperature to have small quantity of PVB residues after heat treatment is 450°C . However, all

the thermal treatments in air led to the formation of char that is eliminated at 750°C. [61]

Therefore, a new sintering was done with the NBT-BT monolayers using two temperature plateaus, the first one at 450°C for 12h, to oxidize the PVB, and another one at 800°C for 30 minutes, to guarantee the elimination of all organic residues in the tape. The final step of the sintering was done at 1050°C for 3h, as for the first one.

However, the as-sintered NBT-BT tape showed a smaller density of 53% compared to the density of the sample sintered without the 450°C plateau. Table 5.1 show the final densities obtained for the different sintering parameters.

Table 5.1 shows that the low density of the NBT-BT monolayers is not due to a sintering

Sintering time (h)	Sintering temperature (°C)	Temperature plateau (°C - h)	Relative density (%)
3	1050	800 - 0.5	58
6	1050	800 - 0.5	47
1	1050	800 - 0.5	49
3	1000	800 - 0.5	42
3	1150	800 - 0.5	62
3	1150	450 - 12 + 800 - 0.5	53

TABLE 5.1: Sintering parameters for the NBT-BT monolayers and as-sintered sample densities (the uncertainties are $\pm 2.5\%$).

problem. The "green" tapes have good mechanical resistance, no cracks and uniform thickness, as mentioned before, indicating that the parameters used in the ball-milling for slurry synthesis are adapted to the MLCC production. So, the next step to solving the density problem of the NBT-BT layers would be to press multiple "green" layer together, to decrease the porosity of the multilayer device before sintering, to increase the NBT-BT powder concentration and to decrease the PVB concentration in the slurry.[38]

5.2 Structure and thickness of the monolayers

The XRD measurements of the monolayer before sintering and as-sintered at 1050°C for three hours are shown in Fig. 5.2.

The measurements show no second phase peak after sintering, since the only peaks not related to the NBT-BT are the ones coming from the ZrO₂ atmosphere powder.

A peak widening similar to the ones observed for the polished and strain-relaxed bulk NBT-BT samples is also observed. The insets in Fig. 5.2 show the pseudocubic (110) and (111) peaks details. The widening is present for all the peaks as a lower-angle-side shoulder peak and is probably also related to a phase coexistence in NBT-BT (see section 2.3.2.2). So, in the as-sintered NBT-BT monolayers, there is a coexistence of pseudo-cubic, rhombohedral, and tetragonal phases at the surface.

The SEM images of the monolayer sintered at 1050°C for three hours are shown in Fig. 5.3. Samples sintered in different conditions show similar structures.

As it can be confirmed from Fig. 5.3, the synthesised NBT-BT monolayers show low density and porous structure. Ceramic layers with low density could not be applied to MLCC production, since it would create problems such as the penetration of the electrodes in the ceramic layer, the increase in the dielectric losses, the decrease of the insulation resistance, and the decrease of the dielectric strength. So an optimization of the slurry composition and the sintering after pressing the layers together in a multilayer device are needed before being able to characterize a layer that could be used in MLCCs (see section 5.1.2).

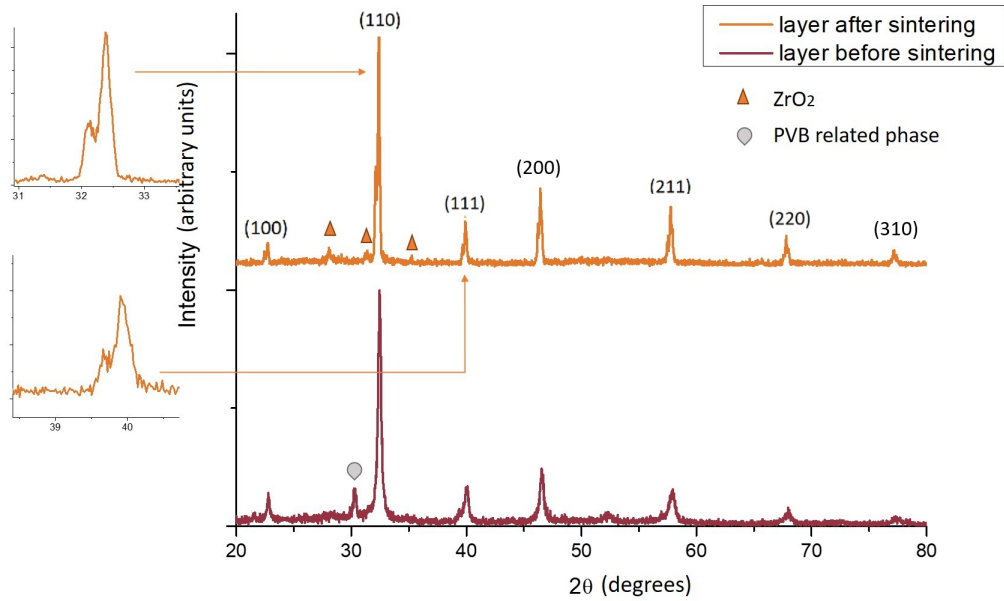


FIGURE 5.2: XRD measurements of the NBT-BT monolayer before and after sintering with phase identification. The insets show the pseudocubic (110) (top) and (111) (bottom) peaks of the layer after sintering.

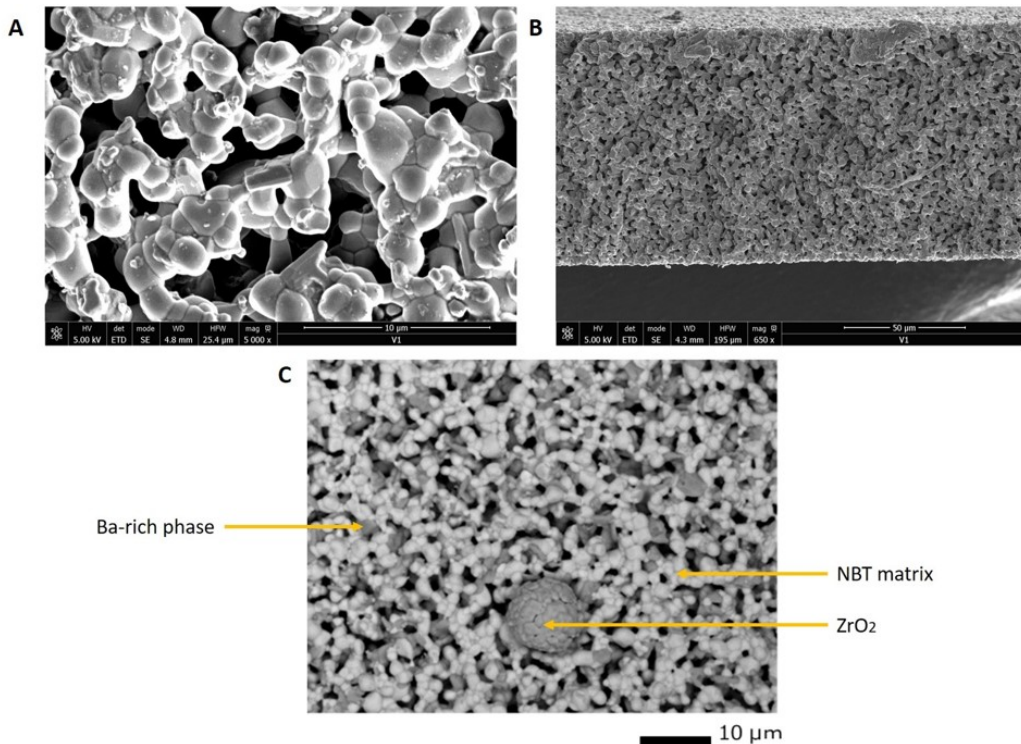


FIGURE 5.3: SEM images of the NBT-BT monolayer sample sintered at 1050°C for three hours. A - grain sizes in 5000x magnification image, B - monolayer thickness and porous structure in 650x magnification image, C - sample's surface showing the secondary Ba-containing phases separation and the ZrO_2 powder grain attached to the surface in 1900x magnification image.

The SEM images showed in Fig. 5.3 also show the presence of secondary Ba-containing phases grains. As for the bulk samples, this phase is formed due to the Na evaporation during sintering. However, the morphology of this phase is different from the one in the bulk samples, as it can be seen in Fig. 5.4, probably due to the low density of the material.

The volume fraction of the secondary Ba-containing phases could not be estimated, due to the impossibility to have a polished surface image. The average grain surface of the secondary Ba-containing phases is $2.9 \pm 0.8 \mu\text{m}^2$ in the monolayer. This is in the moderate average grain surface values necessary to obtain samples compliant with Exxelia requirements (see section 3.2.1.2).

Table 5.2 presents the composition of the matrix and the secondary Ba-containing

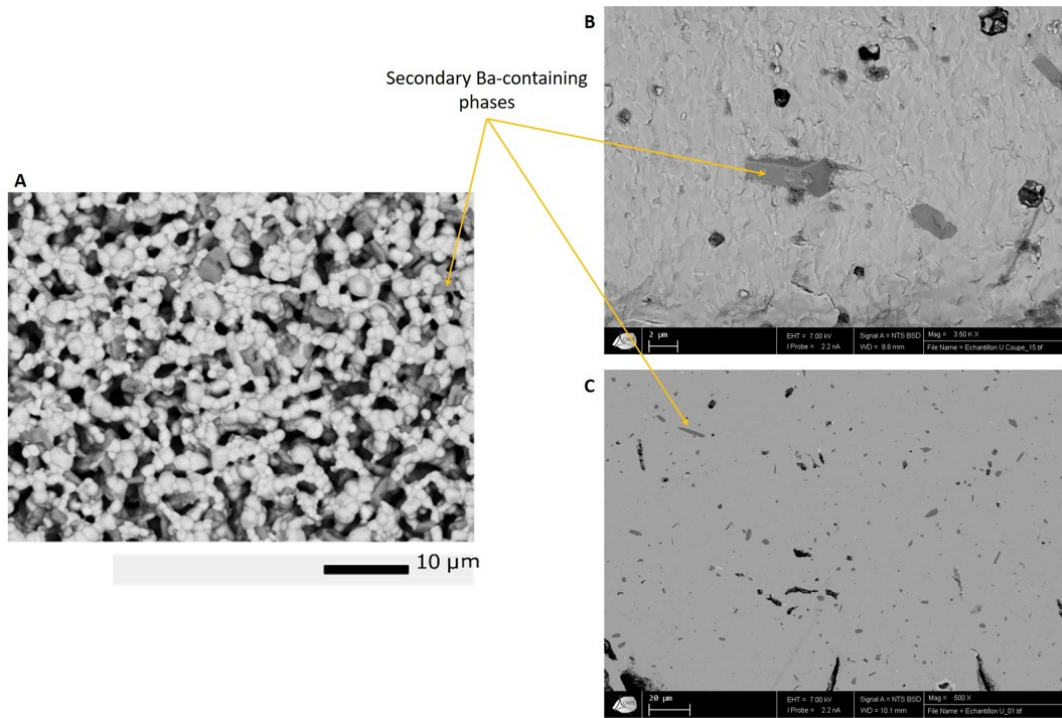


FIGURE 5.4: SEM images showing the morphology of the secondary Ba-containing phases of A - NBT-BT monolayer sample sintered at 1050°C for three hours, B - core of the NBT-BT bulk equivalent sample ("U"), C - surface of the NBT-BT bulk equivalent sample ("U").

phases present in the sample sintered at 1050°C for 3h measured via EDS analysis.

Comparing the monolayer composition with the equivalent "U" bulk sample compo-

Phase	O	Na	Ti	Ba	Bi	Zr
Secondary Ba-containing phases	19.7 ± 0.5	0.35 ± 0.05	9.0	1.97 ± 0.08	0.54 ± 0.03	0.41 ± 0.03
NBT matrix	2.4 ± 0.1	0.31 ± 0.02	1.0	0.05 ± 0.01	0.51 ± 0.02	0.03 ± 0.01

TABLE 5.2: Matrix and secondary Ba-containing phases composition measured via EDS considering stoichiometry for the Ti as 1.0 for the matrix and 9.0 for the secondary Ba-containing phases for the NBT-BT sample after sintering.

sition in Table 2.3 p. 51, it can be seen that for both samples, the Bi is stoichiometric in the matrix NBT phase. However, the Na quantity in the matrix is smaller in the monolayer

sample, indicating that the evaporation during sintering is more important in the monolayer when compared to the bulk. This also indicates that the secondary Ba-containing phases volume fraction should be higher in the layers, even if this could not be measured due to the low density of the samples.

Comparing now the composition of the secondary Ba-containing phases of the layer with to the bulk ones (see Table 2.10 p. 73), it can be seen that, in both cases, there is a Zr contamination in this phase. However, the contamination is more important for the monolayers, due to the higher contact surface of the material with the ZrO_2 powder during sintering. This can also explain the lower Ba quantity in the secondary Ba-containing phases of the layers. The Zr doping favours the $\text{Ba}_2\text{Ti}_9\text{O}_{20}$ formation over Ba_2TiO_4 and $\text{Ba}_2\text{Ti}_9\text{O}_{20}\backslash 2\text{BaO}\cdot\text{TiO}_2$, resulting in a lower Ba content in this phase.

Finally, the SEM analysis shows an average grain size of $2.4 \pm 0.8 \mu\text{m}^2$ after sintering and a monolayer thickness of $97 \mu\text{m}$. The measured grain size is slightly larger than Exxelia's specifications ($2 \mu\text{m}$), but it could still be used for the MLCC production (see section 1.3.1.7). However, the monolayer thickness is considerably larger than the minimum thickness specifications ($20 \mu\text{m}$ as specified in section 1.3.1.7), so the synthesis of thinner layers should also be tested after the density is increased (see section 5.6).

In conclusion, all the synthesized monolayers presented a porous structure due to their low density. This is not ideal for the MLCC production, so an optimization of the slurry synthesis is needed. This optimization can be done by changing the ceramic powder and the binder concentrations on the slurry and by pressing multiple layer together, forming a multilayer device before sintering, to obtain a higher relative density after sintering.

Moreover, the NBT-BT layers present the same secondary Ba-containing phases separation as the bulk samples. However, a more reliable estimation of the volume fraction and the grain surface average values for this secondary phase can be done only after obtaining a dense NBT-BT layer.

5.3 Dielectric properties of the monolayers in temperature

The dielectric properties were measured only for the NBT-BT monolayer sintered at 1050°C . The results for the temperature cycling measurements and for frequencies from 1kHz to 1MHz for the second cooling are shown in Fig. 5.5.

A reliable comparison of the dielectric properties between the equivalent bulk and monolayer samples is difficult, due to the large density difference between them. So a synthesis optimization should be done before.

However, it can be seen that the relative permittivity of the monolayer is drastically smaller compared to the bulk one, with an of average half of the bulk value. The dielectric losses are also increased for temperatures higher than 150°C on the monolayer sample compared to the bulk one. The decrease of the relative permittivity is expected due to the low density of the monolayer sample that decreases the average permittivity of the material due to the low permittivity of the air. The higher dielectric losses are also expected due to the low density of the sample. Due to the high number of pores in the material, the ionization loss coming from the air in the pores contributes to the dielectric losses. Moreover, the high concentration of impurities and defects in the low density materials creates weakly bounded ions, resulting in conduction loss. [40]

Nonetheless, the most important observation related to the dielectric properties of the monolayer sample is the huge temperature hysteresis when measuring it in consecutive thermal cycles. The measurement could not be properly done for temperatures higher than 275°C

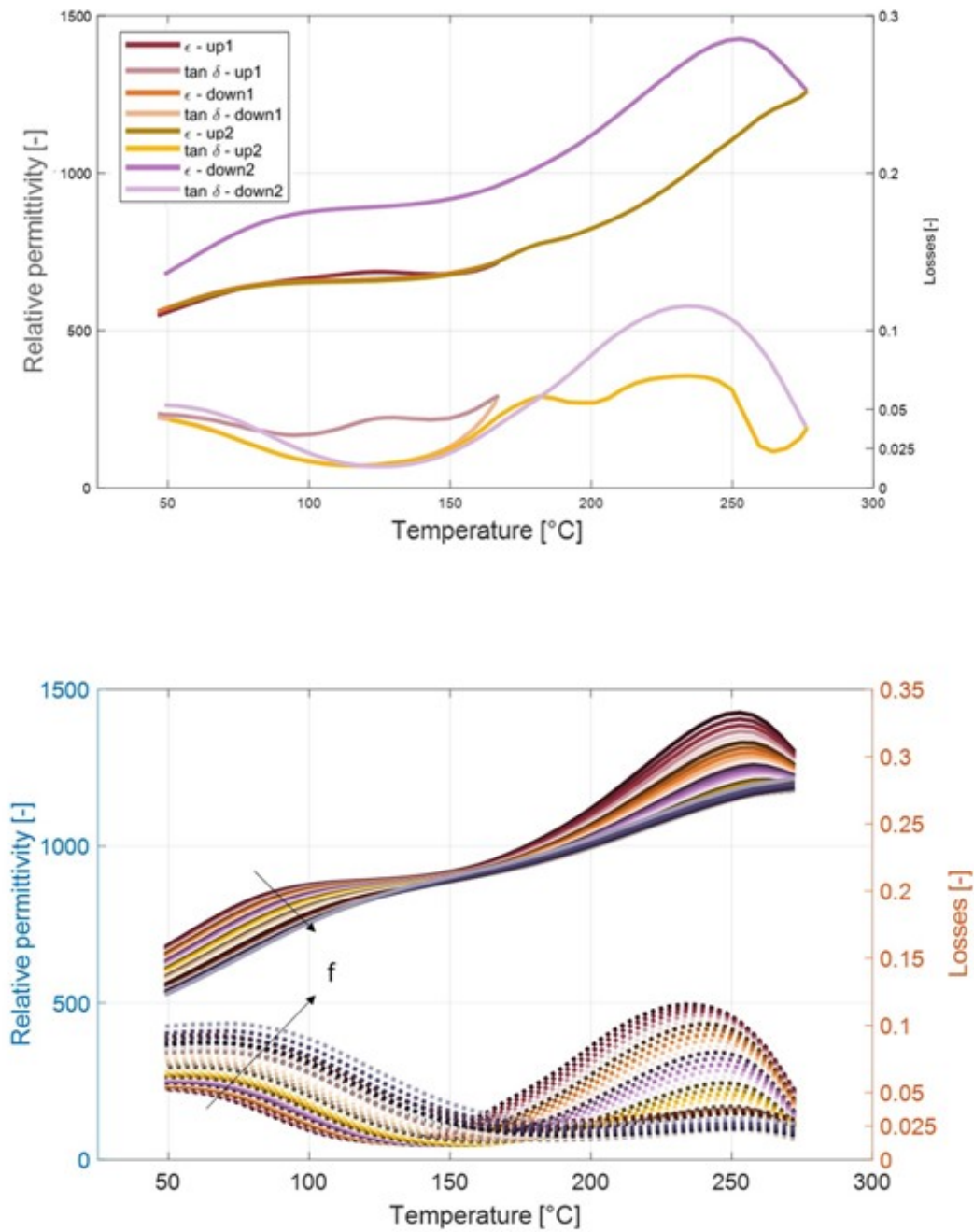


FIGURE 5.5: Relative permittivity and dielectric losses ($\tan \delta$) for the NBT-BT "U" monolayer sample over consecutive temperature cycles from 25 to 170°C in the first cycle and from 25 to 270°C in the second cycle (top panel) and for the second cooling measurement over frequencies from 1kHz to 1MHz (bottom panel).

due to the sample degradation (see Fig. 5.6).

The effect of increasing dielectric losses when measuring the dielectric properties in

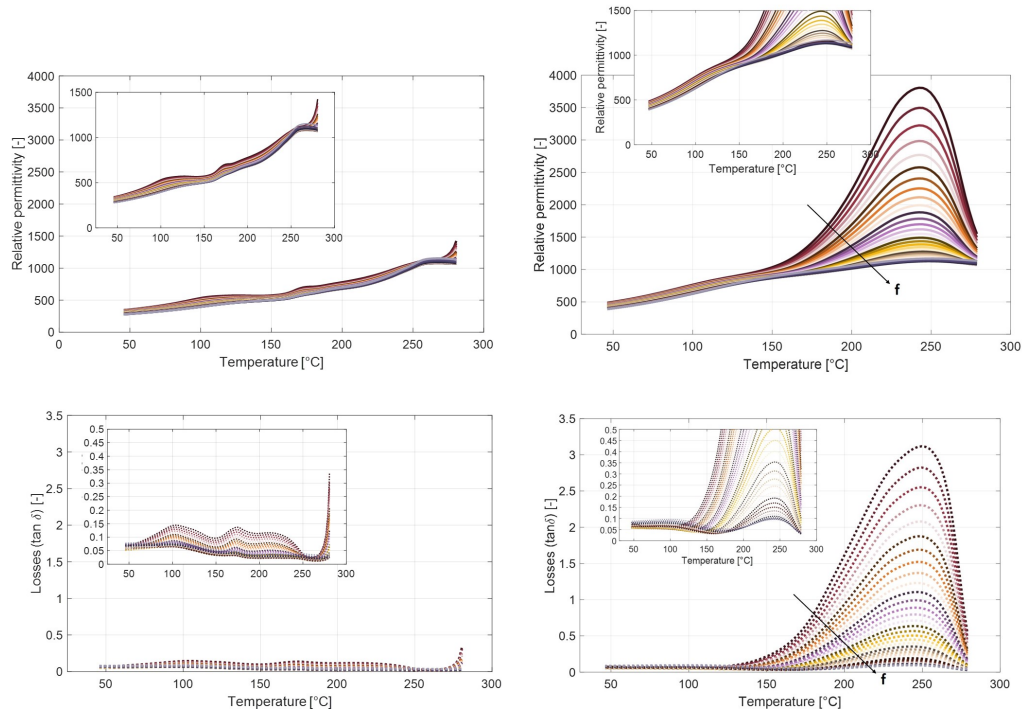


FIGURE 5.6: Relative permittivity (top) and dielectric losses (bottom) for a NBT-BT monolayer sample measured during heating (left) and cooling (right) using a thermal cycle from room temperature to 280°C showing high hysteresis and thermal degradation. The inset show the details for lower values of relative permittivity and dielectric losses, showing the shape of the curves and the dielectric losses values lower than 15% for temperature lower than 250°C.

thermal cycles was already shown in chapter 4 for the bulk samples. However, the effects are magnified for the monolayer samples and they are also present for the relative permittivity.

The effect may be due to the influence of the silver paste electrodes and their morphology in the effective dielectric properties. It is also possible that it is due to changes in the sample's microstructure influenced by the high temperature (see section 4.2.2.3).

The SEM image of the monolayer after measuring its dielectric properties in a temperature cycle from 25 to 350°C using silver paste metallization is shown in Fig. 5.7.

This image shows that there is a penetration of the silver coming from the silver paste electrodes in the material pores during measurement in thermal cycling. This supports the hypothesis that the electrode influences the measured dielectric properties, increasing them by changing its morphology. However, the hypothesis of the material morphology change in temperature cannot be excluded, since the low density and the high specific area of the monolayer samples increase the defect concentration and facilitate the material morphology changes.

Finally, the insulation resistance of the NBT-BT monolayer sample is shown in Fig. 5.8. Comparing the measured value at 200°C (the highest measured value before the curve extrapolation by exponential decrease) of the monolayer sample (0.5s) with its corresponding bulk counterpart "U" (87s), an important decrease in the insulation resistance is observed for the layer sample, corresponding to a temperature variation of 100°C. This difference is due to the low density of the sample that facilitate the creation of defects and the evaporation of

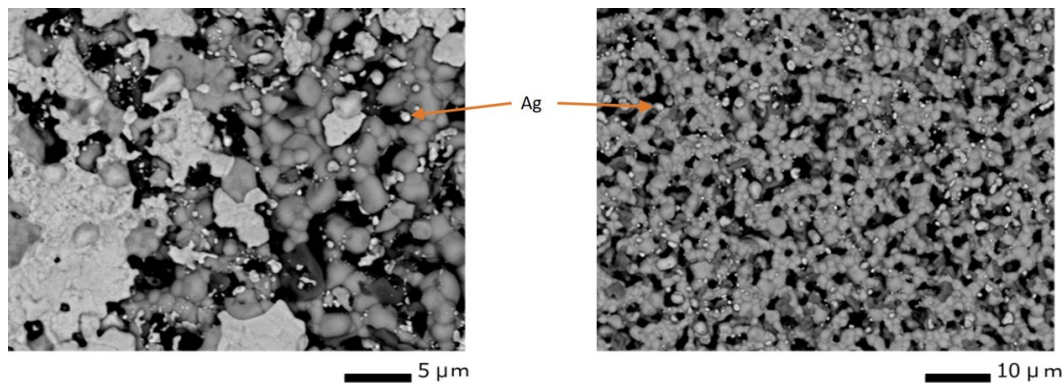


FIGURE 5.7: SEM image of the NBT-BT monolayer surface after measuring its dielectric properties in a temperature cycle from 25 to 350°C using silver paste metallization.

volatiles during sintering, increasing the material's conductivity.

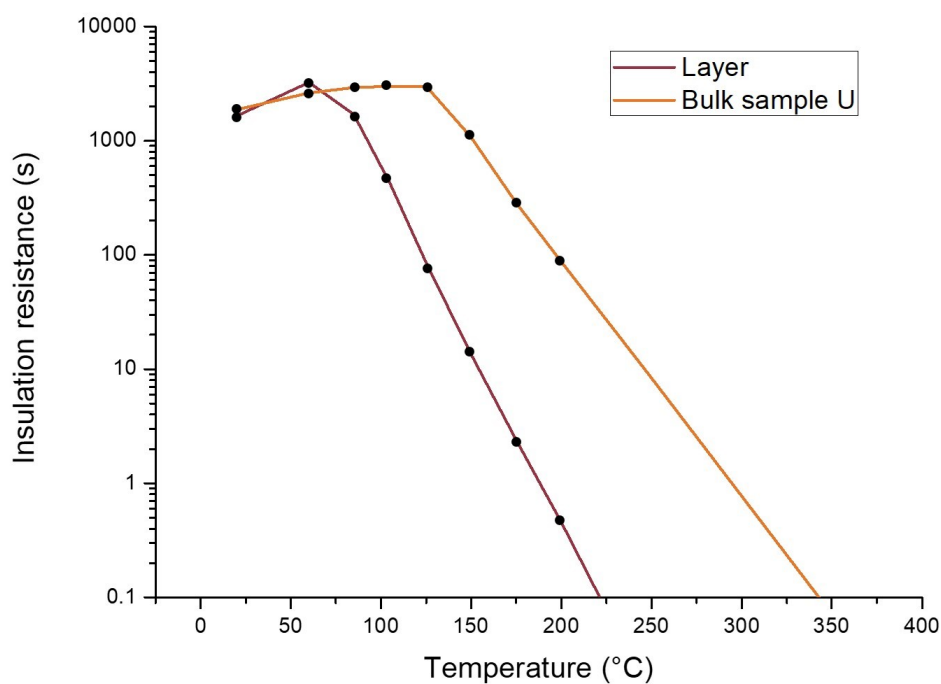


FIGURE 5.8: Insulation resistance of the NBT-BT monolayer sample and of its bulk equivalent (sample "U").

5.3.1 Compatibility of the dielectric properties with Exxelia's specifications

The relative density of the NBT-BT monolayer sample should be improved, to allow a more reliable assessment of NBT-BT layer properties and to meet Exxelia's MLCC requirements (see section 5.2).

However, considering the dielectric properties of this NBT-BT monolayer sample in Fig. 5.5 p. 159, it can be concluded that the losses are lower than 2.5% at 1kHz (the required

maximum value for the MLCCs) from 100 to 150°C. Considering the reference temperature as 213°C (see section 3.2.2.1) the relative permittivity variation of $\pm 15\%$ takes place from 180 to 240°C. If the reference temperature was changed to 125°C (the middle point of the temperature range to have $\tan \delta \leq 2.5\%$ at 1kHz), the variation of $\pm 15\%$ would take place from 68 to 187°C.

Considering now the minimum value of the insulation resistance allowed for the MLCCs (1s, as explained in section 1.3), the the maximum operational temperature of this sample would be 180°C.

In conclusion, even for the low density NBT-BT monolayer sample, considering the reference temperature as 125°C, this sample shows a compatible relative permittivity from 68 to 187°C, a compatible dielectric losses from 100 to 150°C and a compatible insulation resistance from the room temperature to 180°C.

A new dielectric characterization and the comparison between the layer and the equivalent bulk samples should be done after increasing the layer's relative density. This will allow a more reliable assessment of the NBT-BT layer properties, in order to evaluate the real compatibility with Exxelia's requirements and the effect of reducing the sample's thickness on its dielectric and insulating properties.

5.4 Structure and density of the pressed multilayers

As suggested by Exxelia, the effects of pressing multiple "green" ceramic layers together before sintering, forming a multilayer device, was studied. This pressing step is normally important thereby high density ceramics, since it decreases the porosity of the "green" material.

The first step for testing the effects of the pressing step on the density and structure of the layers was to sinter a monolayer of a material that is commercially used. The sintered monolayer was then compared with its equivalent commercial MLCC. The chosen layer material is composed of BaTiO₃ doped with Bi (K2200), since it has a similar sintering temperature to the NBT-BT. The monolayer synthesis was done using the same temperature program as for the NBT-BT layer (120°C/h heating, a plateau of 30 minutes at 800°C, sintering at 1150°C for 3h and 200°C/h cooling) and it was sintered either with or without covering the monolayer with the ZrO₂ powder. The SEM images of the two sintered monolayers and the equivalent commercial MLCC are shown in Fig. 5.9.

The density of the sintered monolayers could not be measured directly due to the low

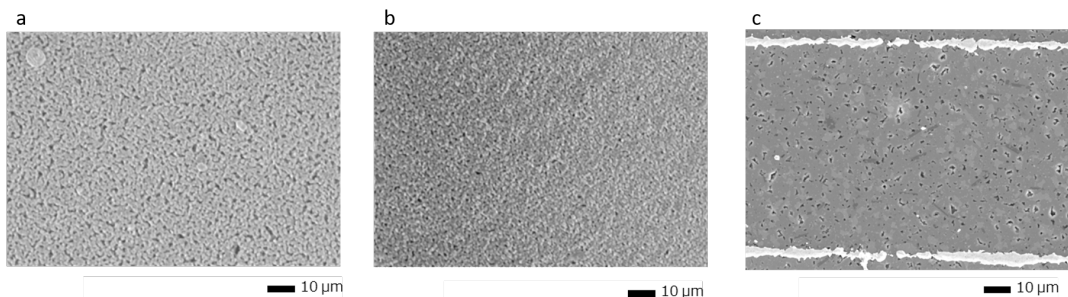


FIGURE 5.9: SEM images of the commercially used material (K2200) monolayers sintered in ZrO₂ powder (a), without ZrO₂ powder (b) and its equivalent commercial MLCC (c).

thickness of the "green" layers (40 μm). However, it can be seen from Fig. 5.9 that the monolayers show a much lower density (higher porosity) compared their corresponding MLCC.

Moreover, the monolayer sintered in ZrO_2 powder also shows a lower density compared to the one sintered without using the ZrO_2 powder. This indicates that the multilayer pressing step is essential to obtain a high density material after sintering and that the use of ZrO_2 powder to control the volatile species evaporation also contributes to limit the final density of the layers.

From the results obtained for the K2200 commercial monolayers, a second test was done, sintering multiple layers of NBT-BT pressed together before sintering. To do that, the same "green" NBT-BT layers were stacked and pressed together using uniaxial pressing in the stacking machine used in Exxelia for the MLCC production. No electrode was applied between the ceramic layers. The pressed ceramic multilayers were cut into squares of around two to three millimeters side and they were sintered in ZrO_2 powder using the same temperature cycle than the 3h at $1150^\circ C$ sintering. Fig 5.10 shows the SEM images of the pressed NBT-BT multilayers and the comparison with their corresponding monolayer.

The measured density of the sintered NBT-BT multilayer is 89.5%, much higher than

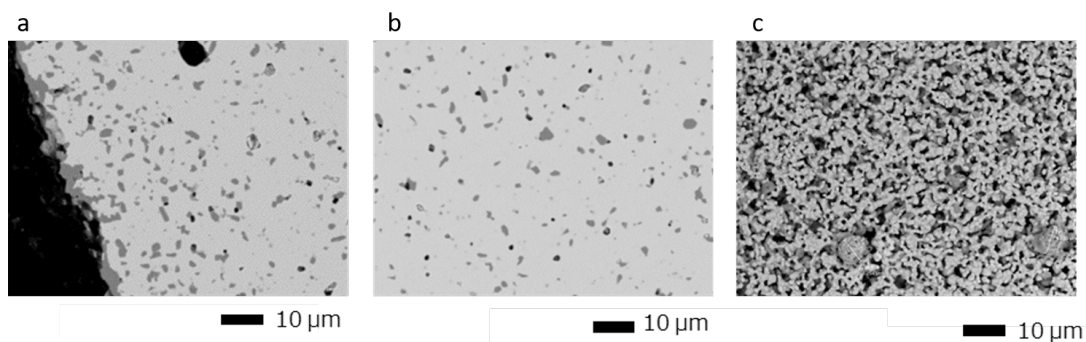


FIGURE 5.10: SEM images of the stacked and pressed NBT-BT multilayers sintered in ZrO_2 powder in the core (a) and in the surface of the sample (b) and the equivalent NBT-BT monolayer (c).

the equivalent monolayer (62%) and compatible with the MLCC production. This density increase can also be observed in the SEM images of the sintered NBT-BT multilayer in Fig. 5.10, since the surface and the core of the sample show much lower porosity compared to the monolayer.

Fig. 5.10 also shows a phase separation and the presence of the secondary Ba-containing phases grains. As for the bulk samples, this phase is formed of grains due to the evaporation of Na during sintering and it concentrates at the surface of the sample. Contrary to the NBT-BT monolayer, the secondary Ba-containing phases in the NBT-BT multilayer show a similar structure as in the bulk samples, with elongated grains. However a higher concentration of this secondary phase is observed in the NBT-BT multilayer compared to the bulk samples, specially at the sample's surface. This indicated that a higher Na evaporation is present in the multilayers, as expected from their lower thickness.

The average volume fraction and average grain surface of the secondary Ba-containing phases could only be estimated for the core of the sample, due to the extremely high concentration of these phases at the surface of the sample. However, since there is a polishing step planned in the MLCC production, the volume fraction and the grain surface of the secondary Ba-containing phases in the surface of the sample do not influence the final MLCC properties.

The estimated average volume fraction of the secondary Ba-containing phases in the core of the sample is $5.5 \pm 2.4 \%$ and the estimated average grain surface of these phases is $1.6 \pm 0.5 \mu m^2$. Comparing these values with the ones for the bulk samples ($1.6 \pm 0.5 \%$ of average volume fraction and $1.9 \pm 1.0 \mu m^2$) it is observed that the average volume fraction

of the secondary Ba-containing phases in the pressed multilayers are similar to the ones in the bulk "U" samples. However, there is a great increase in the average volume fraction for the pressed multilayers, due to the higher Na evaporation during sintering. It is, then, indicated to measure the evolution of the dielectric properties as function of the temperature for the pressed NBT-BT multilayers, to evaluate the effects of this increase on the average volume fraction of the secondary Ba-containing phases.

Another difference in the structure of the pressed multilayers compared to the equivalent "U" bulk sample is that the multilayers do not show a Bi-containing secondary phase in the core of the sample, whereas the bulk samples do. This indicates that there is also a higher evaporation of Bi in the pressed multilayers, which can also affect the dielectric properties of the material. Therefore, the measurement of the evolution of the dielectric properties as function of temperature is also important for evaluating these effects.

In conclusion, the pressing of multiple "green" ceramic layers together before sintering is an important step to obtain high density NBT-BT or commercially used ceramic layers after sintering. The NBT-BT pressed multilayers showed a density of 89.5% after sintering at 1150°C, much higher than the equivalent monolayer (62%) and compatible with the MLCC application.

The NBT-BT pressed multilayer showed a similar structure as its equivalent bulk "U" sample, with the same secondary Ba-containing phases. However, the average volume fraction of this secondary phase was higher than the one in the bulk samples and it did not show a third secondary Bi-containing phase. This indicates a higher Na and Bi evaporation during sintering and could influence the dielectric properties of the material in temperature. So a measurement of the evolution of the dielectric properties as function of temperature should be done for the pressed multilayers, to evaluate its compatibility with the industrial demands.

Anyhow, these results show that, the low density of the monolayers are not due to a problem in the slurry composition. Moreover, even though the density of the monolayers are not sufficient for the MLCC application, giving rise to dielectric properties that are not compatible with the industrial requirements, this does not mean the the multilayer device produced from these layers will have the same problem.

5.5 Conclusion

This chapter discussed the synthesis of NBT-BT layers and its compatibility with the industrial specifications and compared the differences in structure and properties of the best samples in bulk with the layer form.

Bulk sample "U" showed the best properties considering Exxelia's requirements for MLCC applications. For this reason, this sample was chosen to be studied in layer form.

For the layer synthesis, the second ball milling was adapted and the slurry was prepared based on Exxelia's slurry composition as well as a binder and additives optimization for NBT-BT reported in the literature.

The "green" tapes (before sintering) showed good mechanical resistance, no cracks, and a uniform thickness, indicating that the slurry is well dispersed and stable. However, the monolayers sintered using the same temperature program as sample "U" (30-minute temperature step at 850°C and sintering at 1050°C for 3h) showed low relative density of 58%.

For this reason, a sintering optimization was initiated. The sintering parameters that resulted in the highest relative density for the monolayers (62%) were a sintering with a 30 minutes temperature step at 850°C and a sintering at 1150°C for 3h. This is still insufficient for the MLCC applications.

Concerning the monolayers structure, the as-sintered samples showed the presence of ZrO_2 powder in surface, as for the bulk "U" sample. A XRD peak widening was observed due to a skin effect (coexistence of pseudo-cubic, rhombohedral and tetragonal phases in the skin). The same secondary Ba-containing phases as bulk samples were present with an average grain surface of $2.9 \pm 0.8 \mu\text{m}^2$, being compliant with Exxelia requirements. However, the morphology of this phase was different from the one in the bulk, due to the low density of the monolayer. Finally, a higher Zr contamination in the secondary Ba-containing phases was observed for the monolayers, being the reason for its lower Ba concentration.

An average grain size of $2.4 \pm 0.8 \mu\text{m}$ after sintering and a monolayer thickness of $97 \mu\text{m}$ were obtained. These values are not compatible with Exxelia's specifications, but they could still be used for the MLCC production.

It is not possible to do a reliable comparison between bulk and monolayer sample's dielectric properties, due to the low density of the monolayers. However, for the synthesized monolayer, the measured relative permittivity is smaller and the dielectric losses for temperatures greater than 150°C are higher than the bulk. This is expected due to the low density values. Moreover, a huge temperature hysteresis is observed when measuring it in consecutive thermal cycles, making the measurement impossible temperatures higher than 275°C .

This hysteresis and thermal degradation of the sample may be due to the influence of the electrodes and its morphology in the effective dielectric properties, since there is a penetration of the silver paste in the material pores during thermal cycling. However, it may also be due to the material morphology change in temperature, since the low density and the high specific area of the monolayer facilitates the material morphology changes.

Finally, the insulation resistance for the monolayers are lower than for the bulk corresponding to a temperature decrease of 100°C , as expected for lower density materials.

Even for the low density NBT-BT monolayer sample, considering the reference temperature as 125°C , this sample shows a compatible relative permittivity from 68 to 187°C , a compatible dielectric losses from 100 to 150°C and a compatible insulation resistance from the room temperature to 180°C .

So, in order to make a more reliable evaluation of the NBT-BT layers and to achieve the requirements for the MLCC production, the increase in density is imperative.

Finally, as suggested by Exxelia, the effects of pressing multiple "green" NBT-BT layers together before sintering, forming a multilayer device, was studied. It was shown that a high density material (89.5%) can be obtained after sintering the pressed multilayers at 1150°C . This indicates that the low density of the monolayers are not due to a slurry composition problem and that, even though the monolayers do not show dielectric properties compatible with the industrial demands from room temperature up to 300 or 350°C , this does not necessarily mean that the multilayer device prepared from these layers will have the same problem. However, since the pressed NBT-BT multilayers show more Na and Bi evaporation, a new measurement of the evolution of the dielectric properties as function of temperature should be done to evaluate the temperature range of compatibility with the industrial requirements.

5.6 Future works for NBT-BT layers

Even if the NBT-BT monolayers show a relative permittivity compatible with Exxelia's specifications from 68 to 187°C , a compatible dielectric losses from 100 to 150°C and a compatible insulation resistance from the room temperature to 180°C , their properties are not optimal for the MLCC production. The increase in the dielectric losses should be restricted for their industrial application. The increasing dielectric losses were also observed on a much smaller scale for the bulk NBT-BT samples. However, due to the low thickness

and low density of the ceramic monolayers, they were magnified.

In order to meet the industrial density requirements (see section 1.3), to restrain the dielectric losses increase, and the material degradation at high temperatures, the key factor is the final density of the ceramic layers. A high density material was obtained after pressing multiple NBT-BT "green" layers together before sintering (see section 5.4), indicating that, even though the dielectric properties of the monolayer were only compatible with the industrial requirements from 100 to 150°C, this does not necessarily mean that the multilayer device prepared from these monolayers will have the same temperature range restriction.

However, the higher Na and Bi evaporation in the pressed NBT-BT multilayers can affect the final dielectric properties of the material, as explained in section 5.4. So, the next step to evaluate the compatibility of the NBT-BT layers with the industrial MLCC requirements would be to do a new measurement of the evolution of the dielectric properties as function of temperature with the pressed NBT-BT multilayers.

If the density increase is not sufficient to guarantee compatible dielectric properties, an optimization of the slurry could be done, increasing the solid content and decreasing the PVA. Moreover, if the dielectric properties of the pressed NBT-BT multilayers are not compatible with the industrial demands, a modification of the reactants stoichiometry is also proposed. This would compensate for the higher Na and Bi evaporation during sintering and it would decrease the average volume fraction of the secondary Ba-containing phases, affecting the final dielectric properties.

Another parameter that should be optimized during synthesis and characterized for the industrial application is the grain-size distribution. This parameter is important since the surface energy and the sintering results vary depending on the grain-size distribution. For this reason, this is a usual information in the product specification and it is controlled by companies before the MLCC production starts. A reliable characterization of the NBT-BT powders grain size distribution was not possible during the thesis, due to the small average grain size ($\leq 1 \mu\text{m}$) that hinders the SEM resolution of separated grains. However, Exxelia requires a grain size between 300 and 500nm before sintering and between 0.5 and $2\mu\text{m}$ after sintering. So the grain size of the NBT-BT powder and layer samples agree with the required values.

To meet Exxelia's specifications and to ensure that the layers could have a thickness of a minimum between 5 and 20 μm after sintering, the thickness of the tape-casted layers should be gradually decreased.

Finally, a MLCC should be synthesized with the optimized powder synthesis method, slurry composition and reactants stoichiometry, to obtain a prototype. To do that, the industrially used Ag-Pd (70 - 30) ink should be used instead of the silver paste or the Cr-Au sputtering (see section 4.2.2.2). The metallization should be done through a screening method, to guarantee that the electrodes will have a correct and homogeneous thickness and to create some electrode defects (some places without metallic ink) to allow the contact between consecutive ceramic layers and the mechanical integrity of the MLCC. The dielectric properties of this new MLCC prototype should be characterized and compared with Exxelia's specifications afterwards.

The last step of this work would be to optimize the MLCC inside Exxelia (including form and thickness of layers), to do the transition from laboratory scale to industrial scale.

Chapter 6

Conclusion

The MLCCs are the most consumed capacitor type in the world, due to their high volumetric efficiency, good reliability, and frequency features. The annual MLCCs production is more than 100 billion units and their market has grown around 20% each year since the beginning of the decade. The increase of the electronics production and its use in high-technology fields is one key factor for this accelerated growth.

Due to its importance, new requirements are constantly created to allow the miniaturization, property improvement, and reliability. In this context, the high-temperature electronics demands are growing, due to the miniaturization trend and to the new applications such as the deep oil.

However, the environmental demands are also increasing. The REACH and RoHS regulations are especially important for the MLCCs since the use of lead will be soon forbidden for non-military or aerospace applications.

It is estimated that the electronic systems should be capable of working at a maximum temperature of 300 to 350°C. Today, however, the high-temperature MLCC are limited to temperatures up to 200-250°C. *It is therefore imperative to bring out new lead-free materials capable of meeting the expectations of electronics at around 300-350°C.*

The MLCC production process in Exxelia is based on the tape casting of a ceramic slurry. The "green" ceramic tapes are screen printed with a Ag-Pd electrode and the blocks of alternating ceramic and metal layers are co-sintered between 1000 and 1300°C. Sintering is done in industrial furnaces, where the sintering atmosphere and the pressure cannot be controlled.

The compatibility with the current production methods, including the use of a tape casting, the sintering process in a furnace without controlling atmosphere, pressure or other heating sources, the compatibility with the Ag-Pd electrodes, and the price and market limitations are an important limitations.

Considering this, the objectives of this work was the study of a material that can be used for MLCCs with: an operation temperature range from 25°C to 300-350°C, an operation frequency range from 400Hz to 100MHz with a standard measurement frequency of 1kHz, a relative permittivity between 1000 and 2000 at 1kHz, a permittivity variation of $\pm 15\%$ in the operating temperature range when compared to a reference temperature within this range, a maximum loss value of $\tan \delta < 2.5\%$ at 1 kHz, an insulation resistance of 10s from 250 to 300°C and 1s from 300 to 350°C, a layer thickness between 5 to 20 μm or less, a grain size of the ceramics of 0.3 to 0.5 μm before sintering and 0.5 to 2 μm after sintering, and a dielectric strength of 25 to 60 V/ μm .

A study of the main available lead-free dielectric families was done. The choice of the final material took into account the permittivity value, the dielectric losses and the similarity between the temperature range to have $\tan \delta \leq 2.5\%$ and the desired operating temperature range, the insulation resistance at 300°C, the industrial feasibility, and the similarity of the temperature range corresponding to a variation of 15% in the permittivity at 200°C and the desired operating temperature range.

Three important families of lead-free materials were reviewed: the BaTiO₃-based materials, the K_{0.5}Na_{0.5}NbO₃-based materials and the Na_{0.5}Bi_{0.5}TiO₃-based materials.

The NBT-BT solid solution at the MPB was chosen as the base dielectric material. It presents two dielectric anomalies: the first at the depolarization temperature T_d is a frequency dependent shoulder and the second at the maximum relative permittivity temperature T_m is a permittivity maximum. These phase transitions give the NBT-BT a stable permittivity in temperature. It also shows low dielectric losses from T_d to T_m .

Moreover, the MPB with 6% BT improves the permittivity values and its variation in temperature. Finally, the NBT-BT has a double hysteresis loop between 200°C and 300°C, even though it is actually an ergodic-relaxor. This makes it interesting for energy storage applications.

The NBT-BT may also be improved thanks to some small quantity additives, such as Co and Mn, to increase the final density and to decrease the dielectric losses.

Different synthesis methods and parameters were studied, to determine the best synthesis conditions for the NBT-BT, considering Exxelia's requirements.

Initially, two syntheses of the NBT-BT powder were analyzed, the sol-gel and the solid-state synthesis. The solid-state synthesis was chosen, considering the industrial limitations and the expected properties of the final material.

Three sintering methods were then analyzed: the microwave, the SPS, and the traditional sintering. Considering again the industrial limitations and the required properties, the traditional sintering method was chosen.

Finally, three different methods for controlling atmosphere during sintering, avoiding the evaporation of volatiles were tested: the sintering in air (atmosphere not controlled), the sintering on powders of NBT or reactants + ZrO₂ and the sintering on pure ZrO₂ powder. The first method resulted in a material that is not NBT-BT and the second one needed post-sintering treatment to obtain a clean surface. So the sintering on ZrO₂ powder was chosen to control the sintering atmosphere.

The shaping of the ceramic layers was done through tape casting, since it is the only available method for Exxelia's synthesis of MLCCs.

All the samples showed a separation of secondary Ba-containing phases, due to the Na evaporation during sintering. These phases were identified as a mixture of Ba₂TiO₄, the Ba₂Ti₉O₂₀ and the Ba₂Ti₉O₂₀·2BaO·TiO₂. They concentrate at the sample's surface due to the higher Na evaporation and also because the ZrO₂ favours the formation of Ba₂Ti₉O₂₀.

The drying on the hygroscopic reactants was the first tested parameter. It intensified the effects of the ball-milling energy, creating large grain surfaces of secondary Ba-containing phases for 250 rpm and 4h ball-milling and large volume fraction of small grain surfaced secondary phases for 350 rpm and 8h ball milling.

Two ball-milling jars and balls materials were also tested. The ball milling with tungsten carbide jars resulted in a contaminated, high conductive, and dielectric lossy material. Using the yttrium stabilized zirconia jars and balls and the ZrO₂ powder to cover the sample during sintering, the final material showed some ZrO₂ contamination at the surface that could be removed with polishing.

A skin effect due to a phase coexistence (tetragonal, rhombohedral and cubic) was observed for the polished and strain-relaxed materials through low-angle-side peaks on the XRD diagrams. It is not present in the as-sintered samples, due to the lower local concentration of Ba in the NBT lattice at the surface.

Two ball-milling solvents were also tested: pure ethanol and a mixture of ethanol and methyl-ethyl-ketone (MEK). However, the change in the solvent did not affect the structure and phase separation of the NBT-BT. A similar result is found when changing the Na₂CO₃ reactant grain size.

The energy (speed and duration) of ball-milling were also investigated testing a ball-milling at 250 rpm for 4h and another at 350 rpm for 8h. The effects of the ball-milling energy were evident in the samples ball-milled without using a dispersing agent, where the increase in energy resulted in a smaller grain surface and higher volume fraction of the secondary Ba-containing phases. However, this effect is not observed in samples ball-milled with a dispersing agent, since they showed intermediary secondary Ba-containing phases average grain surface and volume fraction.

The use of a second ball-milling after calcination was also tested, to increase the density of bulk ceramic samples. The higher density for samples with no second ball-milling was 91.5% vs 93.5% for the samples prepared with a second ball-milling. It was achieved in both cases for the sintering at 1150°C for 3h. The temperature ramps used were 120°C/h for the heating and 200°C/h for the cooling, to avoid cracks during sintering.

Two ball sizes were tested for the second ball-milling: 1mm-diameter and 10mm-diameter balls. The 1mm-diameter balls were chosen, since their use increased the density without changing the micro-structure and phase separation, and without introducing oxygen vacancies.

Finally, the nominal stoichiometry changes of Na and Bi were also studied. The increase in the Bi and Na concentrations decreased the secondary Ba-containing phases volume fraction and samples without phase separation could be obtained with Na excess. The decrease in the nominal Na/Bi ratio created a matrix stoichiometric in Bi and a separation of the Bi excess in a Bi-rich phase concentrated in the sample's core.

To estimate the permittivity of the NBT-BT samples from their impedance measurement, an RC model was used. The analysis of the variation of the complex impedance in frequency showed that the resistance and the capacitance of the setup can be neglected and validated the use of the RC model.

The dielectric-property uncertainties were estimated through the measurement noise from the characterization of one sample that showed results compatible with two curves. This was considered since the dielectric-property uncertainties were evaluated as being lower than the measurement noise. So a 13% uncertainty was considered for the relative permittivity and a 14% uncertainty was considered for the dielectric losses.

A temperature shift correction was also apported, due to the method initially used to fix the wires on the bottom of the samples (silver paste on the sample surface). The correction was done after measuring a reference BaTiO₃ sample. The shift in the Curie temperature in this sample comparing the heating and the cooling measurements showed that there is no significant temperature gradient in the samples.

Finally, a new method to fix the wires on the bottom of the samples was used (Cr-Au sputtering metallization and displaced fixation over a copper plate) to estimate a 3.5% uncertainty in the temperature measurements.

After estimating uncertainties, the dielectric properties and the insulation resistance of the NBT-BT in temperature were measured. The effects of the stoichiometry, structure, phase separation, synthesis parameters, and internal strain on these properties were analyzed.

The NBT-BT properties are particularly sensitive to stoichiometry and to the Na/Bi ratio. The increase in Na content inhibits the secondary Ba-containing phases separation and decreases the relative Bi content in the main phase, increasing the sample's conductivity. The increase in the Bi content initially compensates for the oxygen vacancy formation and decreases the conductivity before forming a second phase, increasing again the conductivity at higher Bi-excess.

Considering Exxelia's requirements for the high-temperature MLCC, the stoichiometry of sample "U" is the most adapted one, due to its high insulation resistance, lower dielectric losses and permittivity variation in temperature when compared to others.

Due to the phase separation and the secondary Ba-containing phases, the final material

can be considered as a composite where the matrix phase is composed of non-stoichiometric NBT and the inclusions are composed of the secondary Ba-containing phases. However, due to the physical characteristics and the properties of the phases, no classical composite model could be applied.

The increase of the volume fraction and the average grain surface of this phase initially is beneficial to the MLCCs, since it increases the permittivity, decreases the dielectric losses, and increases the insulation resistance, due to the elimination of oxygen vacancies.

Above a critical volume fraction and grain surface, the tendency reverts, due to the conducting character of the secondary phase. So, an intermediary volume fraction (2.5 to 3.0%) and average grain surface (0.9 to $3.0\mu\text{m}^2$) of the secondary Ba-containing phases is desirable.

For this reason, the effect of multiple synthesis parameters on the secondary Ba-containing phases average grain surface and volume fraction were studied.

To obtain this intermediary average grain surface and volume fraction of secondary Ba-containing phases as well as the best dielectric and insulation properties, a dispersing agent should be used during ball milling in MEK and ethanol mixture and the reactants should not be dried before weighing. In this case, the average Na_2CO_3 grain size and the energy of ball milling do not affect significantly the final bulk properties.

Finally, the polishing and strain relaxation are an important step to have a lower ZrO_2 contamination without introducing internal strains. The thermal treatment should be done at 400°C during 3h.

Several hypothesis were considered to explain the dispersion of the dielectric properties in frequency: a composite model with a conducting phase in an insulating matrix (Maxwell-Wagner model), two parallel and frequency dependent RC circuits representing a grain core and grain boundary with different conductivity (Nyquist plot), and a relaxor behaviour (modified Curie-Weiss law).

The three frequency-dispersion models could be applied to the NBT-BT samples, even if the fits could not be done for the Maxwell-Wagner and the Nyquist plot models, due to a limited frequency range of measurement.

The Maxwell-Wagner confirmed the hypothesis that the Ba-containing phases are more conducting than the NBT-matrix phase and so, that there is an interfacial polarization.

The Nyquist plot indicated that two circuits associated with the grain cores and boundaries could be used and that the resistance associated with the grain boundaries is larger and it increases with temperature up to a critical temperature.

Finally, the modified Curie-Weiss law indicated that all the samples, except for sample "E", showed a relaxor character, with γ close to 2. Since sample "E" shows a much higher volume fraction and a much smaller average grain surface of the secondary phases, the influence of these phases and the interaction between their neighbouring grains are greater in this sample. So, the fact that this is the only sample with lower γ value indicated that the interaction between neighbouring grains of the secondary Ba-containing phases can tune the relaxor behaviour in NBT-BT.

Lastly, Co_3O_4 and MnCO_3 were added to NBT-BT, to try to improve the dielectric properties of the samples, acting as a sintering aid. However, in both cases, the conductivity was increased and the dielectric losses were either unchanged or increased. So, it is not ideal for the MLCC production.

Besides the dielectric and insulation properties, other factors were considered: the dielectric strength and the co-sintering with the electrodes.

The dielectric strength could only be measured for sample "P" and was $7.5\text{ V}/\mu\text{m}$. It should be increased for the MLCC application, but it is expected that sample "U" shows a higher value. The possibility to co-sinter with 70% Ag and 30% Pd electrodes was confirmed, since there is no chemical reaction between the Bi and the Pd and since the sintering temperature is lower than the maximum co-sintering temperature.

After analysing the dielectric properties vs temperature and frequency, some reasons for the origin of the incompatibilities in the dielectric properties NBT-BT reported in the literature were discussed. The importance of having a strict synthesis and measurement method was presented.

The literature reports differences in the relative permittivity and dielectric losses values, in their dispersion in frequency, in the hump of the relative permittivity at T_d , and in the shape of the dielectric properties vs temperature curves. To explain these differences, the influence of stoichiometry, metallization, phase separation, synthesis parameters, and polishing and strain relaxation on the material's dielectric properties were analyzed in heating and cooling.

The stoichiometry has a crucial effect on the properties of NBT-BT. The increase in the nominal Na/Bi ratio and Na quantity increases the conductivity and the quantity of free charges. This increases, the dielectric losses and the frequency dispersion. It may also change the value of the relative permittivity, and the shape of the relative permittivity and dielectric losses vs temperature curves. Finally, the increase in the nominal Na/Bi ratio makes T_d less evident in the relative permittivity curve, increases T_d and decreases T_m .

Another important difference in the measured dielectric properties of NBT-BT samples is the temperature cycle hysteresis. All the heating / cooling cycle measurements are similar, except for the first heating that shows decreased permittivity and may show increased noise. This is neither due to the synthesis method, nor to the phase separation, nor to the strain level, nor to the stoichiometry of the material. So this hysteresis should not be an intrinsic characteristics of the material.

The hypothesis that the first heating hysteresis is due to the silver paste metallization and electric wire fixing method was confirmed. Since the silver paste is commonly used in research, it also may be responsible for the literature incompatibilities.

The variability in the measured dielectric properties from sample to sample is also an important factor to explain the differences observed in the literature depending on the heating / cooling cycle considered.

Finally, a change in the dielectric losses at high temperatures after each heating and cooling cycle is observed. It is present regardless of the metallization and method to contact the electrical leads, the stoichiometry, the phase separation, the synthesis parameters, or the polishing and strain relaxation. Moreover, it is present for temperature cycles where the maximum temperature is greater than 300°C and it increases with increasing maximum temperatures. This indicates that a thermally degradation takes place at high temperatures (over 300°C).

Comparing samples with different metallization methods it was possible to conclude that changes in the electrode's morphology during heating increases the measured dielectric losses. However, it is also possible that there is a change in the sample's microstructure influenced by the high temperature.

After analysing the bulk NBT-BT samples, the synthesis of NBT-BT layers and its compatibility with Exxelia's specifications was performed.

Bulk sample "U" showed the best properties for MLCC applications. So this sample was chosen to be studied in the layer form.

For the layer synthesis, the second ball-milling was adapted and the slurry was prepared considering Exxelia's slurry composition and a binder and additives optimization for NBT-BT reported in the literature.

The "green" tapes (before sintering) showed good mechanical resistance, no cracks and a uniform thickness. However, the monolayers sintered with a 30-minute temperature step at 850°C and a sintering at 1050°C for 3h showed low relative density of 58%.

For this reason, a sintering optimization was done. The sintering parameters that resulted in the highest density of the monolayers (62%) were a sintering with a 30 minutes temperature step at 850°C and a sintering at 1150°C for 3h. This is still insufficient for the MLCC

applications, so the next step would be to study the effects of pressing the NBT-BT layers together before sintering and to increase the NBT-BT powder concentration and decrease the PVB concentration in the slurry.

Concerning the monolayers structure, a XRD peak widening was observed due to a skin effect (coexistence of pseudo-cubic, rhombohedral and tetragonal phases). The same secondary Ba-containing phases as in the bulk samples were present with an average grain size of $2.9 \pm 0.8 \mu\text{m}^2$, being compliant with Exxelia requirements. However, the morphology of this phase was different from the bulk one, due to the low density of the monolayer. Finally, a higher Zr contamination from the powder used to create a sintering atmosphere in the secondary Ba-containing phases was observed, being the reason for its lower Ba concentration.

An average grain surface of $2.4 \pm 0.8 \mu\text{m}^2$ after sintering and a layer thickness of $97 \mu\text{m}$ were obtained for the monolayer. These values are not compatible with Exxelia's specifications, but they could still be used for the MLCC production.

The dielectric properties measured for the monolayer are not reliable, due to their low density. However, for the synthesized monolayer, the measured relative permittivity is smaller and the dielectric losses for temperatures greater than 150°C are higher than the bulk. This is expected for low-density materials. Moreover, a huge temperature hysteresis is observed when measuring it over consecutive thermal cycles, making the measurement impossible at temperatures higher than 275°C .

This hysteresis and thermal degradation may be due to the influence of the electrodes, since there is a penetration of the silver paste in the material pores during thermal cycling. However, it may also be due to the material morphology change in temperature, since the low density and the high specific area of the layer facilitates the material morphology changes.

Finally, the insulation resistance for the monolayers are much lower than for the bulk, corresponding to a temperature decrease of 100°C , as expected for low density materials.

These properties are not yet compatible with Exxelia's requirements for the MLCC production. Nevertheless, dielectric losses are lower than 2.5% at 1kHz from 100 to 150°C , permittivity variation of $\pm 15\%$ takes place from 180 to 240°C and insulation resistance is only higher than 1s up to 180°C .

So, to make a more reliable evaluation of the NBT-BT layers and to achieve the requirements for the MLCC production, the increase in density is imperative.

To solve this density problem, the effects of pressing multiple "green" NBT-BT layers together before sintering, forming a multilayer device, was studied. It was shown that a high density material (89.5%) can be obtained after sintering the pressed multilayers at 1150°C . This indicates that the low density of the monolayers are not due to a slurry composition problem and that, even though the monolayers do not show dielectric properties compatible with the industrial demands from room temperature up to 300 to 350°C , this does not necessarily mean that the multilayer device prepared from these layers will have the same temperature range limitation. However, since the pressed NBT-BT multilayers show a higher Na and Bi evaporation, a new dielectric properties measurement in temperature should be done to evaluate the temperature range of compatibility with the industrial requirements.

Appendices

Appendix A

Extract of patent number 17 58575 publication number 3071244

The following extract shows the patent published by Exxelia Technologies and it concerns the material studied in this thesis for the MLCC application.

The complete document can be found in:

<https://bases-brevets.inpi.fr/fr/document/FR3071244.html?s=1568633240025p=5cHash=8ba b94d228065aa6087dd0d15cc42d56>

①9 RÉPUBLIQUE FRANÇAISE
INSTITUT NATIONAL
DE LA PROPRIÉTÉ INDUSTRIELLE
COURBEVOIE

①1 N° de publication : **3 071 244**
(à n'utiliser que pour les
commandes de reproduction)

②1 N° d'enregistrement national : **17 58575**

⑤1 Int Cl⁸ : **C 04 B 35/468** (2018.01), C 04 B 35/475, 35/622

①2 **DEMANDE DE BREVET D'INVENTION** **A1**

②2 Date de dépôt : 15.09.17.

③0 Priorité :

④3 Date de mise à la disposition du public de la demande : 22.03.19 Bulletin 19/12.

⑤6 Liste des documents cités dans le rapport de recherche préliminaire : *Se reporter à la fin du présent fascicule*

⑥0 Références à d'autres documents nationaux apparentés :

Demande(s) d'extension :

⑦1 Demandeur(s) : **EXXELIA TECHNOLOGIES** Société par actions simplifiée — FR.

⑦2 Inventeur(s) : MUSSI TOSCHI VITORIA et LAVILLE HENRI.

⑦3 Titulaire(s) : **EXXELIA TECHNOLOGIES** Société par actions simplifiée.

⑦4 Mandataire(s) : LAVOIX.

⑤4 **MATERIAU DIELECTRIQUE.**

⑤7 La présente invention concerne un matériau du type $(\text{Na}_{>0.5}\text{Bi}_{>0.5}\text{TiO}_{>3})_{>(1-x)} - (\text{BaTiO}_{>3})_{>x}$, dit « NBT-BT », où x est supérieur à 0 et va jusqu'à 0,08, ledit matériau comprenant un cœur et une surface, le cœur comprenant une proportion atomique moyenne des éléments présents suivants par rapport à la composition totale du matériau :

- Sodium: moins de 10 %, de préférence de 6 à 8 %;
- Bismuth: de 5 à 10 %, de préférence de 8 à 10%;
- Baryum: moins de 1 %, de préférence de 0,05 à 0,2 %;
- Titane: de 15 à 25 %, de préférence de 16 à 19 %.

La présente invention concerne également un procédé de préparation d'un tel matériau et ses applications en particulier comme matériau diélectrique.

FR 3 071 244 - A1



Matériau diélectrique

L'invention concerne un matériau, en particulier pour des applications diélectriques, comprenant du Sodium, du Bismuth, du Baryum et du Titane. Plus particulièrement, l'invention concerne des matériaux du type $\text{Na}_{0.5}\text{Bi}_{0.5}\text{TiO}_3 - \text{BaTiO}_3$, dit « NBT-BT », leur procédé de fabrication et leurs applications en électronique.

État de la technique

On connaît déjà des matériaux du type NBT-BT dans la littérature comme par exemple décrit dans la publication F. Craciun et al., 2012 (Electric-field-induced and spontaneous relaxor-ferroelectric phase transitions in $(\text{Na}_{1/2}\text{Bi}_{1/2})_{1-x}\text{Ba}_x\text{TiO}_3$, Journal of Applied Physics 112, 124106 (2012); doi: 10.1063/1.4770326). Cependant ces matériaux demandent à être optimisés notamment du point de vue de la composition afin d'améliorer leurs applications à titre de matériau diélectrique, notamment en termes de permittivité et de pertes diélectrique en particulier à température d'utilisation, typiquement entre 120 et 300 °C.

On connaît également le brevet US 8,976,257 concernant des céramiques diélectriques haute température. De telles céramiques sont composées du mélange d'un composé du type $\text{Me}_x(\text{Na}_{0.5}\text{Bi}_{0.5})_{(1-x)}\text{TiO}_3$ où Me représente Ba ou Sr avec un oxyde d'un cation faiblement donneur comprenant un oxyde de Nb^{5+} , Ta^{5+} ou W^{6+} , d'un oxyde d'un cation accepteur, d'un cation largement donneur comme Nd_2O_3 et d'un composé formant un verre choisi parmi SiO_2 , B_2O_3 , GeO_2 et V_2O_5 . Un tel mélange nécessite un procédé particulier de préparation mais surtout nécessite le mélange du composé de type NBT (comprenant les atomes Na, Bi et Ti) avec différents précurseurs pour arriver à la composition souhaitée, ce que l'on souhaite éviter pour obtenir ce type de matériaux sans qu'il se dégrade rapidement en fonctionnement (dégradation des performances générant moins d'isolement).

Buts de l'invention

L'invention a pour but de fournir un matériau, en particulier pour des applications diélectriques, comprenant du Sodium, du Bismuth, du Baryum et du Titane.

L'invention a en particulier pour but de résoudre le problème technique consistant à améliorer la performance diélectrique d'un matériau à base de Sodium, Bismuth et Titane, connu sous la dénomination « NBT ».

L'invention a également pour but de résoudre le problème technique consistant à fournir un procédé simple de préparation d'un matériau diélectrique comprenant du Sodium, du Bismuth, du Baryum et du Titane.

5 L'invention a également pour but de résoudre le problème technique consistant à fournir un matériau diélectrique présentant une composition chimique plus simple que le composé du type $Me_x(Na_{0,5}Bi_{0,5})_{(1-x)}TiO_3$ décrit dans le brevet US 8,976,257.

10 L'invention a également pour but de résoudre le problème technique consistant à fournir un matériau diélectrique présentant une bonne permittivité et de faibles pertes diélectrique, de préférence inférieures à 8 % et encore de préférence inférieures à 4 % et encore de préférence inférieures à 2 %, en particulier à température d'utilisation, typiquement entre 120 et 300 °C.

15 L'invention a également pour but de résoudre le problème technique consistant à fournir un matériau diélectrique ne présentant pas de dégradation significative de ses performances, de préférence après au moins 1000 heures de fonctionnement à haute température et présentant donc ainsi un fonctionnement amélioré en particulier vis-à-vis de matériaux du type NBT ou NBT-BT tel que décrit dans l'art antérieur ci-dessus..

Description de l'invention

20 L'invention concerne un nouveau matériau de type $(Na_{0,5}Bi_{0,5}TiO_3)_{(1-x)} - (BaTiO_3)_x$, dit « NBT-BT », où x est supérieur à 0 et va jusqu'à 0,08.

25 Avantageusement, l'invention permet de fournir une composition présentant une faible teneur en Baryum. En particulier, l'invention concerne un matériau du type $(Na_{0,5}Bi_{0,5}TiO_3)_{(1-x)} - (BaTiO_3)_x$, dit « NBT-BT », où x est supérieur à 0 et va jusqu'à 0,08, ledit matériau comprenant un cœur et une surface, ledit matériau comprenant dans le cœur une proportion atomique moyenne des éléments présents suivants par rapport à la composition totale du matériau :

30 Sodium : moins de 10 %, de préférence de 6 à 8 % ;
 Bismuth : de 5 à 10 %, de préférence de 8 à 10% ;
 Baryum : moins de 1 %, de préférence de 0,05 à 0,2 % ;
 Titane : de 15 à 25 %, de préférence de 16 à 19 %.

Les éléments sont « présents » au sens où ils sont en quantité détectable et non uniquement sous forme de traces apportées par exemple par les impuretés résiduelles des matières premières utilisées.

Les matériaux de ce type connus dans l'art antérieur souffrent de l'évaporation en particulier du Bismuth et du Sodium lors de leur préparation. L'invention permet de résoudre ce problème technique par la fourniture d'un nouveau procédé de préparation de ce type de matériaux.

5 L'invention concerne en particulier un procédé de préparation d'un matériau du type $(\text{Na}_{0.5}\text{Bi}_{0.5}\text{TiO}_3)_{(1-x)} - (\text{BaTiO}_3)_x$, dit « NBT-BT », où x est supérieur à 0 et va jusqu'à 0,08, et de préférence tel que défini selon l'invention, le procédé comprenant la calcination du matériau en présence d'une atmosphère confinée comprenant du Bismuth et du Sodium.

10 Les matériaux selon l'invention forment des matériaux céramiques.

Selon un mode de réalisation, le procédé de préparation du matériau selon l'invention comprend le mélange de poudres d'oxyde de bismuth, d'oxyde de titane, de carbonate de sodium et de carbonate de baryum. Alternativement, on peut réaliser le mélange de poudres pré-préparées de NBT (Sodium, Bismuth et Titane) et BT (Baryum et
15 Titane). On préfère partir d'un mélange d'oxydes et de carbonates sans réaction ou mélange préalable des poudres entre elles.

Le procédé selon l'invention comprend selon un mode de réalisation préféré le broyage du mélange, par exemple en utilisant un broyeur planétaire avec des billes présentant un premier diamètre. Par exemple, le premier diamètre des billes est compris
20 entre 5 et 20 mm. Un premier diamètre peut être par exemple de 10 mm. On peut par exemple utiliser un rapport massique de masse de billes sur la masse de poudre de 5 à 15, et de préférence de 10. Typiquement, le broyage est réalisé en présence d'un solvant, par exemple un alcool comme par exemple l'éthanol. Typiquement, le broyage est réalisé dans un broyeur planétaire avec une vitesse de rotation de 200 à 400 tours/minute, et par
25 exemple de 250 tours/minute. La période effective de broyage est en général comprise entre 2 et 8 heures, et par exemple est de 4 heures. Avantagement, on peut réaliser des rotations alternées par brèves périodes, par exemple de quelques minutes et en général inférieures à 10 minutes. Cette durée n'est pas comptabilisée dans la période de broyage. On peut réaliser par exemple un temps de pause entre chaque variation de
30 rotation pour limiter l'échauffement de mélange de poudre.

Le procédé selon l'invention comprend, selon un mode de réalisation avantageux, un séchage de la poudre de préférence broyée. Le séchage peut se réaliser par exemple sous étuves à une température typiquement de 70 à 100 °C. On peut par exemple utiliser une température de 80 °C.

Le procédé selon l'invention comprend avantageusement la calcination de la poudre séchée, de préférence broyée. Selon un mode de réalisation, on préfère désagglomérer la poudre séchée avant calcination. Le séchage permet par exemple d'éliminer le solvant utilisé pendant le broyage.

5 La calcination a en général lieu à une température comprise entre 800 et 1000 °C, pendant un temps suffisant pour réaliser la calcination souhaitée. On peut par exemple utiliser une température de calcination de 900 °C. En général, le temps de calcination est compris entre 1 et 5 heures, et peut être par exemple de 2 heures. On utilise
10 avantageusement une pente de chauffage pour limiter la rapidité de la montée en température et ainsi limiter les contraintes à l'intérieur du matériau. Une pente de chauffage peut être comprise entre 100 °C/heure et 250 °C/heure. On utilise de préférence par exemple une température inférieure à 200 °C/heure, comme par exemple 180 °C/heure. De la même manière, on peut utiliser avantageusement une pente de refroidissement limitant la vitesse de descente en température pour limiter les contraintes
15 à l'intérieur du matériau. Cependant, le refroidissement peut être plus rapide que le chauffage. On peut ainsi par exemple utiliser une pente de refroidissement comprise entre 100 °C/heure et 400 °C/heure. On utilise par exemple une pente de 300 °C/heure. Le temps total de l'étape calcination est compris par exemple entre 5 et 48 heures, et par exemple typiquement d'environ 10 heures en comptant la rampe de chauffage, le
20 maintien à la température de calcination puis la rampe de refroidissement. Le chauffage du matériau se réalise en général à partir de la température ambiante. Le refroidissement s'effectue en général jusqu'à la température ambiante.

Avantageusement, pour limiter, voire éviter l'évaporation de certains composés volatiles pendant la calcination, on utilise une atmosphère comprenant de Bismuth et du
25 Sodium. Cette atmosphère est en contact avec le matériau pendant la calcination. Selon un mode de réalisation l'atmosphère est avantageusement générée par une poudre qui s'évapore lors de la calcination. La poudre ne doit pas être directement en contact avec la poudre précurseur du matériau selon l'invention pour qu'il n'y ait pas de diffusion de solution solide entre ces poudres. On peut par exemple placer la poudre précurseur du
30 matériau selon l'invention dans un creuset, par exemple un creuset d'alumine. La poudre générant l'atmosphère peut être avantageusement déposée autour du creuset comprenant la poudre précurseur du matériau de l'invention. Typiquement on dépose plutôt en premier la poudre générant l'atmosphère puis le creuset sur la poudre ou dans un emplacement déterminé de préférence de manière à ce que la poudre entoure le
35 creuset.

Selon un mode de réalisation, l'atmosphère en contact avec le matériau pendant la calcination comprend un mélange d'oxyde de zirconium, d'oxyde de bismuth et de carbonate de sodium. On peut par exemple utiliser un mélange de 40 à 60 % en masse d'oxyde de zirconium et de 20 à 30 % en masse d'oxyde de bismuth et 20 à 30 % en masse de carbonate de sodium. Typiquement, on peut par exemple utiliser un mélange de 50 % d'oxyde de zirconium, de 25 % d'oxyde de bismuth et 25 % de carbonate de sodium, les pourcentages étant exprimés en masse par rapport à la masse totale de la poudre générant l'atmosphère.

Afin de conserver l'atmosphère spécifique précitée lors de la calcination, on préfère que l'ensemble comprenant la poudre générant l'atmosphère et le creuset comprenant la poudre précurseur du matériau de l'invention soit placé dans un récipient fermé, par exemple un creuset en alumine fermé. Selon un mode de réalisation, on peut fermer par un couvercle les deux creusets.

L'atmosphère de calcination est ainsi spécifique à l'invention et permet de maintenir les éléments Bismuth et Sodium de manière particulièrement avantageuse dans la composition du matériau de l'invention est ainsi en améliorer les propriétés diélectriques.

Après calcination, on peut en général broyer à nouveau la poudre pour la désagglomérer. On peut par exemple utiliser un pilon.

Le procédé selon l'invention comprend selon un mode de réalisation préféré un broyage de la poudre après calcination, selon des conditions de préférence similaires ou identiques à celles du premier broyage avant calcination, si cette étape est réalisée (ce qui est préféré). Par exemple, on utilise un broyeur planétaire avec des billes d'un deuxième diamètre. Le deuxième diamètre est avantageusement inférieur au premier diamètre. Le deuxième diamètre est en général compris entre 0,1 mm et 5 mm, et de préférence est par exemple de 1 mm.

Après broyage, on sépare les billes de la poudre par exemple sur un tamis. On peut par exemple utiliser un alcool comme par exemple l'éthanol lors de la séparation.

Le séchage de la poudre broyée est de préférence réalisé dans des conditions similaires ou identiques au séchage avant calcination. On cherche à obtenir une poudre sèche.

Le procédé selon l'invention comprend donc avantageusement après la calcination, et de préférence après le broyage/séchage de la poudre après calcination, une mise en forme puis un frittage.

Selon le mode de réalisation préférée, on utilise un liant pour la mise en forme de la poudre. Selon une variante avantageuse, le procédé comprend la mise en forme de poudre calcinée avant frittage, de préférence en présence d'un liant, par exemple le PVA.

5 Comme exemples de liants, on peut citer les résines thermodurcissables en particulier choisies parmi les résines époxyde, silicone, polyimide, polyester ou phénolique, les alcools polyvinyliques (PVA), les résines acryliques, comme par exemple les méthacrylates de méthyle, en particulier des polyméthacrylates de méthyle (PMMA), et des polyéthylènes glycols (PEG), en particulier à basse densité. Selon une variante on peut par exemple utiliser l'alcool polyvinylique (PVA) comme liant. Selon un mode de
10 réalisation, on utilise une proportion massique de liant de 5 à 15 %, et par exemple de 8 %, en masse par rapport à la masse totale du matériau mis en forme. Avantageusement, la présence d'un liant permet d'éviter les fissures dans le matériau mis en forme. En général, on mélange la poudre et le liant de manière à obtenir un mélange homogène. Selon un mode de réalisation, le mélange poudre/liant est séché avant mise en forme. On
15 peut par exemple réaliser un séchage sous air. La mise en forme peut être par exemple effectuée par densification de la poudre selon les techniques connues par l'homme du métier. On peut par exemple utiliser une presse hydraulique pour mettre en forme la poudre. On peut ainsi par exemple produire des disques de quelques millimètres de diamètre, typiquement de 5 à 10 mm de diamètre.

20 Avantageusement avant frittage, selon un mode de réalisation préféré, on recouvre la poudre mise en forme par une poudre d'oxyde de zirconium. Cette opération a pour avantage de diminuer l'évaporation des composés volatiles pendant le frittage. Avantageusement la poudre d'oxyde de zirconium recouvre la totalité de la surface du matériau mis en forme. En général, la poudre d'oxyde de zirconium est traitée
25 thermiquement, selon une méthode connue de l'art antérieur.

Le procédé selon l'invention comprend avantageusement le frittage de la poudre mise en forme. Selon une variante, le frittage est réalisé à une température comprise entre 1000 et 1300 °C, de préférence en présence d'une poudre d'oxyde de zirconium.

30 On préfère réaliser le frittage à une température de frittage allant de 1000 à 1200°C, et de préférence de 1050 °C à 1200°C. On préfère une température de frittage de 1050 °C, notamment pour améliorer les caractéristiques cristallographiques et diélectriques du matériau ou de 1150 °C pour améliorer sa densité. Le choix de la température finale de frittage optimise les propriétés électriques du matériau de l'invention. Le frittage comprend typiquement un maintien à la température de frittage
35 pendant une durée suffisante pour obtenir un matériau céramique. Ce maintien est en

général réalisé par un palier à la température de frittage. La durée du palier (durée de frittage) est par exemple de 1 à 10 heures, et par exemple de 3 heures.

5 Selon un mode de réalisation, le frittage comprend une élévation de la température à une vitesse de 80 à 200 °C/heure, et par exemple de 100 à 150 °C/heure. On peut par exemple utiliser une rampe de chauffage de 120 °C/heure.

Selon un mode de réalisation, le frittage comprend une diminution de la température à partir de la température de frittage avec une rampe de refroidissement de 80 à 400 °C/heure, et par exemple de 100 à 300 °C/heure. On peut par exemple utiliser une rampe de refroidissement de 200 °C/heure.

10 Selon un mode de réalisation, on réalise lors du chauffage un palier à une température comprise entre 700 et 900 °C, et de préférence de 800 °C. Ce palier a pour but de garantir le brûlage du liant éventuellement présent. Sa durée est donc suffisante pour permettre ce brûlage.

15 Selon un mode de réalisation, le procédé selon l'invention comprend avantageusement un polissage du matériau fritté. Le polissage peut être réalisé par exemple avec du papier de verre. Le polissage permet de limiter la rugosité de la surface.

20 Selon un mode de réalisation, le procédé selon l'invention comprend avantageusement, par exemple après le polissage précité, un traitement thermique de relaxation. Ce traitement thermique a pour but de limiter les contraintes internes du matériau et donc d'enlever les tensions en particulier générées lors du procédé de fabrication. Un tel traitement thermique de relaxation enlève ou limite en général au moins les tensions de surface. Selon un mode de réalisation, le traitement thermique de relaxation comprend un maintien à une température de 300 à 800 °C. Avantagement, on préfère que la température ne dépasse pas 500 °C, en particulier pour limiter la possible évaporation de Bismuth. Selon une variante, le traitement thermique de relaxation des contraintes est réalisé à une température comprise entre 300 et 800 °C.

30 Selon un mode de réalisation préféré, la température de traitement thermique de relaxation est de 400 °C. On peut réaliser une montée en température avec une rampe de chauffage et un refroidissement avec une rampe de refroidissement. Typiquement, selon un mode de réalisation, les rampes de chauffage et de refroidissement, identiques ou différentes, sont comprises entre 100 et 300 °C/h, et par exemple de 200 °C/h.

Ainsi, selon un mode de réalisation, un procédé selon l'invention peut être le suivant :

35 (i) un broyage de poudre d'oxyde de bismuth, d'oxyde de titane, de carbonate de baryum et de carbonate de sodium ;

(ii) un séchage de la poudre broyée ;

(iii) un calcination de la poudre séchée en présence d'une atmosphère confinée comprenant un mélange d'oxydes de zirconium, d'oxyde de bismuth et de carbonate de sodium;

5 (iv) éventuellement un broyage de la poudre calcinée ;

(v) un frittage de la poudre calcinée, éventuellement broyée, pour former une poudre frittée,

(vi) densification de la poudre frittée pour former une poudre densifiée,

(vi) éventuellement un polissage de la poudre densifiée ;

10 (vii) un traitement thermique de relaxation des contraintes de la poudre densifiée éventuellement polie.

L'invention concerne en particulier un matériau selon l'invention, et ses applications comme matériau diélectrique.

15 L'invention concerne un matériau NBT-BT à frontière de phase morphotropique (MPB pour « morphotropic phase boundary » en anglais) entre la phase alpha et beta.

L'invention concerne également un matériau du type $(\text{Na}_{0.5}\text{Bi}_{0.5}\text{TiO}_3)_{(1-x)} - (\text{BaTiO}_3)_x$, dit « NBT-BT », où x est supérieur à 0 et va jusqu'à 0,08, ledit matériau comprenant une phase formant une matrice et une phase formant des aiguilles, et de préférence comprend un cœur et une surface avec dans le cœur de préférence une proportion atomique moyenne des éléments présents suivants par rapport à la composition totale du matériau :

Sodium : moins de 10 %, de préférence de 6 à 8 % ;

Bismuth : de 5 à 10 %, de préférence de 8 à 10% ;

25 Baryum : moins de 1 %, de préférence de 0,05 à 0,2 % ;

Titane : de 15 à 25 %, de préférence de 16 à 19 %.

La phase formant des aiguilles est caractérisée par des dimensions de la forme d'une aiguille avec une longueur supérieure, et de préférence au moins deux fois supérieure, et encore de préférence au moins trois fois supérieure, à sa largeur et à son épaisseur. Selon un mode de réalisation, le matériau selon l'invention présente deux phases distinctes, à savoir une matrice et une phase formant des aiguilles, et en particulier des aiguilles dispersées dans la matrice, en général à la fois en surface et dans le cœur du matériau. Un matériau selon l'invention peut comprendre également d'autres phases, en général minoritaires, comme notamment des phases avec de faibles concentrations de Bismuth et/ou Sodium.

30

35

Selon un mode de réalisation, le matériau présente une densité, exprimée en pourcents, d'au moins 80 %, de préférence supérieure à 90 %. La densité est mesurée en faisant le rapport de la masse (pesée) et du volume (mesures dimensionnelles).

5 On peut également constater la présence d'oxyde de titane et d'autres phases contenant du baryum et/ou du titane.

Selon une variante, l'invention concerne un matériau poli.

Selon une variante l'invention concerne un matériau broyé au moins une fois et de préférence broyé deux fois, de préférence avant et après calcination.

10 Selon une variante, le matériau selon l'invention présente en surface une proportion atomique moyenne des éléments suivants présents par rapport à la composition totale du matériau :

Sodium : moins de 3 %, de préférence de 0,5 à 5 % ;

Bismuth : de 5 à 10 %, de préférence de 6 à 10 % ;

Baryum : moins de 5 %, de préférence de 0,5 à 3 % ;

15 Titane : de 15 à 25 %, de préférence de 16 à 19 %.

Selon une variante, le matériau selon l'invention présente une matrice du cœur présentant une proportion atomique moyenne des éléments suivants présents par rapport à la composition totale du matériau :

Sodium : moins de 10 %, de préférence de 6 à 8 % ;

20 Bismuth : de 5 à 10 %, de préférence de 8 à 10 % ;

Baryum : moins de 1 %, de préférence de 0,05 à 0,2 % ;

Titane : de 15 à 25 %, de préférence de 16 à 19 %.

25 Selon une variante, le matériau selon l'invention présente en matrice de la surface présentant une proportion atomique moyenne des éléments suivants présents par rapport à la composition totale du matériau :

Sodium : de 1 à 7 %, de préférence de 3 à 5 % ;

Bismuth : de 5 à 10 %, de préférence de 6 à 9 % ;

Baryum : moins de 1 %, de préférence de 0,05 à 0,2 % ;

30 Titane : de 15 à 25 %, de préférence de 20 à 23 %.

Selon une variante, le matériau selon l'invention présente des aiguilles de surface présentant une proportion atomique moyenne des éléments suivants présents par rapport à la composition totale du matériau :

35 Sodium : moins de 1 %, de préférence de 0,01 à 0,5 % ;

Bismuth : moins de 1 %, de préférence de 0,1 à 0,5 % ;

Baryum : de 1 à 9 %, de préférence de 3 à 6 % ;

Titane : de 20 à 40%, de préférence de 25 à 35 %.

5 Typiquement, le cœur du matériau de l'invention présente une phase rhomboédrique, par exemple de type R3c, riche en Bismuth et Sodium et une phase tétragonale, par exemple de type P4bm ou P4mm, riche en Baryum et Titane.

10 Selon un mode de réalisation, le matériau de l'invention comprend 75 à 90 % d'oxyde de titane (TiO_2) dans la phase formant les aiguilles. Selon une variante, la phase formant les aiguilles peut présenter de 70 à 90 % d'oxyde de titane, 15 à 20 % de phase BT (Baryum et Titane) et 1 à 5 % de phase NBT (Sodium, Bismuth et Titane). Selon une variante, la phase formant les aiguilles peut présenter une phase $\text{BaTi}_5\text{O}_{11}$ et une phase NBT.

15 Selon une variante, les aiguilles présentent une longueur de 20 à 150 μm , par exemple de 30 à 100 μm pour les aiguilles en surface et de 2 à 50 μm , par exemple de 7 à 30 μm pour les aiguilles dans le cœur (mesuré par un microscope électronique à balayage (MEB)).

20 Selon un mode de réalisation, le matériau de l'invention comprend dans la matrice 95,0 à 99,9 %, par exemple environ 99,2 %, de phase NBT (Na, Bi, Ti) et 5,0 % à 0,1 %, par exemple 0,8 %, de phase BT (Ba, Ti).

Ainsi, selon une variante, le matériau selon l'invention présente un cœur et une surface biphasés.

25 Le matériau selon l'invention est particulièrement intéressant pour des applications à titre de matériau diélectrique, et en particulier pour des applications dans des dispositifs électroniques à composant(s) électronique(s).

30 Avantageusement, le matériau selon l'invention présente une permittivité supérieure à 2400 à une température comprise entre 120 °C et 350 °C, à une fréquence variant de 1 kHz à 1 MHz, et de préférence une permittivité supérieure à 2800 à une température de 180 °C. Avantageusement, le matériau selon l'invention présente une permittivité supérieure à 3000 à une température comprise entre 200 °C et 300 °C, à une fréquence variant de 1 kHz à 1 MHz. Avantageusement, un matériau selon l'invention présente une permittivité supérieure à 3200 et encore de préférence supérieure à 3400 à une température de 280 °C, à une fréquence variant de 1 kHz à 1 MHz.

35 Avantageusement, le matériau selon l'invention présente une perte diélectrique inférieure à 8 % à une température comprise entre 120° et 240°C, et de préférence une

perte diélectrique inférieure à 6 % une température comprise entre 140 et 220 °C, et encore de préférence une perte diélectrique inférieure à 2 % à une température de 180 °C, mesurée à une fréquence de 10 kHz à 1 MHz. Avantageusement, le matériau selon l'invention présente une perte diélectrique inférieure à 2 % à une température de 180 à 200 °C, mesurée à une fréquence de 10 kHz à 1 MHz.

Selon une variante, le matériau selon l'invention présente un maximum local des pertes diélectriques à une température comprise entre 80 à 120°C, voire entre 90 et 110 °C.

L'invention concerne également un dispositif diélectrique comprenant ou constitué d'un matériau selon l'invention, ou susceptible d'être obtenu par un procédé selon l'invention.

L'invention concerne également l'utilisation du matériau selon l'invention, ou susceptible d'être obtenu par un procédé selon l'invention comme matériau diélectrique susceptible de fonctionner à une température supérieure à 100°C, et de préférence à une température comprise entre 120 et 300 °C.

L'invention concerne également un dispositif électronique comprenant un dispositif diélectrique selon l'invention utilisant un courant électrique et ledit dispositif diélectrique étant susceptible de fonctionner à une température supérieure à 100°C, et de préférence à une température comprise entre 120 et 300 °C.

Les termes « selon l'invention » désignent tout mode de réalisation, variante, caractéristique préférée et/ou avantageuse, aspect de la présente invention, y compris selon l'une quelconque de leurs combinaisons.

Sur les figures :

Figure 1 représente la densité mesurée en fonction de la température de frittage pour le NBT-BT préparé selon l'exemple 1, non rebroyé ;

Figure 2 représente la densité mesurée en fonction de la température de frittage pour le NBT-BT préparé selon l'exemple 1, rebroyé avec des petites billes ;

Figure 3 représente une image de la surface de la pastille de NBT-BT rebroyée avec des petites billes et frittée à 1150°C selon l'exemple 1, obtenue à l'aide d'un MEB. L'image est faite par électrons rétrodiffusés (agrandissement de 500x) ;

Figure 4 représente la permittivité en fonction de la température pour la pastille de NBT-BT rebroyé avec des petites billes, frittée à 1050°C, poli et décontrainte (ayant subi un traitement thermique de relaxation) selon l'exemple 1 ;

Appendix B

Résumé de thèse

Les MLCCs (condensateurs céramiques multicouches) sont le type de condensateur le plus consommé au monde, en raison de leur haute efficacité volumique, leur bonne fiabilité et leurs caractéristiques en fréquence. La production annuelle des MLCC s'élève à plus de 100 milliards d'unités et leur part sur le marché a augmenté d'environ 20% chaque année depuis le début de la décennie.

L'importance prise par les MLCCs implique que de nouvelles exigences soient constamment créées pour permettre la miniaturisation et l'amélioration de leurs propriétés. Dans ce contexte, les exigences en matière d'électronique haute température augmentent en raison de la tendance à la miniaturisation et également avec l'apparition de nouvelles applications telles que la perforation pétrolière profonde.

Cependant, les exigences environnementales augmentent aussi. Les réglementations REACH et RoHS sont particulièrement importantes pour les MLCCs car l'utilisation du plomb sera bientôt interdite pour des applications non militaires ou aérospatiales. On estime que les systèmes électroniques devraient être capables de fonctionner à une température maximale de 300 à 350°C. Cependant, les MLCCs sont aujourd'hui limités à des températures allant jusqu'à 200-250°C. Il est donc impératif d'utiliser de nouveaux matériaux sans plomb capables de répondre aux attentes de l'électronique à environ 300-350°C.

Le processus de production des MLCCs chez Exxelia est basé sur le coulage en bande d'une suspension céramique (barbotine). Les feuilles céramiques "vertes" (non frittées) sont sérigraphiées avec une électrode d'Ag-Pd et les blocs de couches alternées de céramique et de métal sont co-frittés entre 1000 et 1300°C. Le frittage est effectué dans des fours industriels où l'atmosphère de frittage et la pression ne peuvent être contrôlées.

La compatibilité avec les méthodes de production actuelles, y compris l'utilisation du coulage en bande, le processus de frittage dans un four sans contrôle de l'atmosphère, de la pression ou d'autres sources de chauffage, la compatibilité avec les électrodes d'Ag-Pd et les limites de prix et de marché constituent des limites importantes.

Par conséquent, les objectifs de ce travail sont d'étudier un matériau sans plomb qui pourra être utilisé pour les MLCCs avec les caractéristiques suivantes : une plage de température de fonctionnement de 25°C à 300-350°C, une plage de fréquence de fonctionnement de 400Hz à 100MHz avec une fréquence de mesure standard de 1kHz, une permittivité relative entre 1000 et 2000 à 1kHz, une variation de permittivité de 15. Trois familles importantes de matériaux sans plomb ont été examinées : les matériaux à base de BaTiO₃, les matériaux à base de K_{0,5}Na_{0,5}NbO₃ et les matériaux à base de Na_{0,5}Bi_{0,5}TiO₃. Le choix du matériau final a pris en compte : la valeur de permittivité, les pertes diélectriques et la similitude entre la plage de température pour avoir $\tan \delta \leq 2.5$. La solution solide NBT-BT à la frontière morphotropique de phase (MPB) a été choisie comme matériau de base. Il présente deux anomalies diélectriques : la première, à la température de dépolarisation T_d, est un épaulement dépendant de la fréquence, et la seconde, à la température T_m, est un maximum de permittivité. Ces transitions de phase confèrent au NBT-BT une permittivité stable en température. Il montre également des faibles pertes diélectriques de T_d à T_m. De plus, la MPB à

6% BT améliore les valeurs de permittivité et sa variation en température. Enfin, le NBT-BT a un double cycle d'hystérésis entre 200°C et 300°C, bien que ce soit un relaxeur ergodique. Cela le rend intéressant pour les applications de stockage d'énergie.

Différentes méthodes et paramètres de synthèse ont été étudiés, pour déterminer les meilleures conditions de synthèse pour le NBT-BT, compte tenu des exigences d'Exxelia. Dans un premier temps, deux méthodes de synthèse de la poudre de NBT-BT ont été analysées, la synthèse via sol-gel et la synthèse à l'état solide. La synthèse à l'état solide a été choisie en tenant compte des limites industrielles et des propriétés attendues du matériau final. Trois méthodes de frittage ont ensuite été analysées : le micro-ondes, le SPS et le frittage traditionnel. Compte-tenu encore une fois des limites industrielles et des propriétés requises, la méthode de frittage traditionnelle a été choisie. Enfin, trois méthodes différentes pour contrôler l'évaporation de volatiles pendant le frittage ont été testées : le frittage sous l'air (atmosphère non contrôlée), le frittage sous poudre de NBT ou réactifs + ZrO₂ et le frittage sous poudre de ZrO₂ pure. La première méthode a permis d'obtenir un matériau qui n'est pas du NBT-BT et la seconde a nécessité un traitement post-frittage pour obtenir une surface propre. Donc, le frittage sous poudre de ZrO₂ a été choisi pour contrôler l'évaporation de volatiles pendant le frittage. La mise en forme des couches céramiques a été faite par coulage en bande, car c'est la seule méthode disponible chez Exxelia.

Tous les échantillons ont montré une séparation de phase et la formation de phases secondaires contenant du Ba, due à l'évaporation du Na lors du frittage. Ces phases ont été identifiées comme un mélange de Ba₂TiO₄ et Ba₂Ti₉O₂₀. Elles se concentrent à la surface des échantillons en raison de l'évaporation plus élevée de Na et aussi parce que le ZrO₂ favorise la formation de Ba₂Ti₉O₂₀.

Le séchage des réactifs hygroscopiques a été le premier paramètre de synthèse étudié. Il a intensifié les effets de l'énergie de broyage, en créant une grande surface moyenne de grain des phases secondaires pour le broyage à 250 rpm pendant 4h et une grande fraction volumique de petits grains des phases secondaires pour un broyage à 350 rpm pendant 8h.

Deux matériaux des jarres et des billes de broyage ont également été testés. Le broyage avec la jarre et les billes en carbure de tungstène a entraîné la formation d'un matériau contaminé, hautement conducteur et avec des pertes diélectriques élevées. En utilisant la jarre et les billes de zircone stabilisées à l'yttrium (YSZ), le matériau final a montré des bonnes propriétés diélectriques et une petite contamination par Zr à la surface qui pourrait être enlevée par polissage. Le broyage avec la jarre et les billes en ZrO₂ a donc été choisi pour la synthèse du NBT-BT.

Un effet de peau dû à une coexistence de phases (tétragonale, rhomboédrique et cubique) a été observé pour les matériaux polis et décontraints dû à des pics élargis et asymétriques sur les diagrammes de diffraction de rayons-X (XRD). Il n'est pas présent dans les échantillons non polis, en raison de la plus faible concentration locale de Ba dans le réseau cristallin du NBT en surface.

Deux solvants de broyage ont aussi été testés : l'éthanol pur et un mélange d'éthanol et de méthyléthylcétone (MEK). Toutefois, le changement de solvant n'a pas eu d'influence sur la structure et la séparation des phases du NBT-BT. Un résultat similaire a été obtenu en changeant la granulométrie du réactif Na₂CO₃.

L'énergie (vitesse et durée) du broyage a également été étudiée en utilisant un broyage à 250 rpm pendant 4h et un autre à 350 rpm pendant 8h. Les effets de l'énergie du broyage étaient évidents dans les échantillons broyés sans utiliser d'agent dispersant, où l'augmentation de l'énergie a entraîné une plus petite surface moyenne des grains et une plus grande fraction volumique des phases secondaires contenant du Ba. Toutefois, cet effet n'est pas observé dans les échantillons broyés avec un agent dispersant, qui avaient des valeurs intermédiaires de surface moyenne des grains et de fraction volumique des phases secondaires.

L'utilisation d'un deuxième broyage après calcination a été testée pour augmenter la densité des céramiques. La densité la plus élevée pour les échantillons sans deuxième broyage a été de 91,5% contre 93,5% pour les échantillons préparés avec un deuxième broyage. Dans les deux cas, la densité maximale a été atteinte le frittage à 1150°C pendant 3h. Les rampes de température utilisées ont été de 120°C/h pour le chauffage et 200°C/h pour le refroidissement, pour éviter les fissures lors du frittage.

Deux diamètres de billes ont été testés pour le deuxième broyage : 1mm et de 10mm. Les billes de 1mm de diamètre ont été choisies, car leur utilisation a augmenté la densité sans modifier la microstructure et la séparation des phases, et sans introduire des lacunes d'oxygène.

Enfin, les changements de stœchiométrie nominale du Na et du Bi ont aussi été étudiés. L'augmentation de la concentration de Bi et de Na a diminué la fraction volumique des phases secondaires contenant du Ba et des échantillons sans séparation de phase ont pu être obtenus avec un excès de Na. La diminution du rapport Na/Bi nominal a créé une matrice stœchiométrique en Bi et une séparation de l'excès de Bi dans une phase riche en Bi et concentrée dans le centre de l'échantillon.

Pour estimer la permittivité des échantillons de NBT-BT à partir de leur mesure d'impédance, un modèle RC a été utilisé. L'analyse de la variation de l'impédance complexe en fréquence a montré que la résistance et la capacité du montage peuvent être négligées et a validé l'utilisation du modèle RC. Les incertitudes des mesures diélectriques ont été estimées par le bruit de mesure, considéré supérieur aux incertitudes. Ainsi, une incertitude de 13% a été prise en compte pour la permittivité relative et une incertitude de 14% a été prise en compte pour les pertes diélectriques.

Une correction du décalage en température a également été apportée. La correction a été effectuée en utilisant un échantillon de BaTiO₃ comme référence. Le changement de la température de Curie dans cet échantillon entre les mesures en chauffage et en refroidissement a montré qu'il n'y a pas de gradient de température significatif dans les échantillons.

Enfin, une nouvelle méthode de fixation des fils sur les échantillons a été utilisée (métallisation par pulvérisation cathodique de Cr-Au et fixation décalée des fils sur une plaque de cuivre) pour estimer une incertitude de 3.5% dans les mesures de température.

Après avoir estimé les incertitudes, les propriétés diélectriques et la résistance d'isolement du NBT-BT ont été mesurées en température. Les effets de la stœchiométrie, de la structure, de la séparation de phases, des paramètres de synthèse et de la contrainte interne sur ses propriétés ont été analysés.

Les propriétés du NBT-BT sont particulièrement sensibles à la stœchiométrie et au rapport Na/Bi. L'augmentation de la teneur en Na inhibe la séparation des phases secondaires contenant du Ba et diminue la teneur relative en Bi dans la phase principale, augmentant ainsi la conductivité de l'échantillon. L'augmentation de la teneur en Bi compense d'abord la formation de lacunes d'oxygène et diminue la conductivité avant de former une deuxième phase, en augmentant à nouveau la conductivité à un Bi-excès supérieur.

Considérant les exigences d'Exxelia pour les MLCCs haute température, la stœchiométrie de l'échantillon "U" (rapport Na/Bi réduit) est la plus adaptée, en raison de sa résistance d'isolation élevée, de ses pertes diélectriques plus faibles et de sa faible variation de permittivité en température par rapport aux autres stœchiométries.

En raison de la séparation de phases et des phases secondaires contenant du Ba, le matériau final peut être considéré comme un composite où la phase matrice est composée de NBT non-stœchiométrique et les inclusions sont constituées des phases secondaires contenant du Ba. Cependant, en raison des caractéristiques physiques et des propriétés des phases, aucun modèle composite classique n'a pas pu être appliqué.

L'augmentation de la fraction volumique et de la surface moyenne des grains de cette phase est d'abord bénéfique pour les MLCCs, puisqu'elle augmente la permittivité, diminue

les pertes diélectriques et augmente la résistance d'isolement, grâce à l'élimination des lacunes d'oxygène. Au-dessus d'une fraction volumique et d'une la surface moyenne de grain critiques, la tendance s'inverse, en raison du caractère conducteur de la phase secondaire. Ainsi, une fraction de volume intermédiaire (2.5 à 3.0%) et une surface moyenne de grain (0.9 à 3.0 μm^2) des phases secondaires contenant du Ba est souhaitable.

Pour obtenir cette fraction volumique et cette surface moyenne de grain des phases secondaires contenant du Ba ainsi que les meilleures propriétés diélectriques et isolantes, il est recommandé d'utiliser un dispersant lors du broyage dans un mélange MEK et éthanol et de ne pas sécher les réactifs avant pesage. Dans ce cas, la granulométrie moyenne du Na_2CO_3 et l'énergie du broyage n'affectent pas significativement les propriétés finales.

Enfin, le polissage et la décontrainte sont une étape importante pour avoir une contamination par ZrO_2 limitée sans introduire de contraintes internes. Le traitement thermique pour relaxer les contraintes doit être fait à 400°C pendant 3h.

Plusieurs hypothèses ont été considérées pour expliquer la dispersion des propriétés diélectriques en fréquence : un modèle composite avec une phase conductrice dans une matrice isolante (modèle de Maxwell-Wagner), deux circuits RC parallèles et dépendant en fréquence représentant le cœur et les joints de grain avec des conductivités différentes (modèle de Nyquist) et un comportement relaxeur (loi de Curie-Weiss modifiée). Les trois modèles de dispersion de fréquence ont pu être appliqués aux échantillons de NBT-BT, même si les tests n'ont pas pu être effectués pour les modèles Maxwell-Wagner et Nyquist, en raison d'une gamme de fréquences de mesure limitée.

Le modèle de Maxwell-Wagner a confirmé l'hypothèse que les phases contenant du Ba sont plus conductrices que la phase matrice de NBT et donc qu'il y a une polarisation interfaciale. Le modèle de Nyquist indique que la résistance associée aux joints des grains est plus élevée et qu'elle augmente avec la température jusqu'à une température critique. Enfin, la loi de Curie-Weiss modifiée indique que tous les échantillons, à l'exception de l'échantillon "E", présentent un caractère relaxeur, avec γ proche de 2. Puisque l'échantillon "E" présente une grande fraction de volume et une petite surface moyenne de grain des phases secondaires contenant du Ba et puisqu'il a une valeur inférieure de γ , cela indique que l'interaction entre les grains voisins des phases secondaires peut influencer le comportement relaxeur dans les NBT-BT.

Enfin, du Co_3O_4 et du MnCO_3 ont été ajoutés au NBT-BT, pour essayer d'améliorer les propriétés diélectriques des échantillons. Cependant, dans les deux cas, la conductivité a été augmentée et les pertes diélectriques ont été soit inchangées, soit augmentées. Donc, ces ajouts ne sont pas idéaux pour la production de MLCCs. En plus des propriétés diélectriques et de la résistance d'isolement, d'autres facteurs ont été pris en compte : la rigidité diélectrique et le cofrittage avec les électrodes. La rigidité diélectrique n'a pu être mesurée que pour l'échantillon "P" et elle était de 7.5 V/ μm . On s'attend toutefois à ce que l'échantillon "U" montre une valeur supérieure. La possibilité de cofritter avec des électrodes 70% Ag et 30% Pd a été confirmée, puisqu'il n'y a pas de réaction chimique entre le Bi et le Pd et que la température de frittage est inférieure à la température maximale de cofrittage.

Après avoir analysé les propriétés diélectriques en fonction de la température et de la fréquence, certaines raisons expliquant l'origine des incompatibilités des propriétés diélectriques du NBT-BT rapportées dans la littérature ont été discutées. L'importance d'avoir une méthode de synthèse et de mesure stricte a été présentée. La littérature montre des incompatibilités dans les valeurs de permittivité relative et de pertes diélectriques, dans leur dispersion en fréquence, dans la permittivité relative à T_d et dans l'allure de la courbe des propriétés diélectriques en fonction de la température.

Pour expliquer ces incompatibilités, l'influence de la stœchiométrie, de la métallisation, de la séparation de phases, des paramètres de synthèse, du polissage et de la décontrainte sur les propriétés diélectriques du matériau a été analysée en chauffage et refroidissement.

La stœchiométrie a un effet crucial sur les propriétés du NBT-BT. L'augmentation du rapport Na/Bi nominal et de la quantité de Na augmente la conductivité et la quantité de charges libres. Ceci augmente les pertes diélectriques et la dispersion en fréquence. Elle peut également modifier la valeur de la permittivité relative et l'allure de la courbe de permittivité et de pertes diélectriques en fonction la température. Enfin, l'augmentation du rapport Na/Bi nominal rend T_d moins évident dans la courbe de permittivité relative, augmente la valeur de T_d et diminue la valeur de T_m .

Une autre différence importante dans les propriétés diélectriques mesurées est l'hystérésis de la permittivité en fonction de la température. Toutes les mesures de la permittivité en chauffage/refroidissement sont similaires, à l'exception de la première mesure en chauffage qui montre une diminution de la permittivité et peut montrer une augmentation du bruit. Ceci est due la métallisation par laque d'argent et à la méthode de fixation du fil électrique. Puisque la laque d'argent est couramment utilisée dans la recherche, elle peut aussi être responsable des incompatibilités rapportées dans la littérature.

La variabilité des propriétés diélectriques mesurées d'un échantillon à l'autre est également un facteur important pour expliquer les différences observées dans la littérature.

Enfin, une variation des pertes diélectriques à haute température est observée après chaque cycle de chauffage et de refroidissement. Elle est présente indépendamment de la métallisation et de la méthode de mise en contact des fils électriques, de la stœchiométrie, de la séparation de phases, des paramètres de synthèse, du polissage et de la relaxation des contraintes. De plus, elle est présente pour les cycles de température où la température maximale est supérieure à 300°C et elle augmente avec l'augmentation des températures maximales. Ceci indique qu'une dégradation thermique a lieu à des températures élevées. En comparant des échantillons avec différentes méthodes de métallisation, il a été possible de conclure que les changements dans la morphologie de l'électrode pendant le chauffage augmentent les pertes diélectriques mesurées. Cependant, il est également possible qu'il y ait un changement dans la microstructure de l'échantillon influencé par la température élevée.

Après avoir analysé les échantillons de NBT-BT en bulk, la synthèse des couches de NBT-BT et la vérification de leur compatibilité avec les spécifications d'Exxelia ont été réalisées. L'échantillon en bulk "U" a montré les meilleures propriétés pour les applications comme MLCC. Cet échantillon a donc été choisi pour être étudié sous forme de couche. Pour la synthèse de la couche, le deuxième broyage a été adapté et la barbotine a été préparée en tenant compte de la composition utilisée par Exxelia et d'une optimisation du liant et des additifs pour NBT-BT mentionnée dans la littérature.

Les couches "vertes" présentaient une bonne résistance mécanique, une épaisseur uniforme et aucune fissure. Cependant, les monocouches frittées avec un palier de température de 30 minutes à 850°C et un frittage à 1050°C pendant 3h ont montré une faible densité relative de 58. Concernant la structure de la monocouche, un élargissement des pics du XRD a été observé en raison d'un effet peau, comme pour les échantillons en bulk. Les mêmes phases secondaires contenant du Ba dans les échantillons en bulk étaient présentes avec une granulométrie moyenne de $2.9 \pm 0.8 \mu\text{m}^2$, conformes aux exigences Exxelia. Cependant, la morphologie de cette phase était différente de celle du bulk, en raison de la faible densité de la monocouche. Enfin, une plus forte contamination en Zr a été observée dans les phases secondaires. Une surface de grain moyenne de $2.4 \pm 0.8 \mu\text{m}^2$ après frittage et une épaisseur de couche de 97 nm ont été obtenues pour la monocouche. Ces valeurs ne sont pas compatibles avec les spécifications d'Exxelia, mais elles pourraient quand-même être utilisées pour la production de MLCCs.

Les propriétés diélectriques mesurées pour la monocouche ne sont pas fiables en raison de leur faible densité. Cependant, la permittivité relative mesurée est plus faible et les pertes diélectriques pour des températures supérieures à 150°C sont plus élevées que le bulk. C'est ce que l'on attend pour les matériaux à faible densité. De plus, une énorme hystérésis en

température est observée lors de sa mesure sur des cycles thermiques consécutifs, rendant la mesure impossible à des températures supérieures à 275°C. Cette hystérésis et cette dégradation thermique peuvent être dues à l'influence des électrodes, puisqu'il y a une pénétration de la laque d'argent dans les pores du matériau pendant les cycles thermiques. Cependant, cela peut aussi être dû au changement de la morphologie du matériau en température, puisque la faible densité et la surface spécifique élevée de la couche facilitent les changements de la morphologie du matériau. Enfin, la résistance d'isolation pour les monocouches est beaucoup plus faible que pour le bulk, comme prévu pour les matériaux basse-densité.

Ces propriétés ne sont pas encore compatibles avec les exigences d'Exxelia pour la production de MLCCs. Néanmoins, les pertes diélectriques sont inférieures à 2.5% à 1kHz de 100 à 150°C, la variation de la permittivité de $\pm 15\%$ a lieu de 180 à 240°C et la résistance d'isolement est supérieure à 1s jusqu'à 180°C. Pour faire une évaluation plus fiable des couches NBT-BT et pour répondre aux exigences de la production de MLCCs, l'augmentation de la densité est impérative.

Pour résoudre ce problème de densité, les effets du pressage de plusieurs couches de NBTBT avant frittage, formant un dispositif multicouche, a été étudié. Il a été démontré qu'un matériau à haute densité (89,5%) peut être obtenu après le frittage des multicouches pressées à 1150°C. Ceci indique que la faible densité des monocouches n'est pas due à un problème de composition de la barbotine et que, même si les monocouches ne présentent pas des propriétés diélectriques compatibles avec les exigences industrielles, cela ne signifie pas nécessairement que le dispositif multicouche préparé avec ces couches aura la même limitation de plage de température. Cependant, comme les multicouches NBT-BT pressées présentent une évaporation de Na et Bi plus élevée, une nouvelle mesure des propriétés diélectriques en température doit être effectuée pour évaluer la plage de température de compatibilité avec les exigences industrielles.

Bibliography

- [1] M Acosta et al. “BaTiO₃-based piezoelectrics: Fundamentals, current status, and perspectives”. In: *Applied Physics Reviews* 4.4 (2017), p. 041305.
- [2] Mickael Anoufa. “Nanocomposites et effet de dimensionnalité pour le stockage de l’énergie”. PhD thesis. CentraleSupélec, 2012, p. 246.
- [3] Kenzo Asaoka and Noritada Kuwayama. “Temperature dependence of thermal expansion coefficient for palladium-based binary alloy.” In: *Dental materials journal* 9 1 (1990), pp. 47–57.
- [4] Ciceron Berbecaru et al. “Structural and Electrical Properties of BNT-BT0.08 Ceramics Processed by Spark Plasma Sintering”. In: *International Journal of Chemical, Molecular, Nuclear, Materials and Metallurgical Engineering* 5.7 (2011), pp. 106–109.
- [5] Alexei A Bokov and Zuo-Guang Ye. “Dielectric relaxation in relaxor ferroelectrics”. In: *Journal of Advanced dielectrics* 2.02 (2012), p. 1241010.
- [6] *Capacitors – Insulation Resistance*. <https://passive-components.eu/capacitors-insulation-resistance/>. Accessed: 2010-09-14.
- [7] *Ceramic Capacitors FAQ*. <https://www.murata.com/en-eu/support/faqs/products/capacitor/mlcc/char/0003>. Accessed: 2010-09-14.
- [8] Henri LAVILLE. “Caractéristiques générales des condensateurs – Condensateurs céramiques”. In: *Techniques de l’ingénieur Matériaux pour l’électronique et dispositifs associés* base documentaire : TIB271DUO.ref. article : e1925 (2018). fre. eprint: [basedocumentaire: TIB271DUO](https://www.techniques-ingenieur.fr/base-documentaire/electronique-photonique-th13/materiaux-pour-l-electronique-et-dispositifs-associes-42271210/caracteristiques-generales-des-condensateurs-condensateurs-ceramiques-e1925/). URL: <https://www.techniques-ingenieur.fr/base-documentaire/electronique-photonique-th13/materiaux-pour-l-electronique-et-dispositifs-associes-42271210/caracteristiques-generales-des-condensateurs-condensateurs-ceramiques-e1925/>.
- [9] Marin Cernea et al. “Sol–gel synthesis and characterization of BaTiO₃-doped (Bi_{0.5}Na_{0.5})TiO₃ piezoelectric ceramics”. In: *Journal of Alloys and Compounds* 490.1-2 (Feb. 2010), pp. 690–694. ISSN: 09258388. DOI: 10.1016/j.jallcom.2009.10.140. URL: <https://linkinghub.elsevier.com/retrieve/pii/S0925838809021161>.
- [10] M Chandrasekhar and P Kumar. “Synthesis and characterizations of BNT–BT and BNT–BT–KNN ceramics for actuator and energy storage applications”. In: *Ceramics International* 41.4 (2015), pp. 5574–5580.
- [11] Xiuli Chen et al. “High relative permittivity, low dielectric loss and good thermal stability of BaTiO₃-bi(Mg_{0.5}Zr_{0.5})O₃ solid solution”. In: *Ceramics International* 41.2 (2015), pp. 2081–2088. ISSN: 02728842. DOI: 10.1016/j.ceramint.2014.10.003. URL: <http://dx.doi.org/10.1016/j.ceramint.2014.10.003>.
- [12] Xiuli Chen et al. “High relative permittivity, low dielectric loss and good thermal stability of novel (K_{0.5}Na_{0.5})NbO₃–Bi(Zn_{0.75}W_{0.25})O₃ solid solution”. In: *Materials Letters* 145 (Apr. 2015), pp. 247–249. ISSN: 0167577X. DOI: 10.1016/j.matlet.2015.01.123. URL: <http://dx.doi.org/10.1016/j.matlet.2015.01.123> <https://linkinghub.elsevier.com/retrieve/pii/S0167577X15001366>.

- [13] Hualei Cheng et al. "MnO₂-modified 0.98(K_{0.5}Na_{0.5})NbO₃-0.02LaFeO₃ ceramics with low dielectric loss for high temperature ceramics capacitors applications". In: *Ceramics International* 40.3 (Apr. 2014), pp. 5019–5023. ISSN: 02728842. DOI: [10.1016/j.ceramint.2013.08.095](https://doi.org/10.1016/j.ceramint.2013.08.095). URL: <https://linkinghub.elsevier.com/retrieve/pii/S0272884213010547>.
- [14] KS Deepa, MT Sebastian, and J James. "Effect of interparticle distance and interfacial area on the properties of insulator-conductor composites". In: *Applied Physics Letters* 91.20 (2007), p. 202904.
- [15] V Dorcet, G Trolliard, and P Boullay. "Reinvestigation of Phase Transitions in Na_{0.5}Bi_{0.5}TiO₃ by TEM. Part I: First Order Rhombohedral to Orthorhombic Phase Transition". In: *Chemistry of Materials* 20.15 (Aug. 2008), pp. 5061–5073. ISSN: 0897-4756. DOI: [10.1021/cm8004634](https://doi.org/10.1021/cm8004634). URL: <https://pubs.acs.org/doi/10.1021/cm8004634>.
- [16] V Dorcet, G Trolliard, and P. Boullay. "Reinvestigation of Phase Transitions in Na_{0.5}Bi_{0.5}TiO₃ by TEM. Part I: First Order Rhombohedral to Orthorhombic Phase Transition". In: *Chemistry of Materials* 20.15 (Aug. 2008), pp. 5061–5073. ISSN: 0897-4756. DOI: [10.1021/cm8004634](https://doi.org/10.1021/cm8004634). URL: <https://pubs.acs.org/doi/10.1021/cm800464d%20https://pubs.acs.org/doi/10.1021/cm8004634>.
- [17] Gui Fen Fan et al. "Effects of manganese additive on piezoelectric properties of (Bi_{1/2}Na_{1/2})TiO₃-BaTiO₃ ferroelectric ceramics". In: *Journal of Materials Science* 42.2 (2007), pp. 472–476. ISSN: 00222461. DOI: [10.1007/s10853-006-1084-6](https://doi.org/10.1007/s10853-006-1084-6).
- [18] Hugo Fricke. "The Maxwell-Wagner dispersion in a suspension of ellipsoids". In: *The Journal of Physical Chemistry* 57.9 (1953), pp. 934–937.
- [19] Wenwei Ge et al. "Evolution of structure in Na_{0.5}Bi_{0.5}TiO₃ single crystals with BaTiO₃". In: *Applied Physics Letters* 105.16 (2014), p. 162913.
- [20] Claudia Groh et al. "High-Temperature Multilayer Ceramic Capacitors Based on 100x(94Bi_{1/2}Na_{1/2}TiO₃-6BaTiO₃)-xK_{0.5}Na_{0.5}NbO₃". In: *Journal of the American Ceramic Society* 99.6 (June 2016). Ed. by J. Ihlefeld, pp. 2040–2046. ISSN: 00027820. DOI: [10.1111/jace.14097](https://doi.org/10.1111/jace.14097). URL: <http://doi.wiley.com/10.1111/jace.14097>.
- [21] Huiling Guo et al. "Improved electrical properties of Co-doped 0.92NBT-0.04KBT-0.04BT lead-free ceramics". In: *Journal of Materials Science: Materials in Electronics* 29.22 (2018), pp. 19063–19069.
- [22] Yiping Guo, Ken-ichi Kakimoto, and Hitoshi Ohsato. "(Na_{0.5}K_{0.5})NbO₃-LiTaO₃ lead-free piezoelectric ceramics". In: *Materials Letters* 59.2-3 (Feb. 2005), pp. 241–244. ISSN: 0167577X. DOI: [10.1016/j.matlet.2004.07.057](https://doi.org/10.1016/j.matlet.2004.07.057). URL: <http://linkinghub.elsevier.com/retrieve/pii/S0167577X04007037>.
- [23] Yiping Guo et al. "Composition-induced antiferroelectric phase and giant strain in lead-free (Na_yBi_z)Ti_{1-x}O₃(1-x)-xBaTiO₃ ceramics Yiping". In: *Physical Review B* 83.5 (Feb. 2011), p. 054118. ISSN: 1098-0121. DOI: [10.1103/PhysRevB.83.054118](https://doi.org/10.1103/PhysRevB.83.054118). URL: <https://link.aps.org/doi/10.1103/PhysRevB.83.054118>.
- [24] S Huband and PA Thomas. "Depolarisation of Na_{0.5}Bi_{0.5}TiO₃-based relaxors and the resultant double hysteresis loops". In: *Journal of Applied Physics* 121.18 (2017), p. 184105.
- [25] Saeed Ullah Jan, Aurang Zeb, and Steven J. Milne. "Dielectric ceramic with stable relative permittivity and low loss from -60 to 300 °C: A potential high temperature capacitor material". In: *Journal of the European Ceramic Society* 36.11 (2016), pp. 2713–2718. ISSN: 1873619X. DOI: [10.1016/j.jeurceramsoc.2016.03.018](https://doi.org/10.1016/j.jeurceramsoc.2016.03.018).

- [26] Saeed ullah Jan, Aurang Zeb, and Steven J Milne. “Electrical properties of Ca-modified Na_{0.5}Bi_{0.5}TiO₃–BaTiO₃ ceramics”. In: *Ceramics International* 40.10 (2014), pp. 15439–15445.
- [27] ZHAO JingBo et al. “Improvement in the piezoelectric temperature stability of (K_{0.5}Na_{0.5})NbO₃ ceramics”. In: *Chinese Science Bulletin* 56.10 (2011), pp. 788–792.
- [28] Liisi Jylhä et al. “Modeling of electrical properties of composites”. In: (2008).
- [29] Liisi Jylhä and Ari Sihvola. “Equation for the effective permittivity of particle-filled composites for material design applications”. In: *Journal of Physics D: Applied Physics* 40.16 (2007), p. 4966.
- [30] Jonas L Kaufman et al. “Permittivity effects of particle agglomeration in ferroelectric ceramic-epoxy composites using finite element modeling”. In: *AIP Advances* 8.12 (2018), p. 125020.
- [31] Walter Arthur Schulze Keith Brudger, Arthur V. Cooke. *High-temperature dielectric materials and capacitors made therefrom*.
- [32] Walter Arthur Schulze Keith Brudger, Arthur V. Cooke. *Patent High-temperature dielectric materials and capacitors made therefrom.pdf*.
- [33] T Kimura et al. “Preparation of crystallographically textured Bi_{0.5}Na_{0.5}TiO₃–BaTiO₃ ceramics by reactive-templated grain growth method”. In: *Ceramics International* 30.7 (2004), pp. 1161–1167.
- [34] Scarlet Kong et al. “Defect-Driven Structural Distortions at the Surface of Relaxor Ferroelectrics”. In: *Advanced Functional Materials* (2019), p. 1900344.
- [35] Jakob König, Matjaž Spreitzer, and Danilo Suvorov. “Influence of the synthesis conditions on the dielectric properties in the Bi_{0.5}Na_{0.5}TiO₃–KTaO₃ system”. In: *Journal of the European Ceramic Society* 31.11 (Oct. 2011), pp. 1987–1995. ISSN: 09552219. DOI: [10.1016/j.jeurceramsoc.2011.04.007](https://doi.org/10.1016/j.jeurceramsoc.2011.04.007). URL: <https://linkinghub.elsevier.com/retrieve/pii/S0955221911001713>.
- [36] Yue-Ming Li et al. “Impedance spectroscopy and dielectric properties of Na_{0.5}Bi_{0.5}TiO₃–NaNbO₃ ceramics”. In: *Physica B: Condensed Matter* 365.1-4 (Aug. 2005), pp. 76–81. ISSN: 09214526. DOI: [10.1016/j.physb.2005.04.039](https://doi.org/10.1016/j.physb.2005.04.039). URL: <https://linkinghub.elsevier.com/retrieve/pii/S0921452605007490>.
- [37] Hamza Lidjici. “Étude, Élaboration Et Caractérisation De Céramiques Piézoélectriques”. PhD thesis. Université Mentouri-Constantine, 2011.
- [38] Zhifu Liu, Yiling Wang, and Yongxiang Li. “Combinatorial study of ceramic tape-casting slurries”. In: *ACS combinatorial science* 14.3 (2012), pp. 205–210.
- [39] Peter Lunkenheimer et al. “Colossal dielectric constants in transition-metal oxides”. In: *The European Physical Journal Special Topics* 180.1 (2009), pp. 61–89.
- [40] Zhen-yu LV. “Study on Dielectric Properties of Aluminum Borate Whisker Reinforced Aluminum Phosphate Composite”. In: *DEStech Transactions on Materials Science and Engineering amst* (2016).
- [41] Dandan Ma et al. “Temperature stability, structural evolution and dielectric properties of BaTiO₃–Bi(Mg_{2/3}Ta_{1/3})O₃ perovskite ceramics”. In: *Ceramics International* 41.5 (June 2015), pp. 7157–7161. ISSN: 02728842. DOI: [10.1016/j.ceramint.2015.02.036](https://doi.org/10.1016/j.ceramint.2015.02.036). URL: <http://dx.doi.org/10.1016/j.ceramint.2015.02.036> <https://linkinghub.elsevier.com/retrieve/pii/S0272884215002552>.
- [42] Amit Mahajen. “Effect of processing on the Structures and Properties of Bismuth Sodium Titanate compounds”. In: *European Materials Research Society (E-MRS) Fall meeting 2017* (Warsaw, Poland). Sept. 2017.

- [43] Deepam Maurya. “Synthesis-Structure-Property Relationships in Lead-Free Piezoelectric Materials”. PhD thesis. Virginia State University, 2012.
- [44] Ryan R. McQuade and Michelle R Dolgos. “A review of the structure-property relationships in lead-free piezoelectric $(1-x)\text{Na}_0.5\text{Bi}_0.5\text{TiO}_3-(x)\text{BaTiO}_3$ ”. In: *Journal of Solid State Chemistry* 242 (Oct. 2016), pp. 140–147. ISSN: 00224596. DOI: 10.1016/j.jssc.2016.01.008. URL: <http://dx.doi.org/10.1016/j.jssc.2016.01.008><https://linkinghub.elsevier.com/retrieve/pii/S0022459616300081>.
- [45] Elisa Mercadelli et al. “Influence of the synthesis route on the properties of BNBT ceramics”. In: *Processing and Application of Ceramics* 3.1-2 (2009), pp. 73–78. ISSN: 1820-6131. DOI: 10.2298/PAC0902073M. URL: <http://www.doiserbia.nb.rs/Article.aspx?ID=1820-61310902073M>.
- [46] R.E. Mistler and E.R. Twiname. *Tape Casting: Theory and Practice*. Wiley, 2000. ISBN: 9781574980295.
- [47] V. R. Mudinepalli et al. “Structural, dielectric and ferroelectric properties of lead-free $\text{Na}_0.5\text{Bi}_0.5\text{TiO}_3$ ceramics prepared by spark plasma sintering technique”. In: *Indian Journal of Physics* 90.2 (Feb. 2016), pp. 131–138. ISSN: 0973-1458. DOI: 10.1007/s12648-015-0743-3. URL: <http://link.springer.com/10.1007/s12648-015-0743-3>.
- [48] Raz Muhammad et al. “ $\text{BaTiO}_3\text{-Bi}(\text{Mg}_{2/3}\text{Nb}_{1/3})\text{O}_3$ Ceramics for High-Temperature Capacitor Applications”. In: *Journal of the American Ceramic Society* 99.6 (2016), pp. 2089–2095. ISSN: 15512916. DOI: 10.1111/jace.14212.
- [49] Xu Ning, Pu Yong Ping, and Wang Zhuo. “Large Dielectric Constant and Maxwell–Wagner Effects in BaTiO_3/Cu Composites”. In: *Journal of the American Ceramic Society* 95.3 (2012), pp. 999–1003.
- [50] M Otoničar et al. “Compositional range and electrical properties of the morphotropic phase boundary in the $\text{Na}_0.5\text{Bi}_0.5\text{TiO}_3\text{-K}_0.5\text{Bi}_0.5\text{TiO}_3$ system”. In: *Journal of the European Ceramic Society* 30.4 (2010), pp. 971–979.
- [51] *Oxford INCA Energy Dispersive Spectrometer (EDS) Training Guide*. <https://pdfs.semanticscholar.org/cd27/97addeb5222d5ddabf67a2e18f77936cdc40.pdf>. Accessed: 2010-08-12.
- [52] Satyanarayan Patel et al. “Tuning of dielectric, pyroelectric and ferroelectric properties of $0.715\text{Bi}_0.5\text{Na}_0.5\text{TiO}_3\text{-}0.065\text{BaTiO}_3\text{-}0.22\text{SrTiO}_3$ ceramic by internal clamping”. In: *AIP Advances* 5.8 (2015), p. 087145.
- [53] He Qi and Ruzhong Zuo. “Linear-like lead-free relaxor antiferroelectric $(\text{Bi}_{0.5}\text{Na}_{0.5})\text{TiO}_3\text{-NaNbO}_3$ with giant energy-storage density/efficiency and super stability against temperature and frequency”. In: *Journal of Materials Chemistry A* 7.8 (2019), pp. 3971–3978. ISSN: 2050-7488. DOI: 10.1039/C8TA12232F. URL: <http://xlink.rsc.org/?DOI=C8TA12232F>.
- [54] Venkata Ramana Mudinepalli et al. “Phase Transitions Of The Ferroelectric $\text{Na}_0.5\text{Bi}_0.5\text{TiO}_3$ By Dielectric And Internal Friction Measurements”. In: *Advanced Materials Letters* 6.1 (Jan. 2015), pp. 27–32. ISSN: 09763961. DOI: 10.5185/amlett.2015.5620. URL: http://vbripress.com/aml/uploads/549fbaff6b95f1419754239%7B%5C_%7Dfullabstratct.pdf.
- [55] M. VENKATA RAMANA et al. “Synthesis of Lead Free Sodium Bismuth Titanate (Nbt) Ceramic By Conventional and Microwave Sintering Methods”. In: *Journal of Advanced Dielectrics* 01.01 (2011), pp. 71–77. ISSN: 2010-135X. DOI: 10.1142/s2010135x11000094.

- [56] Rajeev Ranjan and Akansha Dwiwedi. "Structure and dielectric properties of (Na_{0.50}Bi_{0.50})_{1-x}BaxTiO₃: 0 < x < 0.10". In: *Solid state communications* 135.6 (2005), pp. 394–399.
- [57] *REACH - Les grands principes*. Chanteloup-en-brie, 2018.
- [58] *Règlement CLP*. Chanteloup-en-brie, 2018.
- [59] Richard E. Mistler & Eric R. Twiname. *Tape Casting Theory and Practice*. Westerville, The American Ceramic Society, 2000, p. 291. ISBN: 1574980297.
- [60] *RoHS*. Chanteloup-en-brie, 2018.
- [61] Loey A Salam, Richard D Matthews, and Hugh Robertson. "Pyrolysis of polyvinyl butyral (PVB) binder in thermoelectric green tapes". In: *Journal of the European Ceramic Society* 20.9 (2000), pp. 1375–1383.
- [62] Florian H Schader et al. "Stress-modulated relaxor-to-ferroelectric transition in lead-free (Na^{1/2} Bi^{1/2}) Ti O₃-BaTi O₃ ferroelectrics". In: *Physical Review B* 93.13 (2016), p. 134111.
- [63] Jing Shi et al. "Bi deficiencies induced high permittivity in lead-free BNBT-BST high-temperature dielectrics". In: *Journal of Alloys and Compounds* 627 (2015), pp. 463–467. ISSN: 09258388. DOI: 10.1016/j.jallcom.2014.12.022. URL: <http://dx.doi.org/10.1016/j.jallcom.2014.12.022>.
- [64] *Sol-Gel Science for Ceramic Materials*. <https://www.sigmaaldrich.com/technical-documents/articles/material-matters/sol-gel-science-for.htmls>. Accessed: 2010-09-01.
- [65] Jae-Sung Song et al. "Piezoelectric and dielectric properties in grain oriented (Bi_{0.5}Na_{0.5})TiO₃-BaTiO₃ ceramics". In: *Ferroelectrics* 338.1 (2006), pp. 3–8.
- [66] Matjaž Spreitzer, Matjaž Valant, and Danilo Suvorov. "Sodium deficiency in Na_{0.5}Bi_{0.5}TiO₃". In: *J. Mater. Chem.* 17.2 (2007), pp. 185–192. ISSN: 0959-9428. DOI: 10.1039/B609606A. URL: <http://xlink.rsc.org/?DOI=B609606A>.
- [67] *Technologie et caractéristiques des MLCC*. Chanteloup-en-brie, 1996.
- [68] Karthik Thangavelu, Ranjith Ramadurai, and Saket Asthana. "Evidence for the suppression of intermediate anti-ferroelectric ordering and observation of hardening mechanism in Na^{1/2}Bi^{1/2}TiO₃ ceramics through cobalt substitution". In: *AIP Advances* 4.1 (2014), p. 017111.
- [69] Chun Ming Wang et al. "The temperature-dependent piezoelectric and electromechanical properties of cobalt-modified sodium bismuth titanate". In: *Ceramics International* 42.3 (2016), pp. 4268–4273. ISSN: 02728842. DOI: 10.1016/j.ceramint.2015.11.103. URL: <http://dx.doi.org/10.1016/j.ceramint.2015.11.103>.
- [70] CL Wang. *Theories and Methods of First Order Ferroelectric Phase Transitions*. In-Tech, 2010.
- [71] Defa Wang et al. "Photophysical and photocatalytic properties of SrTiO₃ doped with Cr cations on different sites". In: *The Journal of Physical Chemistry B* 110.32 (2006), pp. 15824–15830.
- [72] L Wang et al. "Dielectric and Piezoelectric Properties of Lead-free BaTiO₃-Bi(Zn_{0.5}Ti_{0.5})O₃ and (Bi_{0.5}Na_{0.5})TiO₃-Bi(Zn_{0.5}Ti_{0.5})O₃ Ceramics". In: *Ferroelectrics* 380.1 (2009), pp. 177–182. ISSN: 0015-0193. DOI: 10.1080/00150190902880282. URL: <http://dx.doi.org/10.1080/00150190902880282>.

- [73] Yiliang Wang et al. “Evolution of phase transformation behavior and dielectric temperature stability of BaTiO₃–Bi(Zn_{0.5}Zr_{0.5})O₃ ceramics system”. In: *Journal of Alloys and Compounds* 551 (Feb. 2013), pp. 365–369. ISSN: 09258388. DOI: [10.1016/j.jallcom.2012.09.127](https://doi.org/10.1016/j.jallcom.2012.09.127). URL: <http://dx.doi.org/10.1016/j.jallcom.2012.09.127> %20<https://linkinghub.elsevier.com/retrieve/pii/S0925838812017306>.
- [74] Chia Ching Wu et al. “The Influences of NaNbO₃ on the Dielectric and Structure Characteristics of (1-X)(Na_{0.5}Bi_{0.5})TiO₃–xNaNbO₃ Ceramics”. In: *Advanced Materials Research* 415–417. Mlcc (2011), pp. 1064–1069. DOI: [10.4028/www.scientific.net/amr.415-417.1064](https://doi.org/10.4028/www.scientific.net/amr.415-417.1064).
- [75] Xiaodong Xia, Zheng Zhong, and George J. Weng. “Maxwell–Wagner–Sillars mechanism in the frequency dependence of electrical conductivity and dielectric permittivity of graphene-polymer nanocomposites”. In: *Mechanics of Materials* 109 (June 2017), pp. 42–50. ISSN: 01676636. DOI: [10.1016/j.mechmat.2017.03.014](https://doi.org/10.1016/j.mechmat.2017.03.014). URL: <http://dx.doi.org/10.1016/j.mechmat.2017.03.014> %20<https://linkinghub.elsevier.com/retrieve/pii/S0167663617300406>.
- [76] Xiangdong Xu. “Enhancements in Dielectric Response Characterization of Insulation Materials”. PhD thesis. Chalmers University of Technology, 2013, p. 71. URL: <http://publications.lib.chalmers.se/records/fulltext/174388/174388.pdf>.
- [77] Zilin Yan. “Microstructure evolution during sintering of multilayer ceramic capacitors: nanotomography and discrete simulations”. PhD thesis. Technischen Universität Darmstadt, 2013.
- [78] F. Yang et al. “Defect chemistry and electrical properties of sodium bismuth titanate perovskite”. In: *Journal of Materials Chemistry A* 6.13 (2018), pp. 5243–5254. ISSN: 20507496. DOI: [10.1039/c7ta09245h](https://doi.org/10.1039/c7ta09245h).
- [79] Pan Yusong, Shen Qianqian, and Chen Yan. “FABRICATION AND MECHANICAL PROPERTIES OF Na_{0.5}Bi_{0.5}TiO₃–BaTiO₃ LEAD-FREE PIEZOELECTRIC CERAMICS”. In: *Ceramics–Silikáty* 58.1 (2014), pp. 50–55.
- [80] A. Zeb and S. J. Milne. “High temperature dielectric ceramics: a review of temperature-stable high-permittivity perovskites”. In: *Journal of Materials Science: Materials in Electronics* 26.12 (Dec. 2015), pp. 9243–9255. ISSN: 0957-4522. DOI: [10.1007/s10854-015-3707-7](https://doi.org/10.1007/s10854-015-3707-7). URL: <http://link.springer.com/10.1007/s10854-015-3707-7>.
- [81] Aurang Zeb and Steven J. Milne. “Low variation in relative permittivity over the temperature range 25–450C for ceramics in the system (1-x)[Ba_{0.8}Ca_{0.2}TiO₃]_{1-x}[Bi(Zn_{0.5}Ti_{0.5})O₃]_x”. In: *Journal of the European Ceramic Society* 34.7 (July 2014), pp. 1727–1732. ISSN: 09552219. DOI: [10.1016/j.jeurceramsoc.2013.12.009](https://doi.org/10.1016/j.jeurceramsoc.2013.12.009). URL: <http://dx.doi.org/10.1016/j.jeurceramsoc.2013.12.009> %20<https://linkinghub.elsevier.com/retrieve/pii/S0955221913005736>.
- [82] Aurang Zeb et al. “Temperature-Stable Relative Permittivity from 70C to 500C in (Ba_{0.8}Ca_{0.2})TiO₃–Bi(Mg_{0.5}Ti_{0.5})O₃–NaNbO₃ Ceramics”. In: *Journal of the American Ceramic Society* 97.8 (Aug. 2014). Ed. by W. Jo, pp. 2479–2483. ISSN: 00027820. DOI: [10.1111/jace.12949](https://doi.org/10.1111/jace.12949). URL: <http://doi.wiley.com/10.1111/jace.12949>.
- [83] Tomas Zednicek. *Capacitors News and Trends*. Noordwijk, 2018.
- [84] Junshan Zhang et al. “Fabrication and Characterization of High-Frequency Ultrasound Transducers Based on Lead-Free BNT-BT Tape-Casting Thick Film”. In: *Sensors* 18.9 (2018), p. 3166.

- [85] Qiang Zhang et al. “Structural and Dielectric Properties of Bi (Mg_{1/2}Ti_{1/2})O₃-BaTiO₃ Lead-Free Ceramics”. In: *Journal of the American Ceramic Society* 94.12 (Dec. 2011). Ed. by S. Zhang, pp. 4335–4339. ISSN: 00027820. DOI: [10.1111/j.1551-2916.2011.04695.x](https://doi.org/10.1111/j.1551-2916.2011.04695.x). URL: <http://doi.wiley.com/10.1111/j.1551-2916.2011.04695.x>.
- [86] Shan-Tao Zhang et al. “Temperature-dependent electrical properties of 0.94 Bi_{0.5}Na_{0.5}TiO₃–0.06 BaTiO₃ ceramics”. In: *Journal of the American Ceramic Society* 91.12 (2008), pp. 3950–3954.
- [87] Jiefeng Zhao et al. “Enhancement of energy-storage properties of K_{0.5}Na_{0.5}NbO₃ modified Na_{0.5}Bi_{0.5}TiO₃–K_{0.5}Bi_{0.5}TiO₃ lead-free ceramics”. In: *Journal of Materials Science: Materials in Electronics* 27.1 (Jan. 2016), pp. 466–473. ISSN: 0957-4522. DOI: [10.1007/s10854-015-3775-8](https://doi.org/10.1007/s10854-015-3775-8). URL: <http://link.springer.com/10.1007/s10854-015-3775-8>.
- [88] Dongxiang Zhou et al. “Influence of ZrO₂ and SnO₂ on the synthesis of Ba₂Ti₉O₂₀ powders”. In: *Ceramics international* 30.5 (2004), pp. 671–673.